

Durham E-Theses

Dual-Phase Electrolyte for Supercapacitors via Non-Aqueous Emulsion Templating

MU, ZHICHAO

How to cite:

MU, ZHICHAO (2025) *Dual-Phase Electrolyte for Supercapacitors via Non-Aqueous Emulsion Templating*, Durham theses, Durham University. Available at Durham E-Theses Online:
<http://etheses.dur.ac.uk/15912/>

Use policy

The full-text may be used and/or reproduced, and given to third parties in any format or medium, without prior permission or charge, for personal research or study, educational, or not-for-profit purposes provided that:

- a full bibliographic reference is made to the original source
- a [link](#) is made to the metadata record in Durham E-Theses
- the full-text is not changed in any way

The full-text must not be sold in any format or medium without the formal permission of the copyright holders.

Please consult the [full Durham E-Theses policy](#) for further details.

Dual-Phase Electrolyte for Supercapacitors via Non-Aqueous Emulsion Templating

Zhichao Mu

A Thesis Presented for the Degree of Doctor of
Philosophy



Department of Engineering

Durham University

United Kingdom

October 2024

Abstract

At present, liquid and solid/quasi-solid electrolytes are the primary types used in the fabrication of supercapacitors (SCs). Liquid electrolytes typically exhibit higher ionic conductivity (10^{-2} to 1 S/cm [1, 2]) but face challenges such as leakage. On the other hand, solid electrolytes address the issue of leakage but generally have lower ionic conductivity (10^{-5} to 10^{-7} S/cm [3]) compared to liquid electrolytes. Quasi-solid electrolytes offer a balance by achieving higher ionic conductivity than solid electrolytes; however, they lack the ability to withstand mechanical pressure, and the ionic conductivity (10^{-4} to 10^{-3} S/cm [3]) is still lower than liquid electrolytes. In this research, a dual-phase electrolyte (DPE) has been fabricated, consisting of a solid phase with a free-flowing liquid phase within its porous structure. The DPE combines good mechanical properties (Young's modulus > 500 kPa [4]) provided by the solid phase and high ionic conductivity (> 1 mS/cm [5]) offered by the liquid phase. This thesis presents a DPE prepared using an emulsion-templating method. This method involves creating an emulsion with dispersed internal phase (liquid phase) droplets within the external phase, followed by the solidification of the external phase (solid phase). The ionic conductivity improves with an increase in the internal phase content; however, this often leads to a decline in mechanical properties. To achieve a balance between desired mechanical properties and ionic conductivity, a polymerised medium internal phase emulsion (polyMIPE) is used. Bisphenol A diglycidyl ether (DGEBA) is selected as the main component of the external phase to provide good mechanical properties, act as a separator, and to ensure the bonding between the DPE and the electrode. Deep Eutectic Solvent (DES) is selected for the internal phase due to its high ionic conductivity (0.02 to 7.61 mS/cm [6]). In the scope of this research, optimal mechanical performance is achieved with a 15 vol.% surfactant content and a 6 ml/min internal phase addition rate. To improve the electrochemical performance of the SC, the polyMIPE is fabricated into a film. The addition of trimethylolpropane triglycidyl

ether (TMPTGE) reduces the viscosity of the emulsion and facilitates film spreading. In polyMIPE films, 5 wt.% TMPTGE content achieves the best combination of ionic conductivity and mechanical performance. Various materials and methods are explored to fabricate SCs based on the polyMIPE films. The maximum specific capacitance of the SC is achieved when carbon (C)-spray is employed to form the electrodes and electrodag is used as the adhesive between the current collector and the electrode, reaching a value of 171.68 ± 6.37 mF/g.

Declaration

The work in this thesis is based on research carried out at the Department of Engineering, Durham University, United Kingdom. No part of this thesis has been submitted elsewhere for any other degree or qualification and it is all my own work unless referenced to the contrary in the text.

Copyright © 2024 by Zhichao Mu.

“The copyright of this thesis rests with the author. No quotations from it should be published without the author’s prior written consent and information derived from it should be acknowledged”.

Acknowledgements

I would like to express my sincere thanks to my supervisor, Dr. Natasha Shirshova. Her inspiring ideas and thoughtful guidance have been essential in completing my PhD research. Her support has been key to reaching this important milestone. I am also grateful to Dr. Andrew Gallant for his guidance throughout my research. His expertise and support have been crucial for the smooth progress of my work.

My appreciation extends to my colleagues and friends at the department. I want to thank Dr. Rajat Sharma for his help with the electrochemical analysis of my samples. His enthusiasm and patience have been invaluable. Additionally, I want to thank the staff of the mechanical workshop for their assistance with the mechanical testing of my samples.

I would like to extend a special thank you to Dr. Akram Karimian. Our bond was deeply strengthened when she offered me comfort during a challenging moment at the café. Her support, both professionally and personally, has been greatly appreciated. Thank you for being there for me not only in my work but also in my life.

I am deeply grateful to my husband for his constant support during my doctoral studies. Despite the challenges, his presence and understanding have been a significant source of strength. I have always been a pessimistic person, but under his influence, I have become more optimistic and better at accepting life's uncertainties. For this positive transformation, I am profoundly thankful.

Finally, I want to thank my parents, my younger brother, and my parents-in-law for their unconditional love and support. Their encouragement has been vital in helping me overcome the challenges of this academic journey.

Contents

Abstract	2
Declaration	4
Acknowledgements	5
Contents	6
List of Figures	9
List of Tables	16
List of Abbreviations and symbols.....	17
1 Introduction	21
2 Theoretical background and literature review.....	24
2.1 Supercapacitor.....	24
2.1.1 Structure of SCs	24
2.1.2 Energy storage mechanisms in SCs	26
2.1.3 Electrolytes of SCs.....	29
2.1.4 Applications of SCs.....	31
2.2 Emulsion-templating method	33
2.2.1 Definition and development.....	33
2.2.2 Instability of emulsions	37
2.2.3 Polymeric surfactants	41
2.2.4 Block copolymer surfactants for O/O emulsions	45
2.2.5 PolyHIPEs/MIPEs based on DGEBA and/or DES	46
2.3 DPE fabricated using different methods	49

2.3.1 DPE fabricated via non-templating method.....	49
2.3.2 DPE fabricated via emulsion-templating method	51
3 Experimental part	53
3.1 Materials.....	53
3.2 Preparation of DES	57
3.3 Preparation of bulk polyMIPE	57
3.4 Preparation of polyMIPE film.....	58
3.5 Fabrication of SCs.....	60
3.6 Characterization	62
3.6.1 Scanning electron microscopy	63
3.6.2 Porosity of polyMIPes.....	64
3.6.3 Compression tests of bulk polyMIPes.....	65
3.6.4 Tension tests of polyMIPE films.....	65
3.6.5 Electrochemical impedance spectroscopy.....	66
3.6.6 Cyclic voltammetry	68
4 The influence of emulsion formulation on various properties of polyMIPes	71
4.1 Summary of sample formulations	72
4.2 The fabrication of polyMIPes with different surfactants.....	73
4.3 The influence of surfactant content on the properties of polyMIPE	77
4.4 The influence of DES addition rate on the properties of polyMIPE.....	86
4.5 The influence of stirring speed on the properties of polyMIPE.....	91
4.6 Summary	96

5	The fabrication and characterization of polyMIPE films.....	98
5.1	Summary of sample formulations	99
5.2	The effect of TMPTGE addition on properties of bulk polyMIPEs	99
5.3	Developing fabrication conditions for polyMIPE films.....	109
5.4	The effect of TMPTGE content on properties of polyMIPE films	112
5.5	Comparison of DPEs prepared in this study with those in existing literatures...	119
5.6	Summary	121
6	Fabrication of SCs based on DES-in-DGEBA polyMIPE	123
6.1	Summary of sample compositions	123
6.2	Exploring the method for fabricating SCs	124
6.3	The effect of TMPTGE addition on the performance of the SCs	133
6.4	The effect of adhesive and current collector type on SC performance	136
6.5	Fabricating SCs using spray-on electrodes	139
6.6	Summary	148
7	Conclusions and recommendation future works	151
7.1	Conclusions	151
7.2	Recommendations for future works	154
8	References	156
9	Appendix	177

List of Figures

Figure 2- 1. The typical structure of a SC.	24
Figure 2- 2. Schematic illustration of charge and discharge of electrical double layer capacitor (the figure adapted from [47]); and the position of the polyMIPE prepared in this study in the SC.	27
Figure 2- 3. Schematic illustration of EDL models: (a) Helmholtz model (b) Gouy-Chaman model (c) Stern model. The figure adapted from [13].	28
Figure 2- 4. The fabrication process of polyH/M/LIPE. The symbol ‘ φ ’ refers to the internal phase volume ratio based on the total emulsion volume.	34
Figure 2- 5. The traditional structure of polyHIPEs. Pores refer to the spaces once occupied by internal phase droplets before their removal, while throats refer to the channels connecting these pores.	36
Figure 2- 6. Schematic diagram of instability mechanisms in an emulsion system.....	37
Figure 2- 7. Three different surfactants: (1) short molecular surfactants; (2) polymeric surfactants; (3) solid particles.	41
Figure 2- 8. Structures of block copolymers: AB type (left) and ABA type (right). A and B indicate different polymers.	43
Figure 2- 9. Schematically illustrate the influence of block length on the packing density of surfactant molecules at the interface. The figure adapted from [155].	44
Figure 2- 10. Schematically illustrate the influence of chain structure on the adsorption of surfactant molecules at the interface (h refers to the separation distance of the droplets, and δ refers to the adsorbed layer thickness). The figure adapted from [155].	45
Figure 3- 1. Structures of the chemicals used in this study.	55
Figure 3- 2. Crosslinking mechanism for epoxy-amine materials.	56
Figure 3- 3. Schematic diagram of film-making stencil (left: top view; right: side view).	60
Figure 3- 4. Definition of specimens from the resulting polyMIPEs used for various characterizations. The specimens 3,4,5,8, and 9 were 10 mm in height and used for	

compression tests; the specimens 1,6, and 10 were 3 mm in height and used for porosity, density and SEM tests; the specimens 2, 7 and 11 were 3 mm in height and used for ionic conductivity tests.....	62
Figure 3- 5. Schematic of a pore in the polyMIPE.....	64
Figure 3- 6. Nyquist plot for bulk polyMIPE or polyMIPE film.	67
Figure 3- 7. Typical EDLC Nyquist plot. ESR refers to equivalent series resistance and R_{ct} refers to charge transfer resistance.	68
Figure 3- 8. CV responses of (a) ideal EDLC, (b) typical EDLC capacitor, and (c) EDLC capacitor involve side electrochemical reactions. The figures adapted from Ref.[229, 232].	70
Figure 4- 1. The SEM image of polyMIPES synthesized using (a) Hypermer B246; (b) Cithrol DPHS; (c) Atlox 4912SF, and the phase separation of (d) Zephyrym PD 2206. (Internal phase ratios - 56 vol.%; surfactant contents - 15 vol.%; DES addition rates - 6 ml/min; stirring speeds - 2000 rpm)	74
Figure 4- 2. The SEM images of polyMIPES based on different surfactant content at two magnifications. (a,b): 10 vol.% surfactant; (c,d): 15 vol.% surfactant; (e,f): 20 vol.% surfactant; (g,h): 25 vol.% surfactant. (Internal phase ratios - 56 vol.%; DES addition rates - 6 ml/min; stirring speeds - 2000 rpm; surfactant - Cithrol DPHS-SO-(MV).)	78
Figure 4- 3. The (a) pore size distribution and (b) throat size distribution of the polyMIPES stabilised with different surfactant content. (Internal phase ratios - 56 vol.%; DES addition rates - 6 ml/min; stirring speeds - 2000 rpm; surfactant - Cithrol DPHS-SO-(MV).)	79
Figure 4- 4. Representative compressive stress-strain curves for polyMIPES produced through the polymerisation of emulsion templates with different surfactant contents. (Internal phase ratios - 56 vol.%; DES addition rates - 6 ml/min; stirring speeds - 2000 rpm; surfactant - Cithrol DPHS-SO-(MV).)	81
Figure 4- 5. Representative compressive stress-strain curves for polyMIPES, one filled with DES (as-synthesized) and after DES extraction. (Internal phase ratios - 56 vol.%; DES addition rates - 6 ml/min; stirring speeds - 2000 rpm; surfactants - Cithrol DPHS-SO-(MV); surfactant content -15 vol.%)	83

Figure 4- 6. The effect of the surfactant content used to stabilize the DES-in-DGEBA MIPE on the ionic conductivity and Young’s modulus of produced in situ filled polyMIPEs. (Internal phase ratios - 56 vol.%; DES addition rates - 6 ml/min; stirring speeds - 2000 rpm; surfactant - Cithrol DPHS-SO-(MV).)	84
Figure 4- 7. The SEM images of polyMIPEs fabricated with different DES addition rates at two magnifications. (a,b): 2ml/min; (c,d): 4ml/min; (e,f): 6ml/min. (Internal phase ratios - 56 vol.%; surfactant contents - 15 vol.%; stirring speeds - 2000 rpm; surfactant - Cithrol DPHS-SO-(MV).).....	88
Figure 4- 8. The (a) pore size distribution and (b) throat size distribution of the polyMIPEs fabricated with different DES addition rates. (Internal phase ratios - 56 vol.%; surfactant contents - 15 vol.%; stirring speeds - 2000 rpm; surfactant - Cithrol DPHS-SO-(MV).)	89
Figure 4- 9. Representative compressive stress-strain curves for polyMIPEs produced through the polymerisation of emulsion templates with different DES drop rates. (Internal phase ratios - 56 vol.%; surfactant contents - 15 vol.%; stirring speeds - 2000 rpm; surfactant - Cithrol DPHS-SO-(MV).)	90
Figure 4- 10. The effect of the DES addition rate on the ionic conductivity and Young’s modulus of produced in situ filled polyMIPEs. (Internal phase ratios - 56 vol.%; surfactant contents - 15 vol.%; stirring speeds - 2000 rpm; surfactant - Cithrol DPHS-SO-(MV).)	91
Figure 4- 11. The SEM images of polyMIPEs fabricated with different stirring speed at two magnifications. (a,b): 500rpm; (c,d): 1000rpm; (e,f): 2000rpm. (Internal phase ratios - 56 vol.%, DES addition rates - 6 ml/min, surfactants - Cithrol DPHS-SO-(MV), surfactant contents -15 vol.%)	93
Figure 4- 12. The pore and pore throat size distribution of the polyMIPEs fabricated with different stirring speed. (Internal phase ratios - 56 vol.%, DES addition rates - 6 ml/min, surfactants - Cithrol DPHS-SO-(MV), surfactant contents -15 vol.%).....	94
Figure 4- 13. Representative compressive stress-strain curves for polyMIPEs produced through the polymerisation of emulsion templates with different stirring speed. (Internal phase ratios - 56 vol.%, DES addition rates - 6 ml/min, surfactants - Cithrol DPHS-SO-(MV), surfactant contents -15 vol.%)	95

Figure 4- 14. Effect of the stirring speed on the ionic conductivity and Young’s modulus of produced in situ filled polyMIPes. (Internal phase ratios - 56 vol.%, DES addition rates - 6 ml/min, surfactants - Cithrol DPHS-SO-(MV), surfactant contents -15 vol.%)	96
Figure 5- 1. The effect of TMPTGE addition on fluidity of the resultantMIPes. The red line in the picture indicates the same scale ‘15’ of the centrifuge tubes. (internal phase ratios - 56 vol.%, DES addition rates - 6 ml/min, stirring speeds - 1000 rpm, surfactants - Cithrol DPHS-SO-(MV), the surfactant contents - 15 vol.%)	102
Figure 5- 2. The SEM images of polyMIPes fabricated with different TMPTGE content at two magnifications. (a,b): 0%TMPTGE-bulk; (c,d): 5%TMPTGE-bulk; (e,f): 10%TMPTGE-bulk; (g,h): 15%TMPTGE-bulk; (i,j): 20%TMPTGE-bulk. (internal phase ratios - 56 vol.%, DES addition rates - 6 ml/min, stirring speeds - 1000 rpm, surfactants - Cithrol DPHS-SO-(MV), surfactant contents - 15 vol.%)	104
Figure 5- 3. The (a) pore size distribution and (b) throat size distribution of polyMIPes fabricated with different TMPTGE content. (internal phase ratios - 56 vol.%, DES addition rates - 6 ml/min, stirring speeds - 1000 rpm, surfactants - Cithrol DPHS-SO-(MV), surfactant contents - 15 vol.%).....	105
Figure 5- 4. Representative compressive stress-strain curves for polyMIPes containing different TMPTGE content. (Internal phase ratios - 56 vol.%, DES addition rates - 6 ml/min, stirring speeds - 1000 rpm, surfactants - Cithrol DPHS-SO-(MV), surfactant contents - 15 vol.%)	107
Figure 5- 5. The structure formula of DGEBA (above) and TMPTGE (below).	108
Figure 5- 6. Effect of TMPTGE content on the ionic conductivity and Young’s modulus of bulk polyMIPes. (Internal phase ratios - 56 vol.%, -DES addition rates - 6 ml/min, -stirring speeds - 1000 rpm, surfactants - Cithrol DPHS-SO-(MV), surfactant contents -15 vol.%)	109
Figure 5- 7. Two instruments for making polyMIPE films: a: film applicator; b: blade, and the appearance of the films prepared by the corresponding instruments. The red rectangles in c and d indicate the sections of the two instruments that come into direct contact with the MIPE film. (internal phase ratio - 56 vol.%, DES addition rate -6 ml/min, the stirring speed - 1000 rpm, surfactants - Cithrol DPHS-SO-(MV), surfactant contents -15 vol.%, the TMPTGE content - 0 wt.%)	111

Figure 5- 8. Schematic diagram illustrating the area of direct contact between the film fabrication tool and the MIPE film.	112
Figure 5- 9. The SEM images of polyMIPE films based on different TMPTGE content with two magnifications. (a,b): 0%TMPTGE- film; (c,d): 2.5%TMPTGE- film; (e,f): 5%TMPTGE- film; (g,h): 7.5%TMPTGE- film; (i,j): 10%TMPTGE- film.....	113
Figure 5- 10. Comparison of bulk polyMIPEs (a,c and e) and polyMIPE film (b, d and f): a: 0%TMPTGE-bulk; b: 0%TMPTGE- film; c: 5%TMPTGE-bulk; d: 5%TMPTGE- film; e: 10%TMPTGE-bulk; f: 10%TMPTGE-film. (Internal phase ratios – at 56 vol.%, DES addition rates – 6 ml/min, stirring speeds – 1000 rpm, surfactants – Cithrol DPHS-SO-(MV), surfactant contents – 15 vol.%)	114
Figure 5- 11. Representative tensile stress-strain curves for polyMIPE films produced through the polymerisation of emulsion templates containing different TMPTGE contents.	115
Figure 5- 12. Effect of TMPTGE content on the ionic conductivity and tensile modulus of polyMIPE films. (Internal phase ratios - 56 vol.%, DES addition rates - 6 ml/min, stirring speeds - 1000 rpm, surfactants - Cithrol DPHS-SO-(MV), surfactant contents - 15 vol.%).....	119
Figure 5- 13. Comparison between this work and existing literature data of DPEs. The mechanical properties are determined using tensile tests. The data presented in the figure are sourced from 1: [188]; 2: [309]; 3: [191]; 4: [310]; 5: [192]; 6: [311]; 7: [193]; 8: [194]; 9: [312]; 10: [253]; 11:[189]; 12: [195]; 13: [196].....	121
Figure 6- 1. Images of (a) MIPE film applied onto the CF mat directly; (b) MIPE film applied onto the CF mat after the MIPE was polymerised for 20 minutes at 60°C; (c) MIPE film applied onto the CF mat after the MIPE was polymerised for 25 minutes at 60°C.....	126
Figure 6- 2. (a) Image of the appearance of the prepared SC. The maximum bending degree of (b) 25min-Cu-P-CF; (c) 40min-Cu-P-CF; and (d) Fully cured-Cu-P-CF.	128
Figure 6- 3. The electrochemical performance of the SCs: (a) CV curves at the scan rate of 5 mV/s; (b) CV curves for Fully cured-Cu-P-CF at the scan rate of 5 mV/s; (c) variation of specific capacitance as a function of scan rate; (d) variation of specific capacitance as a function of scan rate for Fully cured-Cu-P-CF.....	129

- Figure 6- 4.** The SEM images of the surface of polyMIPE film after peeling off the CF mat. (a,c, and e) show the surfaces of the MIPE side that were exposed to air; (b,d, and f) show the surfaces formed by MIPE side in Contact with the substrate. Specifically, (a, b) correspond to 25min-Cu-P-CF; (c,d) correspond to 40min-Cu-P-CF; (e,f) correspond to Fully cured-Cu-P-CF. 131
- Figure 6- 5.** The electrochemical performance of the SCs: (a,c) Nyquist plots of the SCs and (b,d) extended Nyquist plots. 133
- Figure 6- 6.** The electrochemical performance of the SCs fabricated with different TMPTGE content. (a) CV curves at the scan rate of 5 mV/s; and (d) variation of specific capacitance as a function of scan rate; (c) Nyquist plots of the SCs; and (d) extended Nyquist plots..... 136
- Figure 6- 7.** The effect of the adhesive and current collectors on the electrochemical performance of the SCs. (a) CV curves at the scan rate of 5 mV/s; (b) variation of specific capacitance as a function of scan rate; (c) Nyquist plots of the SCs; and (d) extended Nyquist plots..... 138
- Figure 6- 8.** (a) Appearance and (b) the maximum bending degree of the SC using C-spray as the electrodes; (c,d) cross-section of C-spray electrode, ‘Air side’ means the side that contacts the air, and ‘polyMIPE side’ means the side that contacts the polyMIPE film. (Since it is necessary to remove DES for SEM analysis, there is currently no method to do so without damaging the C-spray film. Therefore, the figures c and d present SEM images of the C-spray film that was applied onto a dry polyMIPE film.) 141
- Figure 6- 9.** Surface structure of the polyMIPE film. Figures (a)(c) and (e) show the surface of the polyMIPE film on the side facing the air: (a) as synthesized film, (c) sanded film, and (e) enlarged view of the sanded film. Figures (b)(d) and (f) show the surface structure of the polyMIPE film on the side facing the substrate: (b) as synthesized film; (d) sanded film; and (f) enlarged view of the sanded film. 143
- Figure 6- 10.** The electrochemical performance of the SCs fabricated using C-spray as the electrode. (a) cyclic voltammetry (CV) curves at the scan rate of 5 mV/s; (b) variation of specific capacitance as a function of scan rate; (c) Nyquist plots of the SCs. Nyquist plot for (d)As synthesized-Al-E-C spray; (e) Sanded-Al-E-C spray; and (f) Sanded+DES-Al-E-C spray..... 145

Figure 6- 11. (a) Appearance and (b) the maximum bending degree of the SC using Ni-spray as the electrodes; (c,d) SEM image of the Ni-spray electrode.	146
Figure 6- 12. The electrochemical performance of the SCs fabricated using Ni-spray electrode. (a) cyclic voltammetry (CV) curves at the scan rate of 5 mV/s; (b) variation of specific capacitance as a function of scan rate; and (c) Nyquist plots of the SCs.	148
Figure 6- 13. Variation in specific capacitance of all SCs in this chapter as a function of scan rate. (a) 25min-Cu-P-CF; (b) 40min-Cu-P-CF; (c) Fully cured-Cu-P-CF; (d) 2.5%TMPTGE-Cu-P-CF; (e) 5%TMPTGE-Cu-P-CF; (f) 25min-Cu-E-CF; (g) 25min-Al-E-CF; (h) As synthesized-Al-E-C spray; (i) Sanded-Al-E-C spray; (j) Sanded+DES-Al-E-C spray; (k) Sanded+DES-Al-E-Ni spray.	150

List of Tables

Table 3- 1. chemicals used and their properties.....	54
Table 3- 2. Summarization of the used surfactants and their important properties.	54
Table 4- 1. Compositions of the studied emulsion templates.	72
Table 4- 2. The properties of surfactants used in DES/DGEBA emulsion.....	73
Table 4- 3. The effect of surfactant content on the properties of polyMIPes.	80
Table 4- 4. The effect of DES addition rate on the properties of the resultant polyMIPes.	90
Table 4- 5. The effect of stirring speed on the properties of the resultant polyMIPes...	95
Table 5- 1. Compositions of the studied emulsion templates.	99
Table 5- 2. The influence of TMPTGE addition on the properties of the bulk polyMIPes.	107
Table 5- 3. The influence of TMPTGE content on the properties of polyMIPE films.	116
Table 6- 1. Compositions of SCs in this chapter.....	124

List of Abbreviations and symbols

Abbreviation	Definition
AC	Alternating current
BCP	Block copolymer
C	Carbon
CF	Carbon fibre
ChCl	Choline chloride
CV	Cyclic voltammograms
DES	Deep eutectic solvent
DGEBA	Bisphenol A diglycidyl ether
DGEBOH	Diglycidyl ether of 1,4-butanediol
DPE	Dual phase electrolyte
DVB	Divinylbenzene
EDL	Electrical double-layer
EDLC	Electrical double-layer capacitor
EG	Ethylene glycol
EIS	Electrochemical impedance spectroscopy
EP	Epoxy resin
ESR	Equivalent series resistance
HC	Hybrid capacitors
HIPE	High internal phase emulsion
HLB	Hydrophilic-lipophilic balance
HSP	Hansen solubility parameter
IHP	Inner Helmholtz plane
IL	Ionic liquid
IPA	Isopropanol
IPDA	Isophorondia-mine, mixture of cis and trans
LIPE	Low internal phase emulsion
MIPE	Medium internal phase emulsion
MWCNT	Multi-walled carbon nanotubes
Ni	Nickel
O/O	Oil-in-oil
O/W	Oil-in-water
OHP	Outer Helmholtz plane

PC	Pseudo-capacitors
PEG	Polyethylene glycol
PI	Polyisoprene
PLA	Poly(lactic acid)
PMMA	Poly (methyl methacrylate)
PolyHIPE	Polymerised high internal phase emulsion
PolyLIPE	Polymerised low internal phase emulsion
PolyMIPE	Polymerised medium internal phase emulsion
RIPS	Reaction-induced phase separation
RT	Room temperature
R_{ct}	Charge transfer resistance
SC	Supercapacitor
SEM	Scanning electron microscopy
TMPTGE	Trimethylolprop-ane triglycidyl ether
W/O	Water-in-oil

Symbol	Parameter	Unit
A	Electrode area on the sample surface	cm ²
α_1	Solubility of the internal phase in the external phase	mol/m ³
AHEW	Amine hydrogen equivalent weight	g/eq
C _s	Specific capacitance	F/g
d	Translational diffusion coefficient	m ² /s
D ₁₀	Average pore diameter	μm
D ₃₂	Sauter mean diameter	μm
D _i	Diameter of each pore	μm
E	Young's modulus	Mpa
EEW	Epoxy equivalent weight	g/eq
g ₁	Gravitational acceleration	m/s ²
h	Height of the tested sample	cm
I	Current	A
l	Length of the pore edge	m
L	Length of the base of the porous foam	m
m	Mass of the electrodes	g
n _i	Number of pores	
phr	per hundred resins	
r	Droplet radius	m
R	Gas constant	J/(mol · K)
R _b	resistance	Ω
Symbol	Parameter	Units
t	Time	s
T	Temperature	K
V	Potential	V
V _{Sam}	Volume of the tested sample	ml
γ	Interfacial tension	N/m
Δm	mass difference between the DES filled and dry samples	g
ΔV	Potential window	V
ε	Porosity	%
ė	Strain rate	s ⁻¹
ε	Strain	
η _{cp}	Shear viscosity of the external phase	kg/(m · s)

μ	Dynamic viscosity of the fluid	Pa·s
v_{Stokes}	Creaming/sedimentation velocity	m/s
ρ	Density of DES	g/ml
ρ_{ep}	Density of the external phase in emulsion	kg/m ³
ρ_{droplet}	Density of the internal phase in emulsion	kg/m ³
σ	Ionic conductivity	S/cm
σ^*	Collapse strength	MPa
σ_g^*	Contribution of cell fluids to the strength of open-cell foam	Pa
v	Scan rate	V/s
v_o	Rate of Ostwald ripening	m ³ /s
φ	Internal phase ratio	vol.%

1 Introduction

Energy is essential for human development, rendering the methods for its storage a critical issue. Energy storage systems are classified into electrical and non-electrical types based on the final energy source. Electrical energy storage systems can both receive and deliver stored energy as electrical energy, while also allowing for the storage of energy in other forms [7]. Batteries and supercapacitors (SCs) are the primary electrical energy storage systems used today [7-9]. Compared to batteries, SCs exhibit higher power density (SC: up to 196000 W/kg vs. battery: <1000 W/kg), faster charging/discharging speed (SC: s to min vs. battery: 1-5 h), and greater cycle life (SC: >500000 vs. battery: about 1000) [10-13]. Because of these advantages, SCs have received significant attention from researchers. SCs are devices that store electrical charges at the electrode/electrolyte interface. A typical SC consists of current collectors, electrodes, electrolyte, and separator. The electrolyte is a vital component of a SC to provide a medium for ion transport and to help form the electrical double layer at the electrode-electrolyte interface [2]. Liquid electrolytes are currently the most commonly used type of electrolyte, known for their high ionic conductivity (10^{-2} to 1 S/cm [1, 2]). However, they are prone to issues such as leakage. In contrast, solid electrolytes address the leakage problem but generally exhibit much lower ionic conductivity (10^{-5} to 10^{-7} S/cm [3]). Quasi-solid electrolytes provide a compromise between solid and liquid electrolytes, exhibiting ionic conductivity in the range of 10^{-4} to 10^{-3} S/cm [3], which is higher than that of solid electrolytes. However, their ionic conductivity remains lower than that of liquid electrolytes, and they are also susceptible to mechanical deformation due to their limited ability to withstand applied pressure. In this study, a DPE composed of both solid and liquid phases is prepared. The solid phase possesses a porous structure, provides mechanical properties, and function as a separator and adhesive; while the liquid phase, which can freely flow through the porous structure of the solid phase, ensures ionic conductivity. The DPE combines the high ionic

conductivity advantage of liquid electrolytes with the good mechanical performance of solid electrolytes.

Emulsion-templating method is employed to fabricate the DPE. This method involves two basic steps: the preparation of an emulsion where the internal phase (liquid phase) is dispersed as droplets within the external phase, and solidification of the external phase (solid phase) [14]. To achieve a balance between the desired mechanical properties and ionic conductivity of the DPE, this study focuses on the polyMIPE system. DGEBA is selected as the primary component of the solid phase due to its good mechanical performance (Young's modulus: 1.6 GPa to 2.7 GPa), adhesive properties, and high-temperature performance (glass transition temperature: 113 °C to 124 °C), etc [15-17]. Isophorondia-mine, mixture of cis and trans (IPDA) is the crosslinking agent in the solid phase. The amino group in IPDA attacks the carbon atom of the epoxy group, opening the epoxide ring. The opened epoxide ring then forms a covalent bond with the amino group. As the crosslinking reaction between IPDA and DGEBA progresses, a three-dimensional network structure is formed [18]. The specific crosslinking mechanism is detailed in Chapter 3. As for the liquid phase, DES is selected due to its good conductivity, ease of preparation, non-toxicity, biocompatibility and biodegradability [16].

In summary, the main objective of this thesis is to prepare a DPE with good mechanical properties (Young's modulus > 500kPa [4]) and high ionic conductivity (> 1 mS/cm [5]) using the emulsion-templating method. Furthermore, the performance of this DPE in SC is investigated. The overall research objectives are as follows:

1. Investigate the effects of various factors in the emulsion preparation process on the performance of the bulk polyMIPEs.
2. Explore a suitable method for spreading the emulsion into a uniform film and discuss the properties of polyMIPE films.

3. Evaluate the performance of SCs based on the polyMIPE prepared in this study. Adjust other components (current collector, electrode, and adhesive type) in the SC except the polyMIPE to maximize the function of the DPE.

Following this brief introduction, Chapter 2 provides essential background information on SCs, emulsion-templating method, and DPEs fabricated using different methods. In Chapter 3, the materials used and the experimental procedures, including sample preparation and characterisation methods are detailed. Chapter 4 examines the impact of various factors—such as surfactant content, internal phase addition rate, and stirring speed—on the performance of bulk polyMIPES. In Chapter 5, TMPTGE is added to the MIPE to reduce its viscosity, allowing the MIPE to be more easily spread into a film. The chapter explores the impact of TMPTGE addition on the performance of both bulk polyMIPES and polyMIPE films. Chapter 6 presents the performance of SCs based on the polyMIPE films fabricated in this study. Chapter 8 summarises the research results and provides suggestions for further research.

2 Theoretical background and literature review

2.1 Supercapacitor

2.1.1 Structure of SCs

A supercapacitor is a device that store electrical charges at the electrode/electrolyte interface. A typical SC (**Figure 2- 1**) consists of two current collectors, two electrodes, an electrolyte, and a separator. Each component occupies a specific position in the SC.

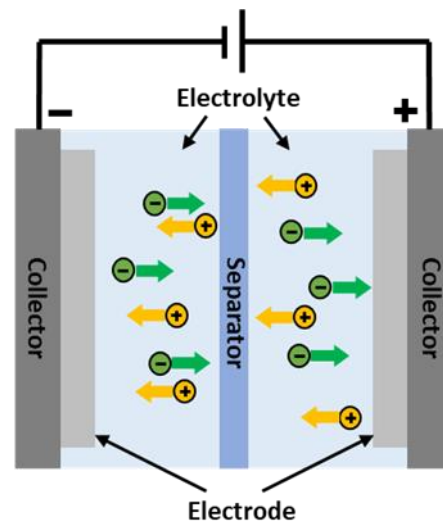


Figure 2- 1. The typical structure of a SC.

The electrode active material determines the charge storage of the SC. Nowadays, the common active electrode materials used for SCs include carbon-based materials, conducting polymers and metal oxides [19-22]. The selection of carbon-based materials (such as carbon foam, graphene, and carbon nanotube[23]) is due to their exceptional electronic conductivity (0.6 to 0.9 S/cm) and large specific surface area (up to 3000 m²/g), [24-27]. Conducting polymers store charge through redox reactions within the material, which enhances energy storage and reduces self-discharge [28-30]. In general, metal oxides deliver high energy density for SCs (20 to 90 Wh/kg) and exhibit good electrochemical stability [31-34].

The electrolyte plays an essential role in SCs as it relates to the charge transfer and balance between electrodes [35]. Each electrolyte has its own advantages and disadvantages. One electrolyte type cannot meet all of the requirements in terms of characteristics. Hence, selecting a proper electrolyte according to demand is essential in the SC field. SC electrolytes can be categorised into two types based on their state: liquid and solid/quasi-solid electrolyte [36-38]. The liquid electrolytes can offer high conductivity (10^{-2} to 1 S/cm [1, 2]) to the SC but also cause leakage problem simultaneously. Solid or quasi-solid electrolytes can avoid the leakage problem and simplify the fabrication process of SC. In addition to providing ionic conduction (10^{-7} to 10^{-3} S/cm [3]), solid/quasi-solid electrolyte also function as separators. However, they face the challenge of lower ionic conductivity compared to liquid electrolytes [35-37]. Apart from the nature of these electrolytes, the interaction between electrolyte and electrode is also the key to a safe and effective SC. A strong interaction is good for charge accumulation, but an extremely strong interaction will decrease the mobility of ions in the electrolytes. It is therefore essential to find an optimal balance of the interaction between electrolytes and electrodes [39]. Section 2.1.3 will provide a detailed description of the electrolyte used in SCs.

The separator is the component placed between two electrodes. The main function of separator is to prevent contact between two electrodes to avoid short-circuiting. The separator should possess ion permeability but no electronic permeability. In addition, the high ionic conductance (0.1 to 10 mS/cm), high mechanical strength (20 MPa to 50 MPa), and low thickness ($< 25 \mu\text{m}$) of the separator can help to achieve the best performance of the SC [40-43]. Similar to the electrolytes, there is no perfect separator which can meet all the requirements for a SC with good performance. The choice of separator should be based on the application involved. For example, the separator used in a structural SC should possess good mechanical performance; SCs in wearable electronics require flexible separators [44].

Generally, two current collectors will be used on the surface of electrodes to collect and transport the electrons. The ideal current collector should possess high electrical conductivity (10^4 to 10^5 S/cm), high mechanical strength (10 to 10^6 GPa), strong bonding with the electrodes, etc [45, 46]. Metal-based current collectors are most used to date; these materials provide high conductivity (2.6×10^4 to 6.0×10^5 S/cm [46]). However, metal-based collectors cannot be used in water-based electrolytes, and the interfacial resistance between the collectors and electrodes cannot be neglected. Carbon and polymer-based collectors are regarded as an alternative to metal collectors. They can effectively reduce the resistance between the electrodes and collectors, but at the same time, these materials are generally expensive [45].

2.1.2 Energy storage mechanisms in SCs

SCs can be classified into three types according to their mechanisms:

(1) Electrical double-layer capacitors (EDLC). This type of SC has two charged layers because of the electrostatically accumulating charges at the electrolyte and electrode interface. This is the type of SC developed in this research. (2) Pseudo-capacitors (PC). This SC's mechanism relates to a Faradaic redox reaction between the electrodes and electrolytes. (3) Hybrid capacitors (HC). This type of SC combines both of the mechanisms mentioned above [47].

In EDLC, the charges are stored by the formation of electric double layer and no charge transfer reactions take place. The electric double layer is formed because of the accumulation of electric charges on the surface of electrodes during the charging process of EDLC [43]. After applying a voltage, the electronic layer of charges is generated on the surface of the electrodes. Ions of opposite polarity from the electrolyte will accumulate on the surface of the electrodes to compensate for these charges on the electrode surface (**Figure 2- 2**) [10].

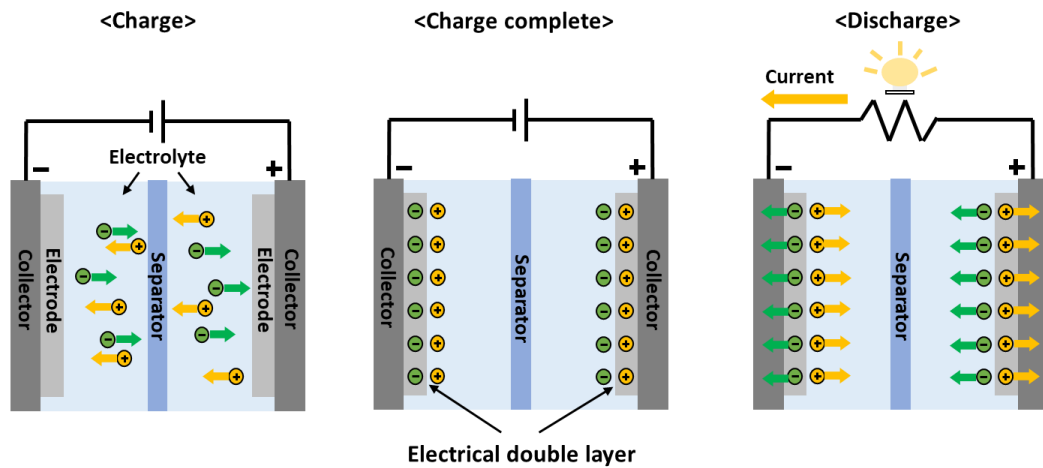


Figure 2- 2. Schematic illustration of charge and discharge of electrical double layer capacitor (the figure adapted from [48]).

The concept of EDLC was firstly proposed by Helmholtz. The Helmholtz model is similar to the conventional two-plate capacitor (**Figure 2- 3**) in which the opposing charges align parallel to the electrode/electrolyte interface [49, 50]. Gouy and Chapman then modified the Helmholtz model into the diffusive layer model. In this model, the charge distribution is a function of distance from the electrode/electrolyte surface. Hence, the electric potential increases exponentially close to the electrode surface (**Figure 2- 3**) [13, 43, 49, 50]. Furthermore, Stern combined the Helmholtz model and Gouy-Chapman model to acknowledge two kinds of charges distribution: Stern layer (compact layer) and a diffusive layer. In the Stern layer, ions are strongly adsorbed by the electrode and the ions can be classified into two types- specifically adsorbed ions and non-specifically adsorbed counterions. These two types of adsorbed ions can be distinguished as inner Helmholtz plane (IHP) and outer Helmholtz plane (OHP) (Figure 2- 3) [13, 43, 51].

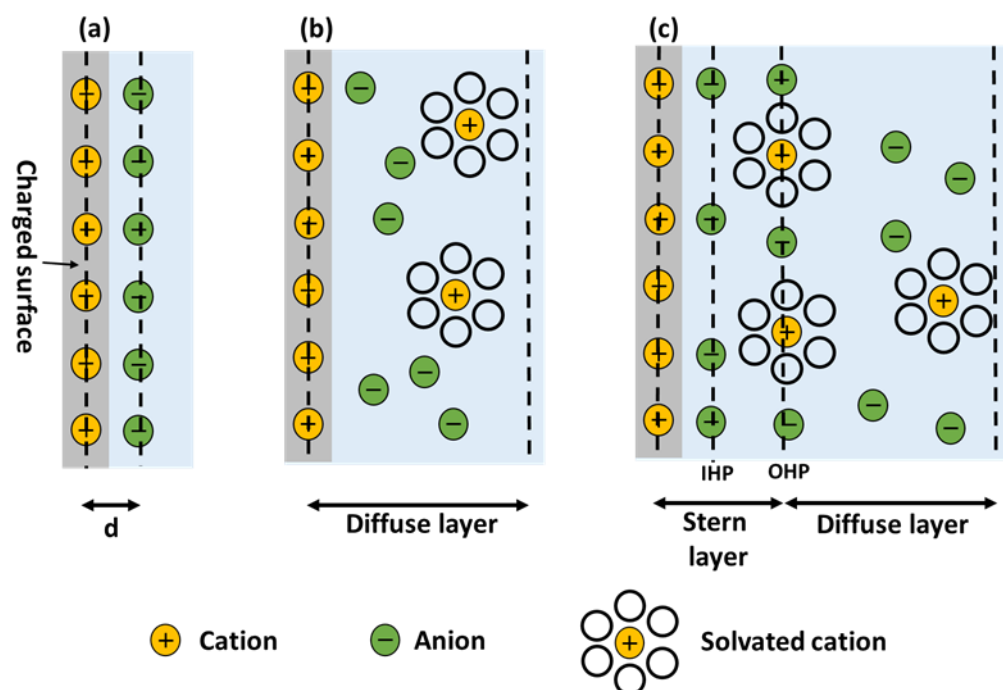


Figure 2- 3. Schematic illustration of EDL models: (a) Helmholtz model (b) Gouy-Chaman model (c) Stern model. The figure adapted from [13].

In addition to electrolyte, the surface area and pore size of the electrodes in SC also influence the formation of the EDL. The ions will not be able to form a double layer when the pore size of electrodes remains smaller than diameter of hydrated ions. Both micropores (pore diameter $<2\text{nm}$) and mesopores ($2\text{ nm}<\text{pore diameter}< 50\text{nm}$) are essential for obtaining good performance SCs. Micropores are the guarantee of a high surface area ($> 1000\text{ m}^2/\text{g}$) which is important for charging the double layer and determining the capacitance value; while mesopores allow good electrolyte penetration which plays an essential role in power density [52, 53].

To describe the materials that possess the similar electrochemical characteristics to the traditional SC (EDLC) but have different energy storage mechanism, Conway firstly proposed the term ‘Pseudocapacitance’ [54]. Pseudocapacitors (PCs) store energy through Faradaic charge process, in which the oxidation or reduction of a chemical species leads to the electron transfer across the electrode/electrolyte interface. The fast and reversible redox reactions happen at the electrode/electrolyte interface by means of

adsorption or intercalation of ions in electrolyte [55]. Charge transfer is the only process taking place between the adsorbed ions and electrodes materials so there are no chemical transformation occurred in electrodes [43]. Meanwhile, there are also some layered materials but undergo Faradic reaction attributed to the intercalation of electrolyte ions in the layers or tunnels [55]. Various materials such as transition metal oxides and electronically conducting polymers are used for pseudo-capacitor electrodes [56]. The capacitance of these SCs are higher than EDLCs due to the electrode materials undergo reversible redox reaction for a long time (10-100 times larger than EDLCs) [13].

The energy storage mechanism of hybrid capacitors is a combination of both EDL formations and Faradaic reactions [57]. The term 'hybrid' means that the electrodes consist of two or more different materials and asymmetric electrodes are used for energy storage [58]. Generally, the electrodes of HCs are classified as asymmetric, composite and battery type. In asymmetric capacitors, one electrode will follow EDLC behaviour, and the other one will be made up of PC electrode material. In composite electrodes, carbon-based materials are combined with PC electrode materials. The battery type electrodes are composed with one carbon-type electrode and one battery-type electrode [43].

2.1.3 Electrolytes of SCs

Electrolytes used in SCs can be categorised into two main types: liquid electrolytes and solid/quasi-solid electrolytes [38, 59, 60]. A detailed discussion of these electrolytes will be presented based on these classifications.

Liquid electrolytes can be further divided into aqueous electrolytes and non-aqueous electrolytes. Aqueous electrolytes exhibit higher ionic conductivity (10^{-2} to 1 S/cm), attributed to their rapid ion transport [59, 61]. Acids such as H_2SO_4 and alkalines such as KOH are frequently used as aqueous electrolytes in SC due to their high ionic

conductivity (0.1 S/cm for 1M KOH) [62]. However, their corrosive properties limit their cyclic stability and effectiveness. In comparison, neutral electrolytes like Na₂SO₄ and KCl are less corrosive. Nonetheless, they tend to have lower ionic conductivity (KOH > KCl > Na₂SO₄) [2, 59, 63]. Organic electrolytes are another commonly used electrolyte in SCs, with an operating window typically ranging from 2.5 to 2.8 V. In contrast, to prevent water decomposition, the cell voltage of SCs based on aqueous electrolytes is generally limited to 1.0 V [61]. Organic electrolytes possess larger operating windows (2.5 to 2.8 V), however, some associated factors must be considered when using organic electrolytes, including flammability and toxicity [64]. Organic electrolytes in SCs are primarily based on conductive organic salts dissolved in organic solvent. Commonly used solvents for organic electrolytes include acetonitrile, ethylene carbonate, and propylene carbonate. The commonly used electrolyte salts are tetraethylammonium tetrafluoroborate, trimethylethylammonium tetrafluoroborate, LiClO₄, and LiPF₆ [64, 65]. Ionic liquids are also commonly used liquid electrolytes, defined as salts composed entirely of ions (cations and anions) with melting points below 100 °C [66]. They possess several advantages, including thermal and chemical stability and negligible volatility [38, 66]. Commonly used cations of ionic liquid for SCs include imidazolium, phosphonium, ammonium, and pyrrolidinium, et al. The frequently used anions include tetrafluoroborate, hexafluorophosphate, and bis (fluorosulfonyl imide) [59].

Solid electrolytes effectively avoid the leakage issue associated with liquid electrolytes and can also function as separator in SC. However, their ionic conductivity (10⁻⁵ to 10⁻⁷ S/cm) is generally lower compared to that of liquid electrolytes. Solid electrolytes can be divided into two types: polymer-based electrolytes and inorganic solid electrolytes [67, 68]. Dry polymer electrolytes and polyelectrolytes are both polymer-based electrolytes. In dry polymer electrolytes, ionic conductivity arises from the movement of salt ions within the polymer, while the ionic conductivity of polyelectrolytes is due to the charged

polymer chains [61]. Dry polymer electrolytes typically consists of high molecular weight polymers, such as poly(ethylene oxide) and poly(propylene oxide), dissolved with lithium-ion salts [67]. The ionisable groups found in common polyelectrolytes include quaternary amines (e.g., $-\text{NH}_2$, $=\text{NH}$, $=\text{N}^+=$), carboxylates (e.g., $-\text{COO}^-$), and phosphonates (e.g., $-\text{PO}_3\text{H}_2$, $-\text{PO}_3^{2-}$) [69]. Inorganic solid electrolytes, which are crystalline or amorphous glassy ionic conductors, typically conduct a single type of ion [67]. Materials such as perovskite, amorphous $\text{Li}_2\text{S}-\text{P}_2\text{S}_5$ and thio-LiSICON have been studied as inorganic electrolytes [68].

Quasi-electrolytes generally exhibit better ionic conductivity (10^{-4} to 10^{-3} S/cm) compared to solid electrolytes, though their mechanical performance tend to be poor. Gel electrolytes are the most widely studied quasi-solid electrolytes. The fundamental structure of gel electrolytes consists of a host polymer that swells with a liquid electrolyte [70]. A variety of polymers have been investigated for the fabrication of gel electrolytes, including poly(vinyl alcohol), poly(ethylene oxide), poly(methyl methacrylate) (PMMA), and poly(acrylic acid) [71].

The electrolyte studied in this research is a bi-continuous DPE composed of solid phase and liquid phase. Due to the highly cross-linked solid phase, it is anticipated to exhibit better mechanical properties compared to liquid and gel electrolytes. Furthermore, the free movement of ions within the liquid phase is expected to contribute to higher ionic conductivity than that of solid electrolytes (10^{-5} to 10^{-7} S/cm). Section 2.3 will provide a detailed discussion of various DPEs based on different preparation methods.

2.1.4 Applications of SCs

SCs possess a broad range of applications due to their capability of delivering huge power within short timeframes. They have been widely used in several sectors like hybrid electric vehicles and in electrical generation and distribution networks.

Electric vehicles have now received considerable attention. One application of SCs in electric vehicles is in the ‘regenerative braking process’ and ‘start and stop system’ [72]. The rapid energy change during these processes can cause stress on the battery and will reduce its life span. SCs could be used as an effective substitute due to the rapid charge and discharge rate [72, 73]. Additionally, SCs require no maintenance and typically endure throughout the entire lifespan of the vehicle [72].

Portable electronics such as smart-phones, laptops, cameras, smart-watches are indispensable in our daily life. These electronics favour lightweight energy storage devices. Arrays of SCs, either in conjunction with batteries or on their own, are used as the energy storage system for the electronics. The hybrid system offers mixed advantages such as large energy density of batteries and rapid charging of SCs [74].

The bulky size of conventional batteries limits their application in wearable electronics. Flexible SCs have been developed recently to resolve this problem [74-77]. Additionally, stretchable, transparent, shape memory, self-healing and thermal chargeable SCs were also researched, which broaden the application of the SC in further [78-82].

Renewable energy systems (e.g. solar energy, wind energy and tidal energy) often experience power fluctuations due to their intermittent, irregular, and cyclical nature. This problem could be resolved by employing a hybrid storage system combining batteries with SCs where the SC responds rapidly to the instantaneous and dynamic power demands and the battery supplies continuous power [43, 83].

SCs are also a good choice for other applications, such as microgrid, medical and health care and buildings, etc. Microgrid refers to an autonomous power grid that operates on a small scale. A microgrid combined with renewable energy sources could be an advantageous solution to the growing energy crises [84]. However, due to the intermittent nature of the renewable energy resources, maintaining a high-quality standalone micro-

grid is challenging [85]. The usage of hybrid energy storage system based on SCs and batteries can address the basic issues such as current stress on battery and intermittency [86]. SCs also play a role in medical and health care applications. For example, SCs can be used in implantable healthcare devices such as insulin pump and cardiac pacemakers [87]; The SCs with flexibility, stretchability and compressibility could be used in medical wearables, sensors and artificial skin [88]. The SCs used in elevators prevent from voltage drop and makes energy efficient and electrochromic SCs can be used in smart homes [89, 90].

2.2 Emulsion-templating method

2.2.1 Definition and development

Emulsion-templating method is a promising and convenient route for producing porous materials. The technique mainly consists of the following steps (**Figure 2- 4**): 1) the preparation of an emulsion consisting of at least two immiscible liquids, in which one liquid (dispersed phase, internal phase) is dispersed in the other liquid (continuous phase, external phase). Typically, surfactants are used to stabilise the emulsion; 2) The polymerisation of the external phase; 3) The removing of the internal phase (if needed). According to the internal phase volume ratio, the emulsions can be divided into three categories. The emulsions are classified as high internal phase emulsions (HIPE) when the internal phase fraction is higher than 74 vol.%; The emulsions are classified as medium internal phase emulsions (MIPE) when the internal phase ratio is between 30 vol.% to 74 vol.% and low internal phase emulsion (LIPE) when the fraction is lower than 30 vol.%. HIPE is the most widely studied among the three types of emulsions [91-93].

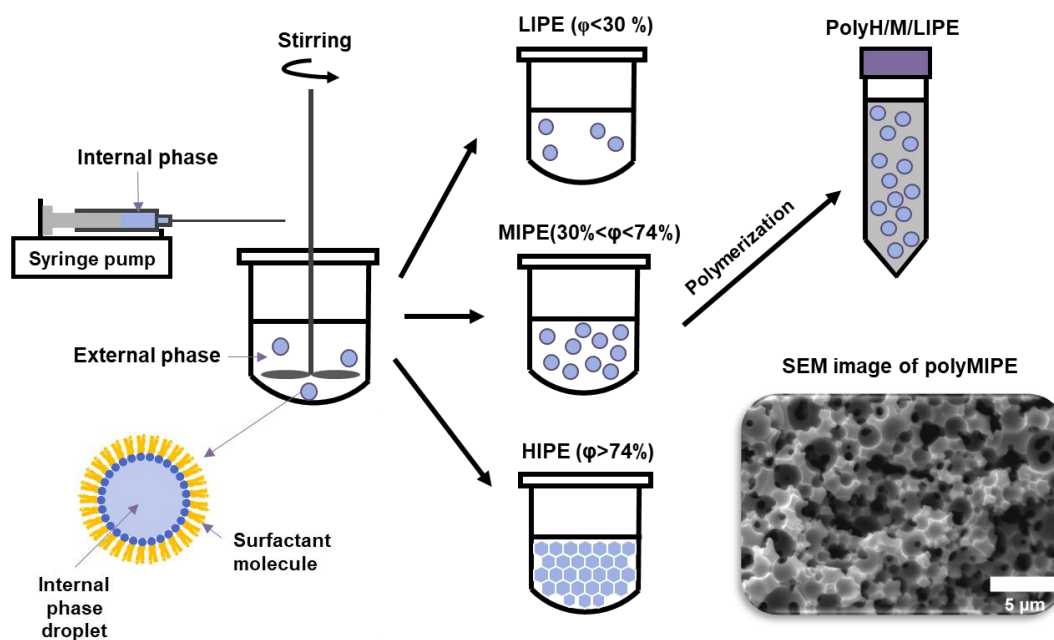


Figure 2- 4. The fabrication process of polyH/M/LIPE. The symbol ‘ ϕ ’ refers to the internal phase volume ratio based on the total emulsion volume.

Polymerised HIPE (polyHIPE) is a porous polymer fabricated within HIPE. The internal phase volume ratio of HIPEs should be more than 74 % which is the maximum packing density of monodispersed spheres. Hence, the droplet shapes in HIPEs are usually polyhedral, which would create large contact areas between the droplets [94]. The thin film that developed at the contact areas often rupture after polymerisation, these ruptures give rise to interconnections, referred to as throat between the pores (**Figure 2- 5**) [95, 96]. The highly distributed throats contribute to the remarkable permeability of polyHIPEs. In the early stages of the emulsion-templated method development, the most researched system is the styrene and divinylbenzene (DVB) based HIPE, which was firstly proposed by Barby and Haq in 1982 [97]. In this study, an aqueous phase (internal phase) in styrene/DVB emulsion was stabilised by non-ionic surfactant. A low-density polystyrene foam with open cellular structure was obtained followed by curing the emulsion and removing the aqueous phase. In the early 1990’s, Williams et al. [98, 99] conducted a more in-depth study of this system, the effects of internal phase content, monomer content, the hydrophilic-lipophilic balance (HLB) of the surfactant and the

locus of initiation on the properties of polystyrene HIPE were investigated. Subsequently, the emulsion-templated polymeric material began to develop rapidly, a variety of oil and water phase materials were used in the study of HIPEs. The hydrophobic polyHIPEs from water-in-oil (W/O) HIPEs are the most common. Apart from styrene, propylene fumarate, thiolene, polycaprolactone tetramethacrylate, trimethylolpropane triacrylate and methyl methacrylate [100-104] are all studied for the fabrication of W/O emulsions. Simultaneously, the study on the hydrophilic polyHIPEs from oil-in-water O/W HIPEs is progressively deepening. Naotaka Kitagawa [105] firstly describe the production of hydrophilic polyHIPEs in O/W emulsions. Thereafter, many polymers have been studied to fabricate polyHIPEs using O/W emulsions. For instance, Barbetta et al. [106] developed gelatin-methacrylate polyHIPEs using Triton X-405 as the surfactant. The produced architecture was highly interconnected, a feature that is vital for three-dimensional colonisation within the realm of tissue engineering. Haifei Zhang et al. [107] prepared an O/W emulsion with the continuous phase composed of N-isopropylacrylamide (NIPAM), N,N'-methylenebisacrylamide(MBAM) and surfactant Triton X-40, and the discontinuous phase consisted of chloroform and Oil Red O (OR). After polymerising the emulsion, the produced polyHIPE was freeze-dried to make a polyHIPE with OR nanoparticles attached to the polymer surface. The authors [107] pointed that a potential use of this kind of polyHIPE is for the delivery of water immiscible drugs in the form of organic nanoparticles. Other polyHIPEs from O/W emulsions include those based on acrylic acid, poly(ϵ -caprolactone), hydroxyethyl methacrylate (HEMA) and 1-vinyl-5-aminotetrazole [108-112]. With the expansion of scholarly investigation, the study of HIPEs has been expanded to include non-aqueous oil-in-oil HIPEs, CO₂-in-water HIPEs and oil-in-water-in-oil HIPEs [15, 113-119]. The polyHIPEs show the potential applications in catalysis, tissue engineering, enzyme support, separation and filtration. However, their widespread industrial deployment is

limited by the lack of sufficient mechanical strength. To address this limitation, a viable strategy involves increasing the foam density by means of decreasing the internal phase ratio of the emulsions, specifically, fabricating L/MIPE would be an effective method.

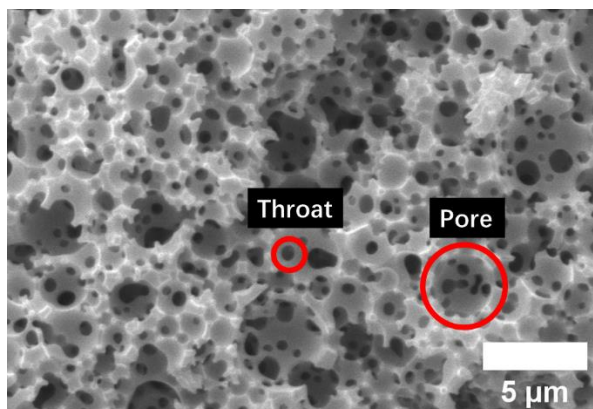


Figure 2- 5. The traditional structure of polyHIPEs. Pores refer to the spaces once occupied by internal phase droplets before their removal, while throats refer to the channels connecting these pores.

Polymerised MIPE (polyMIPE), with a porosity between 30% and 74%, also possesses an interconnected pore structure when using suitable surfactants to stabilise the emulsion. Some studies have demonstrated the preparation of polyMIPEs with both good openness and mechanical properties [120-125]. In their pioneering works, Angelika Menner et al. [120] successfully prepared open-cell styrene/DVB polyMIPEs that were stabilised by non-ionic surfactant Hypermer 1070. The elastic modulus of the polyMIPE was 24 MPa, which is much improved compared to the modulus of the polyHIPE (1MPa) made in their study. The same group [125] also made the styrene/polyethylene glycol dimethacrylate polyMIPEs using Hypermer B246f as the surfactant. Similarly, the Young's modulus increased from 5 MPa to 25 MPa by decreasing the internal phase ratio from 80 vol.% to 60 vol.%; and the interconnected pore structure was observed. Patrick Steindl et al. [124] stabilised an aqueous phase-in-epoxy MIPE with Span 20. It showed that the interconnected pores content increased with increasing the surfactant content, but the mechanical properties exhibited a decline when rising the surfactant content.

Polymerised LIPE (polyLIPE) usually possess low interconnectivity. [121, 126-128] Therefore, polyLIPEs may not be the optimal choice when a good interconnectivity is one of the objectives of this study.

2.2.2 Instability of emulsions

The term ‘stability’ typically denotes the capacity of an emulsion to withstand changes in its physicochemical properties as time progress. Emulsion stability relies on the existence of surfactants at the interface, which retards the natural inclination of the liquids to spontaneously separate. This existence prolongs the stability duration of the emulsion. Hence, to be specific, ‘emulsion stability’ refers to the maintenance of the dispersion within a defined time period while preserving a specific average droplet size and droplet size distribution [129]. An emulsion maybe unstable due to some different mechanisms, including creaming/sedimentation, flocculation, coalescence, Ostwald ripening and phase inversion (**Figure 2- 6**) [129, 130]. The various instability mechanisms are detailed explained as follows.

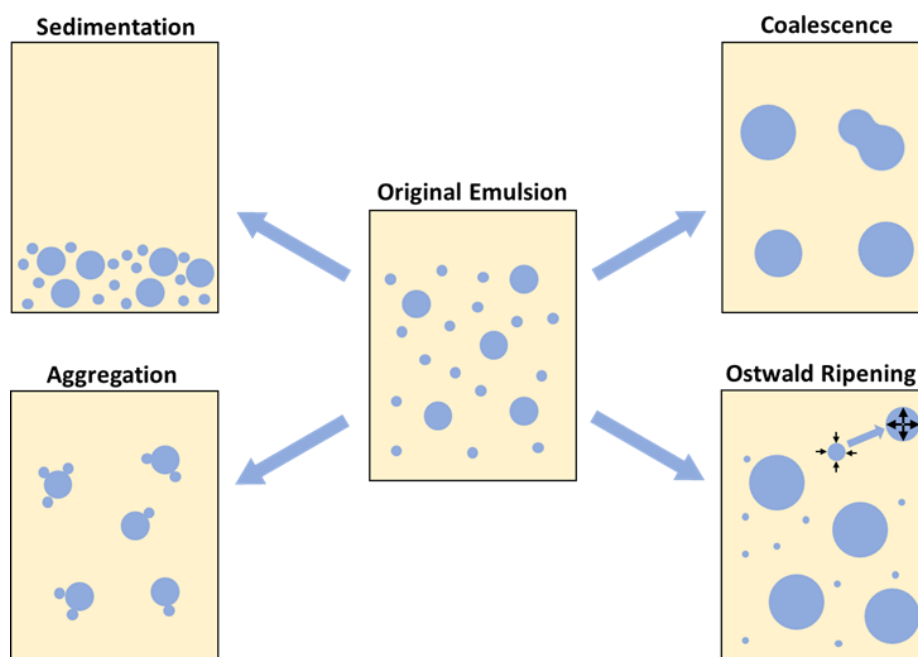


Figure 2- 6. Schematic diagram of instability mechanisms in an emulsion system.

2.2.2.1 Creaming and sedimentation

Both creaming and sedimentation could be classified as gravitational separation. Sedimentation occurs when the density of the internal phase is higher than the external phase, leading to the droplets to moving downward and causing a separated layer; creaming happens when the density of the internal phase is lower than the external phase, resulting the droplets to move upward [131]. Sedimentation is more common in W/O emulsions and solid dispersions, while creaming is more common in O/W emulsions and air dispersions. The degree of creaming/sedimentation can be assessed by measuring the thickness of creaming/sedimentation layer. Fortunately, creaming and sedimentation are reversible, the emulsion can easily be reformed by shaking. The gravitational separation of emulsions can be described by mathematical models [132]:

$$v_{Stokes} = - \frac{2g_1 r^2 (\rho_{droplet} - \rho_{cp})}{9\eta_{cp}} \quad (2-1)$$

where v_{Stokes} refers to the creaming/sedimentation velocity, g_1 is gravitational acceleration, r is the droplet radius, $\rho_{droplet}$ and ρ_{cp} are the densities of the internal phase and external phase (continuous phase) respectively, η_{cp} is the shear viscosity of the external phase. It could be concluded from the function that an appropriate internal phase density (close to the external phase density), larger external phase viscosity and smaller droplet radius can delay and even overcome gravitational separation.

2.2.2.2 Flocculation

Flocculation describes the process that two or more droplets are combined with each other because of mutual attractive interactions, but their integrity is still maintained. Generally, the interaction between droplets is not very strong and could be broken by stirring or just shaking [133, 134]. When flocculation happens, the droplet size can be preserved while the droplets form aggregates or clusters which are larger in size, thereby facilitating gravitational separation. This implies that flocculation is actually damaging to the

emulsion stability [135]. The interactions between droplets are essential to the happening of flocculation, including attraction force (Van der Waals force, hydrophobic interactions and depletion force) and repulsion force (electrostatic repulsion and steric hindrance) [132, 136]. In the case where attraction prevails, the droplets tend to flocculate, whereas when repulsion dominates, the droplets tend to be stable. Typically, surfactants play a role in preventing the flocculation and coalescence of droplets by creating robust electrostatic repulsion and steric hindrance [132].

2.2.2.3 Coalescence

Coalescence describes the process that two or more droplets are merged to form a larger droplet. Coalescence happens when the thin interfacial films between the smaller droplets rupture and the small droplets fuse to form a single larger droplet. The primary characteristic of coalescence is the rupture of the interfacial film. Hence, the viscoelasticity and thickness of the interfacial film are essential to prevent coalescence [132]. For example, Wan et al. [137] made a Pickering emulsion stabilised by alginate/chitosan polyelectrolyte complex. It was found that both the interfacial film thickness and viscoelasticity were increased by increasing the chitosan concentration, which prevents the coalescence, and hence leads to a more stable emulsion.

2.2.2.4 Ostwald ripening

Ostwald ripening describes the process by which larger droplets grow at the cost of smaller droplets due to internal phase molecules migration through the external phase. In a poly-disperse emulsion, the droplet size is inversely related to the chemical potential of molecules in it. As the droplet size decreases, there is an increase in the chemical potential, leading to greater solubility of the smaller droplet molecules within the external phase. [129] The driving mechanism behind Ostwald ripening involves the alternation of the

chemical potential of the internal phase to align with the external phase. The rate of Ostwald ripening can be measured by the following equation [129]:

$$v_o = \frac{dr^3}{dt} = \frac{8Y a_1 d}{9RT} \quad (2-2)$$

where Y is the interfacial tension, r is the radius of the droplet, t is the time, a_1 is the solubility of the internal phase in the external phase, d is the translational diffusion coefficient of the internal phase molecules through the external phase, R is the gas constant and T is the absolute temperature. The equation suggests that reducing the solubility of the internal phase within the external phase would effectively lower the rate of Ostwald ripening. Hence, incorporating external phase-insoluble substances is an effective way to prevent Ostwald ripening. A.S. Kabalnov et al. [138] explained that the existence of poorly soluble components can lead to compositional difference between larger and smaller droplets, which potentially counterbalance the driving force behind Ostwald ripening. In a W/O emulsion, inorganic salt could act as such a substance. For example, M. Yu. Koroleva and E. V. Yurtov [139] found that the addition of NaCl in W/O emulsion could suppress the diffusion of water between the dispersed droplets, thereby decrease the Ostwald ripening greatly. Similarly, adding water-insoluble component to an O/W emulsion would inhibit the Ostwald ripening to good effect. Yurim Jang et al. [140] found that the addition of triacylglycerols, which possess extremely low water solubility, could prevent the Ostwald ripening of orange oil emulsion easily. An alternative way to inhibit Ostwald ripening involves preventing the diffusion of droplet molecules by interfacial engineering methods such as multilayer formation, etc [141].

2.2.2.5 Phase inversion

Phase inversion means the conversion from an O/W emulsion to a W/O emulsion or vice versa. Generally, phase inversion is undesirable because it negatively affects the

appearance and stability of the emulsion. However, phase inversion is desired in some cases, for example, the production of margarine and butter [132]. Hence, it is essential to gain a thorough comprehension of the phase inversion mechanisms. Phase inversion in an emulsion system occurs exclusively when the internal phase possesses a sufficient high-volume fraction (> 13 vol.% [142]), and the continuous stirring must be maintained. The high-volume fraction (> 13 vol.% [142]) increases the likelihood of collisions among the internal phase, facilitating the growth of internal phase droplets. Continuous stirring induces the large droplets to inwardly deform their surfaces, effectively enveloping the external phase [132].

2.2.3 Polymeric surfactants

The application of surfactant is an effective method to guarantee the stability of emulsions. The surfactant establishes an interfacial layer upon adsorption to the droplet's surface, thereby preventing droplet from merging. There are many kinds of surfactants (**Figure 2-7**), such as short molecular weight surfactants, polymeric surfactant as well as solid particles, which have been used in the stabilisation of emulsions.

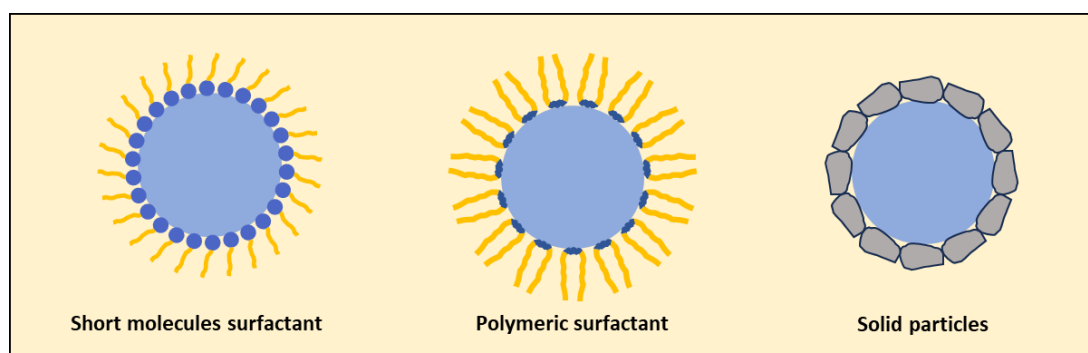


Figure 2- 7. Three different surfactants: (1) short molecular surfactants; (2) polymeric surfactants; (3) solid particles.

Surfactants enhance emulsion stability by forming a steric barrier around the internal phase droplets, which effectively inhibits their agglomeration and coalescence. For a surfactant to effectively stabilise the emulsion, the following criteria need to be satisfied

[143]: (1) ensuring complete coverage of the droplets by the surfactant. Because of van der Waals attraction or bridging, any exposed area may lead to flocculation; (2) there should be strong adsorption of the surfactant to the droplets surface; (3) effective steric stabilisation should be achieved by strong solvation or hydration of the stabilizing chain; (4) an appropriate adsorbed layer thickness should be guaranteed to prevent weak flocculation. Most of the emulsions investigated to date are W/O or O/W emulsions, which can be stabilised by small molecules, polymeric surfactants, or particles. However, this thesis focuses on oil-in-oil (O/O) emulsions, where small molecule surfactants are used much less frequently. This is because small molecule surfactants stabilize emulsions by decreasing the interfacial tension between the two phases; however, the interfacial tension between two immiscible oils is already relatively small, which limits the effectiveness of small molecule surfactants in further reducing it [118]. Compared to small molecule surfactants, polymeric surfactants and particles that offer steric stabilisation at the oil-in-oil (O/O) interface are more frequently employed for the stabilisation of O/O emulsions [118]. For the DES-in-DGEBA emulsion in this research, polymeric surfactants were chosen as the surfactants. Particles were not selected because their use as surfactants often results in polymerised emulsions that exhibit non-permeable or closed-cell structures, characterised by few or no interconnected pores [144]. The interconnected pores are essential to facilitate the free movement of ions in DPE.

Polymeric surfactant molecules can be designed to possess a robust ‘anchor’ chain that attaches to the droplet surface firmly, along with a ‘stabilising’ chain’ that extends from the surface, resulting in a layer thickness δ . When two droplets come within a separation distance h that is smaller than 2δ , the stabilising chains may become compressed and/or overlap, leading to steric repulsion. Block (A-B or A-B-A) copolymer (**Figure 2- 8**) is one of the most used polymeric surfactants. A block copolymer consists of linear segments of different compositions. This polymer surfactant demonstrate surface activity

because one block dissolves in one phase, while the other is miscible in the opposing phase [145]. In addition, with the need to stabilize different emulsions and advancements in synthesis technology, various other types of polymeric surfactants, such as comb-type, dendrimers, and star-shaped, have also been developed [146].

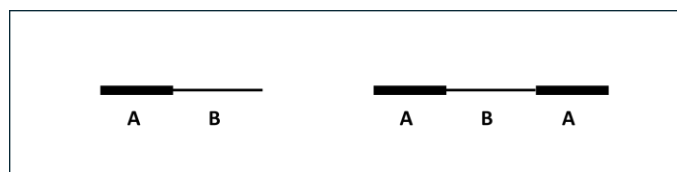


Figure 2- 8. Structures of block copolymers: AB type (left) and ABA type (right). A and B indicate different polymers.

In emulsion systems, polymeric surfactants act as stabiliser that strongly adsorb onto droplet surfaces, providing effective steric stabilisation against coalescence, flocculation, and Ostwald ripening [147-149]. The adsorption of polymeric surfactants is influenced by various factors, such as block structure and length [150], topology [151], molecular weight [143], HLB [152] and concentration [153, 154]. The block length often plays a critical role in dictating the adsorption behaviour at the interface. Specifically, when using the polymeric surfactants, it is essential to consider the folding of the chains at the interface (**Figure 2- 9**). Gref et al. [155] provided a demonstration of this phenomenon using copolymers of poly(ethylene glycol)–poly(lactic acid) (PEG–PLA). When the hydrophobic part (PLA) gets longer, the hydrophobic chains take on a sparser conformation. This special configuration significantly limits their effective adsorption at the interface.

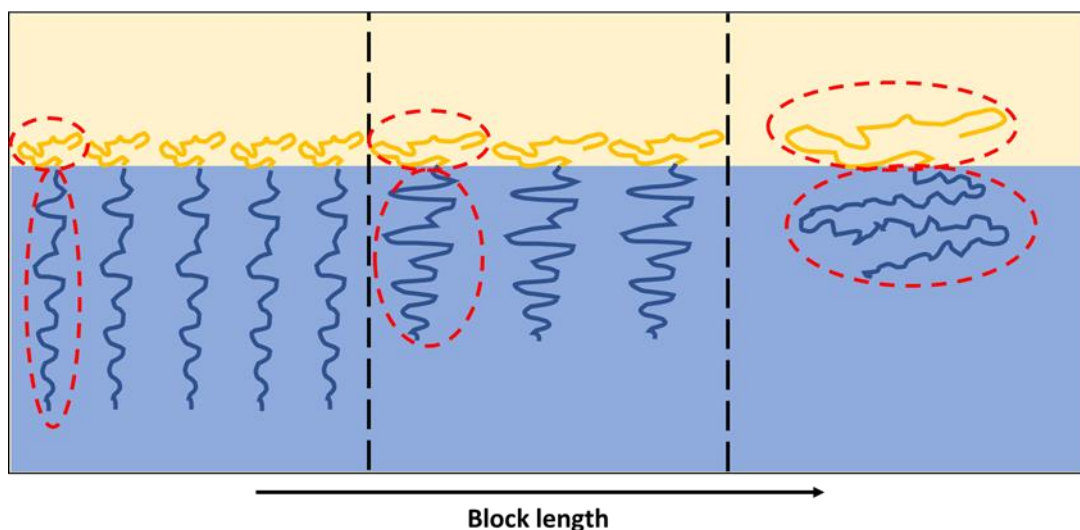


Figure 2- 9. Schematically illustrate the influence of block length on the packing density of surfactant molecules at the interface. The figure adapted from [156].

It becomes more complicated if one considers how the chain topology and the hinderance caused by its structure affects adsorption [157, 158]. Specifically, the distinction between graft and block copolymers always leads to varying chain structures at the interface, consequently resulting in diverse stabilisation mechanisms through steric repulsion (**Figure 2- 10**). Exerowa [159] illustrated this: for the ABA block copolymer, the A-tails within the ‘brush’ can either infiltrate and/or condense when the distance (h) is less than twice the brush thickness (2δ); In contrast, with the graft copolymer, the dominant behaviour tends to be loop-compression rather than loop-penetration. This occurs due to the geometric differences between the brushes and loops, making it highly improbable for the loops to penetrate the brushes [159].

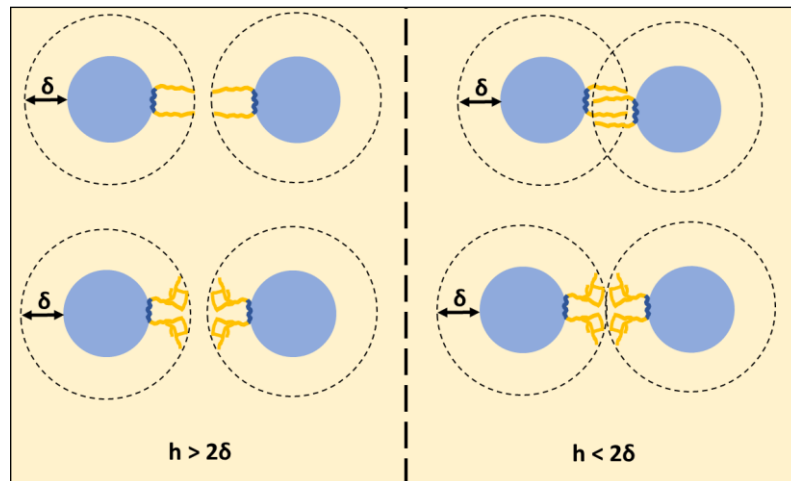


Figure 2- 10. Schematically illustrate the influence of chain structure on the adsorption of surfactant molecules at the interface (h refers to the separation distance of the droplets, and δ refers to the adsorbed layer thickness). The figure adapted from [156].

Additionally, thorough investigations have confirmed the presence of optimal molecular weight, HLB and concentration of polymeric surfactants in emulsion stabilisation, which significantly influence crucial parameters such as adsorbed layer thickness, interfacial tension and steric stabilisation [143, 152-154].

2.2.4 Block copolymer surfactants for O/O emulsions

Block copolymers are widely recognised as effective steric stabilisers for O/O emulsions and serve as the surfactants used in this thesis. Typically, the formation of O/O emulsions using block copolymer (BCP) surfactants requires dissolving the BCP in one oil at a concentration exceeding the critical micelle concentration. At this concentration, the BCP self-assembles into micelles, where one block forms the core and the other constitutes the corona. A second oil, which is miscible with the micelle core but immiscible with the first oil, is then introduced, followed by agitation of the system [118]. The interfacial activity of BCP at a specific O/O interface is influenced by their chemical composition, the size of each block, and molecular weight.

The suitable chemical composition of the BCP for stabilising a specific O/O emulsion can be easily identified through Hansen solubility parameter (HSP). HSP describes the

solubility of a material through three parameters: polarity, hydrogen bonding energy, and dispersion energy [160, 161]. When the HSP of an oil is similar to that of a polymer, it indicates a miscibility between these two materials. This compatibility suggests that the polymer can serve as an effective block in the BCP for stabilizing emulsions that contain the specific oil. For example, an O/O emulsion consisting of hexane and acetonitrile can be stabilised by polyisoprene-b-poly (methyl methacrylate) (PI-b-PMMA), as the HSP of hexane is similar to that of PI, while the HSP of acetonitrile is similar to that of PMMA [162]. In addition to the chemical composition, the size of each block in the BCP also affects the stability of O/O emulsions. Atanase et al. [163] fabricated an oil-in-oil emulsion using PEG400 as the dispersed phase and Miglyol 812, a mixture of caprylic and capric triglycerides, as the continuous phase. Two BCPs with similar molecular weights but different relative block lengths were tested for emulsion stabilisation: poly(2-vinylpyridine)₅₀-block-poly(butadiene)₁₂₈ (P2VP₅₀-b-PBut₁₂₈) and P2VP₃₇-b-PBut₁₈₉. The most stable emulsion was achieved with P2VP₃₇-b-PBut₁₈₉, as the longer PBut chains contribute to enhanced steric stability. Regarding molecular weight, a BCP with larger molecular weight is generally required to stabilise O/O emulsions due to the small interfacial tension between the two phases [118, 164, 165], typically ranging from 5,000 to 50,000 g mol⁻¹ [165].

The selection of an appropriate BCP surfactant for a specific O/O system frequently relies on a guess-and-check approach [118]. It can be challenging to find an exact match in the literature for the system under investigation. In such cases, an initial assessment can be based on HSP, the size of each block, and the molecular weight.

2.2.5 PolyHIPEs/MIPEs based on DGEBA and/or DES

2.2.5.1 PolyHIPEs/MIPEs based on DGEBA

DGEBA is the most widely used epoxy resin, produced through a reaction between bisphenol A and epichlorohydrin. It is widely recognised for its excellent mechanical properties, adhesive properties and chemical resistance [166-168]. The good mechanical properties and chemical resistance of DGEBA contribute to the stability of DPE, while its adhesive property ensures strong bonding between DPE and the electrodes in SC.

There are currently few articles that explore the use of DGEBA as the external phase in the emulsion-templating method for preparing porous polymers. Wang et al. [169] prepared polyHIPEs using DGEBA as the external phase, combined by polyamide resin as the curing agent, nonylphenol polyoxyethylene as the surfactant, and 4-methyl-2-pentanone as the solvent. The internal phase consisted of an aqueous suspension of colloidal silica. The results indicate that the porous polymer could be successfully prepared; however, only partially open pores were achieved, with approximately half of the pores remaining closed. In addition, the use of a colloidal silica suspension as the internal phase was essential, as stable emulsion cannot be produced with water alone. The aqueous suspension of calcium chloride was also used as the internal phase. Steindl et al. [170] prepared polyMIPEs using a kind of epoxy composed of DGEBA and 1,6-hexanediol diglycidyl ether as the external phase, with Pluronic L-81 as the surfactant and a calcium chloride dihydrate solution as the internal phase. At a curing temperature of 23 °C, a polyMIPE with open-porous structure was obtained. However, when the curing temperature raised to 50 °C, the addition of multi-walled carbon nanotubes (MWCNTs) to the external phase became necessary to increase the resin's viscosity and inhibit coalescence; otherwise, phase separation would occur. Nevertheless, some coalescence was still observed even with the incorporation of MWCNTs. The study also examined the compressive mechanical properties of the polyMIPEs, showing that the Young's modulus and crush strength of the samples could reach up to 0.3 MPa and 0.04 MPa, respectively. Steindl et al. [124] subsequently prepared another polyMIPE using a

calcium chloride dihydrate solution as the internal phase. The external phase primarily consisted of a resin containing DGEBA and diglycidyl ether of 1,4-butanediol, along with a crosslinker, cycloaliphatic isophorone diamine. The results indicated that the compressive Young's modulus could reach up to 193.3 MPa, while the crush strength could reach 6.4 MPa.

In conclusion, DGEBA can be used as the external phase in polyHIPE/MIPE; however, the literature to date primarily discusses its application in W/O emulsions. Additionally, these articles do not address the potential use of DGEBA's adhesive properties.

2.2.5.2 PolyHIPES/MIPES based on DES

DESs are binary or ternary mixtures that include at least one hydrogen bond donor and one hydrogen bond acceptor, which are tightly interconnected through hydrogen bonding interactions. A DES exhibits a melting point that is lower than that of each individual component [6, 171]. DESs have attracted widespread attention due to their advantages, including ease of preparation, low toxicity, thermal stability, low volatility, non-flammability, and biodegradability [172-174]. The exploration of DES began in 2001 when Abbott et al. [175] aimed to find alternatives that could address the moisture sensitivity of conventional ionic liquids. Their research tested various mixtures of quaternary ammonium and metal salts, ultimately identifying that a 1:2 molar ratio of choline chloride (ChCl) to zinc chloride exhibited the lowest melting point (23-25 °C). Following this, the same authors [176] further investigated eutectic mixtures of quaternary ammonium salts combined with hydrogen bond donors. They found that a 1:2 mixture of ChCl and urea produced a melting point as low as 12 °C. This remarkable decrease, in contrast to the melting points of pure ChCl (302 °C) and urea (133 °C), can be explained by the hydrogen bonding interactions that occur between urea molecules and chloride ions. Thereafter, various hydrogen bond donors and acceptors were

developed and investigated, with the most commonly studied DESs are typically based on ChCl and various hydrogen bond donors, including ethylene glycol, glycerol, amino acids, and imidazole, et al [173, 177, 178].

There are some studies that have explored the use of DES as the internal phase in polyHIPE. DESs consisting of ChCl and molecules with various functional groups [179-183], such as amides, carboxylic acids, and alcohols have been effectively used as internal phases in HIPEs. While acrylic monomers [179, 180, 184] such as methyl methacrylate, lauryl acrylate, and stearyl methacrylate, as well as styrene (cross-linked with divinylbenzene) [179, 181, 183, 185, 186], have been employed as the external phases. In terms of surfactants, Arlacel P135 [179], Span 60 [179, 181, 183, 185, 186], Cithrol [180, 184], pluronics [180] et al. have been employed. The viscosity of DES is one of the factors that affects the stability of HIPEs. The group of Mota-Morales prepared polyHIPEs based on different DESs [181]. The results showed that the HIPE based on the DES (1ChCl:2Urea) with the highest viscosity demonstrated the highest stability, characterized by minimal coalescence. In addition, the smaller pore size contributed to best mechanical performance of the polyHIPE.

The above studies indicate that DES can effectively serve as the internal phase of polyHIPEs; however, the ionic conductivities of DESs in these polyHIPEs have yet to be explored.

2.3 DPE fabricated using different methods

2.3.1 DPE fabricated via non-templating method

DPE can be prepared either in situ, where the liquid phase forms as part of the initial reaction mixture, or by post-filling, where the liquid phase is introduced into the solid phase after the porous solid phase has been prepared. Reaction-induced phase separation (RIPS) is a non-templating technique typically used to synthesize DPEs formed in situ.

In this method, the initial reaction mixture, which consists of a structure-forming precursor and a liquid electrolyte, is homogeneous. As the polymer starts forming, the compatibility of the different components within the mixture changes, causing them to separate into distinct regions. This results in the formation of a porous solid phase and a freely flowing liquid phase [187].

The properties of DPEs prepared using the RIPS method depend on the composition of the system [188-197]. In general, increasing the liquid phase content tends to enhance the ionic conductivity of the DPE but results in a reduction in Young's modulus. For example, Huang et al. [189] fabricated a DPE using epoxy resin (EP) as the solid phase and ionic liquid (IL) as the liquid phase. They observed that when the IL content increased from 30 wt.% to 50 wt.%, the ionic conductivity of the DPE increased from 10^{-7} S/m to 4.8×10^{-2} S/m, while the Young's modulus decreased from 1688 MPa to 40.52 MPa. Kwon et al. [195] found that as the IL content increased from 30 vol.% to 70 vol.%, the ionic conductivity of the DPE increased from 10^{-6} S/cm to 10^{-4} S/cm, while the Young's modulus decreased from 2 GPa to 40 MPa. The concentration of the liquid phase also impacts the properties of the DPE. Shirshova et al. [188] maintained a 1:1 mass ratio of EP to IL. The experiment revealed that as the concentration of lithium bis(trifluoromethane)sulfonimide (the main component of the IL) increased from 2.3 mol/L to 4.6 mol/L, the Young's modulus rose from 0.23 GPa to 0.51 GPa, but the ionic conductivity decreased from 2.82 mS/cm to 1.04 mS/cm. Adding reinforcement to DPE is an effective way to enhance DPE's performance [190, 192]. Dong et al. [190] found that adding 1.0 wt.% acidified short carbon fibres into the EP/IL system improved both the mechanical properties and ionic conductivity of the DPE. Compared to neat DPE, the Young's modulus of the DPE with 1.0 wt.% fibres increased from 0.52 GPa to 1.08 GPa, and the ionic conductivity rose from 3.14×10^{-2} mS/cm to 9.46×10^{-2} mS/cm. Feng et al. [192] added nano-silica into their DPE system and observed that as the nano-silica content

increased, the interconnectivity of the holes within the DPE structure improved. This enhancement in pore interconnectivity led to an increase in ionic conductivity, accompanied by a decrease in both tensile strength and tensile Young's modulus. Reaction conditions are another factor influencing the properties of DPEs [191, 198]. Quan et al. [191] found that adding room temperature curing into the curing cycle allowed a reduction in microstructural feature size through the suppression of the phase segregation. This reduction in the microstructural features resulted in a reduction in ionic conductivity and an increase in Young's modulus. Schneider et al. [198] prepared a DPE based on bisphenol A ethoxylate dimethacrylate and IL. They found that the UV-cured sample exhibited smaller pore size compared to the thermally cured sample. Both the UV-cured sample and thermally cured sample at 80 °C and 90 °C showed comparable storage modulus at room temperature, while the modulus of the thermally cured sample at 70 °C was lower than that of the other three samples. Additionally, different curing methods and curing temperatures did not significantly affect the ionic conductivity.

2.3.2 DPE fabricated via emulsion-templating method

The emulsion-templating method has been explained in detail in Section 2.2. Compared to RIPS, there are relatively fewer articles that use emulsion-templating method to prepare DPEs. Shirshova and her colleagues [15, 199] were the first to fabricate in-situ filled DPE using emulsion-templating method. They demonstrated the use of IL as the internal phase and lauryl methacrylate as the primary component of the external phase for polyHIPE fabrication. The study resulted in polyHIPE with high porosity level of 84%, and high ionic conductivity ranging from 4.0 to 9.0 mS/cm. Based on this work, researchers [153] from the same group modified the internal phase to increase the internal phase concentration and hence ion flux. They selected a mixture of ethylene carbonate and propylene carbonate as the alternative. This adjustment allowed the organic electrolyte concentration to be improved to 0.8 M, resulting in ionic conductivities of up to 8.90 ± 1.70

mS/cm. The studies successfully prepared in-situ filled DPEs. However, their focuses were primarily on the structure and ionic conductivity of the DPEs, with limited attention given to the mechanical properties. Xiao et al. [200] fabricated a water-in-chloroform gel using emulsion-templating method. The gel possessed an electrical conductivity of 348 μ S/cm. However, it is important to note that gel-state electrolytes often exhibit poor mechanical properties. The above mentioned DPEs are all in-situ filled. Several other polyHIPEs have also been used as DPEs; however, in these instances, it is necessary to remove the internal phase after solidifying the external phase and subsequently refill the porous structure with the desired liquid. This process results in material waste and prolongs the preparation time of the DPE. For example, Jha et al. [201] fabricated polyHIPEs based on trimethylolpropane triacrylate and trimethylolpropane tris(3-mercaptopropionate). After removing the internal phase and filling the polyHIPEs with IL, the resultant DPEs were used in SCs. The devices exhibited excellent capacitive behaviour with symmetric rectangular cyclic voltammograms (CV). The optimal device demonstrated a good energy density of 26.4 Wh/kg 61.1 kW/kg. Ma et al. [202] fabricated a porous material based on gelatin/ polypyrrole/ Ag using the emulsion-templating method. They subsequently filled the porous structure with a mixture of ammonium sulfate/ glycerol/water. The resultant conductive hydrogel exhibited an electrical conductivity of 1.21 S/m.

In this thesis, an in-situ filled DPE is fabricated using the emulsion-templating method. DGEBA is selected as the main component of the external phase in the emulsion, while the internal phase is DES. Our group has previously prepared a similar DPE [203]; however, the loss of ionic conductivity was significant. Furthermore, the study was very preliminary and lacked an in-depth analysis of the various factors influencing the properties of polyMIPEs. It also did not advance to fabricating the resulting polyMIPE into a film and exploring its application in SCs.

3 Experimental part

This chapter summarizes the properties of the raw materials used in this study, the preparation methods for DES and polyMIPE, and the characterization techniques for polyMIPE and SC. DGEBA is selected as the main component of the solid phase due to its good mechanical performance (Young's modulus: 1.6 GPa to 2.7 GPa [15-17]). The choice of crosslinking agent and the curing cycle for DGEBA are based on the successful experiences of previous researchers in the laboratory. Similarly, the selection of raw materials and synthesis methods for DES is informed by prior successful studies conducted in the lab. The choice of surfactant is critical for the successful preparation of polyMIPE. After extensive literature review and considering the available types of surfactants, four surfactants, as outlined in **Table 3- 2**, are ultimately selected for further investigation. In this chapter, the emulsion-templating method is used to synthesize polyMIPE. For the fabrication of SCs based on the polyMIPE developed in this research, two methods are employed depending on the type of electrode: one involves placing partially cured MIPE between two electrodes (CF mat), while the other method involves directly spraying the electrode (C or Ni spray) onto the polyMIPE. The properties of the polyMIPE, as well as the electrochemical performance of the SCs, are characterized using techniques such as SEM, compression testing, tensile testing, cyclic voltammetry (CV), and electrochemical impedance spectroscopy (EIS).

3.1 Materials

All chemicals used in this work and some of their properties are presented in **Table 3- 1** and **Table 3- 2**. All chemicals were used as received without purification.

Table 3- 1. chemicals used and their properties.

Name	Abbreviation	CAS number	Supplier	Form	Purity	Molecular weight (g/mol)	Density (g/cm ³)
Bisphenol A diglycidyl ether	DGEBA	1675-54-3	Merck	Viscous liquid	-	340.41	1.16
Trimethylolpropane triglycidyl ether	TMPTGE	3454-29-3	Merck	Viscous liquid	-	302.36	1.157
Isophorondiamine, mixture of cis and trans	IPDA	2855-13-2	Fisher scientific	Liquid	≥99%	170.30	0.9200
Choline chloride	ChCl	67-48-1	Merck	Crystals	≥98%	139.62	-
Ethylene glycol	EG	107-21-1	Fisher scientific	Liquid	99.5%	62.07	1.1130
Isopropanol	IPA	67-63-0	Merck	Liquid	99.5%	60.10	0.785

Table 3- 2. Summarization of the used surfactants and their important properties.

Surfactant	HLB ^[a]	Viscosity (mPa.s at 50°C)	Form	Density (g/ml)	Melting point (°C)	Ref. ^[b]
Hypermer B246-SO-(MV)	5-6	500-1000	Solid	0.94	Approximately 40	[204-206]
Atlox 4912 SF-SO-(MV)	5-6	1300	Solid	0.92-0.96	40-45	[207-209]
Cithrol DPHS-SO-(MV)	5.5	1300	Solid	0.92-0.96	40-45	[210-212]
Zephrym PD 2206-LQ-(AP)	4	-	Liquid	-	-	[207]

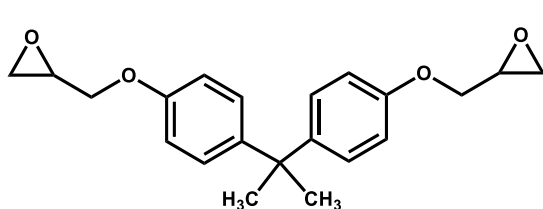
[a]: The values of HLB were obtained from the references.

[b]: The references here specifically indicate the source of the HLB value, while the remaining values are derived from the technical datasheets [213-216].

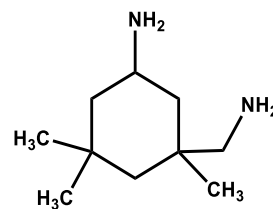
* The surfactants used in this study all exhibits an ABA structure in which B means the Polyethylene glycol (PEG) head and A means dipolyhydroxystearate (DPHS) tail [188].

*: All surfactants were kindly provided by CRODA and used as received.

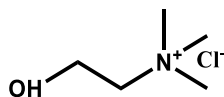
The following figure (**Figure 3- 1**) shows the chemical structures of the main materials.



DGEBA



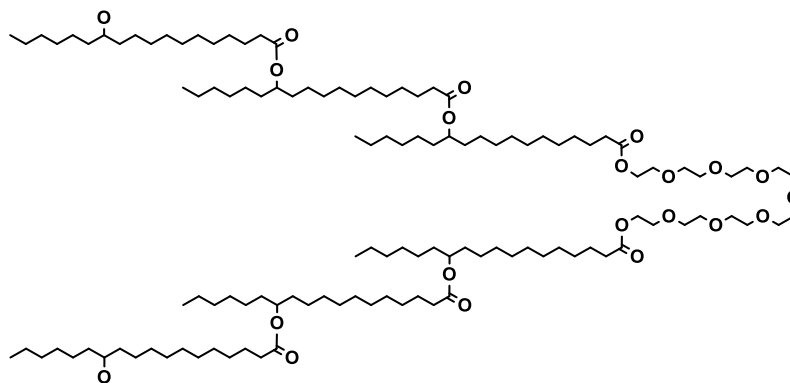
IPDA



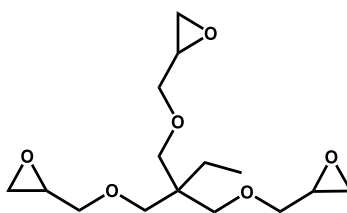
ChCl (hydrogen bond acceptor)



EG (hydrogen bond donor)



General structure of **PEG-DPHS** surfactants. (This a schematic diagram, the exact molecular weight of PEG and DPHS in commercial surfactants is not precisely known)



TMPTGE

Figure 3- 1. Structures of the chemicals used in this study.

The crosslinking mechanisms for DGEBA- IPDA and TMPTGE-IPDA are shown in **Figure 3- 2** [18]. The epoxy group (-C-O-C-) in DGEBA or TMPTGE undergoes a

reaction with the amino group (-NH₂). The reaction is initiated when the amino group attacks the carbon atom within the epoxy group, resulting in the opening of the epoxide ring. The opened epoxide ring subsequently forms a covalent bond with the amino group. Furthermore, the newly formed amino group (-NH-) can react with additional epoxy groups, leading to the development of a three-dimensional network structure. As the reaction progresses, more epoxy groups are consumed. Eventually, the resin completely cures into a solid material.

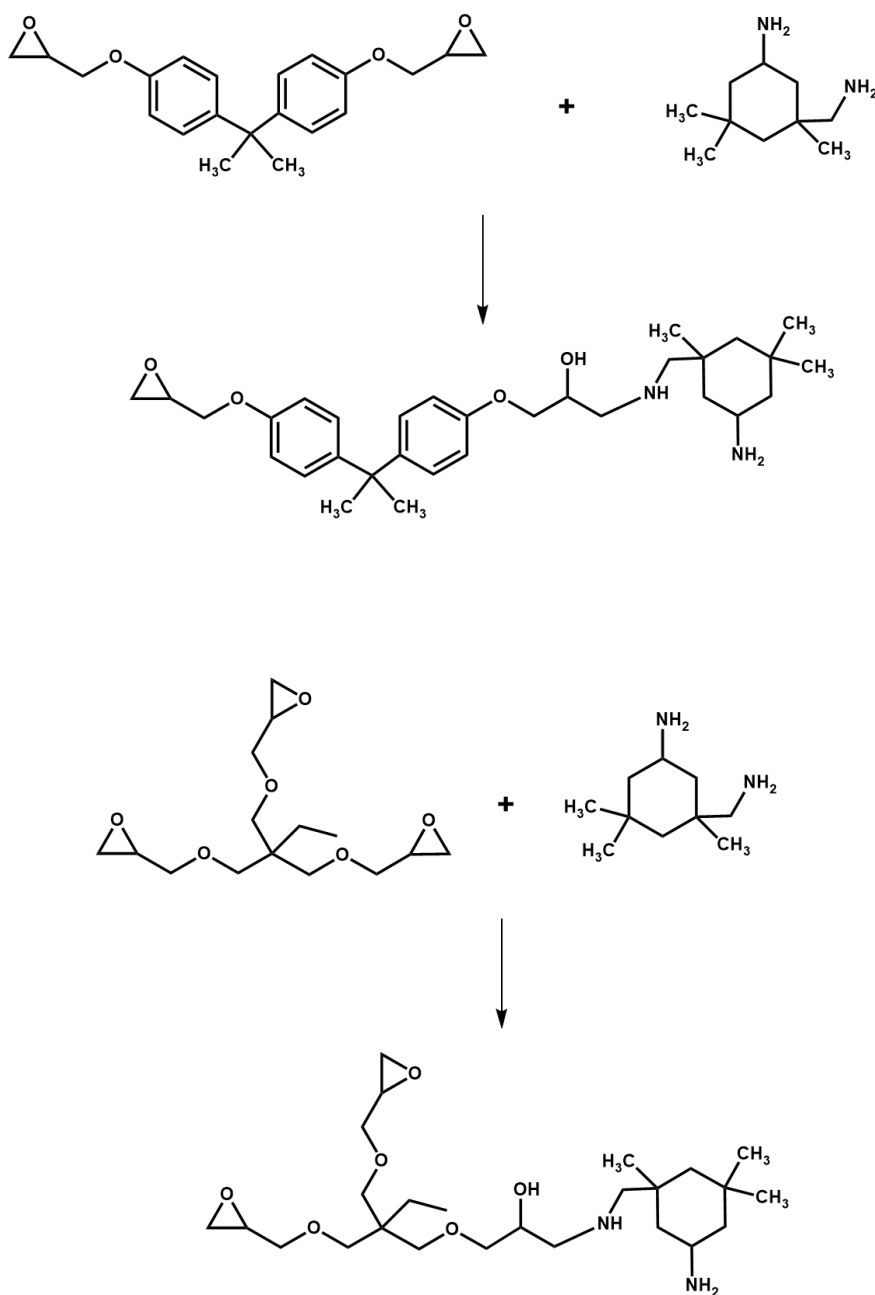


Figure 3- 2. Crosslinking mechanism for epoxy-amine materials.

3.2 Preparation of DES

The DES was synthesised by mixing ChCl and EG in a 1:3 molar ratio in the glass bottle with the screw cap and placing it at 80 °C and constant mixing using a magnetic stirrer for 2 hours, following the procedure described in the literatures: [217-219]. The ionic conductivity of the prepared DES is influenced by the reaction temperature and duration. Therefore, precise control of both these two conditions is essential during the experiments. The prepared DES was stored in a sealed container at room temperature and avoid exposure to light. The measured ionic conductivity of the formed DES was found to be 8.16 mS/cm (20°C), which was consistent with the value of 8.74 mS/cm (20°C) reported in the literature [217].

3.3 Preparation of bulk polyMIPE

MIPES were prepared in a glass reaction vessel equipped with a metal paddle rod connected to an overhead stirrer (IKA EuroStar 60 Control, IKA-Werke, Germany). The external phase was prepared as follows: the surfactant was dissolved in the hardener IPDA using magnetic stirrer, after a homogeneous solution was formed, the stoichiometric amount of epoxy (DGEBA and TMPTGE) was added. The mixture was stirred using an overhead stirrer at 400 rpm for 1 minute to achieve a solution. The DES was added to the external phase dropwise using a syringe pump (780100C, Cole-Parmer, USA), while maintaining the stirring speed at 500 rpm. After all the internal phase was added, the stirring speed was gradually increased to the required level over 30 s, and then maintained at this speed for 120 s to homogenise the emulsion further.

Subsequently, the prepared emulsions were transferred into a 50 ml polypropylene centrifuge for polymerisation. The MIPES are polymerised using the following curing cycle [191]:

(1) ramp to 60 °C at 2°C·min⁻¹;

- (2) hold at 60 °C for 1 h;
- (3) ramp to 80 °C at 3 °C·min⁻¹;
- (4) hold at 80 °C for 2 h;
- (5) cooled down to r.t.

The samples were then removed from the mould and post-cured:

- (1) ramp to 120 °C at 6 °C·min⁻¹;
- (2) hold at 120 °C for 2 h.

Samples were cooled in the oven (WF30, Lenton, UK) to r.t. before their removal.

The stoichiometric calculations were based on the following equations [220, 221]:

$$EEW = \frac{\text{Total weight of the epoxies}}{\frac{\text{Weight of DGEBA}}{EEW \text{ of DGEBA}} + \frac{\text{Weight of TMPTGE}}{EEW \text{ of TMPTGE}}} \quad (3-1)$$

$$AHEW = \frac{\text{Molecular weight of amine hardener}}{\text{Number of active hydrogens}} \quad (3-2)$$

$$phr = \frac{AHEW \times 100}{EEW} \quad (3-3)$$

where *EEW* (g/eq) is the epoxy equivalent weight, *AHEW* (g/eq) is the amine hydrogen equivalent weight and *phr* (per hundred resin) represents the quantity of amine hardener required to cure 100 g of epoxy resin.

3.4 Preparation of polyMIPE film

The method for preparing the emulsion follows the procedure described in Section 3.3. The film was produced using a transparency sheet as mould and a blade as tool in the fabrication process (**Figure 3- 3**). Firstly, create mould by cutting an opening measuring

7 cm in width and 18 cm in length on a transparency sheet (200 μm thick, Foshisy). Place this mould onto a second transparency sheet (100 μm thick, Uninkit), which served as the substrate. Next, put enough emulsion at the knife position indicated in the **Figure 3- 3**, and the knife was moved downward, ensuring that the edge of the knife remains in contact with the mould at all times. Once the knife reaches the end of the mould, both the knife and mould were removed, leaving behind an emulsion film with dimensions of 18 cm in length, 7 cm in width, and 200 μm in thickness on the substrate. The emulsion film together with the substrate was then placed into the oven for polymerisation, following the same curing cycle as for bulk polyMIPEs (see Section 3.3). The choice of substrate is crucial when fabricating the polyMIPE film. The adhesion between the substrate and the MIPE film should not be too weak, as this may lead to the shrinkage of the MIPE film. For example, using baking paper as the substrate results in such an issue. In addition, the adhesion between the substrate and MIPE film also should not be too strong, as this would make it difficult for the polyMIPE film to peel off from the substrate. This issue can occur when using a glass plate as the substrate.

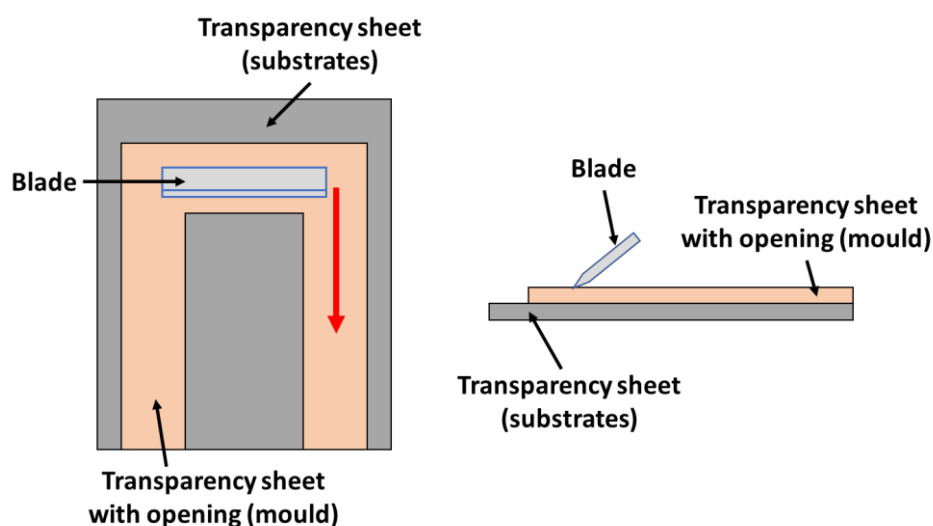


Figure 3- 3. Schematic diagram of film-making stencil (left: top view; right: side view).

3.5 Fabrication of SCs

In this study, various electrode, current collector, and adhesive materials were employed for the fabrication of SCs. The materials used for electrodes include carbon fibre mat (CF mat, CF-PW-210-100, Easycomposites, UK), Carbon spray (C spray, 838AR-340g, MG chemicals, UK), and Nickel spray (Ni spray, 841AR-340g, MG chemicals, UK), all with dimensions of 4 cm x 4 cm (for C spray and Ni spray, this indicates they were sprayed in an area of 4 cm x 4 cm). For the current collectors, Cu tape (AT526, 10 mm x 33 m x 35 μ m, Advance tapes, UK) and Al strip (30 cm x 3 m x 35 μ m, HTM Aluminum foil, China) were used, each cut into 1 cm x 6 cm strips using scissors. The adhesives included a polymer adhesive (the adhesive inherent to the Cu tape AT526) and Electrodag 502 ((Electrodag 502-30g, Agar scientific, UK). This section will provide a detailed description of the process for fabricating SCs using these materials.

Initially, Cu adhesive tape was used as the current collector, while CF mats were used as the electrode material. A Cu tape was first adhered to the edge of a CF mat and cured for 2 h at 130 °C in preparation for subsequent steps. Two CF mats with Cu tape are required to prepare one SC. The curing temperature and duration were determined based on the technical data sheet [222]. Subsequently, a MIPE film with a thickness of 200 μ m and dimension of 6 cm by 6 cm was cast onto the substrate and cured at 60 °C for 25 min. A curing time of less than 25 min will lead to the penetration of the CF mat through the MIPE film. The first CF mat with Cu tape was carefully placed onto the partially polymerised MIPE film and gently pressed. The substrate with the partially polymerised MIPE and CF mat was placed back into the oven for an additional 15 min curing. Afterwards, the partially polymerised MIPE film was peeled off from the substrate, and the second CF mat with Cu tape was placed on the opposite side of the film and pressed gently. Finally, the assembled components were placed into an oven for further curing,

following the curing cycle detailed in Section 3.3. The final polyMIPE film dimensions were 5 cm by 5 cm.

When Cu strip (the Cu strips were obtained by removing the polymer adhesive from the Cu tape using IPA) was used as the current collector, CF mat as the electrode, and Electrodag as the adhesive, it was unnecessary to adhere the current collector to the electrode in advance. Instead, a sandwich structure was prepared firstly, consisting of a layer of partial polymerised MIPE film sandwiched between two pieces of CF mats, following the method described above. After curing the MIPE, Electrodag 502 (0.2 g per CF mat) was used to attach two Cu strips to the respective CF mats.

When Al strip was used as the current collector, CF mat as the electrode, and Electrodag as the adhesive, the process for making SCs was similar to that using Cu strip as the current collector. The only difference was the substitution of the Cu strip with the Al strip. When Al was used as the current collector, the adhesive was always Electrodag. The type of adhesive will not be mentioned again in contexts where Al strip is used as the current collector.

When C spray was used as the electrode and Al strip as the current collector, the following procedure was followed: first, the method detailed in Section 3.4 was employed to prepare a polyMIPE film with dimensions of 5 cm in length and width, and a thickness of 200 μm . Subsequently, C spray was sprayed on both sides of the film with dimensions of 4 cm in length and width, respectively. When applying C spray, position the spray nozzle perpendicular to the polyMIPE film and spray from a height of 20 cm above the film for 5 s. Next, the C spray was cured by heating it at 65 °C for 30 min (according to the technical datasheet [223]). Once the curing process was complete, the two Al strips were adhered onto the corresponding electrodes using Electrodag 502 (0.2 g per CF mat). In addition to using as-synthesized polyMIPE film, sanded polyMIPE film was also used to

prepare SCs. After curing and peeling the polyMIPE film off the substrate, both sides of the polyMIPE film were lightly sanded by sandpaper, and a thin layer of DES was added to the polyMIPE surface to compensate for the loss of DES caused by the sanding. The SC was then fabricated using the same method as with the as-synthesized polyMIPE film. When Ni spray was used as the electrode and Al strip as the current collector, the steps for preparing the SC were the same as when using C spray as the electrode. Only the C spray was replaced with Ni spray in the process.

3.6 Characterization

The prepared bulk polyMIPE, approximately 12 cm in length and 2.5cm in diameter, were cut into 11 specimens (**Figure 3- 4**). Among these specimens, the heights of specimens 3,4,5,8 and 9 were 10mm; and the heights of specimens 1,2,6,7,10 and 11 were 3mm. The five specimens in 10mm height were selected for the compressive tests; the specimens 1,6 and 10 were used for the porosity and density test firstly, after removing the internal phase, these specimens then were used for the SEM characterization; the specimens 2,7 and 11 were selected for the ionic conductivity tests.

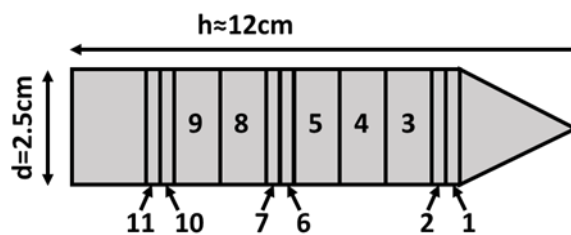


Figure 3- 4. Definition of specimens from the resulting polyMIPEs used for various characterizations. The specimens 3,4,5,8, and 9 were 10 mm in height and used for compression tests; the specimens 1,6, and 10 were 3 mm in height and used for porosity, density and SEM tests; the specimens 2, 7 and 11 were 3 mm in height and used for ionic conductivity tests.

To observe the pore structure of polyMIPE and measure its porosity, it is necessary to extract the internal phase from the polyMIPE. The extraction process was performed as follows: The samples were cut using a band saw and submerged in IPA firstly; To increase the rate of diffusion, the IPA was exchanged three times daily for a week. The completion

of the DES extraction was established using ionic conductivity measurements, as it is expected that the ionic conductivity of the IPA containing DES should be similar to the conductivity of neat IPA. Finally, the samples were dried in an oven at 100°C until reaching a constant weight.

3.6.1 Scanning electron microscopy

The morphology, pore size, and throat size of polyMIPes were determined by scanning electron microscopy (SEM). A Zeiss EVO 10 electron microscope (Zeiss EVO 10, Carl Zeiss, Germany) operating at 10 kV was used for the SEM analysis. A small piece of approximately 0.1 cm³ was broken from the middle of the sample and fixed on the sample stub using carbon cement. The specimen was then placed in a sputter coater (Cressington 108Auto, Cressington company, Watford, UK), where it was carbon sputtered in an argon atmosphere to assure the necessary conductivity. The thickness of the carbon coating was about 35 nm. Three samples taken from the bottom, middle and top of each polyMIPe were investigated and at least 300 pores/sample were measured using the software 'Image J' to determine the pore and throat size distribution. A statistic was introduced to compensate the non-perfect spherical pores (**Figure 3- 5**), with the calculation method referenced from Barbette and Cameron's work [224]. The statistic factor is calculated by $h^2 = R^2 - r^2$, where R is the equatorial diameter, r is the diameter measured on the SEM images and h is the distance from the centre of the sphere to the position where r is measured. The average probability value of h is R/2 and hence it could be obtained that $R/r = 2/\sqrt{3}$. A more accurate estimation of the actual pore diameter and interconnecting throat size can be achieved by multiplying the observed value by the statistic factor.

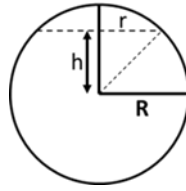


Figure 3- 5. Schematic of a pore in the polyMIPe.

The average diameter (D_{10}) and Sauter mean diameter (D_{32}) were calculated to evaluate the pore size and throat size distribution. The calculation formulas are as follows [225]:

$$D_{10} = \frac{\sum_{i=1}^n n_i D_i^1}{\sum_{i=1}^n n_i} \quad (3-4)$$

$$D_{32} = \frac{\sum_{i=1}^n n_i D_i^3}{\sum_{i=1}^n n_i D_i^2} \quad (3-5)$$

where D_i is the diameter of each pore and n_i is the number of pores with D_i diameter. The pore size distribution and throat size distribution were calculated using the ‘frequency count’ function in Origin software.

3.6.2 Porosity of polyMIPes

Porosity represents the volumetric fraction occupied by all pores within the porous polyMIPes. The porosity of the resulting polyMIPe monolith was determined according to the equation:

$$\varepsilon = \frac{\Delta m / \rho}{V_{sam}} \times 100\% \quad (3-6)$$

where ε is the porosity of the polyMIPe (%); Δm is the mass difference between the DES filled (wet) and dry samples (g); ρ is the density of the DES (g/ml); and V is the volume of the sample (ml).

3.6.3 Compression tests of bulk polyMIPEs

The compressive properties of bulk polyMIPEs were determined by compression tests. The compression tests were carried out using a universal Shimadzu machine (AGS-X Series, Shimadzu UK Limited, UK) with a 50 kN load cell. The tests were performed in accordance with the industrial standard ASTM D1621-10 [226]. Consistently, at least five samples were taken from the polyMIPE, which were 10mm in height and 25mm in diameter [125, 227]. The measurements of each sample were taken using a calliper (accuracy of ± 0.01 mm, Kynup, UK) before conducting the tests. The samples underwent loading at a speed of 1mm/min and the loading continued until a displacement of 20% the height of the sample was reached. The compressive Young's modulus was calculated based on the initial linear slope observed in the stress-strain plot. Because the yield point occurred after 10% deformation of the sample, the point at 10% deformation on the stress-strain plot was chosen to calculate the collapse strength.

3.6.4 Tension tests of polyMIPE films

The tensile properties of polyMIPE films were determined by tension tests. Tensile testing of the polyMIPE film, with dimensions 10mm x100 mm, was performed according to the standard ASTM D882 [228]. The tests were performed using a Lloyd machine (LR5KPlus, Lloyd Instruments/AMETEK, Inc., UK) equipped with a 500N load. The initial distance between grips was set as 50mm and the crosshead speed was fixed at 5mm/min. The Young's modulus was obtained from the initial linear part of the stress-strain curve. The tensile strength was determined by dividing the maximum force at the point of break by the cross-section area of the sample. The percentage elongation was evaluated by the difference in distance between the grips holding the film samples before and after the fracture. The toughness was determined by calculating the area under the stress-strain curve. At least five samples were assessed for each polyMIPE formulation.

3.6.5 Electrochemical impedance spectroscopy

The ionic conductivity (σ) of polyMIPE and equivalent series resistance (ESR) of SCs was determined by electrochemical impedance spectroscopy (EIS). The tests were performed using the VersaSTAT3 potentiostat (AMETEK scientific instrument, UK). To determine ionic conductivity of the bulk polyMIPEs and polyMIPE films, the samples were placed between two stainless steel electrodes, each with a diameter of 1 cm, for measurement. For bulk polyMIPEs (**Figure 3- 4**), the disc-shaped samples were cut from both the bottom, middle and top sections of the polyMIPE. For polyMIPE films (200 μm thick), at least three circular samples with a diameter of half inches were taken from each polyMIPE film for the test. Measurements were conducted at room temperature, covering a frequency range from 250 kHz to 0.5 Hz, with a sinusoidal voltage amplitude set at 5 mV. The calculation of ionic conductivity (σ) relied on sample dimensions and bulk resistance (R_b) (**Figure 3- 6**). The bulk resistance was derived from the high-frequency intercept of the impedance plot with the real axis. The ionic conductivity was calculated as follows:

$$\sigma = \frac{h}{A * R_b} \quad (3-7)$$

where σ is the ionic conductivity (S/cm), h is sample thickness (cm), R_b is the resistance (Ω), and A is the electrode area on the sample surface (cm^2).

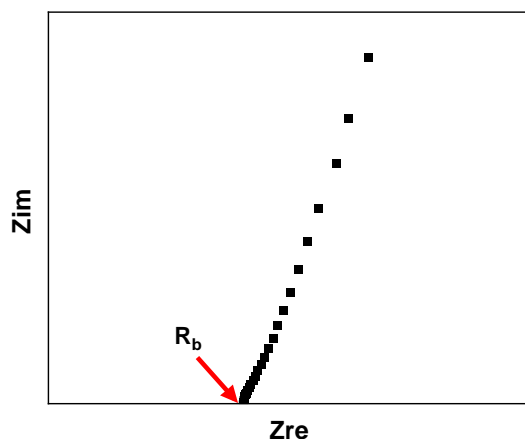


Figure 3- 6. Nyquist plot for bulk polyMIPE or polyMIPE film.

For SCs, the parameter settings align with those used for measuring the ionic conductivity of polyMIPEs. At least three measurements were conducted for each SC. In an ideal situation (**Figure 3- 7**), SCs exhibit a vertical response at low scan frequencies. As the frequency increases, the response gradually develops into a 45° angle, attributed to Warburg resistance due to ion diffusion/transport in the electrolyte. [229] The width of the 45° region increases with electrode thickness [230]. With further increases in frequency, a semi-circle is observed. The distance between the two intersection points of the semicircle and the real axis represents the charge transfer resistance (R_{ct}), which is associated with the electrode–electrolyte interface. R_{ct} includes both ionic resistance and electronic resistance. The ionic resistance is the resistance faced by ions (charge carriers). The electronic resistance arises from the electrode resistance and the contact resistance between the electrodes and the current collectors [231]. The intersection of the real axis with the Nyquist plot observed in the high-frequency region is often referred to as the ESR. It is believed to result from the combined resistances of the electrolyte resistance, electrode resistance, separator resistance, current collector resistance, contact resistance [230, 232].

This study primarily compares the ESR of SCs fabricated using different methods and materials. For different SCs, those with a smaller ESR are preferred, as the larger ESR leads to the reduction of discharge potential along with longer discharge time and consequently lower powder density [47].

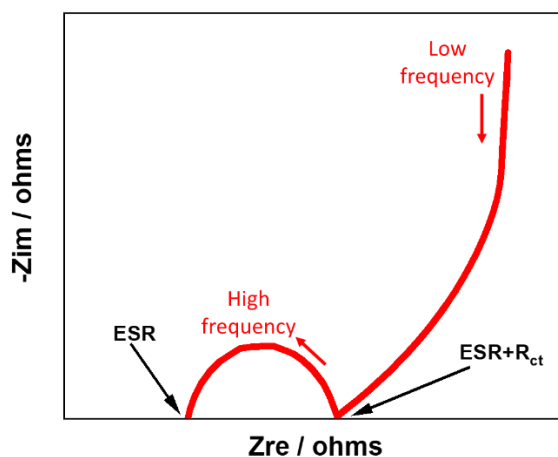


Figure 3- 7. Typical EDLC Nyquist plot. ESR refers to equivalent series resistance and R_{ct} refers to charge transfer resistance.

3.6.6 Cyclic voltammetry

The specific capacitance of SC was determined by cyclic voltammetry (CV). The CV tests were conducted using a VersaSTAT3 potentiostat (AMETEK scientific instrument, UK). The measurements were carried out within the potential window of (-0.1)- (0.8 V) at various scan rates ranging from 5 to 100 mV/s. At least three measurements were conducted for each SC. The specific capacitance was calculated from the CV curves using the following equations [230]:

$$C_s = \frac{\int IdV}{m\Delta V} \quad (3-8)$$

where C_s is the specific capacitance (F/g), I represents the current (A), V is the potential (V), m is the mass of the electrodes, v is the scan rate (V/s), and ΔV is the potential window (V).

In an ideal SC, where capacitance is defined as charge stored divided by voltage change, and current is the rate of change of charge with respect to time, a constant scan rate implies a constant current. Therefore, a rectangular CV response is anticipated (**Figure 3- 8a**).

However, SCs typically deviate from the ideal behaviour in practice, as illustrated in **Figure 3- 8b**. The internal resistance of real SCs contributes to the slight deformation of the CV curves. The higher the resistance of a SC, the more significant the shift of the CV charging-discharging corners towards the centre of the curve [230]. Another factor contributing to CV curve deformation is the inappropriate scan rate. At certain scan rates, the CV curve exhibits a rectangular shape, whereas at increased scan rates, the corners of the CV curve become rounded. This phenomenon results from rate-limiting processes, such as electrical transport limitations within the electrode or ionic transport limitations within the electrolyte. At increased scan rates, the formation of the interfacial double layer is hindered by these transport limitations, as there is insufficient time for its development [233].

Another non-ideal characteristic in real SCs is electrolyte degradation (**Figure 3- 8c**). All electrolytes possess a limited voltage stability window, exceeding which results in faradic reactions within the electrolyte. For instance, aqueous electrolytes typically have a maximum potential window of approximately 1 V. When the potential window is bigger than 1 V, water undergoes oxidation or reduction, producing oxygen and hydrogen, respectively. These reactions necessitate charge transfer across the electrode/electrolyte interface, resulting in an increase in current beyond that of the double-layer charging current. This additional current, denoted as I_{excess} in **Figure 3- 8c**.

In this study, the CV curves of the SCs are of the type shown in **Figure 3- 8b**. The primary comparison in this study focuses on the integrated area of the CV curves, with a larger integrated area corresponding to a higher capacitance. Moreover, the capacitance of the SCs is compared at different scan rates to evaluate the variation in capacitance under varying scan conditions. Capacitance indicates the ability of the SC to store charge at a given voltage. It reflects the SC's energy storage capacity, which is a critical factor for applications requiring efficient energy storage and delivery [43].

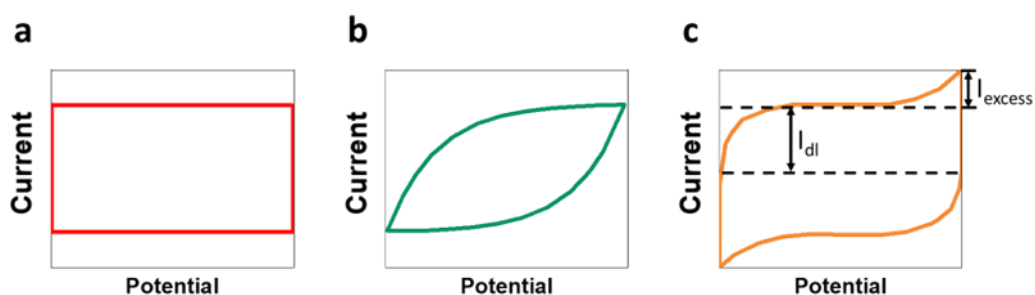


Figure 3- 8. CV responses of (a) ideal EDLC, (b) typical EDLC capacitor, and (c) EDLC capacitor involve side electrochemical reactions. The figures adapted from Ref.[230, 233].

4 The influence of emulsion formulation on various properties of polyMIPES

In the emulsion-templating method, the first and most researched emulsion type is the high internal phase emulsion (HIPE) in which the internal phase, constituting more than 74% of the volume. PolyHIPEs are porous polymers fabricated by polymerising the external phase of HIPEs. They exhibit many distinctive characteristics such as interconnected pore structure and low density (0.1 g/cm^3 [234]). Due to the attractive properties, polyHIPEs show the potential to be used in many applications. However, their actual industrial application is restricted primarily due to the inadequate mechanical properties. There are mainly three ways to improve the mechanical properties of polyHIPEs: firstly, introducing fillers or reinforcing agents such as particles and fibres into the emulsion system; secondly, increasing the external phase volume ratio to increase the resulting foam density, such as LIPE and MIPE; thirdly, altering the composition of the emulsion template to fabricate novel porous polymers with specific desired properties. In this study, dispersing fillers poses a challenge due to the viscous nature of the chosen external phase, DGEBA. Hence, MIPES are fabricated in this research to increase the foam density, which is expected to result in improved mechanical performance. LIPEs are not considered due to their tendency to result in porous polymers with closed pores, which would hinder the ion transport in the internal phase. Ensuring the interconnectivity of the resulting porous polymer is also a priority for the study. In this chapter, after identifying the suitable surfactant for fabricating DES-in-DGEBA polyMIPES, the influence of surfactant content, stirring speed, and internal phase addition rate on the morphological and physical properties of the polyMIPES are investigated. In this chapter, bulk polyMIPE is synthesized. The viscosity of DGEBA has minimal impact on the experimental process; however, its high viscosity makes it challenging to spread MIPE into a thin film. In

Chapter 6, the addition of a reactive diluent (TMPTGE) to reduce the viscosity of DGEBA will be explored.

4.1 Summary of sample formulations

Composition of all prepared samples with the synthesis parameters are presented in the

Table 4- 1.

Table 4- 1. Compositions of the studied emulsion templates.

Sample name	Surfactant content / vol.% ^[a]	DES addition rate / ml/min	Stirring speed / rpm	Surfactant
Cithrol DPHS	20	6	2000	Cithrol DPHS-SO-(MV)
Atlox 4912SF	20	6	2000	Atlox 4912 SF-SO-(MV)
Hypermer B246	20	6	2000	Hypermer B246-SO-(MV)
Zephrym PD 2206	20	6	2000	Zephrym PD 2206-LQ-(AP)
5% surf	5	6	2000	Cithrol DPHS-SO-(MV)
10% surf	10	6	2000	Cithrol DPHS-SO-(MV)
15% surf	15	6	2000	Cithrol DPHS-SO-(MV)
20% surf	20	6	2000	Cithrol DPHS-SO-(MV)
25% surf	25	6	2000	Cithrol DPHS-SO-(MV)
1ml/min	15	1	2000	Cithrol DPHS-SO-(MV)
2ml/min	15	2	2000	Cithrol DPHS-SO-(MV)
4ml/min	15	4	2000	Cithrol DPHS-SO-(MV)
6ml/min	15	6	2000	Cithrol DPHS-SO-(MV)
500rpm	15	6	500	Cithrol DPHS-SO-(MV)
1000rpm	15	6	1000	Cithrol DPHS-SO-(MV)
2000rpm	15	6	2000	Cithrol DPHS-SO-(MV)

[a]: Vol. based on the total volume of the external phase.

*The external phase consisted of DGEBA, IPDA and surfactant; and the internal phase consisted of DES.

*The volume fraction for the internal phase was 56 vol.%.

* The mole ratio of DGEBA to IPDA was fixed at 2:1.

4.2 The fabrication of polyMIPEs with different surfactants

The selection of a suitable surfactant plays a vital role in stabilising MIPE, particularly due to the enhanced mobility of internal phase droplets within MIPE as compared to HIPE [129]. Generally, surfactant molecules containing both lipophilic ‘tail’ and hydrophilic ‘head’ simultaneously, when the hydrophilic droplets dispersed in a lipophilic liquid, the ‘head’ will adsorb to the droplet’s surface whilst the ‘tails’ will extend from the surface to provide a steric repulsion [156, 235]. In this study, the external phase consisted primarily of DGEBA, while the internal phase was composed of DES, resulting in an oil-in-oil emulsion. The stabilization of this kind of system is always achieved by block copolymers (Section 2.2.4), with each phase having an affinity for one of the copolymer blocks. Four surfactants were studied to identify the most suitable option for stabilizing DES-in-DGEBA MIPE (Table 4- 2).

Table 4- 2. The properties of surfactants used in DES/DGEBA emulsion.

Surfactant	HLB	Viscosity (mPa.s at 50°C)	Form at RT ^[a]	Experimental result
Hypermer B246-SO-(MV)	6	500-1000	Solid	Porous polymer (not polyMIPE)
Atlox 4912SF-SO-(MV)	6	1300	Solid	PolyMIPE
Cithrol DPHS-SO-(MV)	5.5	1300	Solid	PolyMIPE
Zephrym PD 2206-LQ-(AP)	4	-	Viscous Liquid	Obvious phase separation

[a]: RT refers to room temperature.

*All the information was obtained from Croda International PLC datasheet or references (details are in Section 3.1). The types of the surfactants are all non-ionic ABA copolymer. A: PEG; B: DPHS.

*The structure of PEG and DPHS can be found in Section 3.1.

The surfactants used in this study are all ABA type polymeric surfactants with ‘tails’ (A) DPHS and ‘head’ (B) PEG. While PEG contains polar groups, DPHS is characterized by its long, nonpolar hydrocarbon chains. MIPEs without phase separation were formed when Atlox 4912SF or Cithrol DPHS-SO-(MV) were used as a surfactant, resulting in polyMIPEs with an open porous structure after curing (Figure 4- 1b and c). Use of

Hypermer B246-SO-(MV) resulted in a stable MIPE but resultant structure after curing did not exhibit conventional polyMIPE appearance (**Figure 4- 1a**). When using Zephyrym PD 2206-LQ-(AP) as the surfactant, it was not possible to form MIPE, as severe phase separation (**Figure 4- 1d**) occurred immediately after all the internal phase was added and the stirring was stopped. For Zephyrym PD 2206-LQ-(AP) and Hypermer B246-SO-(MV), changing the surfactant content, the internal phase addition rate, the stirring speed during emulsion homogenization process, and changing the internal phase ratio did not lead to the formation of the MIPE which produces the polyMIPE with interconnected porous structure.

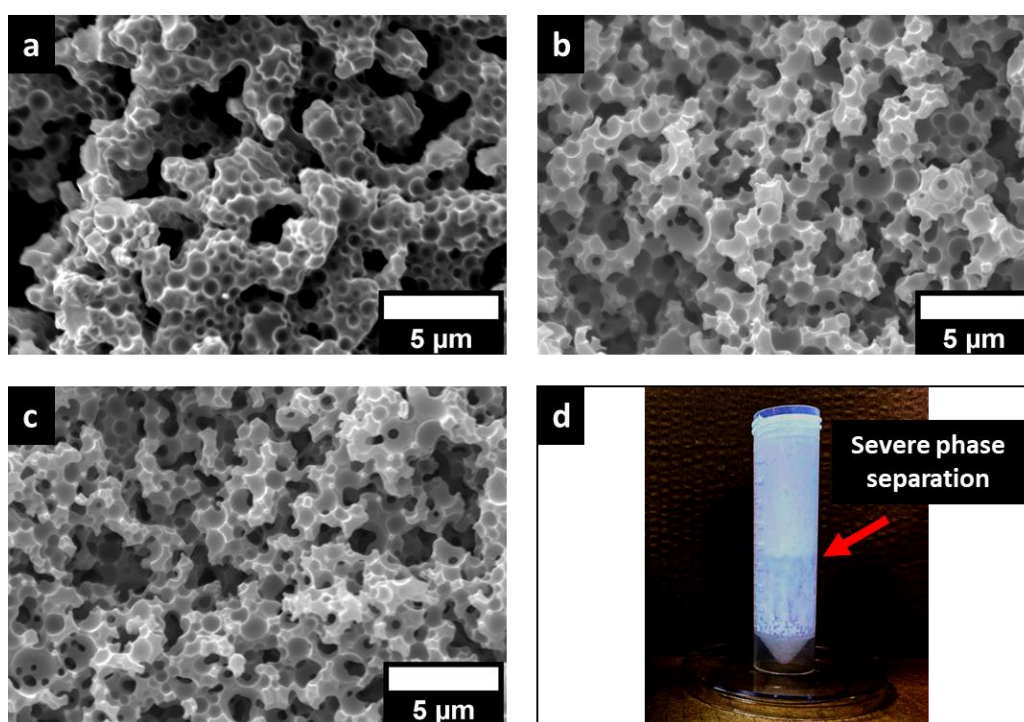


Figure 4- 1. The SEM image of polyMIPEs synthesized using (a) Hypermer B246; (b) Cithrol DPHS; (c) Atlox 4912SF, and the phase separation of (d) Zephyrym PD 2206. (Internal phase ratios - 56 vol.%; surfactant contents - 15 vol.%; DES addition rates - 6 ml/min; stirring speeds - 2000 rpm)

Results have shown that among the four studied polymeric surfactants, Zephyrym PD 2206-LQ-(AP) showed the lowest effectiveness. Through the comparison of the properties of the four surfactants presented in **Table 4- 2**, it is possible that the Zephyrym PD 2206 performance is due to the following factors: the comparatively lower HLB

and/or lower molecular weight. Studies have shown the presence of optimal values in both molecular weight and HLB, affecting crucial parameters such as adsorbed layer thickness and steric stabilisation [152, 236]. It was reported that even a difference of 1 in the HLB value can significantly influence the stability of the emulsion [207]. The HLB of Zephrym PD 2206-LQ-(AP) might be too low for stabilizing DES in DGEBA emulsion. However, it is important to note that this is an assumption and may not be entirely accurate, as some studies suggest that the stabilisation of non-aqueous emulsions is not necessarily related to the HLB of the surfactant [237]. The specific molecular weight of Zephrym PD 2206-LQ-(AP) is unavailable. However, the form of this surfactant is liquid at room temperature, differing from the other three surfactants. The form of a polymer is related to its molecular weight. Monomers with low molecular weight are typically a liquid or a gas. As polymerisation progresses, the chain length, molecular weight, and viscosity of the polymer increases. The resulting macromolecule transitions to a viscous liquid and eventually a solid [238]. In this study, the four surfactants are all composed of PEG and DPHS, with the primary difference being the varying chain length. Consequently, it is speculated that the molecular weight/chain length of Zephrym PD 2206-LQ-(AP) is lower than that of the other three surfactants. The decrease in molecular weight may be attributed to shorter 'head' part, which reduces the surfactant's adsorption ability on the internal phase droplet surface, or to shorter 'tails', which results in insufficient steric repulsion, or both. In any case, the surfactant's ability to stabilise the emulsion decreases. Some studies [239, 240] also suggest that polymeric surfactants should possess adequate molecular weight and chain length to ensure sufficient steric stability. The pore structure of sample Hypermer B246, which differs from that of typical polyMIPE, indicates that aggregation of internal phase occurred in the MIPE. Based on the information currently available, Hypermer B246-SO-(MV) and Atlox 4912-SO-(MV) exhibit similar properties, including the monomer comprising the 'head', the monomer comprising the 'tail', as well

as their HLB values. The difference is that Hypermer B246-SO-(MV) possess a lower viscosity (**Table 4- 2**). Similar to the analysis of Zephyrym PD 2206, the weaker emulsifying ability of Hypermer B246-SO-(MV) is likely related to the polymer's lower molecular weight/ shorter chain length.

The results indicate that out of the four surfactants studied, Atlox 4912 SF-SO-(MV) and Cithrol DPHS-SO-(MV) are the two surfactants suitable for producing DES-in-DGEBA polyMIPE with an interconnecting pore structure. Because the reserve of Cithrol DPHS-SO-(MV) in the laboratory was more sufficient, the subsequent research was based on this surfactant.

Another point to mention is that this study attempted to explore the effect of the internal phase ratio on the properties of the DPE by adjusting the internal phase ratio, specifically exploring ratios of 66 vol.% and 76 vol.%. However, severe phase separation consistently occurred, regardless of the surfactant used or the experimental parameters (DES addition rate, stirring speed, stirring period) adjusted. This phenomenon is attributed to the high viscosity of DGEBA (10-12 mPa.s at 25 °C), which hindered the effective dispersion of DES droplets. Steindl et al. [170] reported similar findings. In their preparation of a W/O polyHIPE, the external phase consisted of an epoxy system (EF80, which the main component is bisphenol-A (epichlorohydrin) and 1,6-hexanediol diglycidyl ether), multi-walled carbon nanotubes, and the surfactant Pluronic L-81. They found that the maximum achievable volume ratio of the internal aqueous phase (a calcium chloride dihydrate solution) was 70 vol.%. Increasing the internal phase ratio beyond this limit was hindered by the high viscosity (10-12 mPa.s at 25 °C) of the external phase. In Chapter 5, this study explores the addition of TMPTGE to reduce the viscosity of the external phase but does not investigate whether polyMIPE/HIPE with a higher internal phase ratio can be fabricated. If there is a specific need in the future, the method of adding TMPTGE could be further explored to determine if it is possible to increase the internal phase ratio.

4.3 The influence of surfactant content on the properties of polyMIPE

Surfactants play a critical role in emulsion fabrication by forming a continuous film around the internal phase. They act as a barrier between the two phases, thereby preventing or retarding coalescence of internal phase droplets and stabilizing the emulsion. In general, an increased surfactant content leads to reduced average pore size and more uniform pore size distribution [241]. However, to the best of my knowledge, there is limited exploration into the impact of surfactant content on the performance of polyMIPE, particularly concerning polyMIPE based on DGEBA and DES. This section aims to study this aspect.

In this study, the surfactant content was initially set in the range of 5 vol.% to 25 vol.%, based on the findings of a previous researcher in our lab. When the surfactant content was 5 vol.%, a stable MIPE could not be obtained. This could be attributed to the surfactant content being inadequate, resulting in insufficient coverage of the DES droplet surface by the surfactant molecules. As the surfactant content was increased to 10 vol.% and then 20 vol.%, microstructure typical for a conventional polyMIPE was observed (**Figure 4- 2a-f**). Further increase of the surfactant content to 25 vol.%, led to formation of the struts like structure (**Figure 4- 2g&h**). This may be due to damage occurring to the structure during the extraction of the internal phase and the subsequent drying process [98, 99, 242]. The following discussion will exclude the sample with 25 vol.% surfactant content. This is because, in addition to failing to achieve a typical polyMIPE structure, the mechanical performance of this porous polymer is also inadequate. The aim of this study is to develop a polyMIPE that combines good mechanical performance and ionic conductivity. However, the compressive Young's modulus and collapse strength of this sample are only 73.6 ± 6.2 MPa and 5.7 ± 0.1 MPa, respectively, which are significantly lower than those of the samples prepared with the other three surfactant contents.

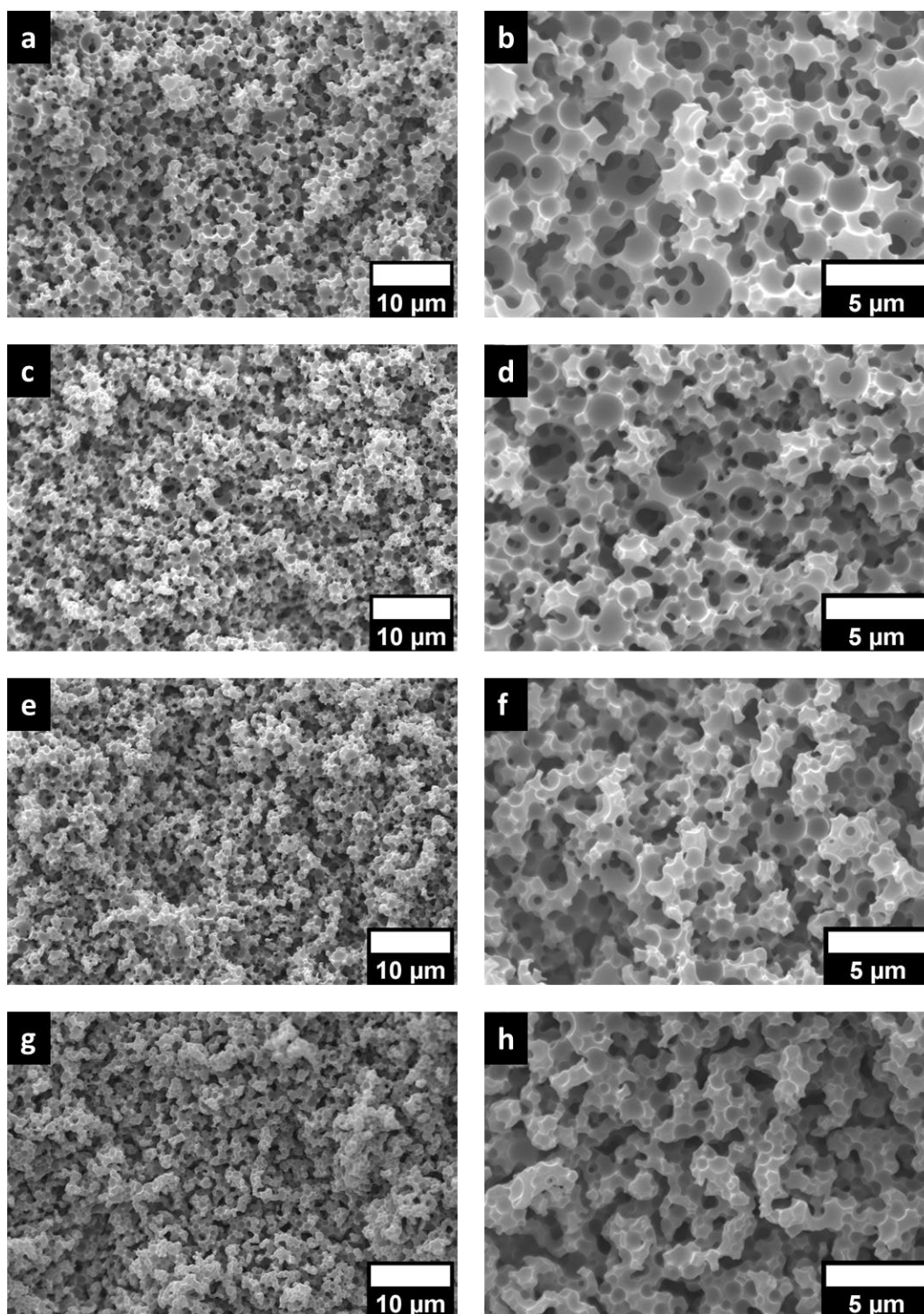


Figure 4- 2. The SEM images of polyMIPES based on different surfactant content at two magnifications. (a,b): 10 vol.% surfactant; (c,d): 15 vol.% surfactant; (e,f): 20 vol.% surfactant; (g,h): 25 vol.% surfactant. (Internal phase ratios - 56 vol.%; DES addition rates - 6 ml/min; stirring speeds - 2000 rpm; surfactant - Cithrol DPHS-SO-(MV).)

After polymerisation, the MIPES stabilized with 10 vol.% to 20 vol.% surfactant exhibited a white and non-chalky characteristic. The pore and pore throat size distribution of polyMIPES can be seen in **Figure 4- 3** and the average values are summarised in **Table**

4- 3. Regarding average sizes, the pore size and pore throat size both decreased with increasing the surfactant content. This phenomenon should be related to the coverage degree of surfactants on DES droplet surfaces. At lower surfactant content, the droplet surface may not be completely covered, resulting in droplet coalescence and the formation of larger pore sizes [243, 244]. As for pore size distribution and throat size distribution **Figure 4- 3**, all the pores are in the range of 0-4 μm . A 20 vol.% surfactant content resulted in the most uniform pore size, indicated by the smallest pore size distribution span. Conversely, a 10 vol.% surfactant content led to the widest pore size distribution. This phenomenon is also attributed to the increased tendency of DES droplets to coalesce at lower surfactant content. The throat sizes and size distributions exhibit a similar trend of change as the pores. This result is consistent with the findings of Dikici's study [204], where a polycaprolactone methacrylate-based polyMIPE was fabricated. In his work, the throat size exhibited the same pattern as the pore size, decreasing as the surfactant concentration increased.

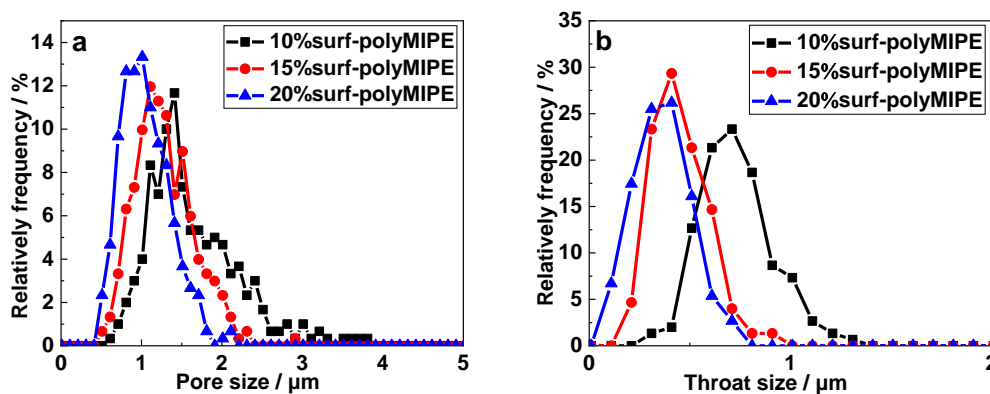


Figure 4- 3. The (a) pore size distribution and (b) throat size distribution of the polyMIPEs stabilised with different surfactant content. (Internal phase ratios - 56 vol.%; DES addition rates - 6 ml/min; stirring speeds - 2000 rpm; surfactant - Cithrol DPHS-SO-(MV).)

The surfactant content did not have a significant impact on the porosity of the resulting polyMIPEs (**Table 4- 3**). This suggests that, within the range of surfactant contents in this study, the amount of surfactant does not significantly impact the porosity. Furthermore,

since the porosity was determined by calculating the volume of DES extracted from polyMIPE, the DES within closed pores would not have been accounted for. Thus, the observed consistency in porosity, which closely aligned with the added internal phase (56 vol.%), suggests that nearly all pores in the synthesized PolyMIPes possess open-pore structures. The presence of these open-pore structures is crucial for the mobility of ions in the DES within the polyMIPE, thereby ensuring polyMIPE's ionic conductivity as a DPE.

Given that the aim of this study is to develop a DPE with simultaneously high mechanical (Young's modulus > 500 kPa [4]) and ionic conductivity (> 1 mS/cm [5]), the influence of surfactant content on the mechanical and ionic conductivity of the resulting polyMIPes was also investigated.

Table 4- 3. The effect of surfactant content on the properties of polyMIPes.

Sample	E ^[a] (MPa)	σ^{*} ^[a] (MPa)	Ionic conducti- vity (mS/cm)	D ₃₂ ^[b] (μ m)	D ₁₀ ^[b] (μ m)	Average throat diameter (μ m)	Poro- sity (%)
10% surf- polyMIPE	126.1 \pm 7.5	9.7 \pm 0.1	5.32 \pm 0.08	2.1	1.6 \pm 0.6	0.7 \pm 0.2	54.1 \pm 1.1
15% surf- polyMIPE	145.6 \pm 5.8	9.9 \pm 0.2	4.60 \pm 0.08	1.5	1.3 \pm 0.4	0.5 \pm 0.1	53.3 \pm 1.4
20% surf- polyMIPE	104.0 \pm 5.5	7.8 \pm 0.3	5.11 \pm 0.06	1.2	1.1 \pm 0.3	0.4 \pm 0.1	54.9 \pm 1.4

[a] E refers to compressive Young's modulus and σ^* refers to collapse strength.

[b] D₃₂ refers to Sauter mean diameter of pores and D₁₀ refers to average pore diameter.

*Internal phase ratios - 56 vol.%; DES addition rates - 6 ml/min; stirring speeds - 2000 rpm; surfactant - Cithrol DPHS-SO-(MV).

A summary of the effect of the surfactant content on mechanical properties is presented in **Table 4- 3** and **Figure 4- 4**. The complete strain-stress curves for porous polymers typically consists of three regions: the linear elasticity region, the plateau region and the densification region [129, 245]. Within the compression range of this study, the

densification region for the foam could not be observed as the sample was compressed by only 20% of its original height. However, the other two commonly observed regions for foams can be identified: the initial linear region and plateau region. The upward slope of the plateau region should be attributed to the combination of cell-wall bending and collapse [246].

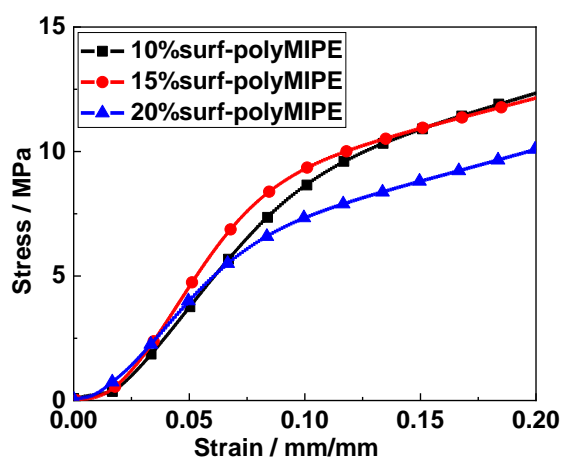


Figure 4- 4. Representative compressive stress-strain curves for polyMIPes produced through the polymerisation of emulsion templates with different surfactant contents. (Internal phase ratios - 56 vol.%; DES addition rates - 6 ml/min; stirring speeds - 2000 rpm; surfactant - Cithrol DPHS-SO-(MV).)

As the surfactant content increases from 10 vol.% to 20 vol.%, the Young's modulus of polyMIPE initially rises from 126.1 ± 7.5 MPa to 145.6 ± 5.8 MPa and subsequently decreases to 104.0 ± 5.5 MPa. Similarly, the collapse strength follows a trend of an initial increase followed by a decrease. At a surfactant content of 15 vol.%, the corresponding polyMIPE demonstrates the highest Young's modulus and collapse strength in the scope of this study. The observed results could be attributed to the influence of both pore morphology and the surfactant content in the polymerised external phase. Some publications [121, 170, 247, 248] have demonstrated that smaller pore sizes in porous materials correlate with higher mechanical properties. A smaller pore size results in more pores, facilitating the distribution of load across a greater number of sites. The improvement in mechanical properties can be attributed to this enhanced distribution of

load. In addition to considering the pore size of polymerised external, the crucial factor to consider is the presence of the internal phase maintained within the structure. While most studies typically remove the internal phase after producing polyHIPE/MIPE, this study retains the internal phase to achieve ionic conductivity. Gibson and Ashby [245] analysed the contribution of cell fluids to the strength of open-cell foam and propose an equation to illustrate the correlation:

$$\sigma_g^* = \frac{C\mu\dot{\epsilon}}{1-\epsilon} \left(\frac{L}{l}\right)^2 \quad (4-1)$$

where σ_g^* refers to the contribution of the fluid in pores to the strength of foam with open cells, C is a constant that contains all various constants of proportionality, μ is dynamic viscosity of the fluid, $\dot{\epsilon}$ is the strain rate, ϵ is strain, L refers to the length of the base of the porous foam, and l refers to the length of the pore edge. The equation implies that the contribution of pore fluid to the strength of open-cell foam is directly proportional to the strain rate and viscosity, and inversely proportional to the square of the cell size. DES was filled in the pores of polyMIPE in this study, serving a supportive role in the structure. This supporting effect is illustrated in **Figure 4- 5**, where the polyMIPE filled with DES exhibits higher Young's modulus and collapse strength compared to the polyMIPE without DES. According to the theory of Gibson and Ashby, the support provided by pore fluids to the porous material increases as the pore size decreases. In one word, it is believed that decreased pore size correlates with increased mechanical performance. Nevertheless, the surfactant present in the polymerised external phase exerts an opposing influence. The existence of surfactant within the polymer network may function as a plasticizer, disrupting the arrangement of polymer chains and compromising the mechanical performance [249-251]. In this study, the decrease in pore size correlates with a simultaneous increase in surfactant content within the external phase. These factors collectively impact the mechanical properties of polyMIPES. Notably, the ultimate

outcome reveals that when the surfactant content reaches 15 vol.%, Young's modulus and strength are maximized. This result is consistent with findings reported in some previous studies. For example, Steindl et al. [124] fabricated polyMIPEs using the mixture of DGEBA and diglycidyl ether of 1,4-butanediol (DGEBOH, reactive diluent) as the external phase. Their findings indicate that increasing surfactant content from 16 vol.% to 20 vol.% led to a decrease in the compressive Young's modulus from 193.3 ± 14 MPa to 71.8 ± 8.7 MPa, while the compressive strength dropped from 6.4 ± 0.2 MPa to 2.2 ± 0.3 MPa. This result aligns with the reduction in mechanical performance observed with similar surfactant content in this study. Rohm et al. [252] prepared polyHIPEs using Span-80 as the surfactant, it was found that the compressive Young's modulus initially increased from 98.7 ± 21.6 kPa to 151 ± 23.1 kPa, followed by a decrease to 16.7 ± 0.1 kPa as the surfactant content increased from 8 wt.% to 12 wt.% and then 16 wt.%. This variation in mechanical behaviour supports the situation observed in the present study. It is important to note, however, that in both examples, the mechanical performances were assessed after the removal of the internal phase, without accounting for the support provided by the internal phase.

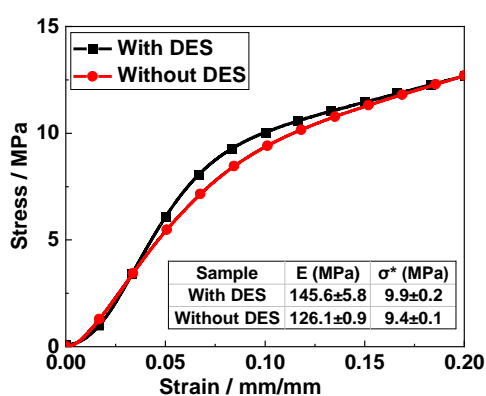


Figure 4- 5. Representative compressive stress-strain curves for polyMIPEs, one filled with DES (as-synthesized) and after DES extraction. (Internal phase ratios - 56 vol.%; DES addition rates - 6 ml/min; stirring speeds - 2000 rpm; surfactants - Cithrol DPHS-SO-(MV); surfactant content -15 vol.%)

The ionic conductivities of polyMIPEs found to be in the range from 4.52 to 5.40 mS/cm depending on the surfactant content, which is lower than that of neat DES (8.16 mS/cm). The reduction is attributed to the restricted ion movement within the tortuous channels of the porous polymer. Additionally, the trend in ionic conductivity as surfactant content increases differs from the trend observed in mechanical performance. As evident from **Table 4- 3** and **Figure 4- 6**, an increase in surfactant content led to an initial decline in ionic conductivity values, decreasing from 5.32 ± 0.08 mS/cm to 4.60 ± 0.08 mS/cm, followed by an increase to 5.11 ± 0.06 mS/cm.

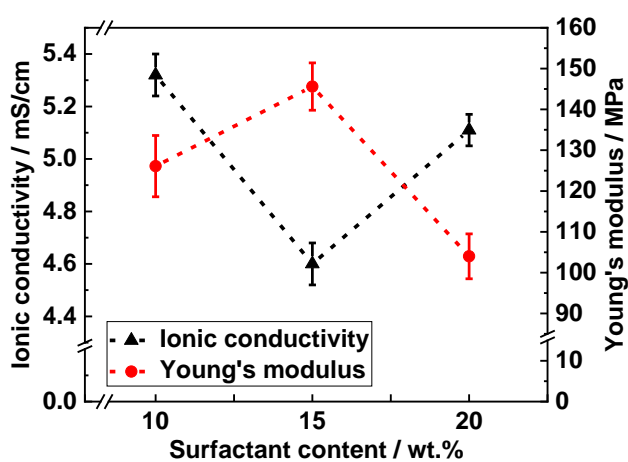


Figure 4- 6. The effect of the surfactant content used to stabilize the DES-in-DGEBA MIPE on the ionic conductivity and Young's modulus of produced in situ filled polyMIPEs. (Internal phase ratios - 56 vol.%; DES addition rates - 6 ml/min; stirring speeds - 2000 rpm; surfactant - Cithrol DPHS-SO-(MV).)

The observed trend is also related to both pore size and surfactant content in the external phase of polyMIPE. The increased ionic conductivity arises from enhanced ion mobility, closely associated with the composition [253, 254], interconnectivity [15, 255, 256], and tortuosity [257, 258] of the porous material. Specifically, increasing the proportion of the liquid phase in DPE enhances its ionic conductivity, whereas a higher proportion of the solid phase results in increased mechanical performance; the enhanced interconnectivity of pores promotes ion transport but negatively impacts mechanical performance; the decrease in pore size increases tortuosity of porous polymers, which hinders ion

movement, but the smaller pore size is beneficial to the material's mechanical performance. It can be noted that all these influencing factors have opposing effects on ionic conductivity and mechanical performance, leading to an inverse relationship between these two properties of polyMIPes. The proportion of DES remains consistently the same in this study. The interconnectivity of polyMIPe is associated with the ratio of throat size to pore size and the quantity of throats present on each pore [224, 259]. It can be seen from **Table 4- 3** and **Figure 4- 2** that the polyMIPes fabricated with different surfactant content exhibit comparable ratios of throat size to pore size and similar numbers of throats on each pore. Consequently, the interconnectivity remains relatively consistent across the different formulations. Tortuosity is another factor that affects ion mobility and is associated with interconnectivity [15], porosity [258], and pore size [260]. Since interconnectivity and porosity remain constant, the primary focus is on the impact of pore size. Tortuosity is defined as the ratio of the actual length through a porous structure to the Euclidean distance between the start and end points of that path [261]. Some studies have suggested that smaller pore sizes are associated with higher tortuosity [262-265]. In other words, smaller pore size associated with reduced ion mobility and lower ionic conductivity. At the same time, however, surfactant will also impact ion transport. Ion pairs present in the DES reduce the concentration of free charged species, thereby decreasing the ionic conductivity [266-268]. The oxygen atoms in the 'head' part of the surfactant PEG can form hydrogen bonds with the cation/anion in DES [269]. This interaction weakens the bond between the cation and anion in the ion pair, thereby enhancing ionic conductivity [270, 271]. In this study, the reduction in pore size hindered ion mobility, whereas the increased surfactant content facilitated enhanced ion movement. Due to the combined effects of these two mechanisms, the ionic conductivity exhibits an initial decrease followed by an increase with the increased surfactant content. Achieving both high mechanical properties (Young's modulus > 500 kPa [4]) and high ionic

conductivity (> 1 mS/cm [5]) simultaneously is challenging. In subsequent explorations, a surfactant content of 15 vol.% was chosen as it yielded the best compression performance among studied formulations. Ionic conductivity is as important as mechanical performance, samples with the highest ionic conductivity can also be considered if specific needs arise.

4.4 The influence of DES addition rate on the properties of polyMIPE

The impact of the internal phase (DES) addition rate on various properties of polyMIPE was investigated. It has been reported that increasing the addition rate of the internal phase leads to larger pore size in emulsions [272]. Therefore, to achieve pore structures that enhances the performance of polyMIPES in this study, it is essential to investigate the impact of the DES addition rate.

The DES addition rates studied were 1 ml/min, 2 ml/min, 4 ml/min and 6 ml/min. The maximum DES addition rate explored was 6 ml/min, aligning with the upper limit of the syringe pump used in this study. The minimum DES addition rate was 1 ml/min, at which point a stable MIPE cannot be obtained, as gross phase separation was observed during the addition of DES. One possible explanation for the instability of the emulsion could be the rise in viscosity. As the drop rate decreases, the time required to introduce all the DES into the system increases. This prolonged duration of the MIPE preparation results in an elevated crosslinking degree of DGEBA and IPDA, leading to an increase in system viscosity [273, 274]. At increased viscosity levels, the shear strength becomes insufficient to break up the DES into small droplets. Consequently, it becomes challenging to achieve a uniform and fine droplet size distribution in the emulsion [275, 276]. When the addition rate was 1 ml/min, the prolonged duration to add the internal phase resulted in the biggest viscosity. Even at the later stages of the DES addition process, DES became completely unable to enter the emulsion due to the viscosity. Increasing the stirring speed might enable the formation of a stable MIPE at a DES addition rate of 1 ml/min. However, this

hypothesis could not be tested, as the maximum speed of the overhead stirrer used in this study was limited to 2000 rpm. The SEM images of polyMIPEs fabricated at different DES addition rates are illustrated in **Figure 4- 7**. At addition rates of 2 ml/min, 4 ml/min and 6 ml/min, conventional polyMIPE structures are observed. The pore size of sample 2ml/min-polyMIPE appears to be larger, and the pore size distribution range is wider among studied formulations. This feature is also evident in the pore size distribution diagram in **Figure 4- 8**. It can be seen that the pore size distribution is widest when the DES addition rate was 2 ml/min. Although there are some variations in pore size distribution at DES addition rates of 4 ml/min and 6 ml/min, they are not significant. DES addition rate had less pronounced effect on throat size distribution, however, polyMIPE synthesized based on 6 ml/min is characterised by the narrower distribution range. The phenomenon could also be attributed to the change in viscosity during the DES addition process. The total times required to add all the DES at 4 ml/min and 6 ml/min are relatively similar - 8.25 min for 4 ml/min and 5.5 min for 6 ml/min. However, at a DES addition rate of 2 ml/min, the addition time increases significantly to 16.5 min. The increased DES addition time led to an increase in the viscosity of the system during the emulsion preparation process. Therefore, the 2 ml/min-polyMIPE exhibits the largest pore size, while the 6 ml/min-polyMIPE shows the smallest pore size. Additionally, given the smaller difference between 8.25 min and 5.5 min, the pore size difference between the 6 ml/min-polyMIPE and the 4 ml/min-polyMIPE is relatively small. Abbasian et al. [272] investigated the effect of internal phase addition rate on polyHIPEs based on styrene/DVB and found that a higher internal phase addition rate resulted in larger pore sizes. This finding is contrary to our observation which can be due to the difference in the viscosity change in two systems. In reported styrene/DVB system, the viscosity of the external phase does not increase significantly over a short period and can be considered negligible. Consequently, the primary factor affecting pore size is the insufficient time to

break up the internal phase droplets into smaller droplets at high addition rates. In our system, however, a higher internal phase addition rate indicates that the shear stress needs to overcome a lower external phase viscosity, which facilitates the breakup of internal phase droplets into smaller droplets.

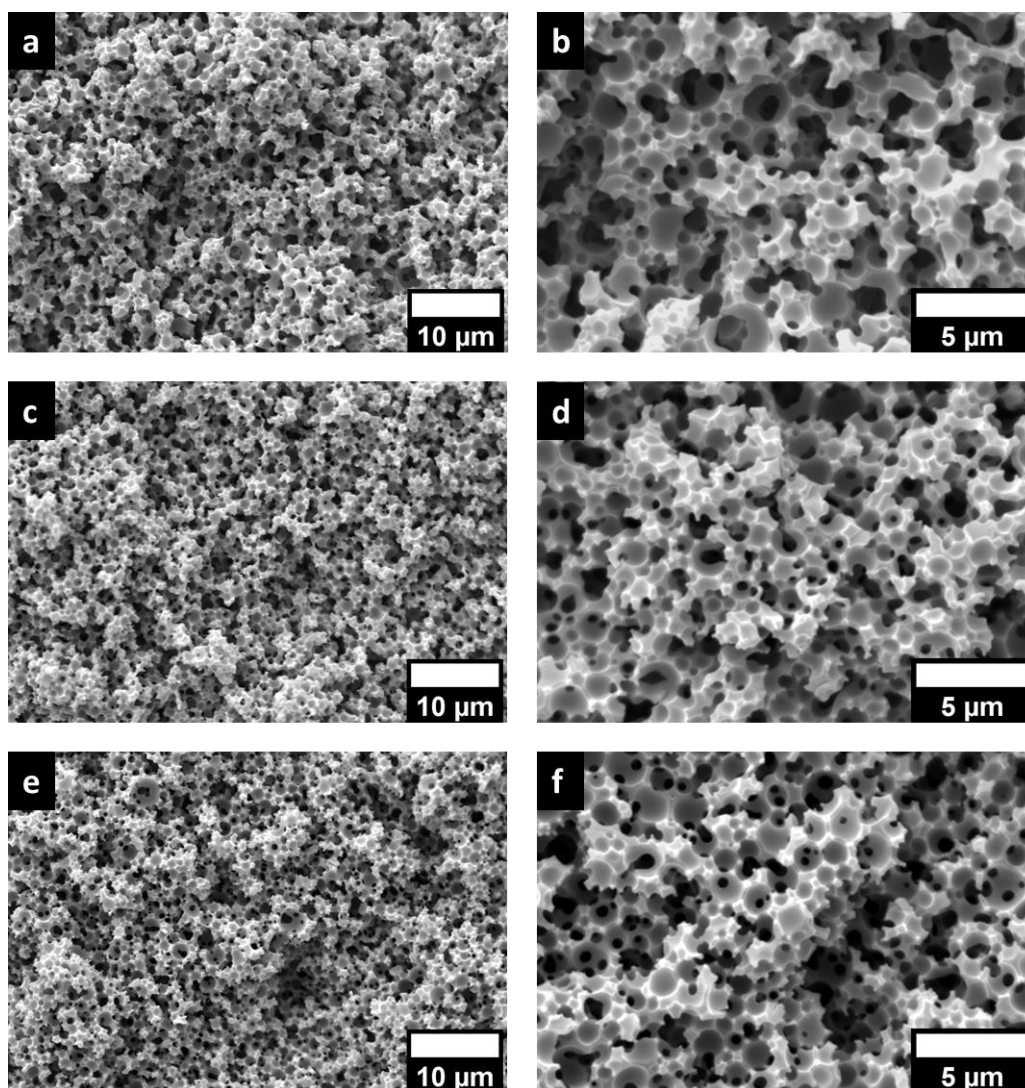


Figure 4- 7. The SEM images of polyMIPES fabricated with different DES addition rates at two magnifications. (a,b): 2ml/min; (c,d): 4ml/min; (e,f): 6ml/min. (Internal phase ratios - 56 vol.%; surfactant contents - 15 vol.%; stirring speeds - 2000 rpm; surfactant - Cithrol DPHS-SO-(MV).)

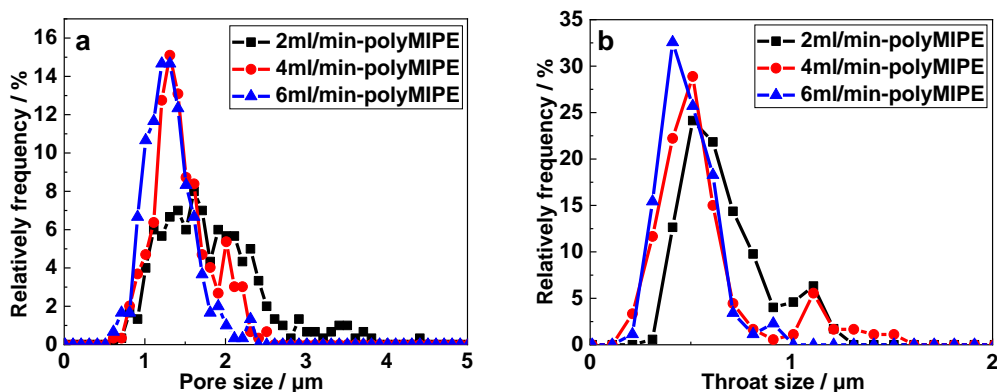


Figure 4- 8. The (a) pore size distribution and (b) throat size distribution of the polyMIPES fabricated with different DES addition rates. (Internal phase ratios - 56 vol.%; surfactant contents - 15 vol.%; stirring speeds - 2000 rpm; surfactant - Cithrol DPHS-SO-(MV).)

The properties and the compressive stress-strain curves of polyMIPES prepared with varying DES addition rates are presented in **Table 4- 4** and **Figure 4- 9**. Similar to polyMIPES fabricated with varying surfactant content, the samples produced with different rates of DES addition exhibited linear deformation regions and upward sloping plateau region. The Young's modulus of polyMIPES is observed to rise from 118.8 ± 4.1 MPa to 142.6 ± 4.2 MPa, and the collapse strength increases from 8.5 ± 0.1 MPa to 9.7 ± 0.2 MPa with increasing the DES addition rates (**Table 4- 4**). The linear elastic behaviour of cellular solids is commonly acknowledged to be correlated with intrinsic material properties and cell geometry [245]. The samples fabricated with different DES addition rates possess identical intrinsic material properties, as no modifications were made to the materials. Hence, the linear elastic behaviour was solely influenced by cell geometry. From **Table 4- 4**, it is evident that the pore size decreased with the increase in DES addition rate, a phenomenon associated with the decrease in system viscosity. When discussing the impact of surfactant content on the mechanical properties of polyMIPES in Section 4.3, the discussion includes the effect of pore size on mechanical properties of polyMIPES. Smaller pore sizes enhance the mechanical properties of porous materials even in the absence of a filled liquid. When filled with liquid, smaller pores provides more support to polyMIPES. The impact of pore size on mechanical properties of polyMIPES,

prepared with different DES addition rates, can be explained using the same theory as discussed in Section 4.3.

Table 4- 4. The effect of DES addition rate on the properties of the resultant polyMIPEs.

Sample	E ^[a] (MPa)	$\sigma^{*[a]}$ (Mpa)	Ionic conductivity (mS/cm)	D ₃₂ ^[b] (μm)	D ₁₀ ^[b] (μm)	Average throat diameter r (μm)	Porosity (%)
2ml/min-polyMIPE	118.8 \pm 4.1	8.5 \pm 0.1	5.15 \pm 0.07	2.3	1.8 \pm 0.6	0.7 \pm 0.2	53.8 \pm 1.2
4ml/min-polyMIPE	128.7 \pm 1.4	8.8 \pm 0.1	4.89 \pm 0.16	1.6	1.5 \pm 0.4	0.6 \pm 0.2	54.2 \pm 1.3
6ml/min-polyMIPE	142.6 \pm 4.2	9.7 \pm 0.2	4.53 \pm 0.21	1.5	1.3 \pm 0.3	0.5 \pm 0.1	55.9 \pm 0.5

[a] E refers to compressive Young's modulus and σ^* refers to collapse strength.

[b] D₃₂ refers to Sauter mean diameter of pores and D₁₀ refers to average pore diameter.

* Internal phase ratios - 56 vol.%; surfactant contents - 15 vol.%; stirring speeds - 2000 rpm; surfactant - Cithrol DPHS-SO-(MV).

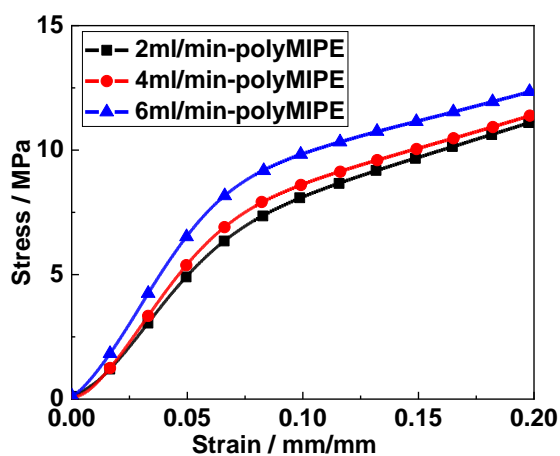


Figure 4- 9. Representative compressive stress-strain curves for polyMIPEs produced through the polymerisation of emulsion templates with different DES drop rates. (Internal phase ratios - 56 vol.%; surfactant contents - 15 vol.%; stirring speeds - 2000 rpm; surfactant - Cithrol DPHS-SO-(MV).)

The variations in ionic conductivity and Young's modulus with the DES addition rate are illustrated in **Figure 4- 10** and it shows the invert relationship between these two properties. With an increase in the DES addition rate, the ionic conductivity decreases from 5.15 \pm 0.07 mS/cm to 4.53 \pm 0.21 mS/cm. Similar to the change in mechanical

properties, variation in ionic conductivity is also associated with the morphology of polyMIPE. **Table 4- 4** indicates that polyMIPEs prepared at different DES addition rates exhibit the similar ratio of throat size to pore size. Additionally, as observed in **Figure 4- 7**, the number of throats contained in each pore is also comparable. Consequently, all polyMIPEs prepared with different DES addition rates display the same interconnectivity. The pore size is another factor that influences ion transport. The pathways for ion movement within porous materials become more tortuous when the pore size is smaller. Increased tortuosity can influence the movement of ions. The pore size of polyMIPE decreased with increasing the DES addition rate, resulting in increased tortuosity. This increase in tortuosity impeded ion movement, leading to a decrease in ion conductivity. The DES addition rate of 6 ml/min was selected for all further experiments, as the resulting polyMIPE exhibited the best mechanical properties.

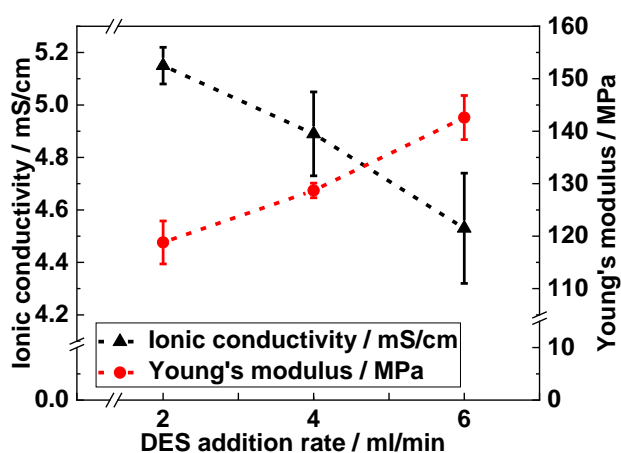


Figure 4- 10. The effect of the DES addition rate on the ionic conductivity and Young's modulus of produced in situ filled polyMIPEs. (Internal phase ratios - 56 vol.%; surfactant contents - 15 vol.%; stirring speeds - 2000 rpm; surfactant - Cithrol DPHS-SO-(MV).)

4.5 The influence of stirring speed on the properties of polyMIPE

When fabricating a polyMIPE, after incorporating the entire internal phase into the external phase under continuous stirring, the stirring speed is typically increased and maintained for a period to homogenize the emulsion. Indeed, the stirring speed has an

impact on shear stress, consequently influencing the droplet size in the emulsion [277]. Hence, the morphology of the polyMIPE is directly impacted. In this section, three stirring speeds, 500 rpm, 1000 rpm, and 2000 rpm were used to investigate the influence of stirring speed on the properties of polyMIPE. The morphology of the resulting polyMIPEs can be observed in the SEM images (**Figure 4- 11**). It is evident that the polyMIPEs fabricated with different stirring speeds exhibit interconnected pore structures with no noticeable difference in pore openness. This observation is further supported by the porosity measurements obtained by extracting the internal phase from the polyMIPEs, revealing comparable porosity values across all samples (**Table 4- 5**). **Figure 4- 12** illustrates the distribution of pore and pore throat sizes, with the pore size and throat size obtained from the SEM images. The pore sizes of the polyMIPEs synthesized at different stirring speeds fall within the range of 0-4 μm and the throat within the range of 0-1.2 μm . In addition, the pore size and throat size distributions of different polyMIPEs remain relatively consistent. It is well-known that an increase in stirring speed leads to higher shear stress, resulting in the formation of smaller droplets of the internal phase and consequently smaller pore sizes in the corresponding polyHIPE/MIPEs [272, 275, 278]. However, this is not the case in this study. The phenomenon might be attributed to the presence of the other mechanisms at play in this work. The DGEBA exhibits shear-thinning behaviour, signifying a decrease in viscosity with an increase in shear rate [279-281]. As the stirring speed increased, the viscosity of the external phase decreased, promoting the coalescence of droplets after stirring stops. The observation during the experiment that the emulsion formed at higher stirring speed had greater fluidity also supported this hypothesis. As the stirring speed increases, shear stress rises, resulting in smaller droplets. However, the decrease in viscosity leads to greater coalescence once stirring stops, causing the droplets to become larger. The combined effect of these factors leads to minimal change in the morphological properties of the polyMIPEs. Steindl et al.

[124] reported similar findings for W/O polyMIPEs prepared with a mixture of DGEBA, DGEBOH, and IPDA as the external phase. The authors did not observe a noticeable effect of stirring speed (400 rpm, 600 rpm, and 800 rpm) on the pore size and pore size distribution of the resulting polyMIPEs.

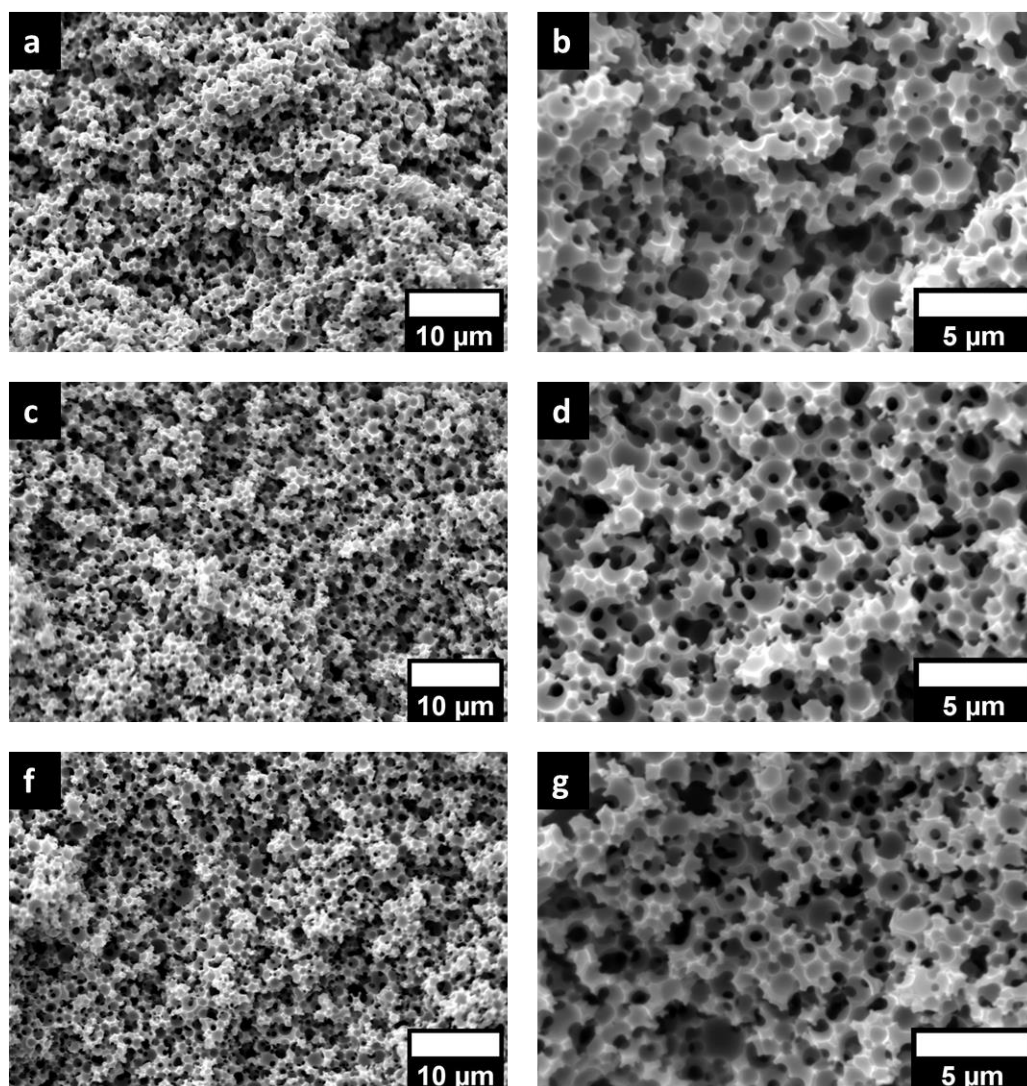


Figure 4- 11. The SEM images of polyMIPEs fabricated with different stirring speed at two magnifications. (a,b): 500rpm; (c,d): 1000rpm; (e,f): 2000rpm. (Internal phase ratios - 56 vol.%, DES addition rates - 6 ml/min, surfactants - Cithrol DPHS-SO-(MV), surfactant contents -15 vol.%)

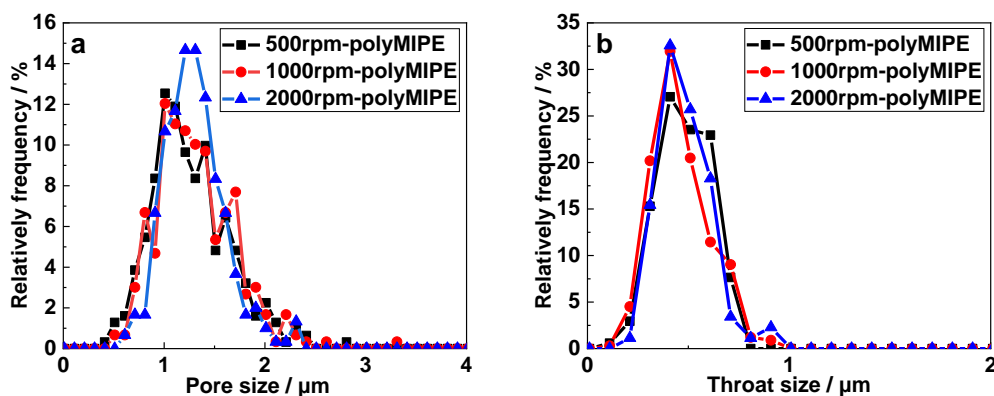


Figure 4- 12. The pore and pore throat size distribution of the polyMIPEs fabricated with different stirring speed. (Internal phase ratios - 56 vol.%, DES addition rates - 6 ml/min, surfactants - Cithrol DPHS-SO-(MV), surfactant contents -15 vol.%)

Change in the stirring speed did not lead to significant changes in the mechanical performance. The Young's modulus values (**Table 4- 5**) for polyMIPEs prepared at 500 rpm, 1000 rpm, and 2000 rpm are 138.8 ± 5.1 MPa, 137.0 ± 8.3 MPa, and 142.6 ± 4.2 MPa, respectively. The corresponding collapse strength values are 9.6 ± 0.2 MPa, 9.8 ± 0.3 MPa, and 9.7 ± 0.2 MPa, respectively. The differences are negligible. The shape of the strain-stress curves (**Figure 4- 13**) is also consistent across the samples. Ionic conductivity similarly exhibits limited sensitivity to changes in stirring speed. The similarity in mechanical properties and ionic conductivity of the resulting polyMIPEs can be attributed to their similar morphological properties and the consistency of their components. No discernible factors have been identified to induce changes in these properties.

Table 4- 5. The effect of stirring speed on the properties of the resultant polyMIPES.

Sample	E ^[a] (MPa)	σ^* ^[a] (Mpa)	Ionic conduc- tivity (mS/cm)	D32 ^[b] (μm)	D10 ^[b] (μm)	Average throat diameter (μm)	Poro- sity (%)
500rpm- polyMIPE	138.8 \pm 5.1	9.6 \pm 0.2	4.55 \pm 0.03	1.5	1.3 \pm 0.4	0.5 \pm 0.1	54.7 \pm 1.6
1000rpm- polyMIPE	137.0 \pm 8.3	9.8 \pm 0.3	4.67 \pm 0.13	1.6	1.3 \pm 0.4	0.5 \pm 0.1	54.9 \pm 0.4
2000rpm- polyMIPE	142.6 \pm 4.2	9.7 \pm 0.2	4.53 \pm 0.21	1.5	1.3 \pm 0.3	0.5 \pm 0.1	55.9 \pm 0.5

[a] E refers to compressive Young's modulus and σ^* refers to collapse strength.

[b] D₃₂ refers to Sauter mean diameter of pores and D₁₀ refers to average pore diameter.

* Internal phase ratios - 56 vol.%, DES addition rates - 6 ml/min, surfactants - Cithrol DPHS-SO-(MV), surfactant contents - 15 vol.%.

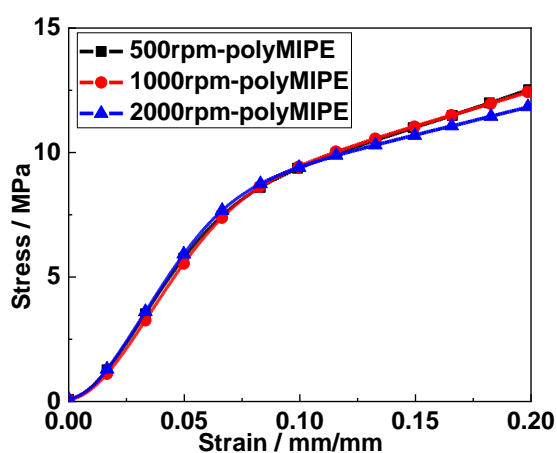


Figure 4- 13. Representative compressive stress-strain curves for polyMIPES produced through the polymerisation of emulsion templates with different stirring speed. (Internal phase ratios - 56 vol.%, DES addition rates - 6 ml/min, surfactants - Cithrol DPHS-SO-(MV), surfactant contents - 15 vol.%)

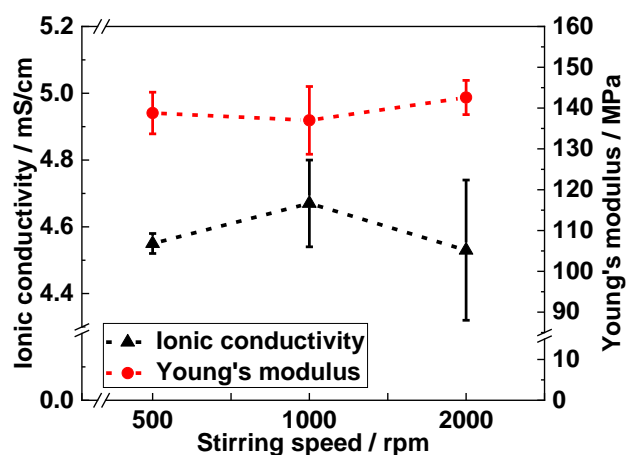


Figure 4- 14. Effect of the stirring speed on the ionic conductivity and Young's modulus of produced in situ filled polyMIPes. (Internal phase ratios - 56 vol.%, DES addition rates - 6 ml/min, surfactants - Cithrol DPHS-SO-(MV), surfactant contents -15 vol.%)

4.6 Summary

This chapter investigated the effects of surfactant type, surfactant content, internal phase addition rate, and stirring speed on various properties of polyMIPE, including morphological properties, compression properties, and ionic conductivity. Among the four surfactants investigated, it was found that the typical polyMIPE structure could be obtained using either Atlox 4912SF-SO-(MV) or Cithrol DPHS-SO-(MV) as the surfactant. Surfactant content is a critical factor influencing the properties of polyMIPE. It was observed that within the surfactant content range of 10 vol% to 20 vol%, the compressive mechanical performance initially increased and then decreased. The change in ionic conductivity as surfactant content increases was opposite to that of mechanical performance. The DES addition rate is also an important factor affecting the properties of polyMIPes. The compressive mechanical properties of polyMIPE increased with increasing the DES addition rate, while the ionic conductivity decreased. The morphological properties, compression mechanical properties and ionic conductivity of polyMIPE were all not affected by the stirring speed.

The above results show that the mechanical performance and ionic conductivity were inversely related. The best mechanical properties were observed with a surfactant content of 15 vol.% and DES addition rate at 6 ml/min. However, the highest ionic conductivities were observed with a surfactant content of 10 vol.% and DES addition rate at 2 ml/min. This study will continue under the conditions that yield optimal mechanical properties. Regarding stirring speed, as its variation did not impact the properties of polyMIPE, a speed of 1000 rpm was arbitrarily chosen from the three speeds investigated for further study.

5 The fabrication and characterization of polyMIPE films

In the previous chapter, the parameters for fabricating the bulk polyMIPEs have been investigated. However, in practical applications, DPEs are typically in the form of thin films, as thinner electrolyte is particularly advantageous for achieving lower ESR [47, 282-285]. The ESR represents the combined resistance of all resistive components within the SC. A smaller ESR is beneficial for faster charging and less power loss [286]. However, a challenge arose when attempting to produce a film from the MIPE formulation developed in Chapter 4, as the MIPE exhibits high viscosity, resulting in a non-uniform film. One factor contributing to the high viscosity of MIPE is the high viscosity of the external phase- DGEBA (10-12 mPa.s at 25 °C). One of the approaches to reduce the viscosity of the resulting MIPEs is by incorporating diluents into the epoxy resin. The diluent type used in this study was reactive diluent. Reactive diluents can chemically bind to the epoxy and become a part of the network [287]. They are generally low-viscosity compounds (4-6 mPa.s at 25 °C [220]) with multiple reactive functionalities that exhibit good compatibility with epoxy resin [288, 289]. The reason for not using non-reactive diluent is that these diluents do not participate in the cross-linking reaction with epoxy [287]. The position of the non-reactive diluents in the MIPE is uncertain due to their lack of participation in the reaction. They may reside in the external phase of the MIPE or migrate into the internal phase as the polymerisation progresses, raising concerns about their potential impact on the performance of polyMIPE, whether in terms of mechanical property or ionic conductivity.

In this study, TMPTGE is chosen as the reactive diluent mainly because TMPTGE is a tri-functional aliphatic epoxy and exhibits a higher cross-linking density compared to di-functional and mono-functional aliphatic epoxies. This increased crosslinking density benefits properties of the cured external phase in polyMIPE, such as the glass transition temperature and flexural strength, within a certain range of TMPTGE addition [290].

Beyond its influence on the viscosity of MIPes, the incorporation of TMPTGE is expected to enhance the ionic conductivity and mechanical properties of polyMIPes, thereby improving their performance in energy storage applications. This chapter investigates the impact of TMPTGE on the viscosity of the MIPes, as well as its effects on the mechanical properties and ionic conductivities of polyMIPes, offering valuable insights for the future design of high-performance DPE in SCs.

5.1 Summary of sample formulations

The MIPE compositions for bulk and polyMIPE films prepared in this chapter are summarised in **Table 5- 1**.

Table 5- 1. Compositions of the studied emulsion templates.

Sample name		TMPTGE content / wt.% [a]	DGEBA /g	TMPTGE /g	IPDA /g [b]
0%	TMPTGE-bulk	0	19.45	0.00	4.76
5%		5	18.48	0.97	4.81
10%		10	17.51	1.95	4.85
15%		15	16.53	2.92	4.90
20%		20	15.56	3.89	4.94
0%	TMPTGE-film	0	19.45	0.00	4.76
2.5%		2.5	18.97	0.49	4.78
5.0%		5.0	18.48	0.97	4.81
7.5%		7.5	17.99	1.46	4.78
10.0%		10.0	17.51	1.95	4.85

[a] weight based on the total weight of DGEBA and TMPTGE.

[b] the masses of IPDA were calculated based on the phr values.

*The external phase consisted of DGEBA, IPDA, TMPTGE and surfactant; and the internal phase consisted of DES.

*The volume fraction of the internal phase was 56 vol.%. The stirring speed - 1000 rpm, DES addition rate - 6ml/min, surfactant (Cithrol DPHS-SO-(MV)) content - 15 vol.%.

5.2 The effect of TMPTGE addition on properties of bulk polyMIPes

This section mainly discusses the impact of TMPTGE addition on MIPE viscosity, as well as on the properties of bulk polyMIPE, including its morphological properties,

mechanical properties, and ionic conductivity. The ability of TMPTGE to reduce the viscosity of DGEBA has been reported in the literature [287, 290, 291]. However, the reported systems do not include emulsions, leaving it unknown whether the reduction in viscosity of TMPTGE-DGEBA blends will have an impact when used as the external phase in MIPE. Therefore, the first task was to determine whether the addition of TMPTGE affects the viscosity of DES-in-DGEBA MIPE. Two challenges arose when attempting to measure the viscosity of the MIPE. Firstly, due to DGEBA's propensity for rapid polymerisation, the MIPE's fluidity diminished significantly within approximately 30 minutes of preparation. Consequently, viscosity testing must be immediately conducted following MIPE preparation. However, due to the absence of a viscosity testing machine (viscometer or rheometer) in the laboratory, it was necessary to transfer the MIPE to an alternative location for measurement. The transfer process makes it impossible to measure the MIPE viscosity accurately. Secondly, the MIPE synthesized in this study exhibits a tendency to adhere to surfaces, posing a risk of instrument damage during testing. Hence, an alternative approach was proposed for evaluating the viscosity of the resultant MIPES. It is well-known that viscosity denotes obstruction to flow. Fluidity, conversely, is defined as the reciprocal of viscosity, indicating the degree of ease of flow [292-294]. Therefore, in this study, the fluidity of the MIPE was used to characterize its viscosity. After the MIPE preparation was completed, 2 ml of the MIPE was immediately injected onto a specific position (between '35' and '45' on the tube scale) of the centrifuge tube using a syringe. During the injecting process, ensure that the centrifuge tube is placed horizontally. The tube was then stood upright, allowing the MIPE to flow under gravity. The change in viscosity after adding TMPTGE was analysed by observing the MIPE's different flow states. Under identical gravitational forces, a greater flow rate correlates with a lower viscosity of the MIPE. The flow behaviour of MIPES with different TMPTGE contents is shown in **Figure 5- 1**. It is evident that the

MIPE with 0 wt.% TMPTGE exhibits the slowest flow rate. Beyond 40 second, all other MIPEs flowed below the mark '15' (red line), with only the MIPE with 0 wt.% TMPTGE remaining above. Furthermore, by observing the situation at the 20 second, it becomes evident that the flow rate of the MIPE increases with the increase of TMPTGE content. However, it is important to note that this change does not follow a linear pattern. Specifically, when the TMPTGE content is 5 wt.%, a notable increase in flow rate is observed; nevertheless, as the TMPTGE content continues to rise to 10 wt.% and beyond, the increase rate in flow rate decreases. This phenomenon aligns with findings in the literature regarding the effects of various reactive diluents- such as TMPTGE[287], Glycidylether C₁₂-C₁₄ alcohol [287], hexanediol diglycidylether [287], polyepoxide cardanol glycidyl ether [291], cardanol glycidyl ether [291], C₁₂-C₁₄ alkyl glycidyl ether [295], butyl glycidyl ether [295], and 1,4-butanediol diglycidyl ether [295]- on the viscosity of DGEBA. Specifically, the viscosity of DGEBA-reactive diluent mixture does not decrease linearly with increasing diluent content. Instead, viscosity decreases rapidly at low diluent content, while the rate of decrease slows as the diluent content increases. This phenomenon can be explained by the concept of critical entanglement concentration. Once the polymer viscosity reaches a critical point where chain entanglements begin, there is a notable increase in viscosity as the polymer concentration rises [204]. Although this study explores the effect of TMPTGE addition on MIPE, the observed viscosity change pattern observed is similar to that reported in the literature regarding the impact of TMPTGE on the viscosity of DGEBA-TMPTGE mixtures [287]. The introduction of DES droplets did not alter this viscosity change pattern.

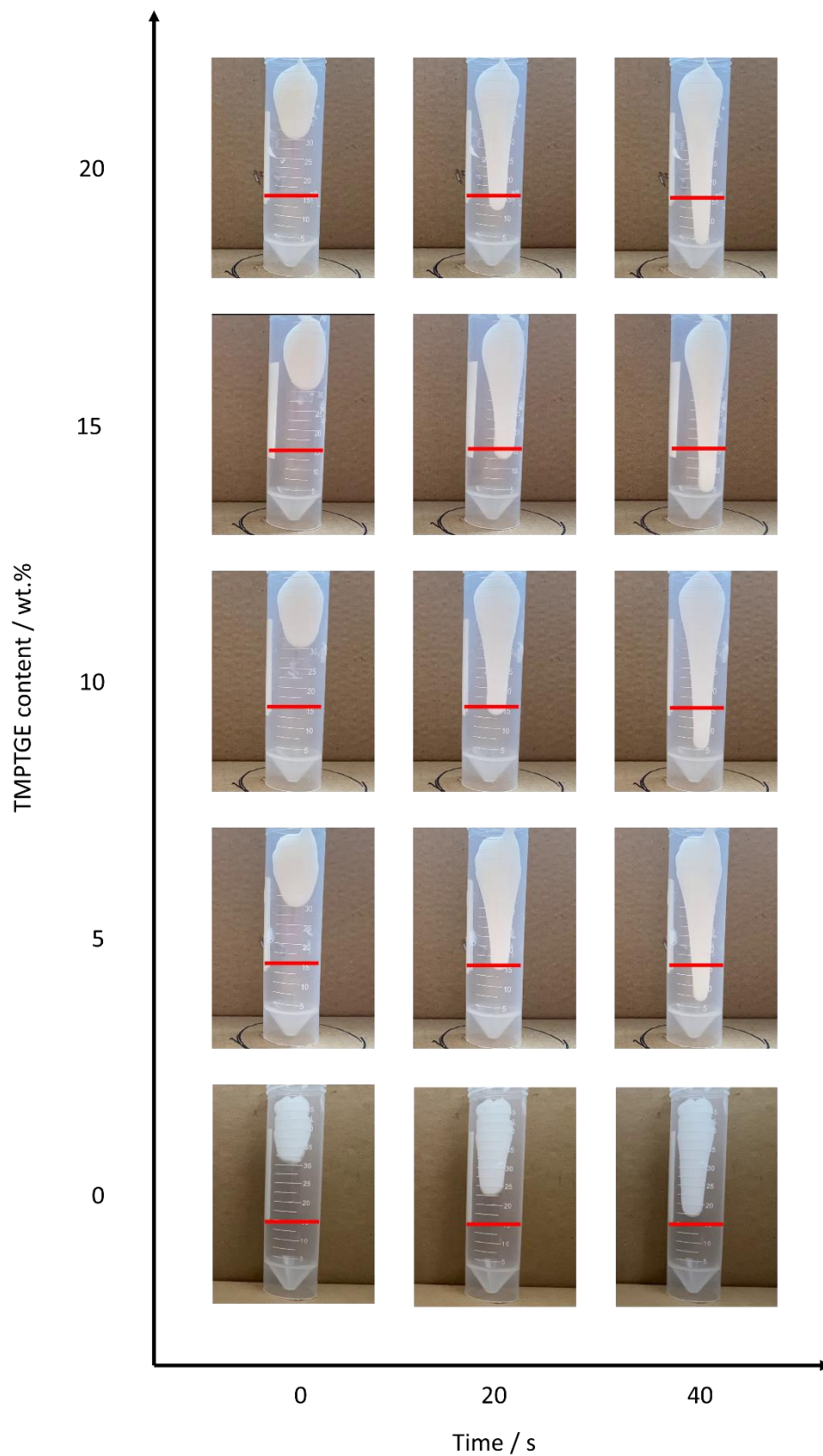


Figure 5- 1. The effect of TMPTGE addition on fluidity of the resultant MIPes. The red line in the picture indicates the same scale '15' of the centrifuge tubes. (internal phase ratios - 56 vol.%, DES addition rates - 6 ml/min, stirring speeds - 1000 rpm, surfactants - Cithrol DPHS-SO-(MV), the surfactant contents - 15 vol.%)

The influence of TMPTGE addition on the morphology of the resulting polyMIPes was also explored. **Figure 5- 2** illustrates the SEM images of polyMIPes synthesised with varying TMPTGE content. As can be seen from the images, all the polyMIPes exhibit an open-cellular structure with interconnected pores. The specific distribution of pore size and throat size are presented in **Figure 5- 3**. It is observed that the addition of TMPTGE and variations in its content within the studied range did not significantly affect the pore size and throat size distributions of the resulting polyMIPes. Moreover, the pore size and throat size remained relatively constant (**Table 5- 2**), measuring 1.3-1.5 μm and 0.5 μm , respectively. The unchanged pore structure may be attributed to the effect of TMPTGE on the viscosity of DGEBA. The addition of TMPTGE reduced DGEBA's viscosity, which facilitated the breakup of DES droplets into smaller sizes [106, 170, 296]. However, this viscosity reduction also decreased the external phase's ability to prevent DES droplet coalescence. Consequently, after stirring was stopped, the DES droplets were more prone to coalescing into larger droplets [277, 297]. Under the combined influence of these two factors, the pore structure of the polyMIPes showed little variation. It is worth noting that Dhavalikar et al. [277, 298] obtained results that differ from those in this study. They investigated the effect of the addition of the reactive diluent 1,4-butanedithiol on the properties of neopentyl glycol diacrylate-based polyHIPes. Their results indicated that, the pore size of the polyHIPes increased with the content of the reactive diluent in the studied range (0- 30 mol.%). The authors attributed the observed relationship to the decreased viscosity of the external phase, which facilitated enhanced coalescence. The difference in results may be due to the different properties of the external phase. The external phase used in our study is based on DGEBA which is easy to polymerise, limiting the time available for DES droplets to coalesce. Although there is currently a lack of effective means to monitor the polymerisation process, the MIPE nearly lost fluidity within 30 min, indicating a fast polymerisation rate of DGEBA.

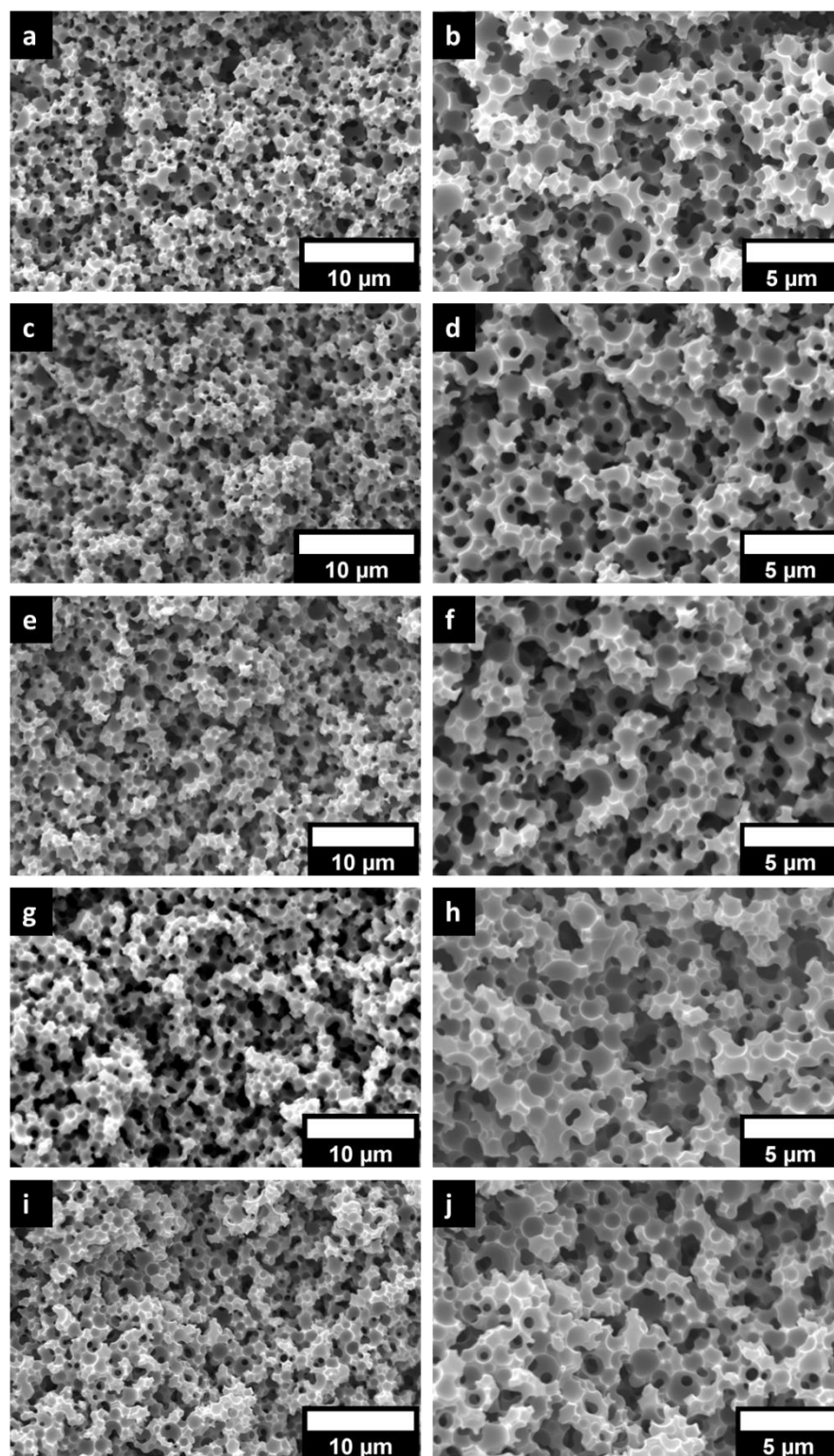


Figure 5- 2. The SEM images of polyMIPEs fabricated with different TMPTGE content at two magnifications. (a,b): 0%TMPTGE-bulk; (c,d): 5%TMPTGE-bulk; (e,f): 10%TMPTGE-bulk; (g,h): 15%TMPTGE-bulk; (i,j): 20%TMPTGE-bulk. (internal phase ratios - 56 vol.%, DES addition rates - 6 ml/min, stirring speeds - 1000 rpm, surfactants - Cithrol DPHS-SO-(MV), surfactant contents - 15 vol.%)

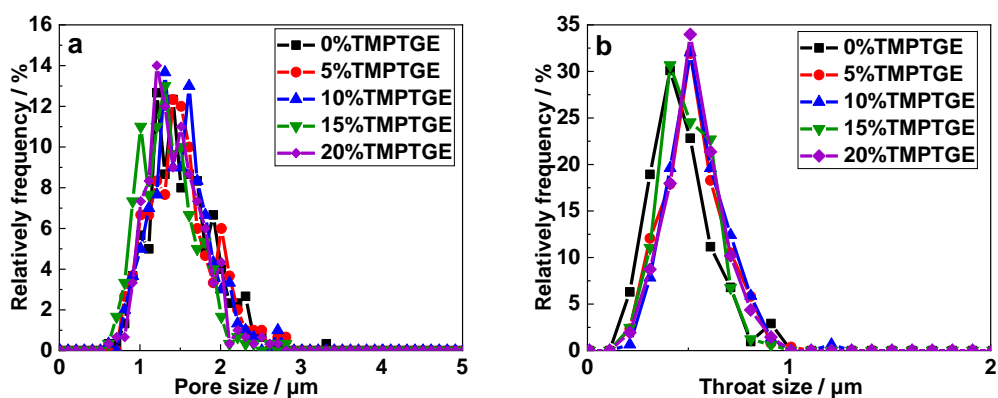


Figure 5- 3. The (a) pore size distribution and (b) throat size distribution of polyMIPes fabricated with different TMPTGE content. (internal phase ratios - 56 vol.%, DES addition rates - 6 ml/min, stirring speeds - 1000 rpm, surfactants - Cithrol DPHS-SO-(MV), surfactant contents - 15 vol.%)

The mechanical properties of the synthesised bulk polyMIPes were evaluated at room temperature using compression testing and summarised in **Table 5- 2** and **Figure 5- 4**. As illustrated in **Figure 5- 4**, the five samples prepared with varying TMPTGE content exhibit similar graphical trends. This indicates that the fracture mechanisms of the samples are similar, suggesting that samples with different TMPTGE contents undergo similar damage accumulation processes during fracture. Notably, both the slope of the linear region of the curve and the strength corresponding to the strain of 0.1 decrease with increasing TMPTGE content, indicating the decrease in Young's modulus and collapse strength. When there is no TMPTGE added, the sample exhibits the best compression mechanical performance, with highest Young's modulus and collapse strength being 141.5 ± 9.1 MPa and 9.2 ± 0.1 MPa, respectively. However, these two values decrease after the addition (5 wt.%- 20 wt.%) of TMPTGE to the MIPes, with the lowest values reaching 111.6 ± 10.4 MPa for Young's modulus and 7.6 ± 0.3 MPa for collapse strength, respectively. Given that the morphology of polyMIPes did not significantly change after the addition of TMPTGE, the decrease in mechanical performance should be attributed to the properties of the polymerised external phase. **Figure 5- 5** shows the chemical formular of DGEBA and TMPTGE. In contrast to DGEBA, the TMPTGE structure lacks aromatic

groups. The aliphatic segments in TMPTGE exhibit smaller rigidity compared to the aromatic segments present in DGEBA. The introduction of TMPTGE results in a decrease in rigid aromatic segments within the system, consequently leading to a decrease in compression performance [287, 290, 291, 299]. The reason for the change in collapse strength differs slightly from that for change in Young's modulus. When the TMPTGE content increases from 0 wt.% to 5 wt.% and then to 10 wt.%, the collapse strength decreases from 9.2 ± 0.1 MPa to 8.6 ± 0.2 MPa, and further to 7.9 ± 0.2 MPa. However, with further increases in TMPTGE content to 15 wt.% and 20 wt.%, the collapse strength remains relatively constant. This initial decrease is likely due to the reduction in rigid aromatic segments, which decrease the sample's resistance to deformation and destruction. At higher TMPTGE content, however, the increased flexibility of the cured epoxy enhances its ability to undergo plastic deformation at the crack tip, allowing for better stress distribution under applied forces [295]. Consequently, the strength does not continue to decrease significantly. In addition, **Table 5- 2** also presents the reduction rate of Young's modulus and collapse strength for each sample relative to the original polyMIPE (0 wt.% TMPTGE). It is evident that when the TMPTGE content is 5 wt.%, the decrease in compression performance is minimal, with only 2.7 % reduction in Young's modulus and a 6.5 % loss in collapse strength. However, when the TMPTGE addition content exceeds 10 wt.%, both Young's modulus and collapse strength decrease begin to exceed 10 %. Therefore, although the addition of TMPTGE can reduce the viscosity of the MIPE, it is beneficial to limit the TMPTGE content to below 10 wt.% to avoid a significant decrease in mechanical performance.

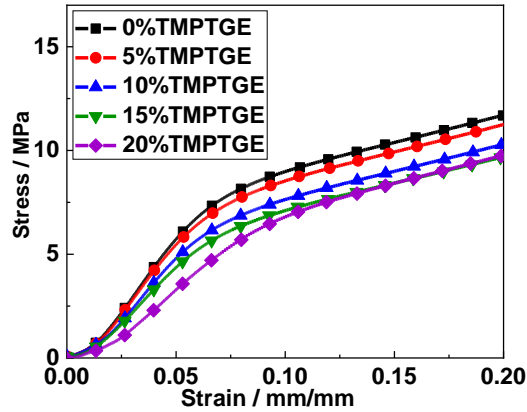


Figure 5- 4. Representative compressive stress-strain curves for polyMIPEs containing different TMPTGE content. (Internal phase ratios - 56 vol.%, DES addition rates - 6 ml/min, stirring speeds - 1000 rpm, surfactants - Cithrol DPHS-SO-(MV), surfactant contents - 15 vol.%.)

Table 5- 2. The influence of TMPTGE addition on the properties of the bulk polyMIPEs.

TMPTGE content	0%	5%	10%	15%	20%
$E^{[a]}$ (MPa)	141.5±9.1	137.7±8.4	126.9±3.7	117.5±7.0	107.6±12.9
Decline rate of $E^{[b]}$ (%)	-	2.7	10.3	17.0	24.0
$\sigma^{*[a]}$ (MPa)	9.2±0.1	8.6±0.2	7.9±0.2	7.6±0.3	7.7±0.5
Decline rate of $\sigma^{*[b]}$ (%)	-	6.5	14.1	17.4	16.3
Ionic conductivity (mS/cm)	4.78±0.06	5.35±0.11	5.61±0.06	5.71±0.10	6.00±0.12
$D_{32}^{[c]}$ (μm)	1.7	1.7	1.7	1.6	1.6
$D_{10}^{[c]}$ (μm)	1.5±0.4	1.5±0.4	1.5±0.5	1.3±0.4	1.4±0.3
Average throat diameter (μm)	0.5±0.2	0.5±0.1	0.5±0.2	0.5±0.1	0.5±0.1
Porosity (%)	55.8±0.5	56.6±0.1	54.9±0.4	55.2±0.7	54.3±0.3

[a] E refers to compressive Young's modulus and σ^* refers to collapse strength.

[b] the decline rate is calculated based on 0% TMPTGE-bulk.

[c] $D_{32}^{[c]}$ refers to Sauter mean diameter of pores and D_{10} refers to average pore diameter.

* Internal phase ratios - 56 vol.%, DES addition rates - 6 ml/min, -stirring speeds - 1000 rpm, - surfactants - Cithrol DPHS-SO-(MV), - surfactant contents - 15 vol.%.

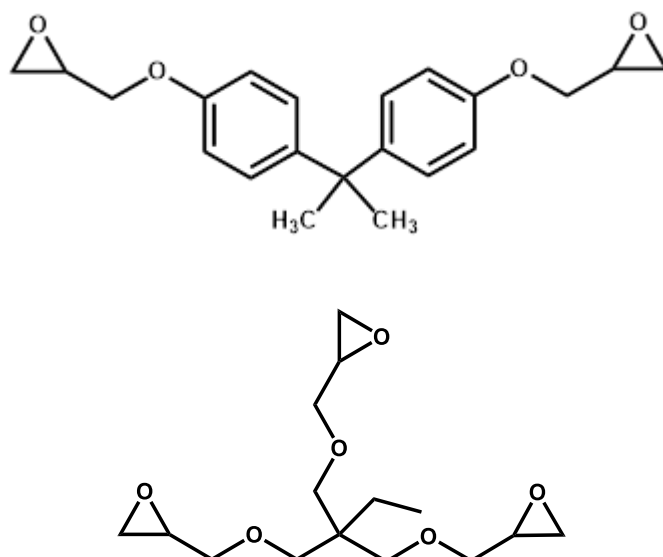


Figure 5- 5. The structure formula of DGEBA (above) and TMPTGE (below).

Ionic conductivity demonstrates an increasing trend with the increasing content of TMPTGE added, exhibiting an inverse relationship with the trend observed for Young's modulus (**Figure 5- 6**). When the TMPTGE content is 20 wt.%, the sample exhibits the maximum ionic conductivity, measured at 6.00 ± 0.12 mS/cm. It can be seen from **Figure 5- 3** and **Table 5- 2** that the addition of TMPTGE does not influence the pore structure and porosity of the polyMIPes. Consequently, the interconnectivity and tortuosity of the polyMIPes should remain similar, thereby exerting minimal impact on the movement of ions. Hence, the increase in ionic conductivity should be related to the presence of TMPTGE. The oxygen atoms in the ether bonds of TMPTGE could form hydrogen bonds with the cations/anions in DES, weakening the interaction between the cation and anion in 'ion pair' and thereby improving ionic conductivity. The DGEBA molecule also contains ether bonds, but its ability to form hydrogen bonds is lower than that of TMPTGE. This is because the oxygen atoms in the ether bonds of DGEBA are connected to the benzene rings. The conjugation effect from the benzene ring can decrease the electron cloud density around these oxygen atoms, which in turn weakens oxygen atoms' ability to form hydrogen bonds. Additionally, the rigidity and larger volume of the benzene ring can create steric hindrance, further impeding hydrogen bond formation [300].

The results of this section indicate that the introduction of TMPTGE could reduce the viscosity of the MIPes, thereby benefiting subsequent polyMIPE film preparation. However, once TMPTGE content exceeds 10 wt.%, there is a significant loss in mechanical performance, with the reduction in Young's modulus and strength exceeding 10 %. Hence, the studies on film fabrication will focus on the range of 0 – 10 wt.% TMPTGE content.

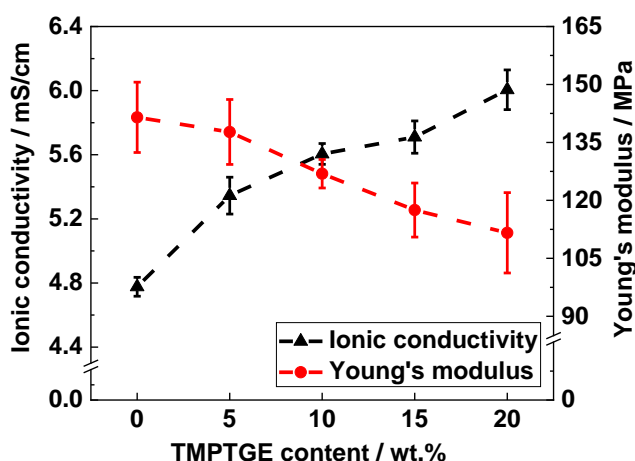


Figure 5- 6. Effect of TMPTGE content on the ionic conductivity and Young's modulus of bulk polyMIPes. (Internal phase ratios - 56 vol.%, -DES addition rates - 6 ml/min, -stirring speeds - 1000 rpm, surfactants - Cithrol DPHS-SO-(MV), surfactant contents - 15 vol.%)

5.3 Developing fabrication conditions for polyMIPE films

To spread bulk MIPE into a uniform film, it is essential to use an appropriate spreading instrument. Under the existing laboratory conditions, two instruments were tried for film fabrication: a film applicator and a blade (**Figure 5- 7a and b**). It is evident from **Figure 5- 7** that the film produced by the film applicator exhibits significant unevenness and irregular surface texture. This unevenness can cause an irregular distribution of force applied to the polyMIPE film, resulting in poor mechanical performance. When using the film applicator for film manufacturing, the conditions to produce a film with a smooth surface were not found, despite adjusting the formulation of the MIPE, the speed of the film applicator's movement, and changing the substrate material. Using a blade for film

manufacturing resulted a film with a smooth surface and no visual defects. It is hypothesized that the uneven film made by film applicator is primarily attributed to the strong adhesion property of DGEBA (the main component of the MIPE's external phase). It is evident that the area of the film applicator in direct contact with the MIPE film is considerable (**Figure 5- 7c**). The part of the MIPE that is close to the applicator will adhere to the film applicator and move along with the film applicator's movement (**Figure 5- 8**). The remaining MIPE constitutes the primary portion of the film. As the volume and shape of the adhered MIPE cannot remain entirely consistent throughout the film production process, the resulting film thickness becomes uneven, leading to a rough surface. The situation is significantly improved when using the sharp blade represented in **Figure 5- 7**. During film fabrication, the direct contact surface between the blade and the MIPE film is minimal (cutting edge of the blade), making it challenging for the MIPE to adhere to the blade. It is known that reducing the contact area decreases the number of contact sites between the adhesive and the adherend, thereby decreasing the adhesion force [301, 302].

In conclusion, this section demonstrates that the blade is effective in producing polyMIPE films with a smooth surface and no visible defects. Therefore, this instrument was used in polyMIPE film fabrication in this research.

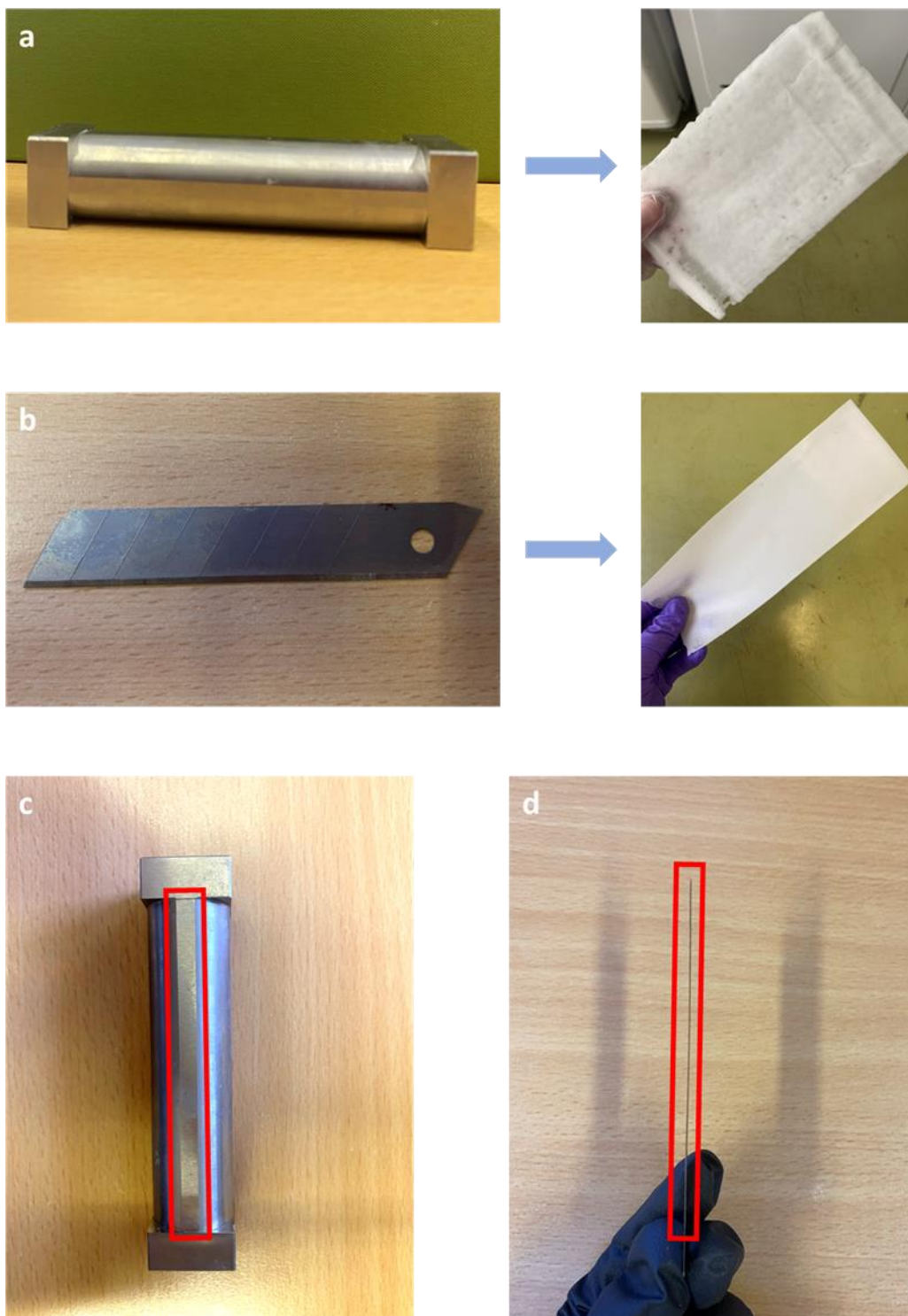


Figure 5- 7. Two instruments for making polyMIPE films: a: film applicator; b: blade, and the appearance of the films prepared by the corresponding instruments. The red rectangles in c and d indicate the sections of the two instruments that come into direct contact with the MIPE film.
 (internal phase ratio - 56 vol.%, DES addition rate -6 ml/min, the stirring speed - 1000 rpm, surfactants - Cithrol DPHS-SO-(MV), surfactant contents -15 vol.%, the TMPTGE content - 0 wt.%)

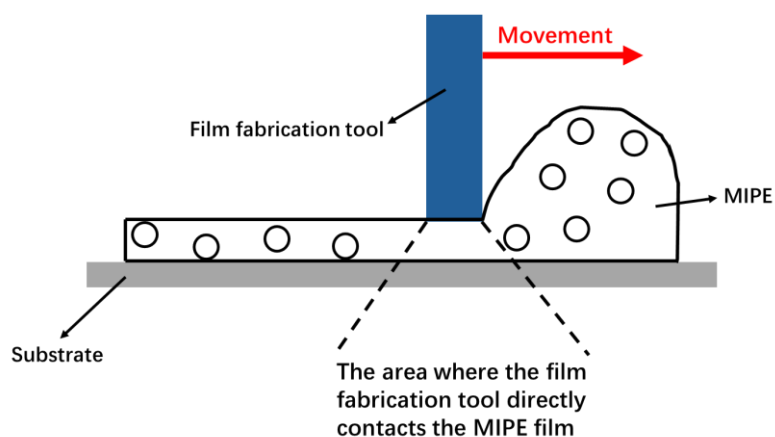


Figure 5- 8. Schematic diagram illustrating the area of direct contact between the film fabrication tool and the MIPE film.

5.4 The effect of TMPTGE content on properties of polyMIPE films

This section explores the impact of TMPTGE content on the morphological properties, mechanical properties, and ionic conductivity of polyMIPE films. The SEM images of polyMIPE films containing different contents of TMPTGE are shown in **Figure 5- 9**. Similar to bulk polyMIPes, polyMIPE films also exhibit interconnected pore structures. However, in comparison to bulk polyMIPE with the same formulations, the polyMIPE films exhibit reduced pore sizes and throat sizes (**Figure 5- 10**). For this phenomenon, it is hypothesized that it is associated with the thickness of MIPes. Compared to bulk MIPE, the reduced thickness of MIPE film facilitated more rapid thermal propagation, resulting in accelerated curing of the MIPE film. Montaserín et al. [292] conducted an in-depth study on the effect of thickness on the curing of DGEBA-amine system. They found that when the system was cured at 90 °C, the 1.5 cm thick sample was fully cured in 43.3 min, but the curing degree of the 4 cm thick sample was below 30 % at this time. In this study, MIPE film exhibits a much lower thickness (200 μm) compared to the bulk MIPE (2.5 cm in diameter). As a result, the curing rate of the MIPE film was higher than that of the bulk MIPE. Consequently, the degree of droplet coalescence and/or Ostwald ripening in the MIPE film was reduced due to the more rapid curing of the external phase. This led

to a reduction in droplet size within the MIPE and consequently results in smaller pore size in the film.

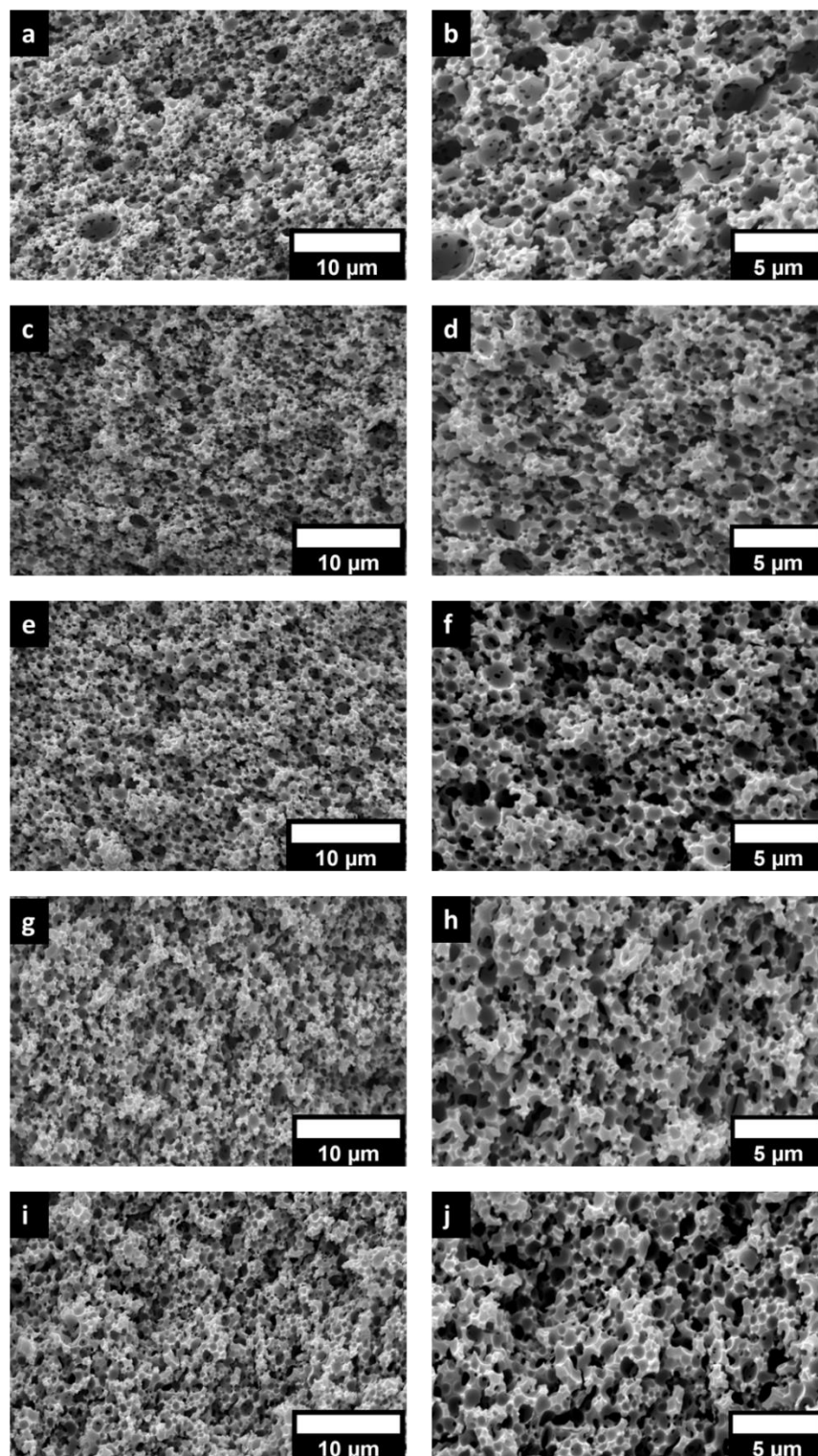


Figure 5- 9. The SEM images of polyMIPE films based on different TMPTGE content with two magnifications. (a,b): 0%TMPTGE- film; (c,d): 2.5%TMPTGE- film; (e,f): 5%TMPTGE- film; (g,h): 7.5%TMPTGE- film; (i,j): 10%TMPTGE- film.

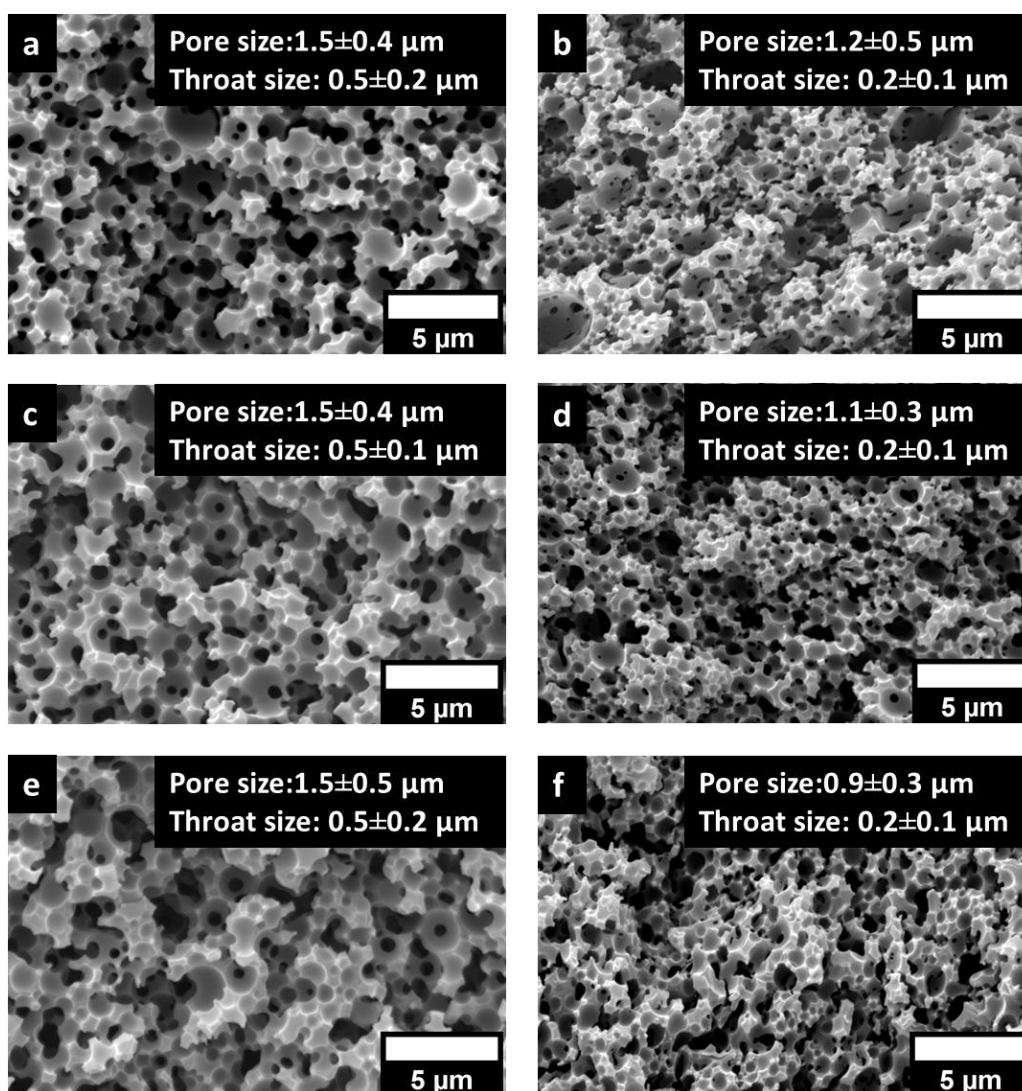


Figure 5- 10. Comparison of bulk polyMIPES (a,c and e) and polyMIPE film (b, d and f): a: 0%TMPTGE-bulk; b: 0%TMPTGE- film; c: 5%TMPTGE-bulk; d: 5%TMPTGE-film; e: 10%TMPTGE-bulk; f: 10%TMPTGE-film. (Internal phase ratios – at 56 vol.%, DES addition rates – 6 ml/min, stirring speeds – 1000 rpm, surfactants – Cithrol DPHS-SO-(MV), surfactant contents – 15 vol.%)

In addition, unlike bulk polyMIPES where TMPTGE content has a very slight effect on pore structure, increasing TMPTGE content in polyMIPE films leads to a more uniform pore size distribution (**Figure 5- 9**). Additionally, both the pore and throat sizes of polyMIPE films decreased as TMPTGE content increased (**Figure 5- 10**). This is because there are two mechanisms in bulk polyMIPES: the addition of TMPTGE reduces the viscosity of the external phase in MIPE, facilitating the breakup of DES into smaller and more uniform droplets under shear forces, while also lowering the resistance to droplet

coalescence once stirring stopped. In polyMIPE films, however, coalescence is reduced due to more rapid polymerisation.

Since the polyMIPE films differ in form from bulk polyMIPEs, tensile testing rather than compression testing was used to evaluate their mechanical properties. The tensile mechanical properties of polyMIPE films containing varying contents of TMPTGE are presented in **Figure 5- 11** and **Table 5- 3**. Compared to the Young's modulus of 540.5 ± 20.3 MPa with no TMPTGE added, the modulus decreases to 423.6 ± 17.0 MPa when the TMPTGE content was 2.5 wt.%. Further increases in TMPTGE content show no significant impact on Young's modulus. However, different trend is observed for the tensile strength of the studied polyMIPE films. The tensile strength of the sample without TMPTGE and that with 2.5 wt.% TMPTGE addition is similar. However, increasing the TMPTGE content to 5.0 wt.% lead to the rise of the tensile strength from 5.6 ± 0.2 MPa to 6.8 ± 0.2 MPa; however, further increases in TMPTGE content to 7.5 wt.% and 10.0 wt.% does not resulted in significant changes in strength. The following paragraph discusses the reasons behind the observed trends in Young's modulus and tensile strength.

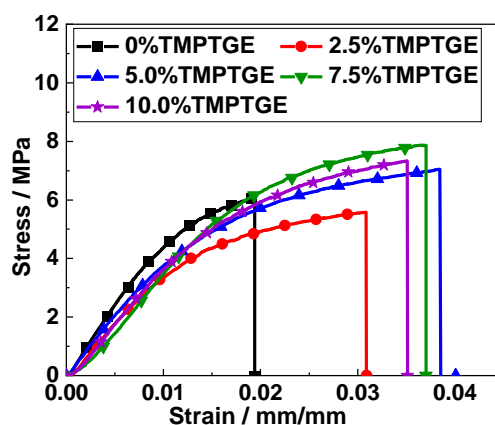


Figure 5- 11. Representative tensile stress-strain curves for polyMIPE films produced through the polymerisation of emulsion templates containing different TMPTGE contents.

Table 5- 3. The influence of TMPTGE content on the properties of polyMIPE films.

TMPTGE content	0%	2.5%	5.0%	7.5%	10%
Tensile Young's modulus (MPa)	540.5±20.3	423.6±17.0	427.9±29.3	424.4±22.7	428.7±31.9
Tensile strength (MPa)	5.8±0.3	5.6±0.2	6.8±0.2	7.3±0.4	7.4±0.3
Toughness(kPa)	72.7±18.1	109.4±7.2	166.1±26.1	173.0±19.7	187.2±33.2
Elongation at break (%)	1.9±0.4	2.9±0.2	3.7±0.4	3.5±0.3	3.8±0.4
Ionic conductivity (mS/cm)	0.74±0.06	0.92±0.04	0.93±0.06	0.92±0.04	0.95±0.03
Thickness (μm)	213±14	210±14	203±5	208±16	200±9
D ₃₂ ^[a] (μm)	1.6	1.5	1.3	1.1	1.0
D ₁₀ ^[a] (μm)	1.2±0.5	1.2±0.4	1.1±0.3	1.0±0.3	0.9±0.3
Average throat diameter (μm)	0.2±0.1	0.2±0.1	0.2±0.1	0.2±0.1	0.2±0.1
Porosity (%)	56.6±1.4	58.5±2.1	57.4±1.8	56.8±1.5	57.2±1.5

[a] D₃₂ refers to Sauter mean diameter of pores and D₁₀ refers to average pore diameter.

* For all samples, the internal phase ratios remained constant at 56 vol.%, the DES addition rates were 6 ml/min, the stirring speeds were 1000 rpm, the surfactants were Cithrol DPHS-SO-(MV), and the surfactant contents were 15 vol.%.

The addition of TMPTGE change the microstructure of the crosslinked DGEBA network and the pore structure of polyMIPEs, impacting the mechanical properties. The highly cross-linked DGEBA structures possess a high Young's modulus (5.5 GPa [303]) but limited flexibility [304]. The incorporation of flexible molecules into the cross-linked epoxy structure leads to a decrease in Young's modulus and increase in deformability [295]. Many studies have shown that the tensile modulus of epoxy decreases after adding a reactive diluent [295, 299, 305, 306]. However, another factor to consider in this study is the pore structure. The pore size decreased with increasing the TMPTGE content, which contributes to the higher Young's modulus. For samples with TMPTGE content greater than 2.5 wt.%, the observed stability of Young's modulus may be attributed to the combined effect of increased flexible chains and decreased pore size. In terms of tensile strength, TMPTGE enhances the flexibility of the cured epoxy, thereby improving its ability to undergo plastic deformation at the crack tip within the epoxy matrix. This

enables the dispersion of stress when external forces are applied. Consequently, TMPTGE contributes to the enhancement of the tensile strength of the resulting polyMIPEs [17, 295]. At a TMPTGE content of 2.5 wt.%, the tensile strength does not exhibit a significant increase, primarily due to the decreased Young's modulus. An increase in tensile strength is observed when the TMPTGE content reaches 5 wt.%. However, increasing the TMPTGE content further to 7.5 wt.% or 10 wt.% does not result in a significant change in strength. This is because a higher number of flexible segments were introduced into the system with increasing TMPTGE content, which may cause a plasticizer effect in the epoxy resin and consequently reduce the tensile strength [307, 308]. However, due to the improved tensile strength of polyMIPE films from reduced pore size, changes in tensile strength for polyMIPE films are not significant in the 5 wt.% to 10 wt.% TMPTGE range. Some studies [291, 306, 309] have observed that with increasing reactive diluent content, the tensile strength of epoxy resin initially increases and then decreases. This result differs slightly from the findings of this study. The observed trend of initially increasing and then remaining unchanged in this study is primarily attributed to the enhancement of tensile strength resulting from the reduced pore size. The samples examined in the referenced studies do not include pore structures.

As the TMPTGE content increases from 0 wt.% to 5.0 wt.%, the tensile toughness demonstrates a gradual enhancement from 72.7 ± 18.1 MPa to 166.1 ± 26.1 MPa (**Table 5-3**). However, beyond 5.0 wt.%, further increases in TMPTGE content do not notably affect the toughness. The improvement in toughness is attributed to the flexible backbone of TMPTGE, which enables the external phase of the polyMIPE to absorb more energy before fracturing [290, 307]. However, as the TMPTGE domain becomes larger at higher content, the stress concentration effect could be higher, which would affect the further improvement of toughness. Sinha A, et al. [307] observed that the tensile toughness of DGEBA/polyethylene glycol 400 (reactive diluent) system initially increases and then

decreases with increasing reactive diluent content. In our study, the toughness did not decrease after the TMPTGE content exceeded 5.0 wt.% primarily due to the reduced pore size in polyMIPE films. Smaller pore size increasing pore density, allowing for better force distribution across the polyMIPE film. This improved dispersion helps spread stress more evenly, reducing stress concentration and enhancing toughness of polyMIPE films.

The ionic conductivity of polyMIPE films with varying contents of TMPTGE is illustrated in **Figure 5- 12**. With increasing TMPTGE content from 0 wt.% to 10 wt.%, the ionic conductivity rises from 0.74 ± 0.06 mS/cm to 0.92 ± 0.04 mS/cm and then stabilizes at approximately 0.92 mS/cm (**Table 5- 3**). The increase in ionic conductivity can be explained by the possibility of the oxygen atoms on the ether bonds in TMPTGE form hydrogen bonding with cations/anions in the DES. While ion pairs present in the DES reduce the concentration of free charged species and thus decrease ionic conductivity [266, 267], the interaction between TMPTGE and cations/anions weakens the bond between cation and anion in the 'ion pair', ultimately enhancing ionic conductivity. After the TMPTGE content exceeds 2.5 wt.%, the ionic conductivity no longer increases, likely due to the reduced pore size. The reduction in pore size increases the tortuosity of the polyMIPE, thereby impeding ion movement. As a result of these two combined effects, further increases in TMPTGE content do not lead to additional improvements in ionic conductivity

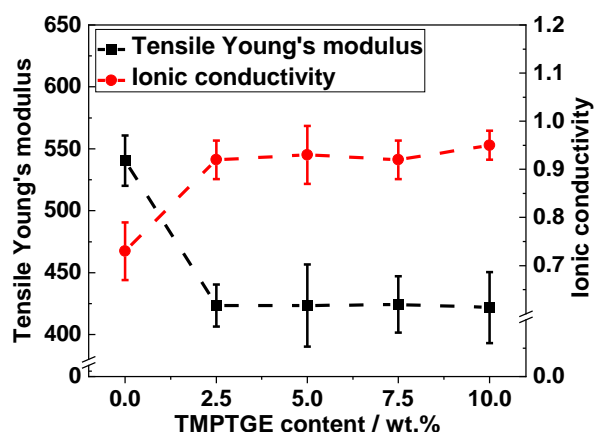


Figure 5- 12. Effect of TMPTGE content on the ionic conductivity and tensile modulus of polyMIPE films. (Internal phase ratios - 56 vol.%, DES addition rates - 6 ml/min, stirring speeds - 1000 rpm, surfactants - Cithrol DPHS-SO-(MV), surfactant contents - 15 vol.%)

5.5 Comparison of DPEs prepared in this study with those in existing literatures

As illustrated in **Figure 5- 13**, the data obtained in this study are compared with the data of DPEs in existing literatures. Specifically, 0%TMPTGE-polyMIPE film (characterized by the highest Young's modulus, 540.5 ± 20.3 MPa) and 2.5%TMPTGE-polyMIPE film (demonstrating the highest ionic conductivity, 0.92 ± 0.04 mS/cm) are used for this comparison. The Young's moduli in the figure are all obtained from tensile tests, and the white squares represent samples with the solid phase based on DGEBA.

Regarding ionic conductivity, samples '6' and '7' exhibit higher ionic conductivity compared to the samples analysed in this study. The liquid phase ratio of sample '6' is 70 wt.%, which is higher than the liquid phase ratio in this study. It is well known that increasing the liquid phase ratio in DPE leads to an increase in ionic conductivity [195-197]. Hence, it remains uncertain whether the increased ionic conductivity is attributable to the higher liquid phase ratio or the intrinsic properties of the liquid phase. The situation for sample '7' is different. The liquid phase ratio for sample '7' is merely 10 wt.%, yet it exhibits a higher ionic conductivity of 1.4 mS/cm. However, the Young's modulus for this sample is relatively low at 0.8 MPa. Future investigations could explore

the use of the liquid phase of sample '7' - specifically, the amphiphilic ionic liquids - as the internal phase of polyMIPE to achieve improved ionic conductivity.

Regarding Young's modulus, samples '8', '10', and '13' demonstrate higher values compared to the samples in our study. The primary component of the solid phase in sample '8' is identical to that in our study, both DGEBA. **Figure 5- 13** presents two data points for sample '8': the point with a higher Young's modulus corresponds to a liquid fraction of 50 vol.%, while the point with a lower Young's modulus relates to a liquid volume fraction of 70 vol.%. If the internal phase volume fraction is adjusted to align with that in our study (56 vol.%), the values of Young's modulus and ionic conductivity are expected to fall between these two points. It is evident that when the internal phase ratio is 56 vol.%, the ionic conductivity of sample '8' will be lower than that of this study. The Young's modulus remains uncertain, but even if it is higher, the difference should not be significant. The liquid phase ratio of sample '10' is 55 vol.% which is similar to the liquid phase ratio in this study. The ionic conductivity of sample '10' reaches 0.7 mS/cm, comparable to the sample 0%TMPTGE-film; the Young's modulus is 700MPa, exceeding the two samples in this study. The relatively high Young's modulus of sample '10' should be related to its solid phase - 5284 epoxy resin. Future research could explore the use of 5284 epoxy resin to improve the mechanical properties of polyMIPE films in our study. In sample '13', the Young's modulus is 900 MPa at a liquid phase ratio of 50 wt.%, while it decreases to 300 MPa at a liquid phase ratio of 70 wt.%. Similar to the sample '8', it remains uncertain whether a higher Young's modulus would be observed if the liquid phase ratio is aligned with that in our study.

In summary, it can be observed from **Figure 5- 13** that while the two samples in our study do not simultaneously possess the highest Young's modulus and ionic conductivity, they both achieve an excellent balance between Young's modulus and ionic conductivity. In

the future, the mechanical properties and ionic conductivity can be further optimised by adjusting the composition and ratio of the internal and external phases.

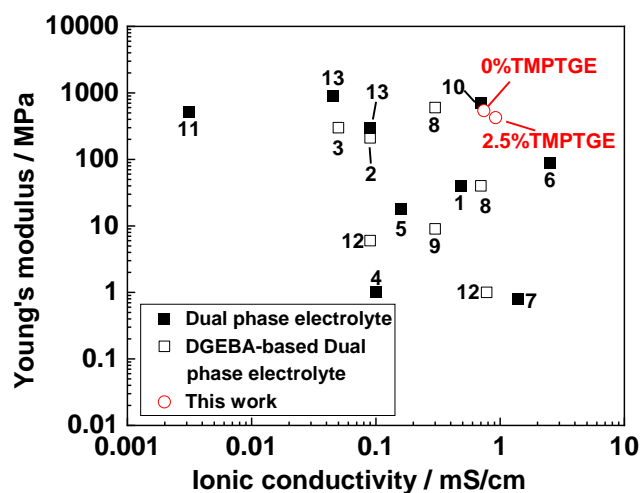


Figure 5- 13. Comparison between this work and existing literature data of DPEs. The mechanical properties are determined using tensile tests. The data presented in the figure are sourced from 1: [189]; 2: [310]; 3: [192]; 4: [311]; 5: [193]; 6: [312]; 7: [194]; 8: [195]; 9: [313]; 10: [254]; 11:[190]; 12: [196]; 13: [197].

5.6 Summary

The primary objective of this chapter was to transform the MIPE investigated in the previous chapter into a thin film suitable for practical applications in SCs. One of the main challenges encountered was the high viscosity of the DES-in-DGEBA MIPE, which could impede the uniform spreading of the film. To address this, a reactive diluent, TMPTGE was introduced to the external phase to reduce the viscosity of the system. In addition to viscosity, the impact of this diluent on the morphological property, mechanical property and ionic conductivity of polyMIPE was also investigated. The addition of 5 wt.% TMPTGE led to a notable reduction in the viscosity of the MIPE. Subsequent increments in TMPTGE addition continued to decrease the MIPE's viscosity, however, the extent of reduction became less significant. Regarding the morphology of polyMIPEs, the addition of TMPTGE did not have a significant impact. Neither the pore size distribution, the throat size distribution, nor the interconnect pore structure of polyMIPE exhibited

substantial alterations. Nevertheless, the mechanical properties and ionic conductivity were changed. As the TMPTGE content increased, there was a gradual decrease in the compressive Young's modulus and collapse strength of polyMIPE. Conversely, there was a gradual increase in the ionic conductivity.

The results indicated that using a blade yields better outcomes compared to film applicator. The pore size of polyMIPE films appeared to be smaller compared to the corresponding bulk polyMIPEs. The sample displayed the highest tensile Young's modulus in the absence of TMPTGE. However, with the addition of TMPTGE, both toughness and elongation at break increased. This trend stabilized once the TMPTGE addition reached 5 wt.%, beyond which there was no further significant increase. The optimal ionic conductivity was achieved at a TMPTGE addition content of 2.5 wt.%, beyond which the ionic conductivity remained unchanged. Based on the above conclusions, which indicate that polyMIPE films with 2.5 wt.% and 5 wt.% TMPTGE exhibit improved performance, Chapter 6 will discuss the effects of adding 2.5 wt.% and 5 wt.% of TMPTGE on SC performance.

6 Fabrication of SCs based on DES-in-DGEBA polyMIPE

After successfully preparing DES-in-DGEBA polyMIPE and casting it into a smooth and uniform film, this chapter focuses on fabricating a SC using the polyMIPE film. Combining polyMIPE with the electrodes presented the initial challenge to be addressed. The simplest solution is to directly sandwich the MIPE between the two electrodes [195], however, due to the MIPE's susceptibility to penetration, this method poses the risk of short circuits. When using plain-woven CF mat as the electrode, the fibre bundles at the edge of the mat consistently curl up. These fibres pose a risk of easily penetrating the MIPE, potentially leading to electrodes contact. The structure of polyMIPE is robust, but fully cured MIPE has lost its viscosity. Hence, the approach used in this study is to assemble the MIPE and the electrode together when the MIPE is partially polymerised. At this stage, the structure is sufficiently robust to withstand the penetration of the electrodes (CF mat) while still maintaining adhesion. After establishing a suitable method for preparing SCs, the discussion will focus on the effect of composition of the MIPE, the binder used to adhere current collector and the electrodes, and the current collectors, on the electrochemical performance of the SCs. In the final part of this chapter, an alternative method for preparing SCs is discussed. This involves using a C spray to form electrodes on the polyMIPE film. This method significantly simplifies the preparation process of SCs while maintaining good electrochemical performance. This chapter discusses the effects of various variables—such as the preparation method, electrodes, adhesive, and current collector—on the CV and EIS performance of SCs. This research aims to advance SC technology and open new possibilities for future applications in wearable devices, portable electronics, and beyond.

6.1 Summary of sample compositions

The compositions for SCs fabricated in this chapter are presented in **Table 6- 1**.

Table 6- 1. Compositions of SCs in this chapter.

Sample name ^[a]		Electrode	Current collector	Binder	TMPTGE content / wt.% ^[b]
25min-	Cu-P-CF	CF mat	Cu strip	Polymer	0
40min-		CF mat	Cu strip	Polymer	0
Fully cured-		CF mat	Cu strip	Polymer	0
2.5% TMPTGE-		CF mat	Cu strip	Polymer	2.5
5% TMPTGE-		CF mat	Cu strip	Polymer	5
25min-Cu-	E-CF	CF mat	Cu strip	Electrodag	0
25min-Al-		CF mat	Al strip	Electrodag	0
As synthesized-	Al-E-C spray	C spray	Al strip	Electrodag	0
Sanded-		C spray	Al strip	Electrodag	0
Sanded+DES-		C spray	Al strip	Electrodag	0
Sanded+DES-Al-E-Ni spray		Ni spray	Al strip	Electrodag	0

[a] the sample names consist of Four parts. The first part is a description of MIPE, the time specified denotes the curing duration (at 60°C) undergone by the eMIPE film before placing the first CF mat. The ‘2.5%TMPTGE’ denotes the content of TMPTGE is 2.5 wt.%. ‘As synthesized’ refers to directly using the prepared polyMIPE film for SC fabrication. ‘Sanded’ indicates that the surface of the polyMIPE film was sanded before use. ‘Sanded+DES’ means that the lost DES caused by sanding was compensated. The second part denotes the material used as the current collector. The third part indicates the adhesive type for bonding the current collector and electrode. In this study, 'P' denotes the polymer-based adhesive, while 'E' refers to the Electrodag. The fourth part indicates the material used for making the electrodes, with ‘CF’ representing carbon fibre mat, 'C spray' indicating carbon spray, and 'Ni spray' signifying nickel spray.

[b] weight based on the total weight of DGEBA and TMPTGE.

*The formula for the polyMIPE film is consistent with that presented in Chapter 5.

6.2 Exploring the method for fabricating SCs

A SC is typically composed of two current collectors, two electrodes, an electrolyte, and a separator. The current collector serves the function of transferring current from the external source during charging and delivering the stored energy to the desired device or machine during discharging. The primary requirements for current collectors including high electrical conductivity (10^4 to 10^5 S/cm [46]) to facilitate efficient transfer of

electrons to external circuits, as well as electrochemical stability. This study initially employed Cu strip as the current collector as it satisfies the requirements mentioned above [314-317]. Charge storage takes place at the electrode/electrolyte interface [47]. For SC electrodes, the primary requirements include high electronic conductivity, rapid charge/discharge rates, and high surface area [318]. Carbon-based materials are frequently used as electrodes due to their excellent electronic conductivity (0.6 to 0.9 S/cm), high surface area (up to 3000 m²/g), and availability in various forms such as sheet, powders, fibres, and tubes [26, 318]. CF mat was chosen as the electrode material in this study due to its accessibility and ease of use. The separator plays a crucial role in preventing physical contact between the electrodes. Throughout the charging and discharging process, the separator enables the free passage of ions while restricting the movement of electrons, thereby ensuring the efficient and safe operation of SCs [319]. In this study, the polyMIPE film served the functions of a separator and an electrolyte, thereby eliminating the necessity of using an additional separator.

The first method for manufacturing the SC containing the polyMIPE film and CF mat, involved applying freshly made MIPE onto one of the CF mats and then placing the other on top of the MIPE film, followed by the solidification of the MIPE. However, as illustrated in **Figure 6- 1a**, this method presents one significant challenge: the edges of the CF mat are partially raised, preventing the MIPE from covering these areas, leaving them without a separator. This can potentially lead to the contact of the two CF mats (electrodes), causing a short circuit. Hence, the second approach was proposed: spread the MIPE film onto a substrate and partially polymerise it until it reaches the gelation stage while still remaining tacky, before peeling it off and placing it between two CF mats. Based on the test results, it is observed that the MIPE needs to be placed in an oven at 60 °C for a minimum of 25 min to become an effective barrier. As illustrated in **Figure 6- 1b**, when the curing time was less than 25 min, the edges of the CF mat are prone to

penetrating the MIPE, resulting in CF exposure. Conversely, when the curing time exceeded 25min (**Figure 6- 1c**), no parts of the CF mat are exposed.

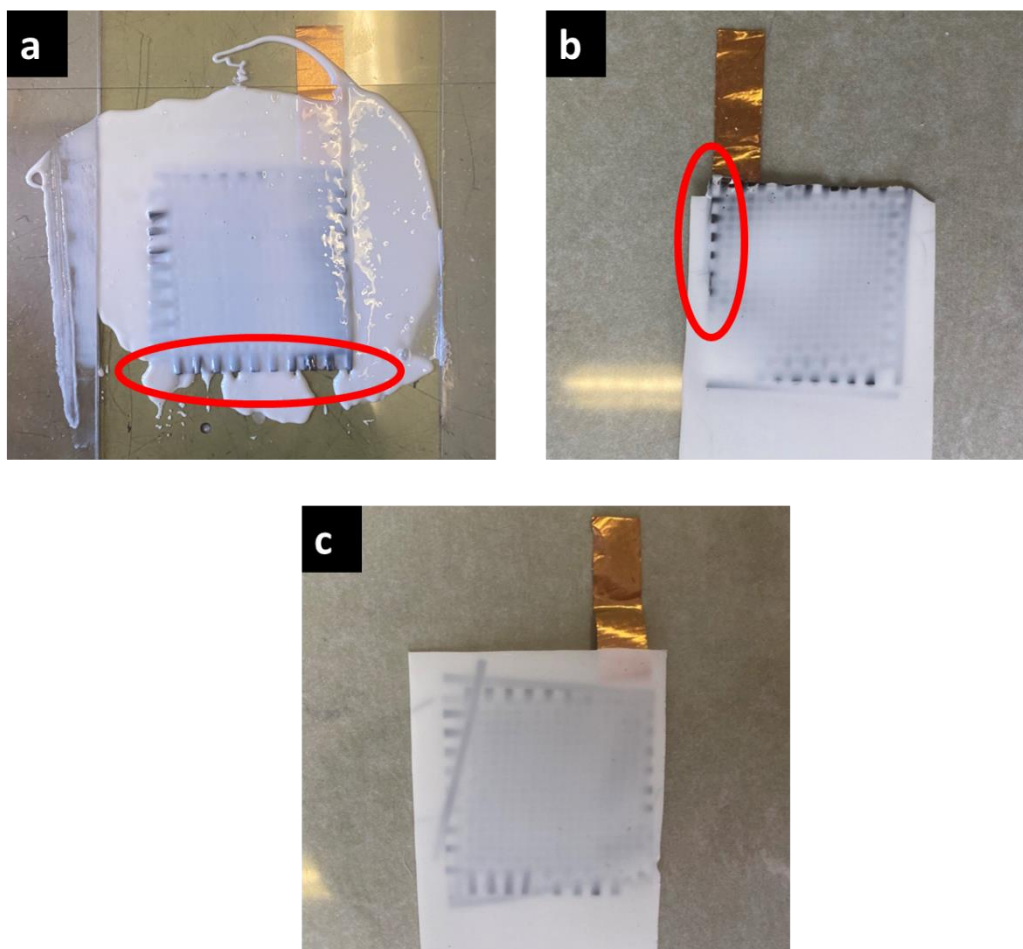


Figure 6- 1. Images of (a) MIPE film applied onto the CF mat directly; (b) MIPE film applied onto the CF mat after the MIPE was polymerised for 20 minutes at 60°C; (c) MIPE film applied onto the CF mat after the MIPE was polymerised for 25 minutes at 60°C.

However, difficulties were encountered when attempting to peel off the MIPE film. At a curing time of 25 min, the MIPE film was still not strong enough to be peeled off from the substrate. It required another 15 min of cure before the MIPE film can be peeled off the substrate. Hence, the method for combining the electrodes and polyMIPE had been tentatively established as follows: the MIPE was cast onto a substrate and cured at 60 °C for 25 minutes. Subsequently, the first CF mat was placed on the MIPE film. After allowing the emulsion to cure at 60 °C for an additional 15 minutes, both the MIPE film and the first CF mat were peeled off from the substrate, and the second CF mat was

positioned on the opposite side of the MIPE film. Finally, the assembly should be placed in an oven for subsequently curing (25min-Cu-P-CF). However, the above method was somewhat cumbersome. Therefore, two alternative methods were proposed. The first method was to peel off the MIPE film from the substrate after curing it at 60 °C for 40 min, then the MIPE film was combined with two CF mats and the assembly was placed in an oven for further curing (40min-Cu-P-CF); The second method was to combine the CF mats with fully cured MIPE film (Fully cured-Cu-P-CF).

The appearance and flexibility of the prepared SCs are shown in **Figure 6- 2**. The polyMIPE film is larger than the CF mat to prevent short circuits caused by the contact of the two CF mat electrodes (**Figure 6- 2a**). The flexibility of the SC prepared by placing the CF mats after complete curing of the MIPE film is greater than that of the other two SCs (**Figure 6- 2b-d**). This is because the loss of adhesiveness in the fully cured MIPE, allowing the CF mat to rest solely on the polyMIPE without providing structural support. In contrast, when the MIPE film was only partially cured, the CF mat can adhere to the MIPE film better, providing support to the polyMIPE. Some studies [320-322] have demonstrated that enhanced adhesion between CFs and the epoxy is beneficial for the structural support of CF for epoxy.

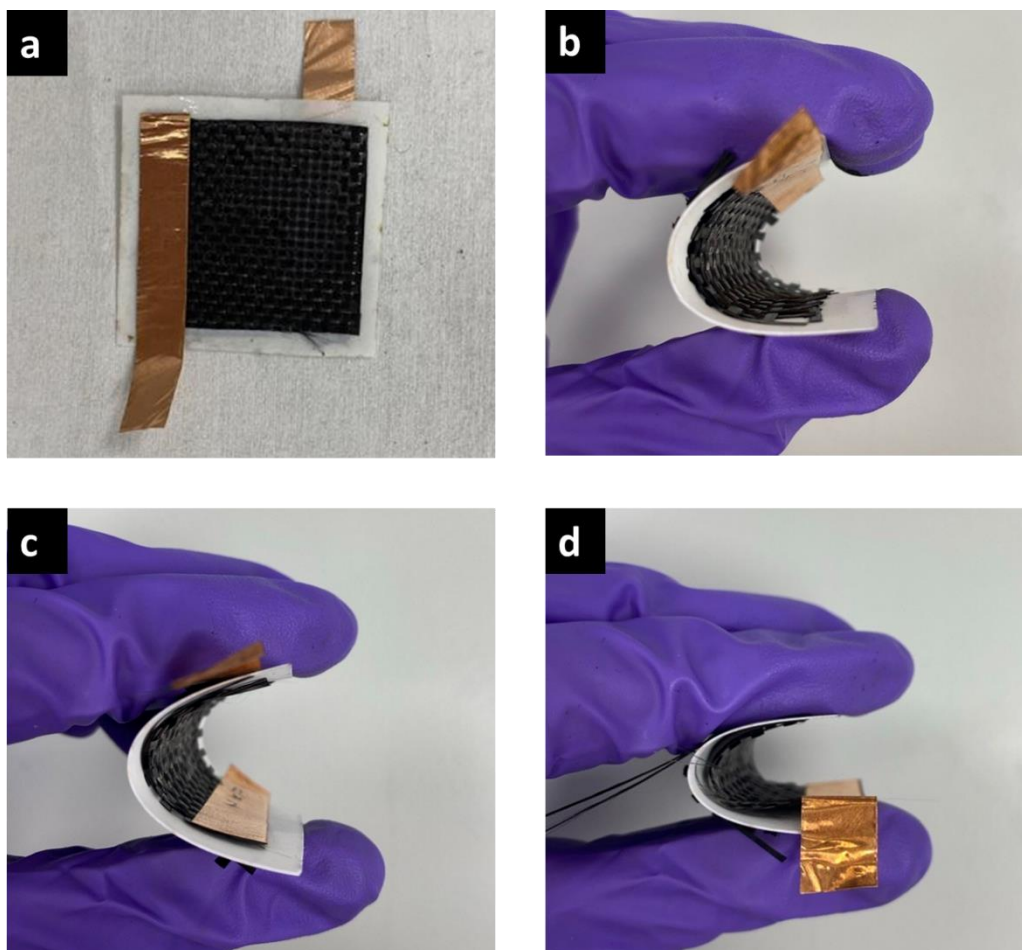


Figure 6- 2. (a) Image of the appearance of the prepared SC. The maximum bending degree of (b) 25min-Cu-P-CF; (c) 40min-Cu-P-CF; and (d) Fully cured-Cu-P-CF.

The electrochemical performances of SCs, fabricated with different deposition times of the CF mats, were evaluated through CV and EIS measurements, as shown in **Figure 6- 3**. The shape of the CV curves (**Figure 6- 3a&b**) at a scan rate of 5 mV/s indicates the formation of the electrical double layer at the electrode-electrolyte interface [323-325]. The absence of evident peaks in the CV curves of all samples indicates the lack of redox reactions, demonstrating the capacitive performance of the EDLC. While an ideal CV curve for EDLCs should be a perfect rectangle [230, 233], the CV curves for the SCs in this study deviate from this trend due to the presence of internal resistance [230, 325]. The greater integral area of the CV curve observed for the sample 25min-Cu-P-CF indicates a higher specific capacitance compared to the other two samples. The specific capacitance values (**Figure 6- 3c&d**) for samples 25min-Cu-P-CF, 40min-Cu-P-CF, and

Fully cured-Cu-P-CF at a scan rate of 5 mV/s are 6.17 ± 0.23 mF/g, 3.95 ± 0.18 mF/g, and 0.03 ± 0.00 mF/g, respectively. Except for Fully cured-Cu-P-CF, the specific capacitances of the other two samples align with previously reported specific capacitances of SCs in the range of 3.0-11.6 mF/g that using unmodified CF electrodes and DPE [326-330].

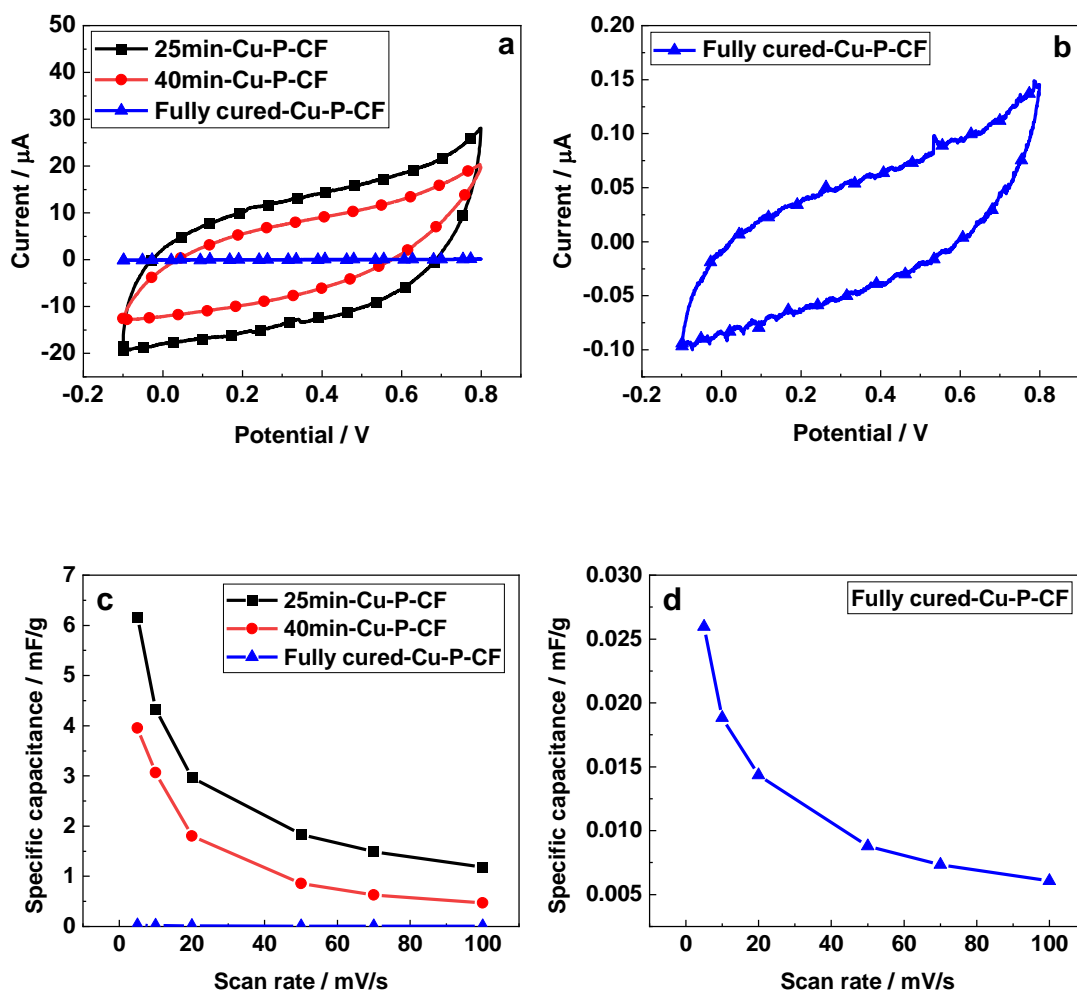


Figure 6- 3. The electrochemical performance of the SCs: (a) CV curves at the scan rate of 5 mV/s; (b) CV curves for Fully cured-Cu-P-CF at the scan rate of 5 mV/s; (c) variation of specific capacitance as a function of scan rate; (d) variation of specific capacitance as a function of scan rate for Fully cured-Cu-P-CF.

The observed difference in specific capacitance of the three samples can be mainly attributed to the differences in the contact areas between the CF mat and the polyMIPE film. When the CF mat was placed after curing the MIPE for 25 min, it formed a strong

bond with the polyMIPE film, making it impossible to peel off the CF mat completely. The strong bond was due to many CFs being embedded in the polyMIPE, as evidenced in **Figure 6- 4a**. The embedded CFs ensure a large contact area between the CF mat and the polyMIPE film, thereby facilitating the contact between the CF mat and the ions in the DES. When the CF mat was placed after curing the MIPE for 40 min, it could be easily peeled off. After the removal of the CF mat, only indentations were left without any CF residue (**Figure 6- 4b-d**). This indicates that the CFs were only partially embedded, resulting lower contact between the CF mat and the polyMIPE film compared to **Figure 6- 4a**. Once the MIPE was fully cured (**Figure 6- 4e&f**), no CF indentations or CFs are observed on the surface of the polyMIPE film, indicating that only the tops of the CFs on the surface of the CF mat were in contact with the polyMIPE film. In addition to the lack of CFs embedding in the polyMIPE, the surface structure of the polyMIPE film also influences the contact between the CF mat and the ions in the DES. When a fully cured polyMIPE film was made, MIPE was applied onto a substrate so that one side of the MIPE film was exposed to air, while the other side remained in contact with the substrate. As shown in **Figure 6- 4e**, the side that was exposed to air displays a film layer with some cracks, and the openness is very low. The different openness of polyMIPE film in contact with CF and air is attributed to the varying affinity of DGEBA for these materials. Jiang's research [331] also demonstrates that when poly(EHA-St-DVB)HIPE is applied to various substrates, the openness of the polyHIPE surface differs, which is believed to be associated with the interfacial tension between the polyHIPE and the substrate. In addition to the limited contact between the CF and the polyMIPE film, the significantly lower openness (**Figure 6- 4e**) of the polyMIPE film surface signifies a further reduction in the contact between the CF and the ions in the DES. It is well-known that capacitance is achieved through the accumulation of charge at the electrode-electrolyte interface, a process reliant on the electrode surface area available for electrolyte ions [332]. The

sample 25min-Cu-P-CF exhibited the largest specific capacitance, primarily due to the greatest contact between the CF mat and the ions in the DES.

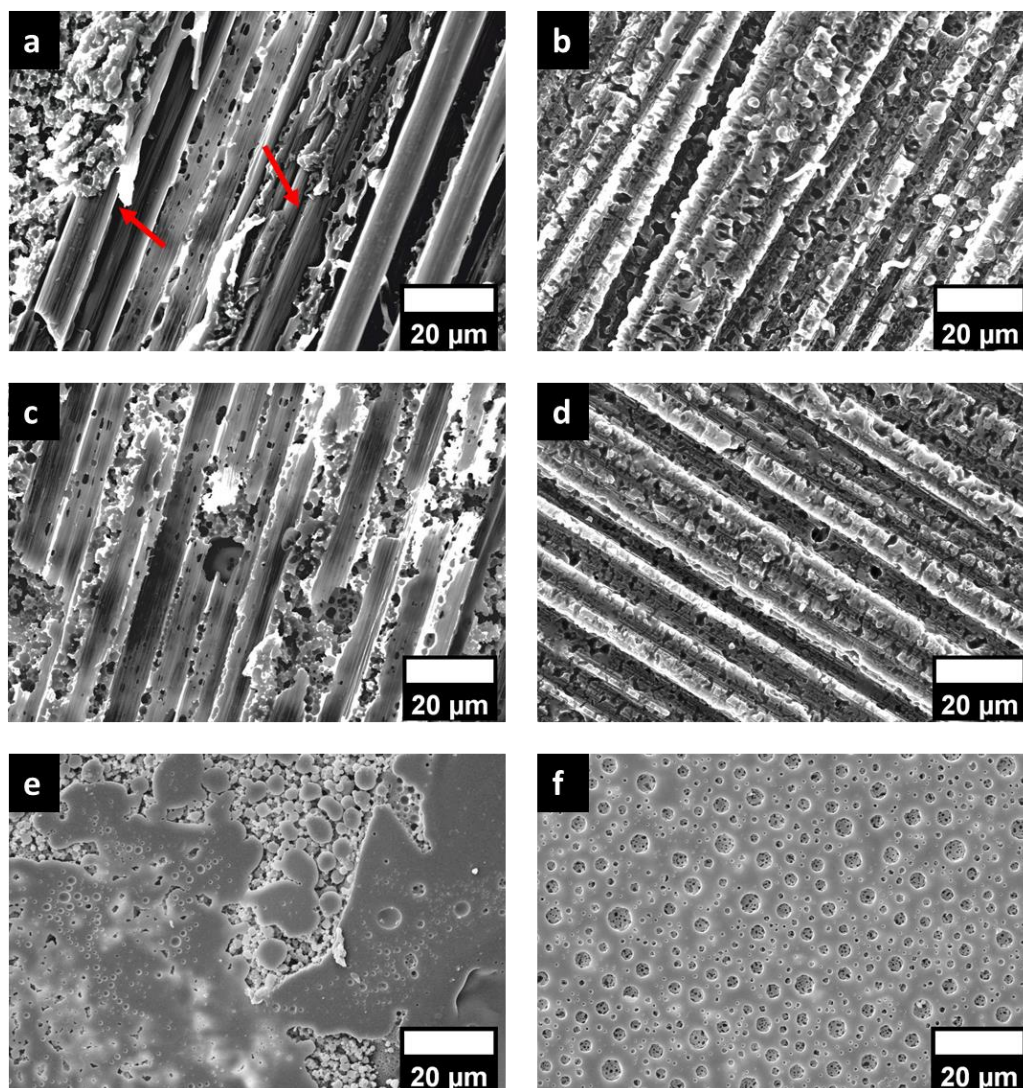


Figure 6- 4. The SEM images of the surface of polyMIPE film after peeling off the CF mat. (a,c, and e) show the surfaces of the MIPE side that were exposed to air; (b,d, and f) show the surfaces formed by MIPE side in Contact with the substrate. Specifically, (a, b) correspond to 25min-Cu-P-CF; (c,d) correspond to 40min-Cu-P-CF; (e,f) correspond to Fully cured-Cu-P-CF.

The SCs exhibit the same trend in specific capacitance with scan rate (**Figure 6- 3c** and **d**), i.e. decrease in specific values with the scan rate. This phenomenon occurs due to rate-limiting processes, such as electrical transport limitation within the electrode or ionic transport limitations within the electrolyte. At higher scan rates, the interfacial double layer formation is affected by these transport limitations, as there is insufficient time for its development [233, 333]. In addition, the sample 25min-Cu-P-CF exhibits the highest

specific capacitance across all scan rates, primarily due to the effective contact between the CF mat and the ions in the DES.

The fundamental behaviour of the resulting SCs was further investigated using EIS test (**Figure 6- 5**). The ESR values for the samples 25min-Cu-P-CF, 40min-Cu-P-CF, and Fully cured-Cu-P-CF are $64.85 \pm 4.40 \ \Omega$, $206.57 \pm 10.33 \ \Omega$, and $295.71 \pm 10.07 \ \Omega$, respectively. The observed differences in ESR can be primarily attributed to the varying contact areas between the CF mat and the DES. Reduced contact area impedes ion transfer to the electrode, thereby increasing ionic resistance and resulting in increased ESR values. The study by Qian et al. [328] supports this perspective. They found that modifying CFs with carbon aerogel significantly reduced the ESRs of the SCs. The reduction in ESR is attributed to the increased contact area between the CF and the electrolyte, as well as the improved transverse conductivity among the primary CFs. All the three samples do not show distinct semi-circle. The absence of semi-circle is common in Nyquist plots for SCs [326, 334-337]. Notably, the absence of semi-circles does not necessarily imply that the R_{ct} of the sample is negligibly small. The semi-circle will deform and even become completely disrupted as the double-layer capacitance increases [338]. In the low-frequency region, an ideal capacitor is typically represented by a vertical 'tail'. However, the 'tails' of the plots for all samples deviate from the expected 90° angle. This phenomenon is common in practical SCs [334, 336, 337, 339].

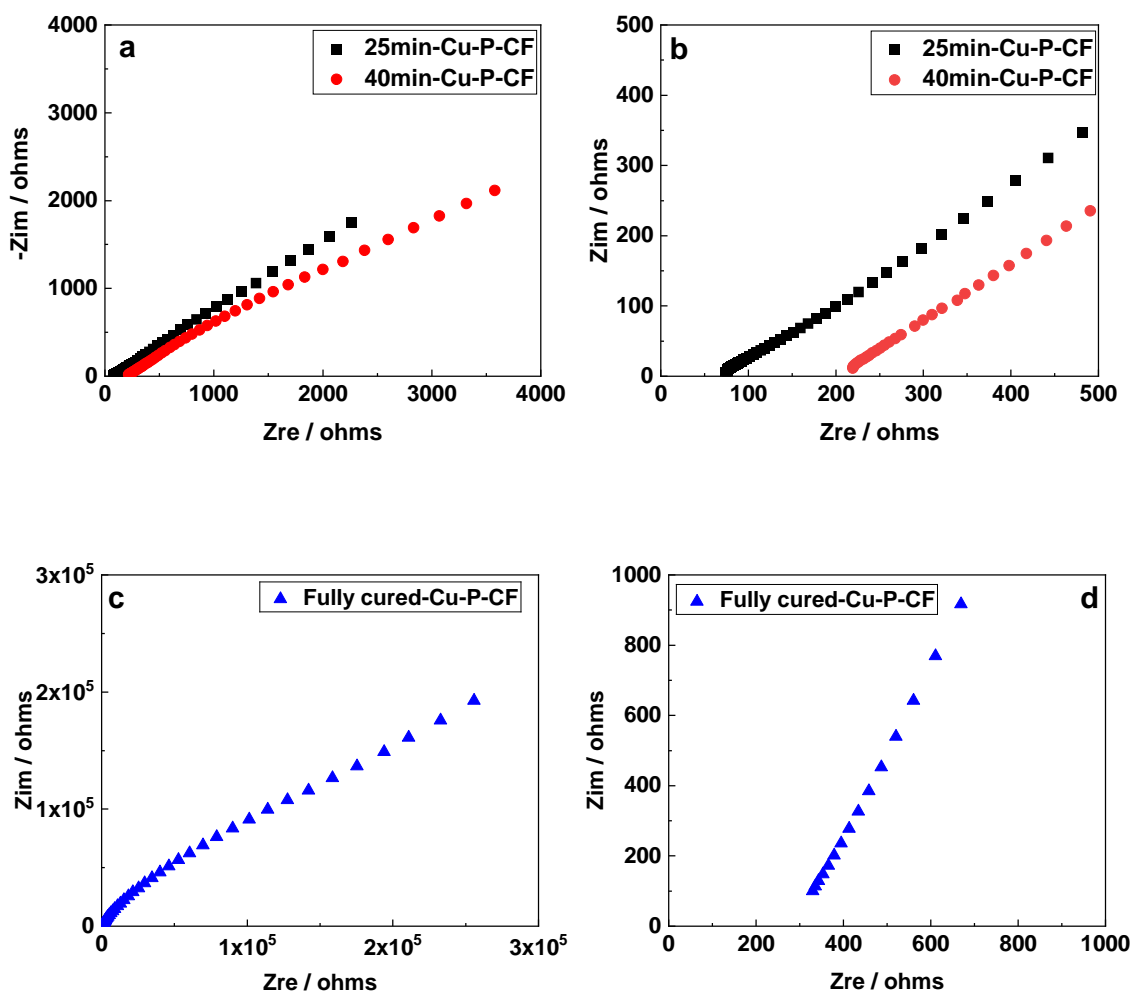


Figure 6- 5. The electrochemical performance of the SCs: (a,c) Nyquist plots of the SCs and (b,d) extended Nyquist plots.

In summary, the sample 25min-Cu-P-CF exhibits the largest specific capacitance and the smallest ESR, and the adhesion between the components in this SC is the best. Subsequent experiments would be conducted based on the preparation method of this sample.

6.3 The effect of TMPTGE addition on the performance of the SCs

After determining a suitable method for fabricating SCs, the effect of TMPTGE addition on the electrochemical properties of SCs was investigated. Based on the findings from Chapter 5, the TMPTGE content of 2.5 wt.% and 5 wt.% were selected for the research. The 5 wt.% TMPTGE was chosen as the resulting polyMIPE film showed the best combination of ionic conductivity and mechanical performance, among studied formulations. The value of 2.5 wt.% falls between 0 wt.% and 5 wt.%. At this content,

the ionic conductivity of the polyMIPE film is comparable to that observed with 5% TMPTGE-polyMIPE film, while the amount of TMPTGE is reduced by half.

The CV graph (**Figure 6- 6a**) demonstrates that the addition of TMPTGE does not change the overall shape of the curve. In addition, it is evident that the SC containing 5 wt.% TMPTGE exhibits the smallest integrated area, suggesting the lowest specific capacitance. The specific capacitance values for the samples 25min-Cu-P-CF, 2.5%TMPTGE-Cu-CF and 5%TMPTGE-Cu-P-CF at a scan rate of 5 mV/s are 6.17 ± 0.23 mF/g, 6.99 ± 0.37 mF/g and 4.44 ± 0.24 mF/g, respectively. When the scan rate exceeds 10 mV/s (**Figure 6- 6b**), the specific capacitance of the sample 25min-Cu-P-CF at various scan rates higher than the other two SCs. Because the polyMIPE film containing TMPTGE exhibits greater ionic conductivity, indicating better ion transport performance, it was anticipated that the specific capacitance of the SC containing TMPTGE would be higher. The experimental results differ from the expected outcomes, which may be related to the contact interface between the electrolyte and the electrode. The result of CV test is affected by various factors, such as current collectors, adhesives, electrolytes, electrode materials, and the contact between components, etc. Except for the polyMIPE film composition, the primary difference in these three SCs is the contact between the polyMIPE film and the electrodes. Hence, it can be concluded that the addition of TMPTGE may affected the properties of this interface. Jiang [331] has demonstrated that the interfacial tension between polyHIPE and substrate influences the openness of polyHIPE surface. The addition of TMPTGE may influence the interfacial tension between the MIPE and the CF mat, leading to lower degrees of pore opening at their interface, which subsequently impacts ion transport. When the TMPTGE content was 2.5 wt.%, the higher ionic conductivity of polyMIPE film mitigated the effect of TMPTGE on the interface. However, as the TMPTGE contents increased to 5 wt.%, the impact of TMPTGE on the

interface increased further; however, the ionic conductivity remained consistent with that observed at 2.5 wt.%. Consequently, the specific capacitance decreased.

The Nyquist plots for the SCs and the corresponding extended plots are shown in **Figure 6- 6c** and **d**. The ESR values for SCs 25min-Cu-P-CF, 2.5%TMPTGE-Cu-P-CF and 5%TMPTGE-Cu-P-CF are $64.85\pm 4.40\ \Omega$, $71.76\pm 5.31\ \Omega$ and $146.36\pm 6.60\ \Omega$, respectively. The addition of 2.5 wt.% TMPTGE has minimal impact on the ESR of the SC. However, the ESR value increases notably when the TMPTGE content rises to 5 wt.%. Similar to the CV test results, the change in ESR should also be related to the ionic conductivity of the polyMIPE films and the openness of the film surface.

In summary, the study finds that the performance of the SC containing 5 wt.% TMPTGE is relatively poor. The EIS results indicate minor differences between the other two SCs. At a scan rate of 5 mV/s, the specific capacitance of the 2.5% TMPTGE-Cu-P-CF is the highest, although it does not significantly exceed that of the 25min-Cu-P-P-CF. When the scan rate exceeds 10 mV/s, the SC 25min-Cu-P-CF exhibits the highest specific capacitance among all tested scan rates. Based on these findings, Subsequent experiments will concentrate on the SC without the addition of TMPTGE.

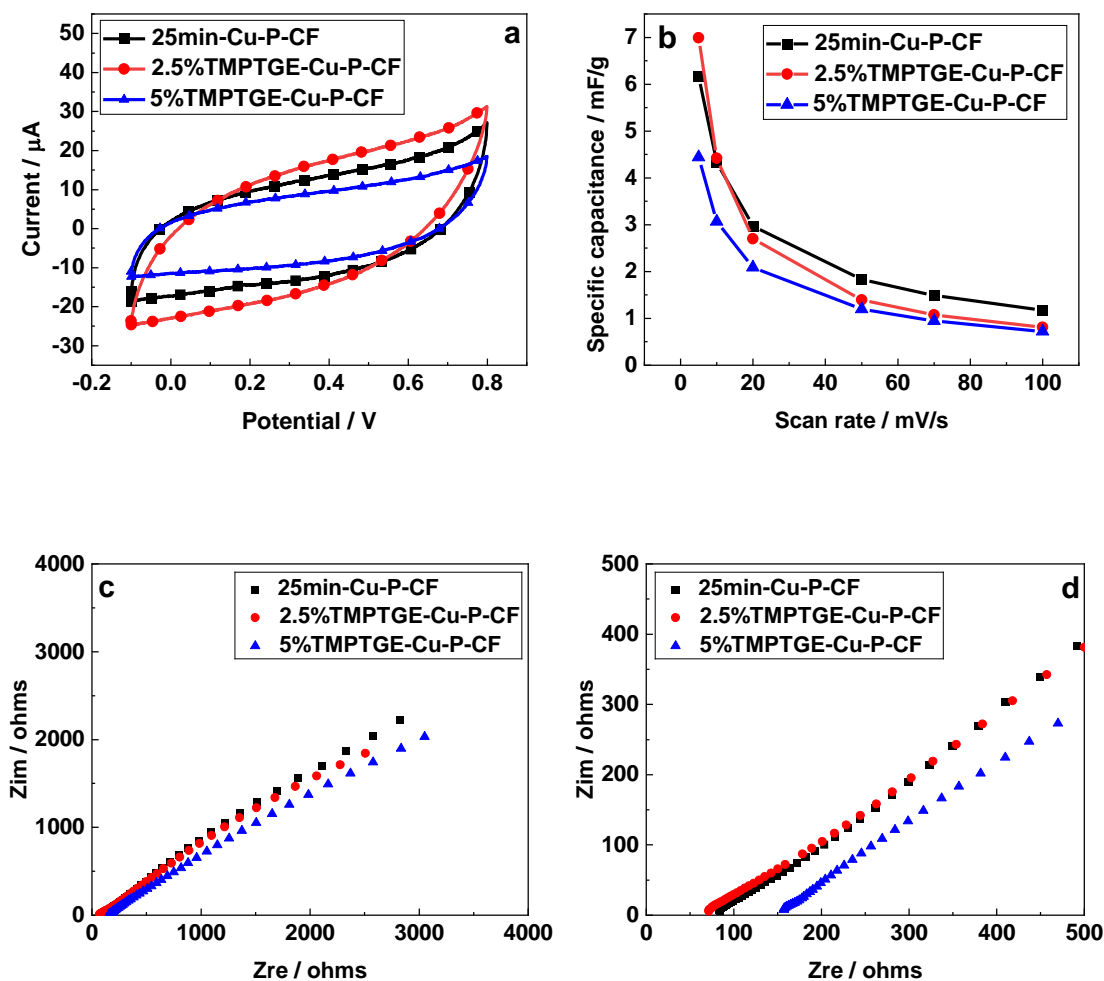


Figure 6- 6. The electrochemical performance of the SCs fabricated with different TMPTGE content. (a) CV curves at the scan rate of 5 mV/s; and (d) variation of specific capacitance as a function of scan rate; (c) Nyquist plots of the SCs; and (d) extended Nyquist plots.

6.4 The effect of adhesive and current collector type on SC performance

The current collector used in the initial study was Cu adhesive tape. However, achieving proper adhesion of this tape to the CF mat requires the two materials to undergo a two-hour curing process to cure the polymer in the adhesive, which is time-consuming. Therefore, Electrodag, containing carbon black and graphite, was used as an alternative adhesive to bond the current collector and electrode material. Electrodag offers conductivity, adhesion, and quick-drying properties (15 min), allowing for the efficient bonding of the Cu strip to CF mat at room temperature. When using electrodag as the

adhesive, the Cu tape used in the previous sections was used as the current collector after removing the polymer adhesive, ensuring that the adhesive was the only variable.

Using electrodag as an adhesive does not change the shape of the CV curves; however, it does result in a significant increase in the area of the CV curves (**Figure 6- 7a**). The larger integral area for 25min-Cu-E-CF suggests a higher specific capacitance. Across all scan rates, the sample employing Electrodag as the adhesive consistently exhibits higher specific capacitance (**Figure 6- 7b**). This phenomenon can be attributed to the enhanced electronic conductivity provided by the Electrodag and/or the improved contact between the current collector and the electrode facilitated by the Electrodag. Within the scope of this study, both SCs achieved their maximum specific capacitance at a scan rate of 5 mV/s, with 25min-Cu-P-CF exhibiting a specific capacitance of 6.17 ± 0.23 mF/g, while 25min-Cu-E-CF showed a value of 24.11 ± 0.31 mF/g. The finding that the specific capacitance of SCs prepared with Electrodag as adhesive is higher than that of using polymer-based adhesives is consistent with the literatures. Kouchachvili et al. [340] employed Electrodag as a binder for the electrode and for attaching the electrode to the current collector. They found that the specific capacitance of SCs using Electrodag is twice that of those employing a polyvinylidene fluoride binder.

The ESR values of 25min-Cu-P-CF and 25min-Cu-E-CF were measured to be 64.85 ± 4.40 Ω and 8.37 ± 0.33 Ω , respectively, with 25min-Cu-E-CF demonstrating a significantly lower ESR value (**Figure 6- 7c and d**). This result is consistent with the findings from the CV test, and the improved performance can be attributed to the use of Electrodag.

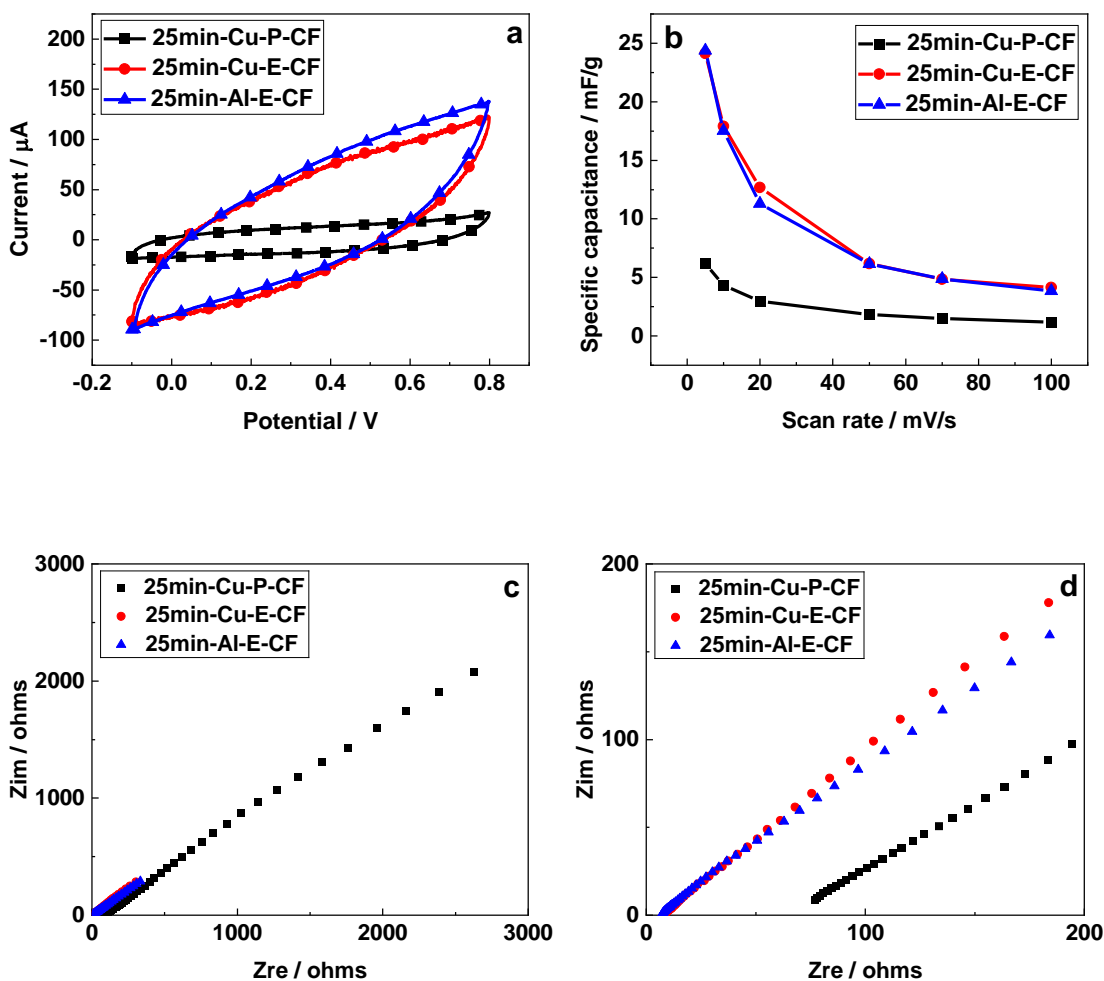


Figure 6- 7. The effect of the adhesive and current collectors on the electrochemical performance of the SCs. (a) CV curves at the scan rate of 5 mV/s; (b) variation of specific capacitance as a function of scan rate; (c) Nyquist plots of the SCs; and (d) extended Nyquist plots.

Subsequently, the performance of the SC using Al strips as the current collector was compared with that of the SC using Cu strips. Al presents several advantages over Cu, including greater flexibility, lighter weight, and cost-effectiveness [341]. The CV curves of the two samples at a scan rate of 5 mV/s are displayed in **Figure 6- 7a**. In addition to their similar shapes, the integrated areas of the two CV curves are also comparable, suggesting that their specific capacitances are similar. This is further illustrated in **Figure 6- 7b**. From 5 mV/s to 100 mV/s, the specific capacitance of the samples remains relatively constant. Within the scope of this study, the samples exhibit their maximum specific capacitance at a scan rate of 5 mV/s, with values of $24.36 \pm 0.36 \text{ mF/g}$ for sample

25min-Al-E-CF and 24.11 ± 0.31 mF/g for sample 25min-Cu-E-CF. The results of the EIS test are shown in **Figure 6- 7c** and d. The patterns of the two Nyquist plots differ slightly. Additionally, the ESR values are 7.52 ± 0.40 Ω for sample 25min-Al-E-CF and 8.37 ± 0.33 Ω for sample 25min-Cu-E-CF. The difference in ESR values is also minimal. The resistance of the Cu strip and Al strip in this study were measured to be 0.02 ± 0.01 Ω and 0.08 ± 0.01 Ω , respectively. This observation confirms that the Cu strip exhibits better conductivity than the Al strip, as support by existing literatures [342-346]. Due to the lower resistance of the Cu strip, it was anticipated that the 25min-Cu-E-CF would demonstrate improved electrochemical performance. However, the SCs based on different strips showed similar CV and EIS results. There are two possible reasons for this phenomenon: first, the Al strip may have better adhesion to the Electrodag, which mitigates the effect of the higher resistance; second, the resistance difference between the Cu and Al strips is relatively small, which not be sufficient to significantly impact the performance of the SCs.

In summary, the use of Electrodag significantly reduces the ESR and increases the specific capacitance of the prepared SC. In addition, compared to Cu adhesive tape, Electrodag greatly shortens the preparation process of SCs, as it eliminates the need for a two-hour curing step. The SCs based on Al strips and Cu strips exhibit similar CV and EIS test results. Considering that the Al strips in this study can be used directly, while the Cu strips require removal of the polymer adhesive from the Cu tape, subsequent experiments will be conducted based on the Al strips.

6.5 Fabricating SCs using spray-on electrodes

When using plain-woven CF mat as the electrode for SCs, the edges of the CF mat tend to curl up, leading to potential short circuit as the two electrodes may come into contact. To address this issue, the MIPE was spread onto a substrate, cured for a period, and then peeled off. However, this method is a bit time-consuming; and the MIPE film's low

degree of solidification at this stage makes it challenging to peel off the film completely from the substrate. Therefore, a new approach was proposed: first, prepare a polyMIPE film, and then apply C spray onto the polyMIPE film. This method has several advantages: (1) it ensures sufficient contact between the electrode and the polyMIPE film, as the carbon black particles in the spray are small and can conform to the surface structure of the polyMIPE film; (2) the fully solidified polyMIPE film can be easily peeled off from the substrate compared to partially solidified MIPE, simplifying the SC preparation process; (3) there is no risk of short circuits caused by electrode contact since the polyMIPE film is fully cured.

The appearance and flexibility of the SC fabricated using C-spray as the electrode material, along with the SEM image of the C-spray electrode are shown in **Figure 6- 8**. Similar to the SC fabricated with CF mats, the polyMIPE film area is larger than the C-spray electrodes to prevent contact between the electrodes (**Figure 6- 8a**). The SC shows high flexibility, as evidenced by the extent to which it can be bent (**Figure 6- 8b**). However, it is important to note that the electrode lacks elasticity, resulting in some observed delamination at the bend. Regarding the morphology of C-spray electrode, as observed in **Figure 6- 8c**, the side of the C-spray in contact with air appears flat, whereas the side in contact with the polyMIPE film appears rough. This roughness is attributed to the C-spray conforming to the irregular surface of the polyMIPE film. The porosity of the C-spray electrode is low (**Figure 6- 8d**). This occurs because the fine carbon particles in the C spray are tightly arranged and bonded together by the polymer in the spray.

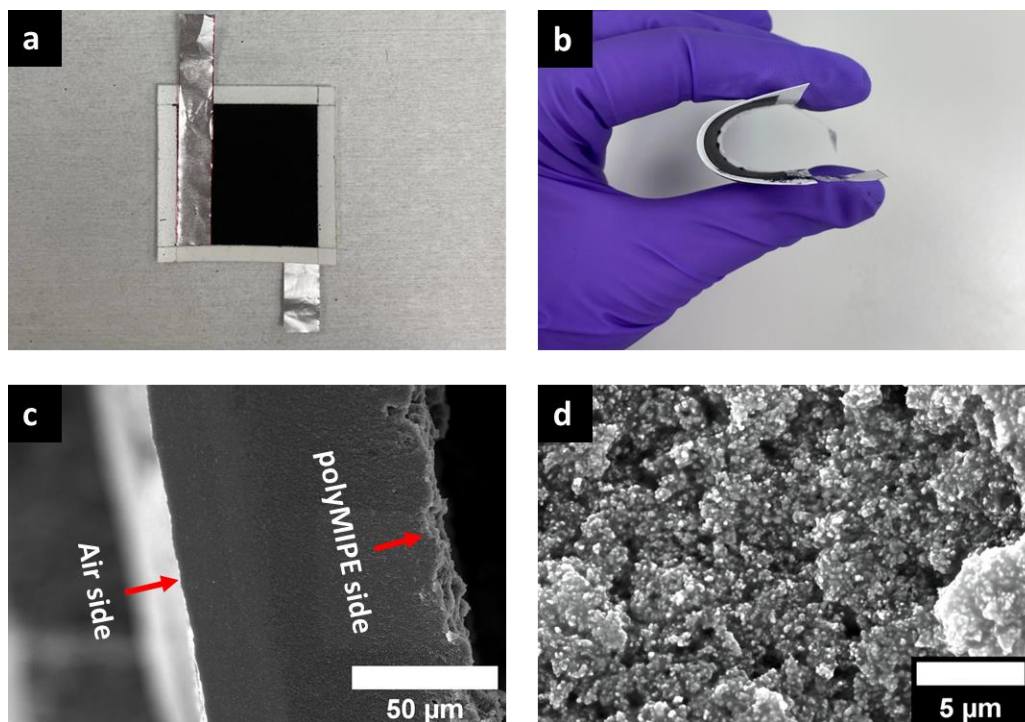


Figure 6- 8. (a) Appearance and (b) the maximum bending degree of the SC using C-spray as the electrodes; (c,d) cross-section of C-spray electrode, ‘Air side’ means the side that contacts the air, and ‘polyMIPE side’ means the side that contacts the polyMIPE film. (Since it is necessary to remove DES for SEM analysis, there is currently no method to do so without damaging the C-spray film. Therefore, the figures c and d present SEM images of the C-spray film that was applied onto a dry polyMIPE film.)

When investigating the electrochemical properties of SCs fabricated with C-spray electrodes, three types of polyMIPE films were employed. The first type is as-synthesized film, which means that the polyMIPE film was not treated in any way; the second type is the sanded polyMIPE film (to remove the skin formed on the surface of the film during the polymerisation); the third type of film is based on the second type of polyMIPE film, with a thin layer of DES was applied onto the polyMIPE film surface to compensate for any loss of DES experienced during the sanding process. The treatment of the polyMIPE film was conducted because the surfaces of the as-synthesized polyMIPE film were not completely open. As illustrated in **Figure 6- 9a** and **b**, independent on the contact surface, i.e. air or substrate, the surface of the resulting film is partially covered with polymer skin. The partial coverage of the polyMIPE film surface aligns with the finding [331], which preparing (EHA-St-DVB) HIPE and cast it onto different substrates. The surface of the

polyMIPE film exposed to air (**Figure 6- 9a**) in this study had a similar structure to the surface of their polyMIPE film exposed to air. Some pores on the skin are attributed to cracking due to shrinkage during polymerisation or air trapped during the experimental process escaping during heating. The skin is attributed to the smaller interfacial tension between DGEBA and air compared to that between DES and air [347, 348]. The surface structure of the polyMIPE film in contact with the substrate (**Figure 6- 9b**) in this study aligns with the observations made in [331] when glass was used as a substrate. The large pores, with diameters exceeding 2 μm , result from the coalescence of the DES droplets. Similar outcomes were reported by Pulko and Krajnc when they cast styrene-DVB HIPE onto a glass substrate [349]. The partially open surfaces could influence the transport of ions in the DES to the electrode, consequently affecting the electrochemical performance of the SC. After sanding (**Figure 6- 9c-f**), the 'skin' on the surface of the polyMIPE can be effectively removed, resulting in the film appearing fully open. Hence, three polyMIPE films were compared to assess the impact of different surface treatments on the performance of SC.

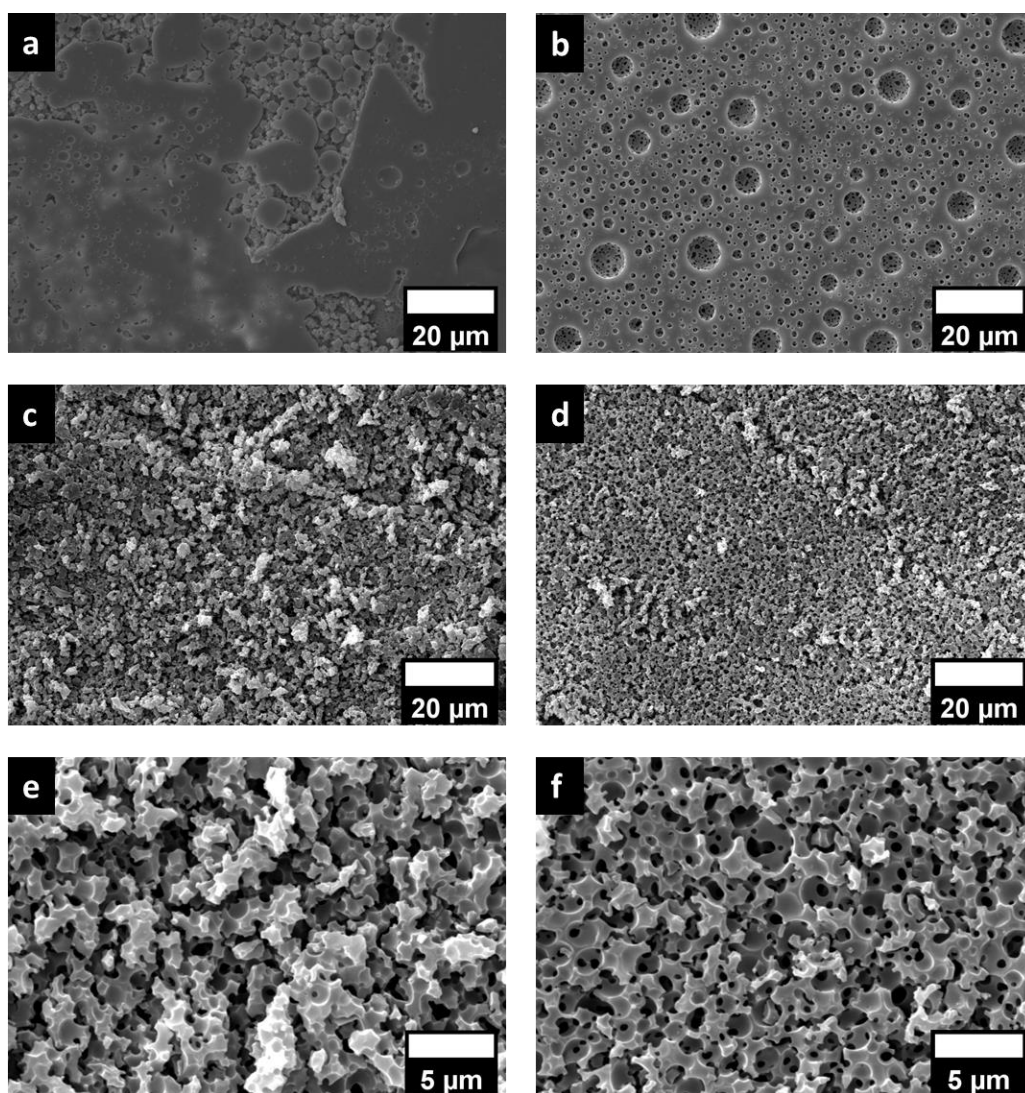


Figure 6- 9. Surface structure of the polyMIPE film. Figures (a)(c) and (e) show the surface of the polyMIPE film on the side facing the air: (a) as synthesized film, (c) sanded film, and (e) enlarged view of the sanded film. Figures (b)(d) and (f) show the surface structure of the polyMIPE film on the side facing the substrate: (b) as synthesized film; (d) sanded film; and (f) enlarged view of the sanded film.

The CV and EIS test results for the SCs fabricated with C-spray as the electrodes are shown in **Figure 6- 10**. In the studied voltage range, all three SCs demonstrate the formation of double layer during the test (**Figure 6- 10a**). The sample based on the sanded polyMIPE film with DES addition shows the largest integrated area. Given that the electrode mass of the three samples is close, this sample exhibits the highest specific capacitance. **Figure 6- 10b** further illustrates the variation in specific capacitance of the sample with the scan rate. Within the scope of this research, the samples As synthesized-Al-E-C Spray, Sanded-Al-E-C Spray, and Sanded+DES-Al-E-C Spray show their

maximum specific capacitance values of 35.16 ± 0.66 , 56.30 ± 1.38 , and 171.68 ± 6.37 mF/g, respectively. Additionally, at all scan rates used, the sample Sanded+DES-Al-E-C Spray exhibits the largest specific capacitances compared to the other two SCs. This improvement is due to the removal of the 'skin' that hinders ion transport after sanding, which facilitates better contact between ions and the electrode. Additionally, compared to the sample that has only been sanded, the sample with DES compensation also addresses the issue of insufficient ions transport medium from the polyMIPE film to the electrodes. For the EIS tests (**Figure 6- 10c-f**), it is evident that two semi-circles appear in the spectra, with the SC based on as-synthesized polyMIPE film shows the largest size for both semi-circles. The semi-circle observed in the higher frequency range could be related to the electrode resistance. Some studies have demonstrated that the electrode resistance will lead to a semi-circle in the high frequency region [350-354]. In this study, when DES is present on the surface of the polyMIPE film, the C spray would be partially dispersed in the DES, which will reduce the thickness of the electrode and the electrode resistance accordingly. The sample As-synthesized-Al-E-C spray exhibits the largest semicircle due to the minimal DES content on the polyMIPE film surface, while the sample Sanded+DES-Al-E-C spray shows the smallest semicircle because there is the most DES on the polyMIPE film surface. The semi-circle observed in the lower frequency region is attributed to ionic resistance [350, 355]. The surface structure of the electrode adjacent to the polyMIPE film is influenced by the surface conditions of polyMIPE, including polyMIPE's structure and DES content. When the polyMIPE film was sanded and then compensated with DES, the C-spray was applied onto the DES and DGEBA. This enables direct contact between the DES and the electrode, allowing for unobstructed ions transport; in the case of as-synthesized polyMIPE film, the polyMIPE surface is partially covered, ions within the DES faced greater challenge in reaching the electrode; sanding the polyMIPE film reduces the size of semi-circle, but it still larger than that observed in

the film after compensation with DES, which is caused by the lack of ions transport medium from the polyMIPE film to the electrodes.

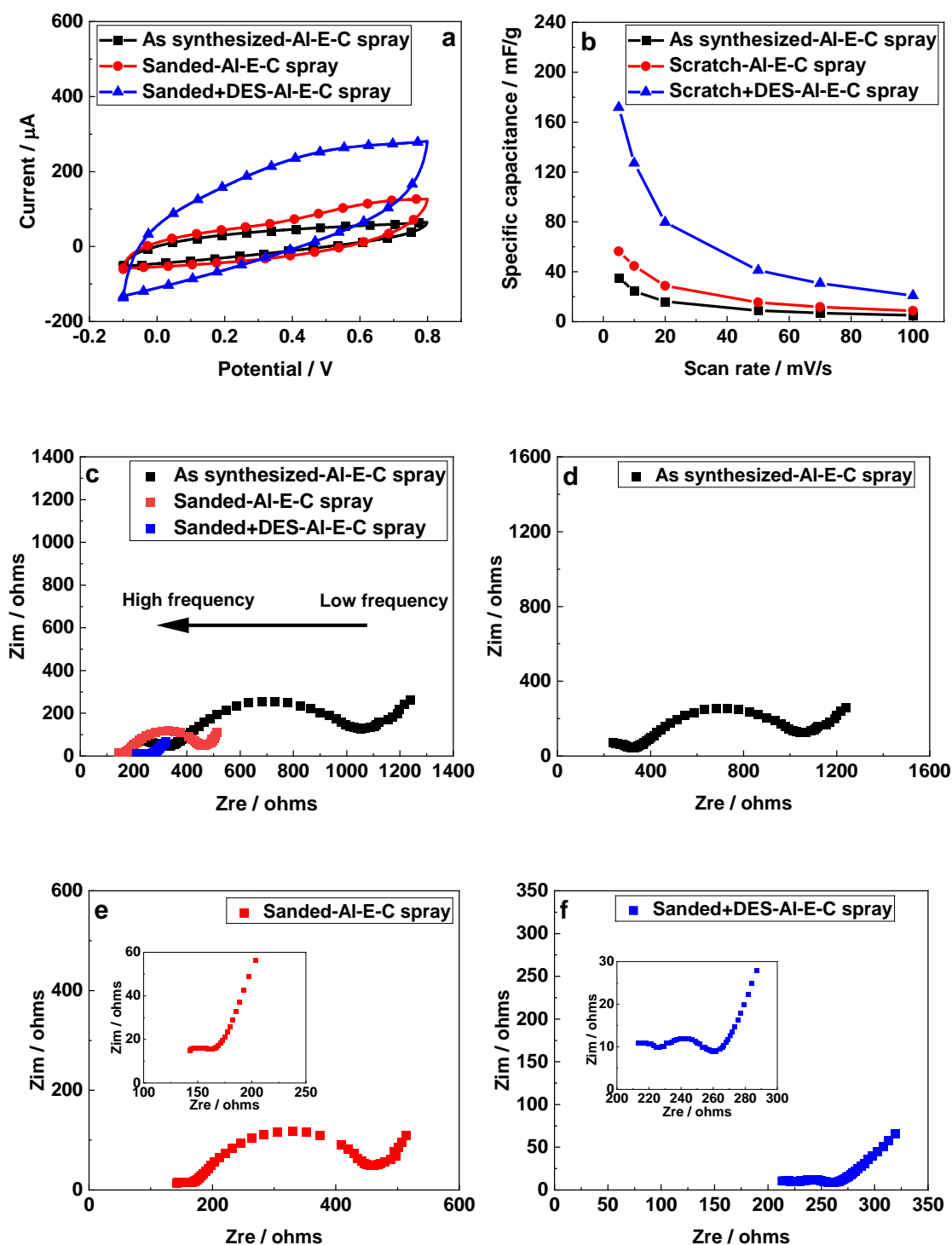


Figure 6- 10. The electrochemical performance of the SCs fabricated using C-spray as the electrode. (a) cyclic voltammety (CV) curves at the scan rate of 5 mV/s; (b) variation of specific capacitance as a function of scan rate; (c) Nyquist plots of the SCs. Nyquist plot for (d)As synthesized-Al-E-C spray; (e) Sanded-Al-E-C spray; and (f) Sanded+DES-Al-E-C spray.

In addition to C-spray, this study also explored the possibility of fabricating SC using Ni-spray to form the electrodes. The primary motivation for choosing Ni-spray is its lower resistance compared to C-spray, as indicated by the technical data sheet [223, 356]. This suggests that a SC fabricated using Ni-spray may offer improved electrochemical performance. The SC fabricated using Ni-spray as the electrode does not exhibit significant difference in appearance and flexibility compared to C-spray (**Figure 6- 11a** and **b**). However, **Figure 6- 11c** and **d** indicate that the Ni-spray electrode possessed larger pores compared to the C-spray electrode. This structural difference stems from the different forms of Ni and carbon black used in the sprays. The Ni is in big flake form, which prevents tight packing to form a compact electrode structure. In contrast, the small size of carbon black particles allows for tighter packing. Furthermore, the bonding polymer present in the C spray further fills the gaps between the carbon black particles.

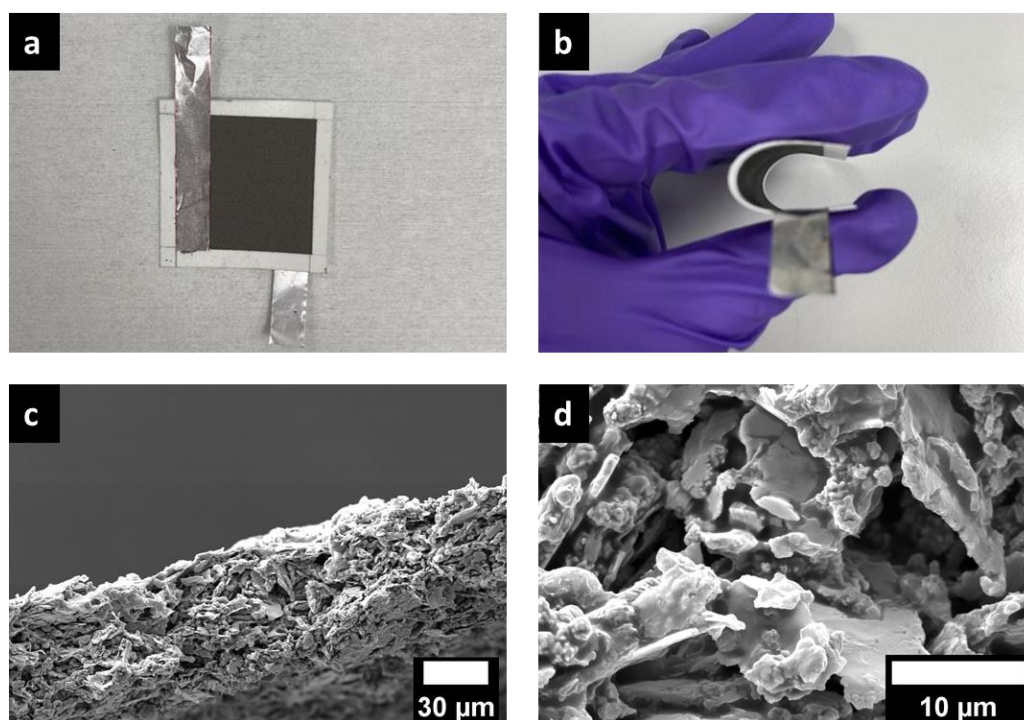


Figure 6- 11. (a) Appearance and (b) the maximum bending degree of the SC using Ni-spray as the electrodes; (c,d) SEM image of the Ni-spray electrode.

The SC based on Ni-spray electrodes stores charges by forming an electrical double layer (**Figure 6- 12a**). A nonlinear increase in current is observed when the voltage exceeds

0.4V, which may be attributed to the Faradic reactions in the SC [285, 357]. The specific capacitance of the SC decreases with increasing scan rate (**Figure 6- 12b**), with a maximum specific capacitance of 1.25 ± 0.04 mF/g. The lower specific capacitance observed when Ni-spray was used as the electrode compared to C-spray may be attributed to the nature of the active material. Compared to C-spray, the active material in Ni-spray are big flakes that cannot fully conform to the porous surface of the polyMIPE film and possess smaller specific surface area, resulting in poorer contact between the ions and the electrodes. The EIS plot (**Figure 6- 12c**) distinctly shows a distorted semi-circle in the high frequency region, representing the R_{ct} , and a straight line in the low frequency region. The ESR of the SC based on Ni-spray is 15.49 ± 0.9 Ω .

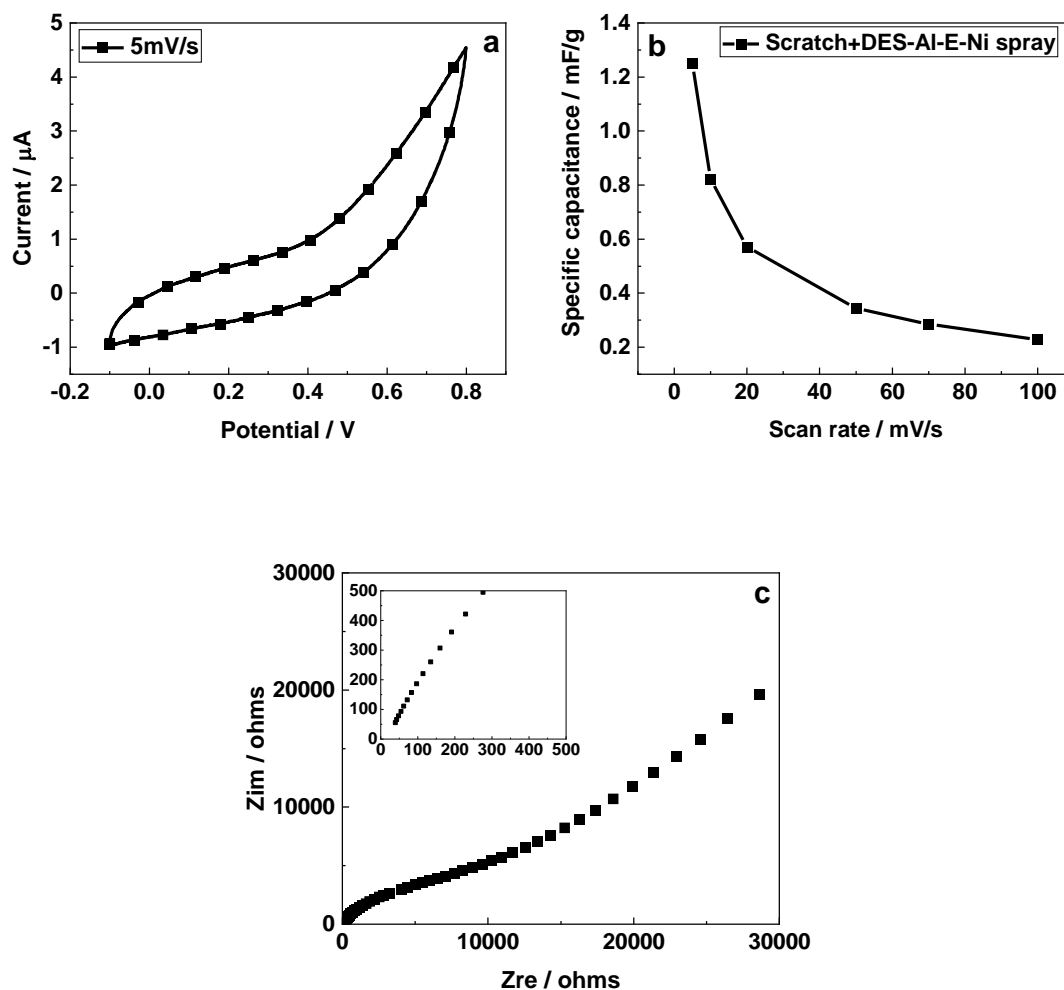


Figure 6- 12. The electrochemical performance of the SCs fabricated using Ni-spray electrode. (a) cyclic voltammetry (CV) curves at the scan rate of 5 mV/s; (b) variation of specific capacitance as a function of scan rate; and (c) Nyquist plots of the SCs.

6.6 Summary

The chapter primarily focuses on the preparation of SC based on polyMIPE film. Initially, we tried to apply MIPE directly on the CF mat, but the MIPE was easily penetrated by the fibre bundle at the edge of the CF mat, causing contact between the two CF mats. To address this issue, it was decided to firstly apply the MIPE film onto a substrate. After allowing the film to partially cure for 25 minutes, the first CF mat was placed onto the film. After an additional 15 minutes, the film could be peeled off the substrate, and the second CF mat was placed on the other side of the film. Since the film was not fully cured at this stage, the bonding between the film and the CF mat was maintained. The effect of

TMPTGE addition on the SC's performance was also investigated. The addition of 5 wt.% TMPTGE resulted in a decrease in specific capacitance and an increase in the ESR of the SC, while the addition of 2.5 wt.% TMPTGE did not significantly impact the performance of the SC. The use of Electrodag as the adhesive between the electrode and the current collector significantly enhanced the electrochemical performance of the SC. Additionally, employing Al and Cu strips as current collectors yields similar results in terms of specific capacitance and ESR of the SCs. The above studies were all conducted using CF mat as the electrode. To simplify the SC fabrication process and enhance the contact area between the polyMIPE film and the electrode, the feasibility of using spray as the electrode was explored. The results indicated that among all the SCs in this study, the specific capacitance of the three samples using C-spray as electrodes ranks in the top three (**Figure 6- 13**), with Sanded+DES-Al-E-C spray exhibiting the highest specific capacitance, primarily due to the excellent contact between the DES and the electrodes. These findings highlight the potential to improve SCs performance through optimization of fabrication methods and constituent materials. The electrochemical performance of SCs was enhanced by improving the contact between key components (current collector and electrode, as well as electrode and polyMIPE). This research will contribute to advancing the practical applications of polyMIPE-based SCs.

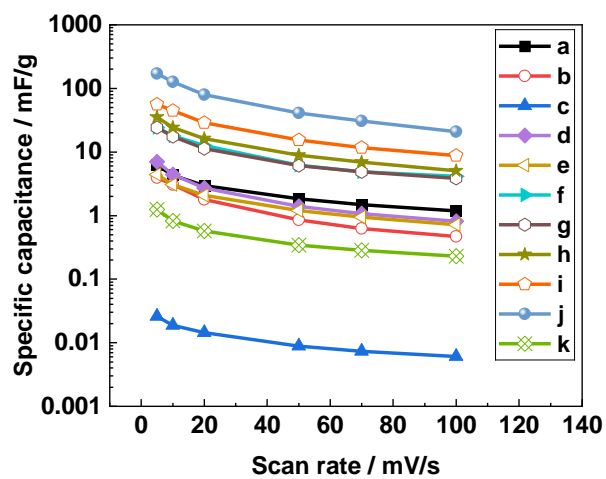


Figure 6- 13. Variation in specific capacitance of all SCs in this chapter as a function of scan rate. (a) 25min-Cu-P-CF; (b) 40min-Cu-P-CF; (c) Fully cured-Cu-P-CF; (d) 2.5%TMPTGE-Cu-P-CF; (e) 5%TMPTGE-Cu-P-CF; (f) 25min-Cu-E-CF; (g) 25min-Al-E-CF; (h) As synthesized-Al-E-C spray; (i) Sanded-Al-E-C spray; (j) Sanded+DES-Al-E-C spray; (k) Sanded+DES-Al-E-Ni spray.

7 Conclusions and recommendation future works

7.1 Conclusions

The aim of this thesis was to develop a DPE for SCs using emulsion-templating method. The DPE is comprised a liquid phase and solid phase, with the liquid phase consisting of a DES that provides ionic conductivity, while the primarily component of the solid phase was DGEBA, which ensured good mechanical performance. The emulsion-templating method involves dispersing the internal phase (liquid phase in the DPE) within the external phase, followed by solidifying the external phase (solid phase in the DPE). This process often employs surfactants to stabilize the emulsion.

This research reported in this thesis firstly explored suitable surfactants for stabilising the MIPE, as well as the effects of surfactant content, DES addition rate, and stirring speed on the properties of polyMIPEs. Among the four surfactants discussed, Atlox 4912SF-SO-(MV) and Cithrol DPHS-SO-(MV) were suitable for preparing polyMIPEs with an interconnected pore structure. The ideal DPE exhibits both high mechanical performance (Young's modulus > 500 kPa [4]) and high ionic conductivity (> 1 mS/cm [5]); however, improving these two properties simultaneously presents challenges as some factors always have opposite effects on them. For example, a smaller pore size enhances mechanical performance of polyMIPEs; but it simultaneously increases the tortuosity of the pore structure, affecting ion transport and consequently reducing ionic conductivity. In this thesis, the compressive mechanical performance of polyMIPE was optimal at a surfactant content of 15 wt.% and a DES addition rate of 6 ml/min, achieving a Young's modulus of 142.6 ± 4.2 MPa. At this point, ionic conductivity was minimised at 4.53 ± 0.21 mS/cm, primarily due to the smallest pore size achieved under these conditions. The change of stirring speed showed no significant effect on the properties of polyMIPEs. The ionic conductivities of all polyMIPEs obtained in Chapter 4 ranged from 4.53 mS/cm to

5.32 mS/cm, which is lower than the 8.16 mS/cm observed for neat DES, as ions in DES were hindered from moving through the tortuous pores of polyMIPEs.

After determining the optimal conditions for preparing polyMIPE, the next step was to cast the MIPE into a film, as the DPE in SCs is typically in film form, which helps reduce the device's ESR. The primary challenge was the high viscosity of the emulsion, which hinders its spreading. This issue becomes even more critical when considering large-scale preparation of polyMIPE films for future industrial applications. The high viscosity of the emulsion primarily stems from its external phase- DGEBA. Hence, a reactive diluent- TMPTGE- was introduced into the external phase. The results show that adding 5 wt.% TMPTGE significantly reduced viscosity, though further additions had diminishing effects. Furthermore, the introduction of TMPTGE resulted in a reduction of the compressive mechanical properties of bulk polyMIPE, while increasing its ionic conductivity. After casting the MIPE into a film and then curing, it was found that the pore size of the polyMIPE film was smaller than that of the bulk polyMIPE under the same formulations. This is attributed to the rapid heat propagation in the thinner MIPE, leading to faster curing and hence a shorter coalescence time for the DES droplets. The tensile modulus (540.5 ± 20.3 MPa) of the polyMIPE film was highest without the addition of TMPTGE. However, the toughness (166.1 ± 26.1 MPa) reached the maximum value when the TMPTGE addition was 5wt.%. In terms of ionic conductivity, the maximum value (0.92 ± 0.04 mS/cm) was achieved at 2.5 wt.% TMPTGE, with further additions having little effect on the conductivity.

The last part of this study was to prepare a SC based on DES-in-DGEBA polyMIPE. Compared to the method where MIPE was fully cured before combining it with CF mats serving as electrodes, combining the CF mats with partially cured MIPE led to an improvement in the specific capacitance and reduction in ESR of the SC. Additionally,

this method ensured effective adhesion between the polyMIPE film and the CF mats, enabling the fabrication of a complete device without the need for an additional adhesive.

The reason for not applying MIPE directly onto the CF mat was that the edges of the CF mat were prone to penetrate the MIPE, which could potentially lead to a short circuit. Subsequently, the effects of varying TMPTGE contents, different adhesives between current collectors and electrodes, and different current collector materials on the performance of the SC were studied. The results indicated that with a TMPTGE addition of 2.5 wt.%, the SC performance was comparable to that observed without TMPTGE. However, increasing the TMPTGE addition to 5 wt.% resulted in a decrease in specific capacitance and an increase in ESR. This phenomenon is likely related to the impact of TMPTGE on the openness of the polyMIPE film surface, which subsequently affects the contact between the DES and the CF mats. The use of Al strips as current collectors yielded results similar to those obtained with Cu current collectors. Notably, when the polymer adhesive was replaced with the electrodag, the specific capacitance of the SC increased from 6.61 ± 0.11 mF/g to 24.11 ± 0.31 mF/g, while the ESR decreased from 73.36 ± 6.40 Ω to 8.37 ± 0.33 Ω . The method of directly spraying the electrode material onto the polyMIPE film was also employed to prepare the SC. In this study, C-spray and Ni-spray were used, with results indicating that C-spray obtained better performance. Compared to CF mat, the active materials in C-spray were tiny particles that better conform to the surface structure of the polyMIPE film, leading to a significant increase in specific capacitance, which reaches 171.68 ± 6.37 mF/g.

The objective of this study was to prepare a DPE for SC that combines both good mechanical performance (Young's modulus > 500 kPa [4]) and ionic conductivity (> 1 mS/cm [5]). The polyMIPE synthesized in this study meets the expectations, with a maximum tensile Young's modulus of 540.5 ± 20.3 MPa and ionic conductivity of 0.95 ± 0.03 mS/cm. This polyMIPE overcomes the limitations of liquid and gel electrolytes,

which suffer from low mechanical performance, as well as the disadvantage of low ionic conductivity in solid electrolytes. SCs fabricated with this polyMIPE exhibit flexibility, making them suitable for applications in wearable devices, foldable electronics, and other similar fields.

7.2 Recommendations for future works

This study successfully prepared DES-in-DGEBA polyMIPE and demonstrated its feasibility for application in SC. Future developments of this research could focus on the following areas:

1. The preferred thickness for commercial separators is less than 25 μm [43]. Although casting MIPE into 25 μm films is feasible, a significant challenge stems from the weakness of polyMIPE films, which makes the films prone to breaking when peeled from the substrate. Future research could investigate the surface openness of polyMIPE films after MIPE is cast onto various substrates, as increased surface openness means there is less DGEBA on the polyMIPE film surface bonding to the substrate, thereby facilitating the peeling of the polyMIPE film.
2. In addition to casting MIPE onto substrates, other methods can also be employed to prepare polyMIPE films, such as slicing bulk polyMIPE to a defined thickness using a microtome or laser cutter. This approach avoids the potential impacts of the casting process on the MIPE structure.
3. The main component of the external phase of MIPE in this study is DGEBA, which polymerises rapidly. After the MIPE was prepared, it lost its fluidity after approximately 30 min. To extend the workable time for spreading MIPE, future work could explore the use of materials with slower polymerisation rates as the external phase.
4. The edges of the CF mat used in this study were prone to curling up and penetrating the MIPE, which prevented the direct spreading of MIPE onto the CF mat. An

alternative approach is to prepare a carbon slurry (electrode) and cast it onto an Al/Cu current collector, followed by spreading MIPE on the dried slurry [358, 359]. This method enables direct spreading of MIPE on the electrode, avoiding the need to peel the polyMIPE film from the substrate, thus simplifying the SC fabrication process. Additionally, this method ensures a strong bond between the electrode and the polyMIPE film.

8 References

- [1] A. Mishra, N. P. Shetti, S. Basu, K. R. Reddy, and T. M. Aminabhavi, "Chapter 7 - Recent developments in ionic liquid-based electrolytes for energy storage supercapacitors and rechargeable batteries," *Green Sustainable Process for Chemical and Environmental Engineering and Science*, Inamuddin, A. M. Asiri and S. Kanchi, eds., pp. 199-221: Elsevier, 2020.
- [2] M. Z. Iqbal, S. Zakar, and S. S. Haider, "Role of aqueous electrolytes on the performance of electrochemical energy storage device," *Journal of Electroanalytical Chemistry*, vol. 858, pp. 113793, 2020/02/01/, 2020.
- [3] S. Samantaray, D. Mohanty, I. M. Hung, M. Moniruzzaman, and S. K. Satpathy, "Unleashing recent electrolyte materials for next-generation supercapacitor applications: A comprehensive review," *Journal of Energy Storage*, vol. 72, pp. 108352, 2023/11/20/, 2023.
- [4] X. Guo, J. Li, F. Wang, J. H. Zhang, J. Zhang, Y. Shi, and L. Pan, "Application of conductive polymer hydrogels in flexible electronics," *Journal of Polymer Science*, vol. 60, no. 18, pp. 2635-2662, 2022.
- [5] Y. Wang, X. Qiao, C. Zhang, and X. Zhou, "Development of all-solid-state structural supercapacitor using an epoxy based adhesive polymer electrolyte," *ECS Transactions*, vol. 72, no. 8, pp. 31, 2016.
- [6] Q. Zhang, K. D. O. Vigier, S. Royer, and F. Jérôme, "Deep eutectic solvents: syntheses, properties and applications," *Chemical Society Reviews*, vol. 41, no. 21, pp. 7108-7146, 2012.
- [7] Y. Wang, L. Zhang, H. Hou, W. Xu, G. Duan, S. He, K. Liu, and S. Jiang, "Recent progress in carbon-based materials for supercapacitor electrodes: a review," *Journal of Materials Science*, vol. 56, no. 1, pp. 173-200, 2021/01/01, 2021.
- [8] V. Molahalli, C. K. M. K. Singh, M. Agrawal, S. G. Krishnan, and G. Hegde, "Past decade of supercapacitor research – Lessons learned for future innovations," *Journal of Energy Storage*, vol. 70, pp. 108062, 2023/10/15/, 2023.
- [9] M. Pershaanaa, S. Bashir, S. Ramesh, and K. Ramesh, "Every bite of Supercap: A brief review on construction and enhancement of supercapacitor," *Journal of Energy Storage*, vol. 50, pp. 104599, 2022/06/01/, 2022.
- [10] L. Zhang, X. Hu, Z. Wang, F. Sun, and D. G. Dorrell, "A review of supercapacitor modeling, estimation, and applications: A control/management perspective," *Renewable and Sustainable Energy Reviews*, vol. 81, pp. 1868-1878, 2018/01/01/, 2018.
- [11] S. Sharma, and P. Chand, "Supercapacitor and electrochemical techniques: A brief review," *Results in Chemistry*, vol. 5, pp. 100885, 2023/01/01/, 2023.
- [12] A. Dutta, S. Mitra, M. Basak, and T. Banerjee, "A comprehensive review on batteries and supercapacitors: Development and challenges since their inception," *Energy Storage*, vol. 5, no. 1, pp. e339, 2023.
- [13] W. Raza, F. Ali, N. Raza, Y. Luo, K.-H. Kim, J. Yang, S. Kumar, A. Mehmood, and E. E. Kwon, "Recent advancements in supercapacitor technology," *Nano Energy*, vol. 52, pp. 441-473, 2018/10/01/, 2018.
- [14] B. Aldemir Dikici, and F. Claeysens, "Basic principles of emulsion templating and its use as an emerging manufacturing method of tissue engineering scaffolds," *Frontiers in bioengineering and biotechnology*, vol. 8, pp. 875, 2020.
- [15] N. Shirshova, P. Johansson, M. J. Marczewski, E. Kot, D. Ensling, A. Bismarck, and J. H. Steinke, "Polymerised high internal phase ionic liquid-in-oil emulsions as potential separators for lithium ion batteries," *Journal of Materials Chemistry A*, vol. 1, no. 34, pp. 9612-9619, 2013.
- [16] F. G. Garcia, B. G. Soares, V. J. R. R. Pita, R. Sánchez, and J. Rieumont, "Mechanical properties of epoxy networks based on DGEBA and aliphatic amines," *Journal of Applied Polymer Science*, vol. 106, no. 3, pp. 2047-2055, 2007.

- [17] X. Mi, N. Liang, H. Xu, J. Wu, Y. Jiang, B. Nie, and D. Zhang, "Toughness and its mechanisms in epoxy resins," *Progress in Materials Science*, vol. 130, pp. 100977, 2022/10/01/, 2022.
- [18] M. Janvier, L. Hollande, A. S. Jaufurally, M. Pernes, R. Ménard, M. Grimaldi, J. Beaugrand, P. Balaguer, P. H. Ducrot, and F. Allais, "Syringaresinol: a renewable and safer alternative to bisphenol A for epoxy-amine resins," *ChemSusChem*, vol. 10, no. 4, pp. 738-746, 2017.
- [19] P. Forouzandeh, V. Kumaravel, and S. C. Pillai, "Electrode materials for supercapacitors: a review of recent advances," *Catalysts*, vol. 10, no. 9, pp. 969, 2020.
- [20] R. Dhillip Kumar, S. Nagarani, V. Sethuraman, S. Andra, and V. Dhinakaran, "Investigations of conducting polymers, carbon materials, oxide and sulfide materials for supercapacitor applications: a review," *Chemical Papers*, vol. 76, no. 6, pp. 3371-3385, 2022.
- [21] B. K. Saikia, S. M. Benoy, M. Bora, J. Tamuly, M. Pandey, and D. Bhattacharya, "A brief review on supercapacitor energy storage devices and utilization of natural carbon resources as their electrode materials," *Fuel*, vol. 282, pp. 118796, 2020.
- [22] N. Kumar, S.-B. Kim, S.-Y. Lee, and S.-J. Park, "Recent advanced supercapacitor: a review of storage mechanisms, electrode materials, modification, and perspectives," *Nanomaterials*, vol. 12, no. 20, pp. 3708, 2022.
- [23] Z. Li, K. Xu, and Y. Pan, "Recent development of supercapacitor electrode based on carbon materials," *Nanotechnology Reviews*, vol. 8, no. 1, pp. 35-49, 2019.
- [24] L. Miao, Z. Song, D. Zhu, L. Li, L. Gan, and M. Liu, "Recent advances in carbon-based supercapacitors," *Materials Advances*, vol. 1, no. 5, pp. 945-966, 2020.
- [25] G. Kothandam, G. Singh, X. Guan, J. M. Lee, K. Ramadass, S. Joseph, M. Benzigar, A. Karakoti, J. Yi, and P. Kumar, "Recent Advances in Carbon-Based Electrodes for Energy Storage and Conversion," *Advanced Science*, vol. 10, no. 18, pp. 2301045, 2023.
- [26] Z. S. Iro, C. Subramani, and S. S. Dash, "A Brief Review on Electrode Materials for Supercapacitor," *International Journal of Electrochemical Science*, vol. 11, no. 12, pp. 10628-10643, 2016/12/01/, 2016.
- [27] A. Barroso Bogeat, "Understanding and Tuning the Electrical Conductivity of Activated Carbon: A State-of-the-Art Review," *Critical Reviews in Solid State and Materials Sciences*, vol. 46, no. 1, pp. 1-37, 2021/01/02, 2021.
- [28] G. A. Snook, P. Kao, and A. S. Best, "Conducting-polymer-based supercapacitor devices and electrodes," *Journal of Power Sources*, vol. 196, no. 1, pp. 1-12, 2011/01/01/, 2011.
- [29] S. Wustoni, D. Ohayon, A. Hermawan, A. Nuruddin, S. Inal, Y. S. Indartono, and B. Yulianto, "Material design and characterization of conducting polymer-based supercapacitors," *Polymer Reviews*, vol. 64, no. 1, pp. 192-250, 2024.
- [30] A. Thejas Prasannakumar, R. R. Mohan, M. V, and S. J. Varma, "Progress in Conducting Polymer-Based Electrospun fibers for Supercapacitor Applications: A Review," *ChemistrySelect*, vol. 8, no. 17, pp. e202203564, 2023.
- [31] A. Sharma, and S. Sharma, "Review of power electronics in vehicle-to-grid systems," *Journal of Energy Storage*, vol. 21, pp. 337-361, 2019/02/01/, 2019.
- [32] S. Y. Attia, S. G. Mohamed, Y. F. Barakat, H. H. Hassan, and W. A. Zoubi, "Supercapacitor electrode materials: addressing challenges in mechanism and charge storage," *Reviews in Inorganic Chemistry*, vol. 42, no. 1, pp. 53-88, 2022.
- [33] I. Shaheen, I. Hussain, T. Zahra, M. S. Javed, S. S. A. Shah, K. Khan, M. B. Hanif, M. A. Assiri, Z. Said, and W. U. Arifeen, "Recent advancements in metal oxides for energy storage materials: design, classification, and electrodes configuration of supercapacitor," *Journal of Energy Storage*, vol. 72, pp. 108719, 2023.
- [34] C. An, Y. Zhang, H. Guo, and Y. Wang, "Metal oxide-based supercapacitors: progress and perspectives," *Nanoscale Advances*, vol. 1, no. 12, pp. 4644-4658, 2019.
- [35] B. Pal, S. Yang, S. Ramesh, V. Thangadurai, and R. Jose, "Electrolyte selection for supercapacitive devices: A critical review," *Nanoscale Advances*, vol. 1, no. 10, pp. 3807-3835, 2019.
- [36] P. Lokhande, and U. Chavan, "Inorganic Electrolytes in Supercapacitor," pp. 11-30, 2019.

- [37] A. Mendhe, and H. Panda, "A review on electrolytes for supercapacitor device," *Discover Materials*, vol. 3, no. 1, pp. 29, 2023.
- [38] S. Biswas, and A. Chowdhury, "Organic supercapacitors as the next generation energy storage device: emergence, opportunity, and challenges," *ChemPhysChem*, vol. 24, no. 3, pp. e202200567, 2023.
- [39] S. Schweizer, J. Landwehr, B. J. M. Etzold, R. H. Meißner, M. Amkreutz, P. Schiffels, and J.-R. Hill, "Combined Computational and Experimental Study on the Influence of Surface Chemistry of Carbon-Based Electrodes on Electrode–Electrolyte Interactions in Supercapacitors," *The Journal of Physical Chemistry C*, vol. 123, no. 5, pp. 2716-2727, 2019/02/07, 2019.
- [40] A. González, E. Goikolea, J. A. Barrena, and R. Mysyk, "Review on supercapacitors: Technologies and materials," *Renewable and sustainable energy reviews*, vol. 58, pp. 1189-1206, 2016.
- [41] S. Ahankari, D. Lasrado, and R. Subramaniam, "Advances in materials and fabrication of separators in supercapacitors," *Materials Advances*, vol. 3, no. 3, pp. 1472-1496, 2022.
- [42] N. Raza, K. Aziz, M. S. Javed, R. Tariq, N. Kanwal, W. Raza, M. Sarfraz, S. Khan, M. A. Ismail, B. Akkinepally, and X. Wang, "Advancements in separator design for supercapacitor technology: A review of characteristics, manufacturing processes, limitations, and emerging trends," *Journal of Energy Storage*, vol. 111, pp. 115328, 2025/03/01/, 2025.
- [43] K. K. Kar, *Handbook of nanocomposite supercapacitor materials II*: Springer, 2020.
- [44] S. S. Ahankari, D. Lasrado, and S. Ramesh, "Advances in materials and fabrication of separators in supercapacitors," *Materials Advances*, 2022.
- [45] A. Abdisattar, M. Yeleuov, C. Daulbayev, K. Askaruly, A. Tolyzbekov, A. Taurbekov, and N. Prikhodko, "Recent advances and challenges of current collectors for supercapacitors," *Electrochemistry Communications*, vol. 142, pp. 107373, 2022/09/01/, 2022.
- [46] H. Hao, R. Tan, C. Ye, and C. T. J. Low, "Carbon-coated current collectors in lithium-ion batteries and supercapacitors: Materials, manufacture and applications," *Carbon Energy*, pp. e604, 2024.
- [47] Y. Xu, W. Lu, G. Xu, and T.-W. Chou, "Structural supercapacitor composites: A review," *Composites Science and Technology*, vol. 204, pp. 108636, 2021/03/01/, 2021.
- [48] "Murata Americas, https://www.mouser.com/pdfDocs/Murata-DMF-DMT_TechnicalGuide.pdf. Accessed Sept 2013.."
- [49] D. L. Chapman, "LI. A contribution to the theory of electrocapillarity," *The London, Edinburgh, and Dublin philosophical magazine and journal of science*, vol. 25, no. 148, pp. 475-481, 1913.
- [50] M. Gouy, "Sur la constitution de la charge électrique à la surface d'un électrolyte," *J. Phys. Theor. Appl.*, vol. 9, no. 1, pp. 457-468, 1910.
- [51] L. L. Zhang, and X. Zhao, "Carbon-based materials as supercapacitor electrodes," *Chemical Society Reviews*, vol. 38, no. 9, pp. 2520-2531, 2009.
- [52] J. Zhao, C. Lai, Y. Dai, and J. Xie, "Pore structure control of mesoporous carbon as supercapacitor material," *Materials Letters*, vol. 61, no. 23, pp. 4639-4642, 2007/09/01/, 2007.
- [53] N. N. Loganathan, V. Perumal, B. R. Pandian, R. Atchudan, T. N. J. I. Edison, and M. Ovinis, "Recent studies on polymeric materials for supercapacitor development," *Journal of Energy Storage*, vol. 49, pp. 104149, 2022/05/01/, 2022.
- [54] T. Brousse, D. Bélanger, and J. W. Long, "To be or not to be pseudocapacitive?," *Journal of The Electrochemical Society*, vol. 162, no. 5, pp. A5185, 2015.
- [55] N. R. Chodankar, H. D. Pham, A. K. Nanjundan, J. F. Fernando, K. Jayaramulu, D. Golberg, Y. K. Han, and D. P. Dubal, "True meaning of pseudocapacitors and their performance metrics: asymmetric versus hybrid supercapacitors," *Small*, vol. 16, no. 37, pp. 2002806, 2020.

- [56] R. Chen, M. Yu, R. P. Sahu, I. K. Puri, and I. Zhitomirsky, "The development of pseudocapacitor electrodes and devices with high active mass loading," *Advanced Energy Materials*, vol. 10, no. 20, pp. 1903848, 2020.
- [57] B. Senthilkumar, Z. Khan, S. Park, K. Kim, H. Ko, and Y. Kim, "Highly porous graphitic carbon and Ni₂P₂O₇ for a high performance aqueous hybrid supercapacitor," *Journal of Materials Chemistry A*, vol. 3, no. 43, pp. 21553-21561, 2015.
- [58] A. Muzaffar, M. B. Ahamed, K. Deshmukh, and J. Thirumalai, "A review on recent advances in hybrid supercapacitors: Design, fabrication and applications," *Renewable and Sustainable Energy Reviews*, vol. 101, pp. 123-145, 2019/03/01/, 2019.
- [59] A. Mendhe, and H. S. Panda, "A review on electrolytes for supercapacitor device," *Discover Materials*, vol. 3, no. 1, pp. 29, 2023/10/26, 2023.
- [60] P. Lokhande, and U. Chavan, "Inorganic electrolytes in supercapacitor." pp. 11-30.
- [61] C. Zhong, Y. Deng, W. Hu, J. Qiao, L. Zhang, and J. Zhang, "A review of electrolyte materials and compositions for electrochemical supercapacitors," *Chemical Society Reviews*, vol. 44, no. 21, pp. 7484-7539, 2015.
- [62] J. Li, J. Qiao, and K. Lian, "Hydroxide ion conducting polymer electrolytes and their applications in solid supercapacitors: a review," *Energy Storage Materials*, vol. 24, pp. 6-21, 2020.
- [63] M. Sajjad, M. I. Khan, F. Cheng, and W. Lu, "A review on selection criteria of aqueous electrolytes performance evaluation for advanced asymmetric supercapacitors," *Journal of Energy Storage*, vol. 40, pp. 102729, 2021/08/01/, 2021.
- [64] A. Acharjee, and B. Saha, "Organic electrolytes in electrochemical supercapacitors: Applications and developments," *Journal of Molecular Liquids*, vol. 400, pp. 124487, 2024/04/15/, 2024.
- [65] C. Xiong, Y. Zhang, and Y. Ni, "Recent progress on development of electrolyte and aerogel electrodes applied in supercapacitors," *Journal of Power Sources*, vol. 560, pp. 232698, 2023/03/15/, 2023.
- [66] P. M. Yeletsky, M. V. Lebedeva, and V. A. Yakovlev, "Today's progress in the synthesis of porous carbons from biomass and their application for organic electrolyte and ionic liquid based supercapacitors," *Journal of Energy Storage*, vol. 50, pp. 104225, 2022/06/01/, 2022.
- [67] M. Akin, and X. Zhou, "Recent advances in solid-state supercapacitors: From emerging materials to advanced applications," *International Journal of Energy Research*, vol. 46, no. 8, pp. 10389-10452, 2022.
- [68] T. Ye, L. Li, and Y. Zhang, "Recent Progress in Solid Electrolytes for Energy Storage Devices," *Advanced Functional Materials*, vol. 30, no. 29, pp. 2000077, 2020.
- [69] X. Fan, C. Zhong, J. Liu, J. Ding, Y. Deng, X. Han, L. Zhang, W. Hu, D. P. Wilkinson, and J. Zhang, "Opportunities of Flexible and Portable Electrochemical Devices for Energy Storage: Expanding the Spotlight onto Semi-solid/Solid Electrolytes," *Chemical Reviews*, vol. 122, no. 23, pp. 17155-17239, 2022/12/14, 2022.
- [70] M. M. Amaral, R. Venâncio, A. C. Peterlevitz, and H. Zanin, "Recent advances on quasi-solid-state electrolytes for supercapacitors," *Journal of Energy Chemistry*, vol. 67, pp. 697-717, 2022/04/01/, 2022.
- [71] H. Dai, G. Zhang, D. Rawach, C. Fu, C. Wang, X. Liu, M. Dubois, C. Lai, and S. Sun, "Polymer gel electrolytes for flexible supercapacitors: Recent progress, challenges, and perspectives," *Energy Storage Materials*, vol. 34, pp. 320-355, 2021/01/01/, 2021.
- [72] K. Subasinghage, K. Gunawardane, N. Padmawansa, N. Kularatna, and M. Moradian, "Modern supercapacitors technologies and their applicability in mature electrical engineering applications," *Energies*, vol. 15, no. 20, pp. 7752, 2022.
- [73] D. Xie, M. Liu, L. Xu, and W. Lu, "Bi-level programming approach for coordinated configuration of distributed generations and automation devices in distribution networks," *International Journal of Electrical Power & Energy Systems*, vol. 133, pp. 107210, 2021.

- [74] R. Nigam, K. D. Verma, T. Pal, and K. K. Kar, "Applications of supercapacitors," *Handbook of Nanocomposite Supercapacitor Materials II: Performance*, pp. 463-481, 2020.
- [75] A. Yadav, B. De, S. K. Singh, P. Sinha, and K. K. Kar, "Facile development strategy of a single carbon-fiber-based all-solid-state flexible lithium-ion battery for wearable electronics," *ACS applied materials & interfaces*, vol. 11, no. 8, pp. 7974-7980, 2019.
- [76] J. Cherusseri, and K. K. Kar, "Hierarchical carbon nanopetal/polypyrrole nanocomposite electrodes with brush-like architecture for supercapacitors," *Physical Chemistry Chemical Physics*, vol. 18, no. 12, pp. 8587-8597, 2016.
- [77] M. Mohan, N. P. Shetti, and T. M. Aminabhavi, "Recent developments in MoS₂-based flexible supercapacitors," *Materials Today Chemistry*, vol. 27, pp. 101333, 2023/01/01/, 2023.
- [78] X. Wang, C. Yang, J. Jin, X. Li, Q. Cheng, and G. Wang, "High-performance stretchable supercapacitors based on intrinsically stretchable acrylate rubber/MWCNTs@conductive polymer composite electrodes," *Journal of Materials Chemistry A*, vol. 6, no. 10, pp. 4432-4442, 2018.
- [79] K. Lee, H. Lee, Y. Shin, Y. Yoon, D. Kim, and H. Lee, "Highly transparent and flexible supercapacitors using graphene-graphene quantum dots chelate," *Nano Energy*, vol. 26, pp. 746-754, 2016.
- [80] Y. Huang, M. Zhu, Z. Pei, Q. Xue, Y. Huang, and C. Zhi, "A shape memory supercapacitor and its application in smart energy storage textiles," *Journal of Materials Chemistry A*, vol. 4, no. 4, pp. 1290-1297, 2016.
- [81] Y. Zou, C. Chen, Y. Sun, S. Gan, L. Dong, J. Zhao, and J. Rong, "Flexible, all-hydrogel supercapacitor with self-healing ability," *Chemical Engineering Journal*, vol. 418, pp. 128616, 2021.
- [82] S. L. Kim, H. T. Lin, and C. Yu, "Thermally chargeable solid-state supercapacitor," *Advanced Energy Materials*, vol. 6, no. 18, pp. 1600546, 2016.
- [83] T. Ma, H. Yang, and L. Lu, "Development of hybrid battery-supercapacitor energy storage for remote area renewable energy systems," *Applied Energy*, vol. 153, pp. 56-62, 2015/09/01/, 2015.
- [84] X. Tan, Q. Li, and H. Wang, "Advances and trends of energy storage technology in Microgrid," *International Journal of Electrical Power & Energy Systems*, vol. 44, no. 1, pp. 179-191, 2013/01/01/, 2013.
- [85] W. Jing, C. Hung Lai, S. H. W. Wong, and M. L. D. Wong, "Battery-supercapacitor hybrid energy storage system in standalone DC microgrids: a review," *IET Renewable Power Generation*, vol. 11, no. 4, pp. 461-469, 2017.
- [86] B. R. Ravada, and N. R. Tummuru, "Control of a supercapacitor-battery-PV based standalone DC-microgrid," *IEEE Transactions on Energy Conversion*, vol. 35, no. 3, pp. 1268-1277, 2020.
- [87] D. P. Dubal, N. R. Chodankar, D.-H. Kim, and P. Gomez-Romero, "Towards flexible solid-state supercapacitors for smart and wearable electronics," *Chemical Society Reviews*, vol. 47, no. 6, pp. 2065-2129, 2018.
- [88] L. Liu, Z. Niu, and J. Chen, "Unconventional supercapacitors from nanocarbon-based electrode materials to device configurations," *Chemical Society Reviews*, vol. 45, no. 15, pp. 4340-4363, 2016.
- [89] J. Zou, M. Zhang, J. Huang, J. Bian, Y. Jie, M. Willander, X. Cao, N. Wang, and Z. L. Wang, "Coupled supercapacitor and triboelectric nanogenerator boost biomimetic pressure sensor," *Advanced Energy Materials*, vol. 8, no. 10, pp. 1702671, 2018.
- [90] Y.-Z. Zhang, Y. Wang, T. Cheng, L.-Q. Yao, X. Li, W.-Y. Lai, and W. Huang, "Printed supercapacitors: materials, printing and applications," *Chemical Society Reviews*, vol. 48, no. 12, pp. 3229-3264, 2019.
- [91] M. S. Silverstein, "Emulsion-templated porous polymers: A retrospective perspective," *Polymer*, vol. 55, no. 1, pp. 304-320, 2014.

- [92] B. Aldemir Dikici, and F. Claeysens, "Basic Principles of Emulsion Templating and Its Use as an Emerging Manufacturing Method of Tissue Engineering Scaffolds," *Front Bioeng Biotechnol*, vol. 8, pp. 875, 2020.
- [93] T. Zhang, R. A. Sanguramath, S. Israel, and M. S. Silverstein, "Emulsion Templating: Porous Polymers and Beyond," *Macromolecules*, vol. 52, no. 15, pp. 5445-5479, 2019.
- [94] M. Tebboth, A. Menner, A. Kogelbauer, and A. Bismarck, "Polymerised high internal phase emulsions for fluid separation applications," *Current Opinion in Chemical Engineering*, vol. 4, pp. 114-120, 2014/05/01/, 2014.
- [95] A. Menner, and A. Bismarck, "New evidence for the mechanism of the pore formation in polymerising high internal phase emulsions or why polyHIPEs have an interconnected pore network structure." pp. 19-24.
- [96] N. Cameron, D. Sherrington, L. Albiston, and D. Gregory, "Study of the formation of the open-cellular morphology of poly (styrene/divinylbenzene) polyHIPE materials by cryo-SEM," *Colloid and Polymer Science*, vol. 274, pp. 592-595, 1996.
- [97] B. Donald, and H. Zia, *Low density porous cross-linked polymeric materials and their preparation*, Eur Pat 0060138, 1982.
- [98] J. M. Williams, A. J. Gray, and M. H. Wilkerson, "Emulsion stability and rigid foams from styrene or divinylbenzene water-in-oil emulsions," *Langmuir*, vol. 6, no. 2, pp. 437-444, 1990/02/01, 1990.
- [99] J. M. Williams, "High internal phase water-in-oil emulsions: influence of surfactants and cosurfactants on emulsion stability and foam quality," *Langmuir*, vol. 7, no. 7, pp. 1370-1377, 1991/07/01, 1991.
- [100] E. M. Christenson, W. Soofi, J. L. Holm, N. R. Cameron, and A. G. Mikos, "Biodegradable Fumarate-Based PolyHIPEs as Tissue Engineering Scaffolds," *Biomacromolecules*, vol. 8, no. 12, pp. 3806-3814, 2007/12/01, 2007.
- [101] S. A. Richardson, T. M. Rawlings, J. Muter, M. Walker, J. J. Brosens, N. R. Cameron, and A. M. Eissa, "Covalent Attachment of Fibronectin onto Emulsion-Templated Porous Polymer Scaffolds Enhances Human Endometrial Stromal Cell Adhesion, Infiltration, and Function," *Macromolecular Bioscience*, vol. 19, no. 2, pp. 1800351, 2019.
- [102] B. Aldemir Dikici, S. Dikici, G. C. Reilly, S. MacNeil, and F. Claeysens, "A novel bilayer polycaprolactone membrane for guided bone regeneration: Combining electrospinning and emulsion templating," *Materials*, vol. 12, no. 16, pp. 2643, 2019.
- [103] M. Sušec, S. C. Ligon, J. Stampfl, R. Liska, and P. Krajnc, "Hierarchically Porous Materials from Layer-by-Layer Photopolymerization of High Internal Phase Emulsions," *Macromolecular Rapid Communications*, vol. 34, no. 11, pp. 938-943, 2013.
- [104] S. Huš, and P. Krajnc, "PolyHIPEs from Methyl methacrylate: Hierarchically structured microcellular polymers with exceptional mechanical properties," *Polymer*, vol. 55, no. 17, pp. 4420-4424, 2014/08/18/, 2014.
- [105] N. Kitagawa, "Hydrophilic polymeric material and method of preparation," Google Patents, 2001.
- [106] A. Barbeta, M. Dentini, E. M. Zannoni, and M. E. De Stefano, "Tailoring the porosity and morphology of gelatin-methacrylate polyHIPE scaffolds for tissue engineering applications," *Langmuir*, vol. 21, no. 26, pp. 12333-12341, 2005.
- [107] H. Zhang, and A. I. Cooper, "Thermoresponsive "Particle Pumps": Activated Release of Organic Nanoparticles from Open-Cell Macroporous Polymers," *Advanced Materials*, vol. 19, no. 18, pp. 2439-2444, 2007.
- [108] P. Krajnc, D. Štefanec, and I. Pulko, "Acrylic Acid "Reversed" PolyHIPEs," *Macromolecular Rapid Communications*, vol. 26, no. 16, pp. 1289-1293, 2005.
- [109] W. Busby, N. R. Cameron, and C. A. B. Jahoda, "Emulsion-Derived Foams (PolyHIPEs) Containing Poly(ϵ -caprolactone) as Matrixes for Tissue Engineering," *Biomacromolecules*, vol. 2, no. 1, pp. 154-164, 2001/03/01, 2001.

- [110] J. Majer, M. Paljevac, E. Žagar, S. Kovačič, and P. Krajnc, "Functionalization of 2-hydroxyethyl methacrylate-based polyHIPEs: Effect of the leaving group," *Reactive and Functional Polymers*, vol. 109, pp. 99-103, 2016/12/01/, 2016.
- [111] J. Majer, and P. Krajnc, "Cross-Linked Porous Poly(Acrylic Acid-co-Acrylamide) from High Internal Phase Emulsions: Preparation and Functionalisation," *ACTA CHIMICA SLOVENICA*, vol. 56, no. 3, pp. 629-634, 2009.
- [112] F. Audouin, M. Birot, E. Pasquinet, O. Besnard, P. Palmas, D. Poullain, and H. Deleuze, "Preparation, Solid-State NMR, and Physicochemical Characterization of Surprisingly Tough Open Cell PolyHIPEs Derived from 1-Vinyl-1,2,4-triazole Oil-in-Water Emulsions," *MACROMOLECULES*, vol. 44, no. 12, pp. 4879-4886, JUN 28, 2011.
- [113] R. Butler, I. Hopkinson, and A. Cooper, "Synthesis of porous emulsion-templated polymers using high internal phase CO₂-in-water emulsions," *Journal of the American Chemical Society*, vol. 125, no. 47, pp. 14473-14481, 2003.
- [114] S. Kovačič, H. Kren, P. Krajnc, S. Koller, and C. Slugovc, "The Use of an Emulsion Templated Microcellular Poly(dicyclopentadiene-co-norbornene) Membrane as a Separator in Lithium-Ion Batteries," *Macromolecular Rapid Communications*, vol. 34, no. 7, pp. 581-587, 2013.
- [115] R. Butler, C. M. Davies, and A. I. Cooper, "Emulsion templating using high internal phase supercritical fluid emulsions," *Advanced Materials*, vol. 13, no. 19, pp. 1459-1463, 2001.
- [116] V. V. Dhanuka, J. L. Dickson, W. Ryoo, and K. P. Johnston, "High internal phase CO₂-in-water emulsions stabilized with a branched nonionic hydrocarbon surfactant," *Journal of Colloid and Interface Science*, vol. 298, no. 1, pp. 406-418, 2006.
- [117] W. Luo, S. Zhang, P. Li, R. Xu, Y. Zhang, L. Liang, C. D. Wood, Q. Lu, and B. Tan, "Surfactant-free CO₂-in-water emulsion-templated poly (vinyl alcohol)(PVA) hydrogels," *Polymer*, vol. 61, pp. 183-191, 2015.
- [118] A. Zia, E. Pentzer, S. Thickett, and K. Kempe, "Advances and opportunities of oil-in-oil emulsions," *ACS applied materials & interfaces*, vol. 12, no. 35, pp. 38845-38861, 2020.
- [119] H. Zhang, G. C. Hardy, Y. Z. Khimyak, M. J. Rosseinsky, and A. I. Cooper, "Synthesis of hierarchically porous silica and metal oxide beads using emulsion-templated polymer scaffolds," *Chemistry of Materials*, vol. 16, no. 22, pp. 4245-4256, 2004.
- [120] A. Menner, R. Powell, and A. Bismarck, "Open porous polymer foams via inverse emulsion polymerization: should the definition of high internal phase (ratio) emulsions be extended?," *Macromolecules*, vol. 39, no. 6, pp. 2034-2035, 2006.
- [121] S. San Manley, N. Graeber, Z. Grof, A. Menner, G. F. Hewitt, F. Stepanek, and A. Bismarck, "New insights into the relationship between internal phase level of emulsion templates and gas-liquid permeability of interconnected macroporous polymers," *Soft Matter*, vol. 5, no. 23, pp. 4780-4787, 2009.
- [122] R. Wu, A. Menner, and A. Bismarck, "Tough interconnected polymerized medium and high internal phase emulsions reinforced by silica particles," *Journal of Polymer Science Part A: Polymer Chemistry*, vol. 48, no. 9, pp. 1979-1989, 2010.
- [123] V. O. Ikem, A. Menner, and A. Bismarck, "Tailoring the mechanical performance of highly permeable macroporous polymers synthesized via Pickering emulsion templating," *Soft Matter*, vol. 7, no. 14, pp. 6571-6577, 2011.
- [124] P. Steindl, A. Menner, and A. Bismarck, "Permeable emulsion-templated porous polyepoxides," *Polymer*, vol. 240, pp. 124476, 2022/02/01/, 2022.
- [125] A. Menner, K. Haibach, R. Powell, and A. Bismarck, "Tough reinforced open porous polymer foams via concentrated emulsion templating," *Polymer*, vol. 47, no. 22, pp. 7628-7635, 2006/10/18/, 2006.
- [126] M. Abshirini, M. C. Saha, L. Cummings, and T. Robison, "Synthesis and characterization of porous polydimethylsiloxane structures with adjustable porosity and pore morphology using emulsion templating technique," *Polymer Engineering & Science*, vol. 61, no. 7, pp. 1943-1955, 2021.

- [127] R. Mat Noor, "Synthesis of Polymer/Graphene Oxide Nanocomposite Foams: A New Dispersion-based Approach," UNSW Sydney, 2022.
- [128] C. Stubenrauch, A. Menner, A. Bismarck, and W. Drenckhan, "Emulsion and Foam Templating—Promising Routes to Tailor-Made Porous Polymers," *Angewandte Chemie International Edition*, vol. 57, no. 32, pp. 10024-10032, 2018.
- [129] N. Graeber, "A study of fundamentals in emulsion templating for the preparation of macroporous polymer foams," Imperial College London, 2013.
- [130] D. J. McClements, "Critical review of techniques and methodologies for characterization of emulsion stability," *Critical reviews in food science and nutrition*, vol. 47, no. 7, pp. 611-649, 2007.
- [131] Y.-T. Hu, Y. Ting, J.-Y. Hu, and S.-C. Hsieh, "Techniques and methods to study functional characteristics of emulsion systems," *Journal of Food and Drug Analysis*, vol. 25, no. 1, pp. 16-26, 2017/01/01/, 2017.
- [132] H. Niu, W. Wang, Z. Dou, X. Chen, X. Chen, H. Chen, and X. Fu, "Multiscale combined techniques for evaluating emulsion stability: A critical review," *Advances in Colloid and Interface Science*, vol. 311, pp. 102813, 2023/01/01/, 2023.
- [133] O. G. Jones, and D. J. McClements, "Recent progress in biopolymer nanoparticle and microparticle formation by heat-treating electrostatic protein-polysaccharide complexes," *Advances in colloid and interface science*, vol. 167, no. 1-2, pp. 49-62, 2011.
- [134] D. J. McClements, E. Newman, and I. F. McClements, "Plant-based milks: A review of the science underpinning their design, fabrication, and performance," *Comprehensive Reviews in Food Science and Food Safety*, vol. 18, no. 6, pp. 2047-2067, 2019.
- [135] T. Yang, X.-T. Li, and C.-H. Tang, "Novel edible pickering high-internal-phase-emulsion gels efficiently stabilized by unique polysaccharide-protein hybrid nanoparticles from Okara," *Food Hydrocolloids*, vol. 98, pp. 105285, 2020.
- [136] T. F. Tadros, A. Vandamme, B. Leveck, K. Booten, and C. V. Stevens, "Stabilization of emulsions using polymeric surfactants based on inulin," *Advances in Colloid and Interface Science*, vol. 108-109, pp. 207-226, 2004/05/20/, 2004.
- [137] S. Wan, Q. Zeng, S. Yang, X. Zhao, Q. Wen, H. Tang, Y. Zhang, J. Huang, G. Yu, Y. Feng, and J. Li, "In Situ Characterization and Interfacial Viscoelastic Properties of Pickering Emulsions Stabilized by AIE-Active Modified Alginate and Chitosan Complexes," *ACS Sustainable Chemistry & Engineering*, vol. 10, no. 31, pp. 10275-10285, 2022/08/08, 2022.
- [138] A. Kabal'Nov, A. Pertzov, and E. Shchukin, "Ostwald ripening in two-component disperse phase systems: Application to emulsion stability," *Colloids and Surfaces*, vol. 24, no. 1, pp. 19-32, 1987.
- [139] M. Y. Koroleva, and E. V. Yurtov, "Effect of Ionic Strength of Dispersed Phase on Ostwald Ripening in Water-in-Oil Emulsions," *Colloid Journal*, vol. 65, no. 1, pp. 40-43, 2003/01/01, 2003.
- [140] Y. Jang, J. Park, H. Y. Song, and S. J. Choi, "Ostwald Ripening Rate of Orange Oil Emulsions: Effects of Molecular Structure of Emulsifiers and Their Oil Composition," *Journal of Food Science*, vol. 84, no. 3, pp. 440-447, 2019.
- [141] S. H. Park, C. R. Hong, and S. J. Choi, "Prevention of Ostwald ripening in orange oil emulsions: Impact of surfactant type and Ostwald ripening inhibitor type," *LWT*, vol. 134, pp. 110180, 2020/12/01/, 2020.
- [142] L. Achour, M. Specklin, M. Asuaje, S. Kouidri, and I. Belaidi, "A review of emulsion flows, their characterization and their modeling in pumps," *Chemical Engineering Research and Design*, vol. 205, pp. 538-555, 2024/05/01/, 2024.
- [143] T. Tadros, "Polymeric surfactants in disperse systems," *Advances in Colloid and Interface Science*, vol. 147-148, pp. 281-299, 2009/03/01/, 2009.
- [144] A. M. Bago Rodriguez, and B. P. Binks, "High internal phase Pickering emulsions," *Current Opinion in Colloid & Interface Science*, vol. 57, pp. 101556, 2022/02/01/, 2022.

- [145] T. F. Tadros, A. Vandamme, B. Leveck, K. Booten, and C. Stevens, "Stabilization of emulsions using polymeric surfactants based on inulin," *Advances in colloid and interface science*, vol. 108, pp. 207-226, 2004.
- [146] G. M. Aleid, A. S. Alshammari, D. B. Tripathy, A. Gupta, and S. Ahmad, "Polymeric Surfactants: Recent Advancement in Their Synthesis, Properties, and Industrial Applications," *Macromolecular Chemistry and Physics*, vol. 224, no. 17, pp. 2300107, 2023.
- [147] M. S. Lim, and H. Chen, "Miniemulsion polymerization of styrene with a block copolymer surfactant," *Journal of Polymer Science Part A: Polymer Chemistry*, vol. 38, no. 10, pp. 1818-1827, 2000.
- [148] M. Bouix, J. Gouzi, B. Charleux, J. P. Vairon, and P. Guinot, "Synthesis of amphiphilic polyelectrolyte block copolymers using "living" radical polymerization. Application as stabilizers in emulsion polymerization," *Macromolecular rapid communications*, vol. 19, no. 4, pp. 209-213, 1998.
- [149] G. Riess, "Block copolymers as polymeric surfactants in latex and microlatex technology," *Colloids and Surfaces A: Physicochemical and Engineering Aspects*, vol. 153, no. 1-3, pp. 99-110, 1999.
- [150] R. Vijay, S. Angayarkanny, B. Reddy, A. Mandal, and G. Baskar, "Adsorption and emulsification properties of amphiphilic poly (styrene-co-octadecyl maleamic acid salt) with comb-like architecture," *Journal of colloid and interface science*, vol. 346, no. 1, pp. 143-152, 2010.
- [151] K. Busse, J. Kressler, D. Van Eck, and S. Höring, "Synthesis of amphiphilic block copolymers based on tert-butyl methacrylate and 2-(N-methylperfluorobutanesulfonamido) ethyl methacrylate and its behavior in water," *Macromolecules*, vol. 35, no. 1, pp. 178-184, 2002.
- [152] P. Alexandridis, and B. Lindman, *Amphiphilic block copolymers: self-assembly and applications*: Elsevier, 2000.
- [153] E. Kot, N. Shirshova, A. Bismarck, and J. H. Steinke, "Non-aqueous high internal phase emulsion templates for synthesis of macroporous polymers in situ filled with cyclic carbonate electrolytes," *RSC Advances*, vol. 4, no. 22, pp. 11512-11519, 2014.
- [154] L. L. Wong, P. M. Baiz Villafranca, A. Menner, and A. Bismarck, "Hierarchical polymerized high internal phase emulsions synthesized from surfactant-stabilized emulsion templates," *Langmuir*, vol. 29, no. 20, pp. 5952-5961, 2013.
- [155] R. Gref, V. Babak, P. Bouillot, I. Lukina, M. Bodorev, and E. Dellacherie, "Interfacial and emulsion stabilising properties of amphiphilic water-soluble poly (ethylene glycol)-poly (lactic acid) copolymers for the fabrication of biocompatible nanoparticles," *Colloids and Surfaces A: Physicochemical and Engineering Aspects*, vol. 143, no. 2-3, pp. 413-420, 1998.
- [156] P. Raffa, D. A. Z. Wever, F. Picchioni, and A. A. Broekhuis, "Polymeric surfactants: synthesis, properties, and links to applications," *Chemical reviews*, vol. 115, no. 16, pp. 8504-8563, 2015.
- [157] R. Francis, D. Taton, J. L. Logan, P. Masse, Y. Gnanou, and R. S. Duran, "Synthesis and surface properties of amphiphilic star-shaped and dendrimer-like copolymers based on polystyrene core and poly (ethylene oxide) corona," *Macromolecules*, vol. 36, no. 22, pp. 8253-8259, 2003.
- [158] C. Burguière, S. Pascual, C. Bui, J.-P. Vairon, B. Charleux, K. A. Davis, K. Matyjaszewski, and I. Bétremieux, "Block copolymers of poly (styrene) and poly (acrylic acid) of various molar masses, topologies, and compositions prepared via controlled/living radical polymerization. Application as stabilizers in emulsion polymerization," *Macromolecules*, vol. 34, no. 13, pp. 4439-4450, 2001.
- [159] D. Exerowa, G. Gotchev, T. Kolarov, K. Kristov, B. Leveck, and T. Tadros, "Comparison of oil-in-water emulsion films produced using ABA or AB_n copolymers," *Colloids and*

- Surfaces A: Physicochemical and Engineering Aspects*, vol. 335, no. 1, pp. 50-54, 2009/03/05/, 2009.
- [160] A. Hussain, M. A. Altamimi, S. S. Imam, and F. Imam, "Green nanoemulsion-based treatment to remove sulfamethoxazole from a contaminated water solution," *Journal of Molecular Liquids*, vol. 384, pp. 122183, 2023/08/15/, 2023.
- [161] A. d. P. Sánchez-Camargo, M. Bueno, F. Parada-Alfonso, A. Cifuentes, and E. Ibáñez, "Hansen solubility parameters for selection of green extraction solvents," *TrAC Trends in Analytical Chemistry*, vol. 118, pp. 227-237, 2019/09/01/, 2019.
- [162] M. Klapper, S. Nenov, R. Haschick, K. Müller, and K. Müllen, "Oil-in-oil emulsions: a unique tool for the formation of polymer nanoparticles," *Accounts of chemical research*, vol. 41, no. 9, pp. 1190-1201, 2008.
- [163] L. I. Atanase, and G. Riess, "Stabilization of non-aqueous emulsions by poly(2-vinylpyridine)-b-poly(butadiene) block copolymers," *Colloids and Surfaces A: Physicochemical and Engineering Aspects*, vol. 458, pp. 19-24, 2014/09/20/, 2014.
- [164] R. Dorresteyn, R. Haschick, M. Klapper, and K. Müllen, "Poly (l-lactide) Nanoparticles via Ring-Opening Polymerization in Non-aqueous Emulsion," *Macromolecular Chemistry and Physics*, vol. 213, no. 19, pp. 1996-2002, 2012.
- [165] L.-I. Atanase, and G. Riess, "Block copolymers as polymeric stabilizers in non-aqueous emulsion polymerization," *Polymer International*, vol. 60, no. 11, pp. 1563-1573, 2011.
- [166] O. Dagdag, R. Hsissou, Z. Safi, O. Hamed, S. Jodeh, R. Haldhar, C. Verma, E. E. Ebenso, A. El Bachiri, and M. El Gouri, "Viscosity of epoxy resins based on aromatic diamines, glucose, bisphenolic and bio-based derivatives: a comprehensive review," *Journal of Polymer Research*, vol. 29, no. 5, pp. 200, 2022/05/06, 2022.
- [167] F.-L. Jin, X. Li, and S.-J. Park, "Synthesis and application of epoxy resins: A review," *Journal of Industrial and Engineering Chemistry*, vol. 29, pp. 1-11, 2015/09/25/, 2015.
- [168] P. Mohan, "A critical review: the modification, properties, and applications of epoxy resins," *Polymer-Plastics Technology and Engineering*, vol. 52, no. 2, pp. 107-125, 2013.
- [169] J. Wang, C. Zhang, Z. Du, A. Xiang, and H. Li, "Formation of porous epoxy monolith via concentrated emulsion polymerization," *Journal of Colloid and Interface Science*, vol. 325, no. 2, pp. 453-458, 2008/09/15/, 2008.
- [170] P. Steindl, H. Decker, B. Retzl, Q. Jiang, A. Menner, and A. Bismarck, "Emulsion-templated flexible epoxy foams," *Polymer*, vol. 215, pp. 123380, 2021/02/12/, 2021.
- [171] F. M. Perna, P. Vitale, and V. Capriati, "Deep eutectic solvents and their applications as green solvents," *Current Opinion in Green and Sustainable Chemistry*, vol. 21, pp. 27-33, 2020/02/01/, 2020.
- [172] K. A. Omar, and R. Sadeghi, "Physicochemical properties of deep eutectic solvents: A review," *Journal of Molecular Liquids*, vol. 360, pp. 119524, 2022/08/15/, 2022.
- [173] B. B. Hansen, S. Spittle, B. Chen, D. Poe, Y. Zhang, J. M. Klein, A. Horton, L. Adhikari, T. Zelovich, B. W. Doherty, B. Gurkan, E. J. Maginn, A. Ragauskas, M. Dadmun, T. A. Zawodzinski, G. A. Baker, M. E. Tuckerman, R. F. Savinell, and J. R. Sangoro, "Deep Eutectic Solvents: A Review of Fundamentals and Applications," *Chemical Reviews*, vol. 121, no. 3, pp. 1232-1285, 2021/02/10, 2021.
- [174] Y. Nahar, and S. C. Thickett, "Greener, Faster, Stronger: The Benefits of Deep Eutectic Solvents in Polymer and Materials Science," *Polymers*, vol. 13, no. 3, pp. 447, 2021.
- [175] A. P. Abbott, G. Capper, D. L. Davies, H. L. Munro, R. K. Rasheed, and V. Tambyrajah, "Preparation of novel, moisture-stable, Lewis-acidic ionic liquids containing quaternary ammonium salts with functional side chains Electronic supplementary information (ESI) available: plot of conductivity vs. temperature for the ionic liquid formed from zinc chloride and choline chloride (2 : 1). See <http://www.rsc.org/suppdata/cc/b1/b106357j>," *Chemical communications*, no. 19, pp. 2010-2011, 2001.
- [176] A. P. Abbott, G. Capper, D. L. Davies, R. K. Rasheed, and V. Tambyrajah, "Novel solvent properties of choline chloride/urea mixtures," *Chemical communications*, no. 1, pp. 70-71, 2003.

- [177] T. El Achkar, H. Greige-Gerges, and S. Fourmentin, "Basics and properties of deep eutectic solvents: a review," *Environmental Chemistry Letters*, vol. 19, no. 4, pp. 3397-3408, 2021/08/01, 2021.
- [178] S. P. Ijardar, V. Singh, and R. L. Gardas, "Revisiting the physicochemical properties and applications of deep eutectic solvents," *Molecules*, vol. 27, no. 4, pp. 1368, 2022.
- [179] A. Carranza, M. G. Pérez-García, K. Song, G. M. Jeha, Z. Diao, R. Jin, N. Bogdanchikova, A. F. Soltero, M. Terrones, Q. Wu, J. A. Pojman, and J. D. Mota-Morales, "Deep-Eutectic Solvents as MWCNT Delivery Vehicles in the Synthesis of Functional Poly(HIPE) Nanocomposites for Applications as Selective Sorbents," *ACS Applied Materials & Interfaces*, vol. 8, no. 45, pp. 31295-31303, 2016/11/16, 2016.
- [180] A. Carranza, J. A. Pojman, and J. D. Mota-Morales, "Deep-eutectic solvents as a support in the nonaqueous synthesis of macroporous poly (HIPEs)," *RSC Advances*, vol. 4, no. 78, pp. 41584-41587, 2014.
- [181] M. Pérez-García, A. Carranza, J. Puig, J. Pojman, F. Del Monte, G. Luna-Bárceñas, and J. Mota-Morales, "Porous monoliths synthesized via polymerization of styrene and divinyl benzene in nonaqueous deep-eutectic solvent-based HIPEs," *RSC Advances*, vol. 5, no. 30, pp. 23255-23260, 2015.
- [182] A. Carranza, K. Song, J. Soltero-Martínez, Q. Wu, J. Pojman, and J. Mota-Morales, "On the stability and chemorheology of a urea choline chloride deep-eutectic solvent as an internal phase in acrylic high internal phase emulsions," *RSC advances*, vol. 6, no. 85, pp. 81694-81702, 2016.
- [183] S. T. Huerta-Marcial, and J. D. Mota-Morales, "Tailoring the morphology of poly(high internal phase emulsions) synthesized by using deep eutectic solvents," *e-Polymers*, vol. 20, no. 1, pp. 185-193, 2020.
- [184] A. Carranza, D. Romero-Perez, H. Almanza-Reyes, N. Bogdanchikova, K. Juarez-Moreno, J. A. Pojman, C. Velasquillo, and J. D. Mota-Morales, "Nonaqueous Synthesis of Macroporous Nanocomposites Using High Internal Phase Emulsion Stabilized by Nanohydroxyapatite," *Advanced Materials Interfaces*, vol. 4, no. 16, pp. 1700094, 2017.
- [185] S. T. Huerta-Marcial, and J. D. Mota-Morales, "Tailoring the morphology of poly (high internal phase emulsions) synthesized by using deep eutectic solvents," *e-Polymers*, vol. 20, no. 1, pp. 185-193, 2020.
- [186] S. T. Huerta-Marcial, A. L. Ruiz-Deance, and J. D. Mota-Morales, "Bringing sustainability to macroporous polystyrene: Cellulose nanocrystals as cosurfactant and surface modifier in deep eutectic solvent-based emulsion templating," *ACS Sustainable Chemistry & Engineering*, vol. 9, no. 45, pp. 15109-15116, 2021.
- [187] E. S. Greenhalgh, S. Nguyen, M. Valkova, N. Shirshova, M. S. P. Shaffer, and A. R. J. Kucernak, "A critical review of structural supercapacitors and outlook on future research challenges," *Composites Science and Technology*, vol. 235, pp. 109968, 2023/04/12/, 2023.
- [188] N. Shirshova, A. Bismarck, E. S. Greenhalgh, P. Johansson, G. Kalinka, M. J. Marczewski, M. S. Shaffer, and M. Wienrich, "Composition as a means to control morphology and properties of epoxy based dual-phase structural electrolytes," *The Journal of Physical Chemistry C*, vol. 118, no. 49, pp. 28377-28387, 2014.
- [189] F. Huang, Y. Zhou, Z. Sha, S. Peng, W. Chang, X. Cheng, J. Zhang, S. A. Brown, Z. Han, and C.-H. Wang, "Surface functionalization of electrodes and synthesis of dual-phase solid electrolytes for structural supercapacitors," *ACS Applied Materials & Interfaces*, vol. 14, no. 27, pp. 30857-30871, 2022.
- [190] G.-H. Dong, F.-L. Guo, Z. Sun, Y.-Q. Li, S.-F. Song, C.-H. Xu, P. Huang, C. Yan, N. Hu, and S.-Y. Fu, "Short carbon fiber reinforced epoxy-ionic liquid electrolyte enabled structural battery via vacuum bagging process," *Advanced Composites and Hybrid Materials*, vol. 5, no. 3, pp. 1799-1811, 2022.
- [191] Q. Wendong, J. Dent, V. Arrighi, L. Cavalcanti, M. S. Shaffer, and N. Shirshova, "Biphasic epoxy-ionic liquid structural electrolytes: minimising feature size through cure cycle and

- multifunctional block-copolymer addition," *Multifunctional Materials*, vol. 4, no. 3, pp. 035003, 2021.
- [192] Q. Feng, J. Yang, Y. Yu, F. Tian, B. Zhang, M. Feng, and S. Wang, "The ionic conductivity, mechanical performance and morphology of two-phase structural electrolytes based on polyethylene glycol, epoxy resin and nano-silica," *Materials Science and Engineering: B*, vol. 219, pp. 37-44, 2017.
- [193] S.-H. Bae, C. Jeon, S. Oh, C.-G. Kim, M. Seo, and I.-K. Oh, "Load-bearing supercapacitor based on bicontinuous PEO-bP (S-co-DVB) structural electrolyte integrated with conductive nanowire-carbon fiber electrodes," *Carbon*, vol. 139, pp. 10-20, 2018.
- [194] W.-J. Cho, S.-K. Cho, J. H. Lee, J. H. Yoon, S. Kwon, C. Park, W. B. Lee, P. J. Yoo, M. Lee, and S. Park, "Solid polymer electrolytes of ionic liquids via a bicontinuous ion transport channel for lithium metal batteries," *Journal of Materials Chemistry A*, vol. 11, no. 4, pp. 1676-1683, 2023.
- [195] S. J. Kwon, T. Kim, B. M. Jung, S. B. Lee, and U. H. Choi, "Multifunctional epoxy-based solid polymer electrolytes for solid-state supercapacitors," *ACS applied materials & interfaces*, vol. 10, no. 41, pp. 35108-35117, 2018.
- [196] J. Y. Lim, D. A. Kang, N. U. Kim, J. M. Lee, and J. H. Kim, "Bicontinuously crosslinked polymer electrolyte membranes with high ion conductivity and mechanical strength," *Journal of Membrane Science*, vol. 589, pp. 117250, 2019.
- [197] S. Deshpande, V. Vidyaprakash, S. Oka, S. S. Dasari, K.-W. Liu, C. Wang, J. L. Lutkenhaus, and M. J. Green, "Low-Temperature Structural Battery Electrolytes Produced by Polymerization-Induced Phase Separation," *ACS Applied Polymer Materials*, 2024.
- [198] L. M. Schneider, N. Ihrner, D. Zenkert, and M. Johansson, "Bicontinuous electrolytes via thermally initiated polymerization for structural lithium ion batteries," *ACS Applied Energy Materials*, vol. 2, no. 6, pp. 4362-4369, 2019.
- [199] N. Shirshova, A. Bismarck, and J. H. G. Steinke, "Ionic Liquids as Internal Phase for Non-Aqueous PolyHIPEs," *Macromolecular Rapid Communications*, vol. 32, no. 23, pp. 1899-1904, 2011/12/01, 2011.
- [200] H. Xiao, J.-F. Yin, Q. Cheng, Q. Zhou, J. Chen, C. Huang, and P. Yin, "Nanometer-Scale Molecular Cluster Surfactants Generate Robust Gel Emulsion Systems for Solid-State Electrolytes," *ACS Applied Nano Materials*, vol. 4, no. 10, pp. 10430-10437, 2021/10/22, 2021.
- [201] M. K. Jha, N. Sunariwal, B. J. Parker, N. Cameron, and C. Subramaniam, "Multi-cationic ionic liquid combination enabling 86-fold enhancement in frequency response and superior energy density in all-solid-state supercapacitors," *Journal of Energy Storage*, vol. 53, pp. 105164, 2022/09/01/, 2022.
- [202] X. Ma, X. Shi, Y. Wang, W. Xiong, C. Xiong, J. Yang, L. You, and S. Wang, "Stretchable porous conductive hydrogel films prepared by emulsion template method as flexible sensors," *Colloids and Surfaces A: Physicochemical and Engineering Aspects*, vol. 676, pp. 132272, 2023/11/05/, 2023.
- [203] B. Clough, L. Hollyman, W. Quan, and N. Shirshova, "Polymerised medium internal phase emulsions as structural separators." pp. 4087-4094.
- [204] B. Aldemir Dikici, S. Dikici, and F. Claeysens, "Synergistic effect of type and concentration of surfactant and diluting solvent on the morphology of emulsion templated matrices developed as tissue engineering scaffolds," *Reactive and Functional Polymers*, vol. 180, pp. 105387, 2022/11/01/, 2022.
- [205] X. Wan, U. Azhar, Y. Wang, J. Chen, A. Xu, S. Zhang, and B. Geng, "Highly porous and chemical resistive P (TFEMA-DVB) monolith with tunable morphology for rapid oil/water separation," *RSC advances*, vol. 8, no. 15, pp. 8355-8364, 2018.
- [206] B. Sergent, M. Birot, and H. Deleuze, "Preparation of thiol-ene porous polymers by emulsion templating," *Reactive and Functional Polymers*, vol. 72, no. 12, pp. 962-966, 2012/12/01/, 2012.

- [207] J. A. Martin, C. A. Mullen, and A. A. Boateng, "Maximizing the Stability of Pyrolysis Oil/Diesel Fuel Emulsions," *Energy & Fuels*, vol. 28, no. 9, pp. 5918-5929, 2014/09/18, 2014.
- [208] M. C. García, J. Muñoz, M. C. Alfaro, and J. M. Franco, "Physical characterization of multiple emulsions formulated with a green solvent and different HLB block copolymers," *Colloids and Surfaces A: Physicochemical and Engineering Aspects*, vol. 458, pp. 40-47, 2014/09/20/, 2014.
- [209] M. C. García, P. Cox, L. Trujillo-Cayado, J. Muñoz, and M. C. Alfaro, "Rheology, microstructural characterization and physical stability of W/ α -PINENE/W emulsions formulated with copolymers," *Colloids and Surfaces A: Physicochemical and Engineering Aspects*, vol. 536, pp. 125-132, 2018/01/05/, 2018.
- [210] T. H. Hassan, H. Metz, and K. Mäder, "Novel semisolid SNEDDS based on PEG-30-dipolyhydroxystearate: Development and characterization," *International Journal of Pharmaceutics*, vol. 477, no. 1, pp. 506-518, 2014/12/30/, 2014.
- [211] M. Nollet, H. Boulghobra, E. Calligaro, and J. D. Rodier, "An efficient method to determine the hydrophile-lipophile balance of surfactants using the phase inversion temperature deviation of CiEj/n-octane/water emulsions," *International Journal of Cosmetic Science*, vol. 41, no. 2, pp. 99-108, 2019.
- [212] J. Linse, "Solid Water in Oil Emulsions with phase transition stability," 2016.
- [213] Croda, "ZEPHYRM PD 2206-LQ-(AP)," *Safety data sheet*, 2022.
- [214] Croda, "HYPERMER™ B246-SO-(MV)," *Safety data sheet*, 2019.
- [215] Croda, "CITHROL™ DPHS-SO-(MV)," *Safety data sheet*, 2019.
- [216] Croda, "ATLOX™ 4912 SF-SO-(MV)," *Safety data sheet*, 2022.
- [217] A. P. Abbott, R. C. Harris, and K. S. Ryder, "Application of hole theory to define ionic liquids by their transport properties," *The Journal of Physical Chemistry B*, vol. 111, no. 18, pp. 4910-4913, 2007.
- [218] A. P. Abbott, G. Capper, D. L. Davies, K. J. McKenzie, and S. U. Obi, "Solubility of metal oxides in deep eutectic solvents based on choline chloride," *Journal of Chemical & Engineering Data*, vol. 51, no. 4, pp. 1280-1282, 2006.
- [219] S. M. Shuwa, B. Y. Jibril, Y. M. Al-Wahaibi, and R. S. Al-Hajri, "Heavy-oil-recovery enhancement with choline chloride/ethylene glycol-based deep eutectic solvent," *SPE Journal*, vol. 20, no. 01, pp. 79-87, 2015.
- [220] S. Malburet, H. Bertrand, C. Richard, C. Lacabanne, E. Dantras, and A. Graillot, "Biobased epoxy reactive diluents prepared from monophenol derivatives: effect on viscosity and glass transition temperature of epoxy resins," *RSC advances*, vol. 13, no. 22, pp. 15099-15106, 2023.
- [221] Y. Ecochard, M. Decostanzi, C. Negrell, R. Sonnier, and S. Caillol, "Cardanol and Eugenol Based Flame Retardant Epoxy Monomers for Thermostable Networks," *Molecules*, vol. 24, no. 9, May 10, 2019.
- [222] A. Tapes, "AT526 35 Micron Copper Foil Shielding Tape," *Technical datasheet*.
- [223] M. chemicals, "838AR Technical Data Sheet Total Ground™ Carbon Conductive Coating," *Technical datasheet*, 2018.
- [224] A. Barbetta, and N. R. Cameron, "Morphology and Surface Area of Emulsion-Derived (PolyHIPE) Solid Foams Prepared with Oil-Phase Soluble Porogenic Solvents: Span 80 as Surfactant," *Macromolecules*, vol. 37, no. 9, pp. 3188-3201, 2004/05/01, 2004.
- [225] K. Rohm, I. Manas-Zloczower, and D. Feke, "Poly(HIPE) morphology, crosslink density, and mechanical properties influenced by surfactant concentration and composition," *Colloids and Surfaces A: Physicochemical and Engineering Aspects*, vol. 583, pp. 123913, 2019/12/20/, 2019.
- [226] H. Kim, "Engineering Porous Polymer Electrolyte for High-Performance Quasi Solid-State Supercapacitor," Northeastern University, 2021.

- [227] T. H. Lau, L. L. Wong, K.-Y. Lee, and A. Bismarck, "Tailored for simplicity: creating high porosity, high performance bio-based macroporous polymers from foam templates," *Green Chemistry*, vol. 16, no. 4, pp. 1931-1940, 2014.
- [228] X. Huang, "Separator technologies for lithium-ion batteries," *Journal of Solid State Electrochemistry*, vol. 15, no. 4, pp. 649-662, 2010.
- [229] B. Hu, X. Shang, P. Nie, B. Zhang, K. Xu, J. Yang, J. Qiu, and J. Liu, "Facile Fabrication of a Highly Porous N-Doped Nanotubular Carbon Aerogel by an In Situ Template-Growth Method for High-Performance Supercapacitors," *ACS Applied Energy Materials*, vol. 4, no. 7, pp. 6991-7001, 2021/07/26, 2021.
- [230] P. Giannakou, "Printed Transition Metal Oxide Electrochemical Capacitors for Energy Harvesting Applications," University of Surrey, 2021.
- [231] R. Muchakayala, S. Song, J. Wang, Y. Fan, M. Benggeppagari, J. Chen, and M. Tan, "Development and supercapacitor application of ionic liquid-incorporated gel polymer electrolyte films," *Journal of Industrial and Engineering Chemistry*, vol. 59, pp. 79-89, 2018/03/25/, 2018.
- [232] P. L. Taberna, C. Portet, and P. Simon, "Electrode surface treatment and electrochemical impedance spectroscopy study on carbon/carbon supercapacitors," *Applied Physics A*, vol. 82, no. 4, pp. 639-646, 2006/03/01, 2006.
- [233] B. Hsia, *Materials synthesis and characterization for micro-supercapacitor applications*: University of California, Berkeley, 2013.
- [234] R. Foudazi, "HIPEs to polyHIPEs," *Reactive and Functional Polymers*, vol. 164, pp. 104917, 2021.
- [235] A. Gadhav, "Determination of hydrophilic-lipophilic balance value," *Int. J. Sci. Res*, vol. 3, no. 4, pp. 573-575, 2014.
- [236] T. Tadros, "Polymeric surfactants in disperse systems," *Advances in Colloid and Interface Science*, vol. 147, pp. 281-299, 2009.
- [237] O. Suiythimeathegorn, *Studies on non-aqueous emulsions*: University of London, University College London (United Kingdom), 2006.
- [238] V. Causin, and V. Causin, *Polymers on the crime scene*: Springer, 2015.
- [239] L. I. Atanase, and G. Riess, "Stabilization of non-aqueous emulsions by poly (2-vinylpyridine)-b-poly (butadiene) block copolymers," *Colloids and Surfaces A: Physicochemical and Engineering Aspects*, vol. 458, pp. 19-24, 2014.
- [240] R. Dorresteyn, R. Haschick, M. Klapper, and K. Müllen, "Poly(L-lactide) Nanoparticles via Ring-Opening Polymerization in Non-aqueous Emulsion," *Macromolecular Chemistry and Physics*, vol. 213, no. 19, pp. 1996-2002, 2012.
- [241] R. S. Moglia, J. L. Holm, N. A. Sears, C. J. Wilson, D. M. Harrison, and E. Cosgriff-Hernandez, "Injectable polyHIPEs as high-porosity bone grafts," *Biomacromolecules*, vol. 12, no. 10, pp. 3621-3628, 2011.
- [242] T. Gitli, and M. S. Silverstein, "Bicontinuous hydrogel-hydrophobic polymer systems through emulsion templated simultaneous polymerizations," *Soft Matter*, vol. 4, no. 12, pp. 2475-2485, 2008.
- [243] B. Abismail, J. P. Canselier, A. M. Wilhelm, H. Delmas, and C. Gourdon, "Emulsification by ultrasound: drop size distribution and stability," *Ultrasonics sonochemistry*, vol. 6, no. 1-2, pp. 75-83, 1999.
- [244] S. Tcholakova, N. D. Denkov, and T. Danner, "Role of surfactant type and concentration for the mean drop size during emulsification in turbulent flow," *Langmuir*, vol. 20, no. 18, pp. 7444-7458, 2004.
- [245] M. F. A. L. J. Gibson "Cellular Solids: Structure and Properties," Cambridge, UK: Cambridge University Press, 1997.
- [246] M. C. Saha, H. Mahfuz, U. K. Chakravarty, M. Uddin, M. E. Kabir, and S. Jeelani, "Effect of density, microstructure, and strain rate on compression behavior of polymeric foams," *Materials Science and Engineering: A*, vol. 406, no. 1, pp. 328-336, 2005/10/15/, 2005.

- [247] R. S. Moglia, J. L. Robinson, A. D. Muschenborn, T. J. Touchet, D. J. Maitland, and E. Cosgriff-Hernandez, "Injectable polyMIPE scaffolds for soft tissue regeneration," *Polymer*, vol. 55, no. 1, pp. 426-434, 2014/01/14/, 2014.
- [248] K. Mathieu, C. Jérôme, and A. Debuigne, "Macro- and near-mesoporous monoliths by medium internal phase emulsion polymerization: A systematic study," *Polymer*, vol. 99, pp. 157-165, 2016/09/02/, 2016.
- [249] S. Wang, J. Li, M. Qi, X. Gao, and W.-J. Wang, "Toward Maximizing the Mechanical Property of Interconnected Macroporous Polystyrenes Made from High Internal Phase Emulsions," *Langmuir*, vol. 33, no. 50, pp. 14295-14303, 2017/12/19, 2017.
- [250] T. J. McKenzie, P. S. Heaton, K. Rishi, R. Kumar, T. Brunet, G. Beaucage, O. Mondain-Monval, and N. Ayres, "Storage Moduli and Porosity of Soft PDMS PolyMIPES Can Be Controlled Independently Using Thiol–Ene Click Chemistry," *Macromolecules*, vol. 53, no. 10, pp. 3719-3727, 2020/05/26, 2020.
- [251] Y. Lumelsky, I. Lalush-Michael, S. Levenberg, and M. S. Silverstein, "A degradable, porous, emulsion-templated polyacrylate," *Journal of Polymer Science Part A: Polymer Chemistry*, vol. 47, no. 24, pp. 7043-7053, 2009.
- [252] K. Rohm, I. Manas-Zloczower, and D. Feke, "Poly (HIPE) morphology, crosslink density, and mechanical properties influenced by surfactant concentration and composition," *Colloids and Surfaces A: Physicochemical and Engineering Aspects*, vol. 583, pp. 123913, 2019.
- [253] N. Shirshova, A. Bismarck, S. Carreyette, Q. P. Fontana, E. S. Greenhalgh, P. Jacobsson, P. Johansson, M. J. Marczewski, G. Kalinka, and A. R. Kucernak, "Structural supercapacitor electrolytes based on bicontinuous ionic liquid–epoxy resin systems," *Journal of Materials Chemistry A*, vol. 1, no. 48, pp. 15300-15309, 2013.
- [254] J. Zhang, J. Yan, Y. Zhao, Q. Zhou, Y. Ma, Y. Zi, A. Zhou, S. Lin, L. Liao, and X. Hu, "High-strength and machinable load-bearing integrated electrochemical capacitors based on polymeric solid electrolyte," *Nature Communications*, vol. 14, no. 1, pp. 64, 2023.
- [255] L. L. C. Wong, V. O. Ikem, A. Menner, and A. Bismarck, "Macroporous polymers with hierarchical pore structure from emulsion templates stabilised by both particles and surfactants," *Macromolecular Rapid Communications*, vol. 32, no. 19, pp. 1563-1568, 2011.
- [256] M. Zhou, and R. Foudazi, "Effect of Cosurfactant on Structure and Properties of Polymerized High Internal Phase Emulsions (PolyHIPEs)," *Langmuir*, vol. 37, no. 26, pp. 7907-7918, 2021/07/06, 2021.
- [257] J. Fu, H. R. Thomas, and C. Li, "Tortuosity of porous media: Image analysis and physical simulation," *Earth-Science Reviews*, vol. 212, pp. 103439, 2021/01/01/, 2021.
- [258] J. Song, C. Cheng, Y. Wang, and C. Wan, "Microstructure of poly (vinylidene fluoride)-based polymer electrolyte and its effect on transport properties," *Journal of the Electrochemical Society*, vol. 149, no. 9, pp. A1230, 2002.
- [259] C. T. Desire, A. Khodabandeh, T. L. Schiller, R. Wilson, R. D. Arrua, S. A. F. Bon, and E. F. Hilder, "Preparation of highly interconnected hydrophilic polymers from emulsion templates with improved mechanical properties," *European Polymer Journal*, vol. 102, pp. 56-67, 2018/05/01/, 2018.
- [260] K. Abraham, M. Alamgir, and D. Hoffman, "Polymer electrolytes reinforced by Celgard® membranes," *Journal of The Electrochemical Society*, vol. 142, no. 3, pp. 683, 1995.
- [261] B. Tjaden, D. J. Brett, and P. R. Shearing, "Tortuosity in electrochemical devices: a review of calculation approaches," *International Materials Reviews*, vol. 63, no. 2, pp. 47-67, 2018.
- [262] R. S. Moglia, *Biomedical applications of emulsion templated scaffolds*: Texas A&M University, 2014.
- [263] E. A. Botchwey, M. A. Dupree, S. R. Pollack, E. M. Levine, and C. T. Laurencin, "Tissue engineered bone: Measurement of nutrient transport in three-dimensional matrices," *Journal of Biomedical Materials Research Part A: An Official Journal of The Society for*

- Biomaterials, The Japanese Society for Biomaterials, and The Australian Society for Biomaterials and the Korean Society for Biomaterials*, vol. 67, no. 1, pp. 357-367, 2003.
- [264] J.-H. Cao, B.-K. Zhu, and Y.-Y. Xu, "Structure and ionic conductivity of porous polymer electrolytes based on PVDF-HFP copolymer membranes," *Journal of Membrane Science*, vol. 281, no. 1, pp. 446-453, 2006/09/15/, 2006.
- [265] J. Bear, *Dynamics of fluids in porous media*: Courier Corporation, 2013.
- [266] Y. Marcus, and G. Hefter, "Ion pairing," *Chemical reviews*, vol. 106, no. 11, pp. 4585-4621, 2006.
- [267] F. Zhen, "Electron transfer in deep eutectic solvents: from kinetics to the hydrogen-bonding and ion pairing effects," Université de Rennes, 2022.
- [268] A. Sanchez-Fernandez, A. J. Jackson, S. F. Prévost, J. J. Douch, and K. J. Edler, "Long-range electrostatic colloidal interactions and specific ion effects in deep eutectic solvents," *Journal of the American Chemical Society*, vol. 143, no. 35, pp. 14158-14168, 2021.
- [269] M. Aryafard, M. Abbasi, D. Řeha, A. R. Harifi-Mood, and B. Minofar, "Experimental and theoretical investigation of solvatochromic properties and ion solvation structure in DESs of reline, glyceline, ethaline and their mixtures with PEG 400," *Journal of Molecular Liquids*, vol. 284, pp. 59-67, 2019/06/15/, 2019.
- [270] X. Bu, Y. Ge, L. Wang, L. Wu, X. Ma, and D. Lu, "Design of highly stretchable deep eutectic solvent-based ionic gel electrolyte with high ionic conductivity by the addition of zwitterion ion dissociators for flexible supercapacitor," *Polymer Engineering & Science*, vol. 61, no. 1, pp. 154-166, 2021.
- [271] B. B. Hansen, S. Spittle, B. Chen, D. Poe, Y. Zhang, J. M. Klein, A. Horton, L. Adhikari, T. Zelovich, and B. W. Doherty, "Deep eutectic solvents: A review of fundamentals and applications," *Chemical reviews*, vol. 121, no. 3, pp. 1232-1285, 2020.
- [272] Z. Abbasian, and M. Moghbeli, "Open porous emulsion-templated monoliths: Effect of the emulsion preparation conditions on the foam microstructure and properties," *Journal of applied polymer science*, vol. 116, no. 2, pp. 986-994, 2010.
- [273] J. Hong, D. Radojčić, M. Ionescu, Z. Petrović, and E. Eastwood, "Advanced materials from corn: isosorbide-based epoxy resins," *Polymer Chemistry*, vol. 5, no. 18, pp. 5360-5368, 2014.
- [274] J. Yang, J. Xiao, J. Zeng, C. Peng, X. Feng, and B. Hou, "An Empirical Model for Resin Viscosity During Cure in Vacuum Infusion Molding Process," *Applied Composite Materials*, vol. 19, no. 3, pp. 573-582, 2012/06/01, 2012.
- [275] S. Huš, M. Kolar, and P. Krajnc, "Tailoring morphological features of cross-linked emulsion-templated poly (glycidyl methacrylate)," *Designed Monomers and Polymers*, vol. 18, no. 7, pp. 698-703, 2015.
- [276] A. Barbeta, "Emulsion-derived (PolyHIPE) foams: optimization of properties and morphology for fluid flow applications," Durham University, 2002.
- [277] P. Dhavalikar, J. Shenoi, K. Salhadar, M. Chwatko, G. Rodriguez-Rivera, J. Cheshire, R. Foudazi, and E. Cosgriff-Hernandez, "Engineering toolbox for systematic design of polyHIPE architecture," *Polymers*, vol. 13, no. 9, pp. 1479, 2021.
- [278] M. Tebboth, A. Kogelbauer, and A. Bismarck, "Highly permeable macroporous polymers via controlled agitation of emulsion templates," *Chemical Engineering Science*, vol. 137, pp. 786-795, 2015/12/01/, 2015.
- [279] S. Vahid, V. Burattini, S. Afshinjavid, and A. Dashtkar, "Comparison of Rheological Behaviour of Bio-Based and Synthetic Epoxy Resins for Making Eco-composites. Fluids 2021, 6, 38," s Note: MDPI stays neutral with regard to jurisdictional claims in ..., 2021.
- [280] P. Jajibabu, M. Jagannatham, P. Haridoss, G. D. Janaki Ram, A. P. Deshpande, and S. R. Bakshi, "Effect of different carbon nano-fillers on rheological properties and lap shear strength of epoxy adhesive joints," *Composites Part A: Applied Science and Manufacturing*, vol. 82, pp. 53-64, 2016/03/01/, 2016.

- [281] S. McIntyre, I. Kaltzakorta, J. J. Liggat, R. A. Pethrick, and I. Rhoney, "Influence of the Epoxy Structure on the Physical Properties of Epoxy Resin Nanocomposites," *Industrial & Engineering Chemistry Research*, vol. 44, no. 23, pp. 8573-8579, 2005/11/01, 2005.
- [282] A. Laforgue, and L. Robitaille, "A comparative study of the performance of ultra-porous membranes as separators in supercapacitor devices," *ECS Transactions*, vol. 35, no. 24, pp. 13, 2011.
- [283] P. Aparaj, A. Karandikar, P. Karandikar, N. Bhavana, and R. Gabhane, "Investigation of layered separators for improved performance of supercapacitors." pp. 215-219.
- [284] X.-Z. SUN, X. Zhang, B. Huang, and Y.-W. MA, "Effects of separator on the electrochemical performance of electrical double-layer capacitor and hybrid battery-supercapacitor," *Acta Physico-Chimica Sinica*, vol. 30, no. 3, pp. 485-491, 2014.
- [285] K. Tönurist, T. Thomberg, A. Jänes, T. Romann, V. Sammelselg, and E. Lust, "Influence of separator properties on electrochemical performance of electrical double-layer capacitors," *Journal of Electroanalytical Chemistry*, vol. 689, pp. 8-20, 2013/01/15/, 2013.
- [286] S. Satpathy, S. Das, and B. K. Bhattacharyya, "How and where to use super-capacitors effectively, an integration of review of past and new characterization works on super-capacitors," *Journal of Energy Storage*, vol. 27, pp. 101044, 2020/02/01/, 2020.
- [287] E. Ozeren Ozgul, and M. H. Ozkul, "Effects of epoxy, hardener, and diluent types on the workability of epoxy mixtures," *Construction and Building Materials*, vol. 158, pp. 369-377, 2018/01/15/, 2018.
- [288] K. Johansson, and M. Johansson, "A model study on fatty acid methyl esters as reactive diluents in thermally cured coil coating systems," *Progress in Organic Coatings*, vol. 55, no. 4, pp. 382-387, 2006/04/01/, 2006.
- [289] K. Wutticharoenwong, J. Dzikowski, and M. D. Soucek, "Tung based reactive diluents for alkyd systems: Film properties," *Progress in Organic Coatings*, vol. 73, no. 4, pp. 283-290, 2012/04/01/, 2012.
- [290] M. A. Downey, and L. T. Drzal, "Toughening of aromatic epoxy via aliphatic epoxy copolymers," *Polymer*, vol. 55, no. 26, pp. 6658-6663, 2014/12/15/, 2014.
- [291] J. Chen, X. Nie, Z. Liu, Z. Mi, and Y. Zhou, "Synthesis and Application of Polyepoxide Cardanol Glycidyl Ether as Biobased Polyepoxide Reactive Diluent for Epoxy Resin," *ACS Sustainable Chemistry & Engineering*, vol. 3, no. 6, pp. 1164-1171, 2015/06/01, 2015.
- [292] J. Szöllösi, "Fluidity/viscosity of biological membranes," *Mobility and proximity in biological membranes*, pp. 137-208, 2018.
- [293] C. H. Lee, V. Moturi, and Y. Lee, "Thixotropic property in pharmaceutical formulations," *Journal of controlled release*, vol. 136, no. 2, pp. 88-98, 2009.
- [294] M. Nakagawa, and T. Kawai, "Exploring the Multifunctionality of a Novel Long-Chain Amidoamine Amphiphile," *Journal of oleo science*, vol. 66, no. 1, pp. 13-19, 2017.
- [295] Q. Yuan, Z. Wang, H. Yao, J. Huang, S. Zuo, and H. Huang, "Comparative study of reactive diluents with different molecular structures on the curing properties of epoxy adhesives and the interface bonding properties with mortar," *International Journal of Adhesion and Adhesives*, vol. 126, pp. 103473, 2023/08/01/, 2023.
- [296] H. Tai, A. Sergienko, and M. S. Silverstein, "Organic-inorganic networks in foams from high internal phase emulsion polymerizations," *Polymer*, vol. 42, no. 10, pp. 4473-4482, 2001.
- [297] B. A. Dikici, S. Dikici, and F. Claeysens, "Synergistic effect of type and concentration of surfactant and diluting solvent on the morphology of emulsion templated matrices developed as tissue engineering scaffolds," *Reactive and Functional Polymers*, vol. 180, pp. 105387, 2022.
- [298] P. S. Dhavalikar, *Development of polyHIPE Scaffolds for Improved Bone Regeneration: The University of Texas at Austin*, 2020.
- [299] Y. Hu, Q. Shang, C. Wang, G. Feng, C. Liu, F. Xu, and Y. Zhou, "Renewable epoxidized cardanol-based acrylate as a reactive diluent for UV-curable resins," *Polymers for Advanced Technologies*, vol. 29, no. 6, pp. 1852-1860, 2018.

- [300] J. Clayden, N. Greeves, and S. Warren, *Organic chemistry*: Oxford University Press, USA, 2012.
- [301] A. Ghanem, and Y. Lang, "Introduction to polymer adhesion," *Department of process engineering and applied science, Dalhousie University, Halifax, Nova Scotia, Canada*, 2017.
- [302] C. Cui, and W. Liu, "Recent advances in wet adhesives: Adhesion mechanism, design principle and applications," *Progress in Polymer Science*, vol. 116, pp. 101388, 2021/05/01/, 2021.
- [303] P. Delobelle, L. Guillot, C. Dubois, and L. Monney, "Photo-oxidation effects on mechanical properties of epoxy matrixes: Young's modulus and hardness analyses by nano-indentation," *Polymer Degradation and Stability*, vol. 77, no. 3, pp. 465-475, 2002/01/01/, 2002.
- [304] A. Giuntoli, N. K. Hansoge, A. van Beek, Z. Meng, W. Chen, and S. Keten, "Systematic coarse-graining of epoxy resins with machine learning-informed energy renormalization," *npj computational materials*, vol. 7, no. 1, pp. 168, 2021.
- [305] A. Ömür, and K. Yunus, "Effect of Reactive and Non-Reactive Diluent on Mechanical Properties of Epoxy Resin," *Bilecik Şeyh Edebali Üniversitesi Fen Bilimleri Dergisi*, vol. 8, no. 1, pp. 167-172, 2021.
- [306] L. Kregl, G. M. Wallner, R. W. Lang, and G. Mayrhofer, "Effect of resin modifiers on the structural properties of epoxy resins," *Journal of Applied Polymer Science*, vol. 134, no. 44, pp. 45348, 2017.
- [307] A. Sinha, N. Islam Khan, S. Das, J. Zhang, and S. Halder, "Effect of reactive and non-reactive diluents on thermal and mechanical properties of epoxy resin," *High Performance Polymers*, vol. 30, no. 10, pp. 1159-1168, 2018.
- [308] N. Suderman, M. I. N. Isa, and N. M. Sarbon, "The effect of plasticizers on the functional properties of biodegradable gelatin-based film: A review," *Food Bioscience*, vol. 24, pp. 111-119, 2018/08/01/, 2018.
- [309] S. Huo, H. Ma, G. Liu, C. Jin, J. Chen, G. Wu, and Z. Kong, "Synthesis and properties of organosilicon-grafted cardanol novolac epoxy resin as a novel biobased reactive diluent and toughening agent," *ACS omega*, vol. 3, no. 12, pp. 16403-16408, 2018.
- [310] Y. Yu, B. Zhang, Y. Wang, G. Qi, F. Tian, J. Yang, and S. Wang, "Co-continuous structural electrolytes based on ionic liquid, epoxy resin and organoclay: Effects of organoclay content," *Materials & Design*, vol. 104, pp. 126-133, 2016.
- [311] J. Han, M. J. Lee, K. Lee, Y. J. Lee, S. H. Kwon, J. H. Min, E. Lee, W. Lee, S. W. Lee, and B. J. Kim, "Role of Bicontinuous Structure in Elastomeric Electrolytes for High-Energy Solid-State Lithium-Metal Batteries," *Advanced Materials*, vol. 35, no. 1, pp. 2205194, 2023.
- [312] K. Matsumoto, S. Sogabe, and T. Endo, "Synthesis and properties of methacrylate-based networked polymers having ionic liquid structures," *Journal of Polymer Science Part A: Polymer Chemistry*, vol. 48, no. 20, pp. 4515-4521, 2010.
- [313] U. H. Choi, and B. M. Jung, "Ion conduction, dielectric and mechanical properties of epoxy-based solid polymer electrolytes containing succinonitrile," *Macromolecular Research*, vol. 26, pp. 459-465, 2018.
- [314] S. H. Wang, Y. X. Yin, T. T. Zuo, W. Dong, J. Y. Li, J. L. Shi, C. H. Zhang, N. W. Li, C. J. Li, and Y. G. Guo, "Stable Li metal anodes via regulating lithium plating/stripping in vertically aligned microchannels," *Advanced Materials*, vol. 29, no. 40, pp. 1703729, 2017.
- [315] C.-P. Yang, Y.-X. Yin, S.-F. Zhang, N.-W. Li, and Y.-G. Guo, "Accommodating lithium into 3D current collectors with a submicron skeleton towards long-life lithium metal anodes," *Nature communications*, vol. 6, no. 1, pp. 8058, 2015.
- [316] K. R. Adair, M. Iqbal, C. Wang, Y. Zhao, M. N. Banis, R. Li, L. Zhang, R. Yang, S. Lu, and X. Sun, "Towards high performance Li metal batteries: Nanoscale surface modification of 3D metal hosts for pre-stored Li metal anodes," *Nano Energy*, vol. 54, pp. 375-382, 2018.

- [317] Q. Li, S. Zhu, and Y. Lu, "3D porous Cu current collector/Li-metal composite anode for stable lithium-metal batteries," *Advanced Functional Materials*, vol. 27, no. 18, pp. 1606422, 2017.
- [318] N. Choudhary, C. Li, J. Moore, N. Nagaiah, L. Zhai, Y. Jung, and J. Thomas, "Asymmetric Supercapacitor Electrodes and Devices," *Advanced Materials*, vol. 29, no. 21, pp. 1605336, 2017.
- [319] J. Li, H. Jia, S. Ma, L. Xie, X.-X. Wei, L. Dai, H. Wang, F. Su, and C.-M. Chen, "Separator Design for High-Performance Supercapacitors: Requirements, Challenges, Strategies, and Prospects," *ACS Energy Letters*, vol. 8, no. 1, pp. 56-78, 2023/01/13, 2023.
- [320] P. Banerjee, S. Kumar, and S. Bose, "Thermoreversible bonds and graphene oxide additives enhance the flexural and interlaminar shear strength of self-healing epoxy/carbon fiber laminates," *ACS Applied Nano Materials*, vol. 4, no. 7, pp. 6821-6831, 2021.
- [321] S. Mandal, R. Raj, K. Samanta, S. Kumar, and S. Bose, "Self-Healable Interfaces with Improved Mechanical Properties Induced by Dynamic Network Reconfiguration in Carbon Fiber-Reinforced Epoxy Laminates," *ACS Applied Materials & Interfaces*, 2024.
- [322] S. Mandal, K. Samanta, K. Manna, S. Kumar, and S. Bose, "GO-tagged PEI sizing agent imparts self-healing and excellent mechanical properties to carbon fiber reinforced epoxy laminates," *Nanoscale*, vol. 16, no. 14, pp. 6984-6998, 2024.
- [323] A. J. Bard, L. R. Faulkner, and H. S. White, *Electrochemical methods: fundamentals and applications*: John Wiley & Sons, 2022.
- [324] T. F. Fuller, and J. N. Harb, *Electrochemical engineering*: John Wiley & Sons, 2018.
- [325] H. Tariq, S. U. Awan, D. Hussain, S. Rizwan, S. A. Shah, S. Zainab, and M. B. Riaz, "Enhancing supercapacitor performance through design optimization of laser-induced graphene and MWCNT coatings for flexible and portable energy storage," *Scientific Reports*, vol. 13, no. 1, pp. 21116, 2023.
- [326] Y. Xu, S. Pei, Y. Yan, L. Wang, G. Xu, S. Yarlagadda, and T.-W. Chou, "High-performance structural supercapacitors based on aligned discontinuous carbon fiber electrodes and solid polymer electrolytes," *ACS Applied Materials & Interfaces*, vol. 13, no. 10, pp. 11774-11782, 2021.
- [327] E. S. Greenhalgh, J. Ankersen, L. E. Asp, A. Bismarck, Q. Fontana, M. Houille, G. Kalinka, A. Kucernak, M. Mistry, and S. Nguyen, "Mechanical, electrical and microstructural characterisation of multifunctional structural power composites," *Journal of composite materials*, vol. 49, no. 15, pp. 1823-1834, 2015.
- [328] H. Qian, A. R. Kucernak, E. S. Greenhalgh, A. Bismarck, and M. S. Shaffer, "Multifunctional structural supercapacitor composites based on carbon aerogel modified high performance carbon fiber fabric," *ACS applied materials & interfaces*, vol. 5, no. 13, pp. 6113-6122, 2013.
- [329] N. Shirshova, H. Qian, M. S. Shaffer, J. H. Steinke, E. S. Greenhalgh, P. T. Curtis, A. Kucernak, and A. Bismarck, "Structural composite supercapacitors," *Composites Part A: Applied Science and Manufacturing*, vol. 46, pp. 96-107, 2013.
- [330] N. S. Hudak, A. D. Schlichting, and K. Eisenbeiser, "Structural supercapacitors with enhanced performance using carbon nanotubes and polyaniline," *Journal of The Electrochemical Society*, vol. 164, no. 4, pp. A691, 2017.
- [331] Q. Jiang, "Functionalised macroporous films via emulsion templating: preparation, processing and applications," Imperial College London, 2013.
- [332] Z. S. Iro, C. Subramani, and S. Dash, "A brief review on electrode materials for supercapacitor," *International Journal of Electrochemical Science*, vol. 11, no. 12, pp. 10628-10643, 2016.
- [333] M. A. Brza, S. B. Aziz, H. Anuar, F. Ali, M. H. Hamsan, M. F. Z. Kadir, and R. T. Abdulwahid, "Metal framework as a novel approach for the fabrication of electric double layer capacitor device with high energy density using plasticized Poly(vinyl alcohol):

- Ammonium thiocyanate based polymer electrolyte," *Arabian Journal of Chemistry*, vol. 13, no. 10, pp. 7247-7263, 2020/10/01/, 2020.
- [334] R. Reece, C. Lekakou, and P. A. Smith, "A structural supercapacitor based on activated carbon fabric and a solid electrolyte," *Materials Science and Technology*, vol. 35, no. 3, pp. 368-375, 2019/02/01, 2019.
- [335] H. Lu, L. He, X. Li, W. Zhang, J. Che, X. Liu, Z. Hou, H. Du, and Y. Qu, "Ionic liquid-solvent mixture of propylene carbonate and 1, 2-dimethoxyethane as electrolyte for electric double-layer capacitor," *Journal of Materials Science: Materials in Electronics*, vol. 30, pp. 13933-13938, 2019.
- [336] A. Noofeli, P. J. Hall, and A. J. Rennie, "Ionic liquid based EDLCs: influence of carbon porosity on electrochemical performance," *Faraday Discussions*, vol. 172, pp. 163-177, 2014.
- [337] B. K. Muñoz, A. González-Banciella, D. Ureña, M. Sánchez, and A. Ureña, "Electrochemical comparison of 2D-flexible solid-state supercapacitors based on a matrix of PVA/H₃PO₄," *Polymers*, vol. 15, no. 20, pp. 4036, 2023.
- [338] A. C. Lazanas, and M. I. Prodromidis, "Electrochemical Impedance Spectroscopy—A Tutorial," *ACS Measurement Science Au*, vol. 3, no. 3, pp. 162-193, 2023/06/21, 2023.
- [339] Komal, A. Kumar, Y. Kumar, and V. K. Shukla, "Parthenium hysterophorus derived activated carbon for EDLC device application," *Journal of Materials Science: Materials in Electronics*, vol. 34, no. 27, pp. 1880, 2023/09/27, 2023.
- [340] L. Kouchachvili, N. Maffei, and E. Entchev, "Novel binding material for supercapacitor electrodes," *Journal of Solid State Electrochemistry*, vol. 18, no. 9, pp. 2539-2547, 2014/09/01, 2014.
- [341] C. Lamiel, I. Hussain, X. Ma, and K. Zhang, "Properties, functions, and challenges: current collectors," *Materials Today Chemistry*, vol. 26, pp. 101152, 2022/12/01/, 2022.
- [342] A. Das, A. Barai, I. Masters, and D. Williams, "Comparison of tab-to-busbar ultrasonic joints for electric vehicle Li-ion battery applications," *World Electric Vehicle Journal*, vol. 10, no. 3, pp. 55, 2019.
- [343] A. İrfan, S. Celik, and İ. ÇELİK, "Comparison of properties of friction and diffusion welded joints made between the pure Aluminium and Copper bar," Balıkesir University, Engineering and Architecture Faculty, Department of ..., 1999.
- [344] H. Dhulipati, S. Mukundan, L. Chauvin, C. Riczu, A. Edrisky, M. Kozdras, J. Bauman, S. Habibi, J. Tjong, and N. C. Kar, "Investigation of aluminium and copper wound PMSM for direct-drive electric vehicle application." p. 012002.
- [345] Y. Hanaoka, K. Hinode, K. i. Takeda, and D. Kodama, "Increase in electrical resistivity of copper and aluminum fine lines," *Materials transactions*, vol. 43, no. 7, pp. 1621-1623, 2002.
- [346] K. Savolainen, J. Mononen, T. Saukkonen, and H. Hänninen, "A preliminary study on friction stir welding of dissimilar metal joints of copper and aluminium paper 79."
- [347] M. Orselly, C. Richard, J. Devémy, A. Bouvet-Marchand, A. Dequidt, C. Loubat, and P. Malfreyt, "Impact of the Force Field on the Calculation of Density and Surface Tension of Epoxy-Resins," *The Journal of Physical Chemistry B*, vol. 127, no. 11, pp. 2617-2628, 2023.
- [348] Y. Chen, W. Chen, L. Fu, Y. Yang, Y. Wang, X. Hu, F. Wang, and T. Mu, "Surface tension of 50 deep eutectic solvents: effect of hydrogen-bonding donors, hydrogen-bonding acceptors, other solvents, and temperature," *Industrial & Engineering Chemistry Research*, vol. 58, no. 28, pp. 12741-12750, 2019.
- [349] I. Pulko, and P. Krajnc, "Open cellular reactive porous membranes from high internal phase emulsions," *Chemical communications*, no. 37, pp. 4481-4483, 2008.
- [350] B.-A. Mei, J. Lau, T. Lin, S. H. Tolbert, B. S. Dunn, and L. Pilon, "Physical Interpretations of Electrochemical Impedance Spectroscopy of Redox Active Electrodes for Electrical Energy Storage," *The Journal of Physical Chemistry C*, vol. 122, no. 43, pp. 24499-24511, 2018.

- [351] Y. Suda, A. Mizutani, T. Harigai, H. Takikawa, H. Ue, and Y. Umeda, "Influences of internal resistance and specific surface area of electrode materials on characteristics of electric double layer capacitors."
- [352] D. Maheswari, and P. Venkatachalam, "Enhanced performance of bi-layer Nb₂O₅ coated TiO₂ nanoparticles/nanowires composite photoanode in dye-sensitized solar cells," *Photonics and Nanostructures - Fundamentals and Applications*, vol. 12, no. 5, pp. 515-526, 2014/11/01/, 2014.
- [353] A. Pandolfo, G. J. Wilson, T. D. Huynh, and A. F. Hollenkamp, "The influence of conductive additives and inter-particle voids in carbon EDLC electrodes," *Fuel cells*, vol. 10, no. 5, pp. 856-864, 2010.
- [354] L. Köps, P. Ruschhaupt, C. Guhrenz, P. Schlee, S. Pohlmann, A. Varzi, S. Passerini, and A. Balducci, "Development of a high-energy electrical double-layer capacitor demonstrator with 5000 F in an industrial cell format," *Journal of Power Sources*, vol. 571, pp. 233016, 2023/07/01/, 2023.
- [355] R. Thangappan, S. Kalaiselvam, A. Elayaperumal, R. Jayavel, M. Arivanandhan, R. Karthikeyan, and Y. Hayakawa, "Graphene decorated with MoS₂ nanosheets: a synergetic energy storage composite electrode for supercapacitor applications," *Dalton transactions*, vol. 45, no. 6, pp. 2637-2646, 2016.
- [356] M. chemicals, "Super Shield™ Nickel Conductive Coating 841AR Technical Data Sheet," *Technical datasheet*, 2017.
- [357] S. Senthilkumar, R. K. Selvan, N. Ponpandian, J. Melo, and Y. Lee, "Improved performance of electric double layer capacitor using redox additive (VO²⁺/VO²⁺) aqueous electrolyte," *Journal of Materials Chemistry A*, vol. 1, no. 27, pp. 7913-7919, 2013.
- [358] Y. K. Han, J. Y. Cheon, T. Kim, S. B. Lee, Y. Do Kim, and B. M. Jung, "A chemically bonded supercapacitor using a highly stretchable and adhesive gel polymer electrolyte based on an ionic liquid and epoxy-triblock diamine network," *RSC advances*, vol. 10, no. 32, pp. 18945-18952, 2020.
- [359] S. J. Moon, H. J. Min, C. S. Lee, D. R. Kang, and J. H. Kim, "Adhesive, free-standing, partially fluorinated comb copolymer electrolyte films for solid flexible supercapacitors," *Chemical Engineering Journal*, vol. 429, pp. 132240, 2022/02/01/, 2022.

9 Appendix

Appendix 1. CV plots of the fabricated SCs at various scan rates

